



## Evaluation of In-plane Silicon Microneedles for Allergy Diagnostics

**Bisgaard, Stephanie Ingemann**

*Publication date:*  
2023

*Document Version*  
Publisher's PDF, also known as Version of record

[Link back to DTU Orbit](#)

*Citation (APA):*  
Bisgaard, S. I. (2023). *Evaluation of In-plane Silicon Microneedles for Allergy Diagnostics*. DTU Nanotech.

---

### General rights

Copyright and moral rights for the publications made accessible in the public portal are retained by the authors and/or other copyright owners and it is a condition of accessing publications that users recognise and abide by the legal requirements associated with these rights.

- Users may download and print one copy of any publication from the public portal for the purpose of private study or research.
- You may not further distribute the material or use it for any profit-making activity or commercial gain
- You may freely distribute the URL identifying the publication in the public portal

If you believe that this document breaches copyright please contact us providing details, and we will remove access to the work immediately and investigate your claim.



# **Evaluation of In-plane Silicon Microneedles for Allergy Diagnostics**

PhD thesis by Stephanie Ingemann Bisgaard

Biomaterial Microsystems Group  
National Centre for Nano Fabrication and Characterization

Research Group for Food Allergy  
National Food Institute

Technical University of Denmark, DTU

March 2023



## I) Abstract (English)

The prevalence of allergies is increasing worldwide and is a global burden for the healthcare sector. The skin prick test (SPT) is a common method for screening for allergies. It takes 15-20 min and requires a manual readout by a healthcare professional. However, the response is only qualitative, not quantitative. The aim of the InstaPatch project, which this PhD thesis is a part of, was to improve on the SPT and develop a novel test for fast and quantitative allergy diagnostics in the skin. The InstaPatch is envisioned as an intradermal electrochemical biosensor based on microneedles (MNs) which are sub-mm structures that act like small needles piercing the skin. The first aim of the PhD project was to ensure the mechanical stability and penetration ability of in-plane solid silicon MNs. The MNs should cause as little tissue damage as possible while ensuring sufficient penetration depth to reach the upper dermis skin layer. Five MN shapes with varying dimensions were tested in skin-simulating hydrogels, excised Brown Norway (BN) rat (*rattus norvegicus*) skin, and porcine ear skin samples using a Texture Analyser to obtain force-displacement graphs for the penetration. The MN shape and dimensions were optimized to minimize penetration force while maintaining mechanical stability. Induced tissue damage was examined using histology and the triangular shape was found to cause the least amount of tissue damage. The optimized MNs were a hybrid between a triangular and pencil shape exhibiting good mechanical stability and penetration ability while providing enough surface area for coating and future electrochemical measurements. The optimized MNs were tested in porcine skin and human breast skin samples to evaluate their mechanical stability and penetration ability. The MNs were 1000  $\mu\text{m}$  long, 400  $\mu\text{m}$  wide, and 180  $\mu\text{m}$  thick. The second aim of the PhD project was to deliver an allergen by MN insertion to initiate a local allergic reaction. First, MNs were coated using dip-coating with fluorescent-labeled molecules for visualization and quantification of delivery. It was shown that MNs could be coated with fluorescent-labeled molecules and delivery was confirmed by cryostat histology and fluorescence microscopy. However, by measuring the remaining, fluorescent-labeled coating found on the MNs after insertion, the delivered amounts were found to be exceedingly small and hard to quantify. The final aim of the PhD project was to deliver an allergen in sensitized BN rats using allergen-coated MNs and confirm a local allergic reaction. *In vivo* experiments were performed. One used peanut protein extract (PPE)-sensitized BN rats and another used birch pollen extract (BPE)-sensitized BN rats. MNs were coated with the peanut allergen Ara h 2 at various concentrations for delivery in PPE-sensitized rats while other MNs were coated with BPE or the birch pollen allergen Bet v 1 in various concentrations for delivery in BPE-sensitized rats. Coatings with compound 48/80 were included as positive control and phosphate buffered saline as negative control. Intradermal (i.d.) injections of the same allergen solution concentrations were included as a second control for the coated MNs. The allergic response within the skin was evaluated by intravenously injecting Evans blue into the tail vein to visualize blood accumulations. It was not possible to measure a significant reaction in sensitized BN rats when the delivery was facilitated by the MNs. However, some promising, but sub-optimal dose-response curves were measured for rats receiving i.d. injections. As a last step, delivered Ara h 2 was attempted recovered in homogenized biopsy samples from the BN rats. Ara h 2 could be measured in the homogenized samples for delivery from the highest i.d. injection concentration, however, not from the MNs.

## II) Resumé (dansk)

Allergier er udbredt verden over, og de er en global byrde for sundhedssektoren. Priktesten er en almindelig metode til at screene for allergier. Priktesten tager 15-20 min og kræver en fortolkning fra en sundhedsmedarbejder og denne respons er kun kvalitativ frem for kvantitativ. Målet for InstaPatch projektet, som denne Ph.d.-afhandling er en del af, var at forbedre priktesten og udvikle en ny test til hurtig og kvantitativ diagnosticering i huden. InstaPatchen forudses at være en intradermal elektrokemisk biosensor baseret på mikronåle (MN), der er struktureret på under en mm i form af nåle, der kan prikkes ind i huden. Det første mål for Ph.d.-projektet var at sikre den mekaniske stabilitet og penetrationsevne af solide in-plane silicium MN. MN skulle forårsage så lidt hudbeskadigelse som muligt, men sikre en passende penetrationsdybde til at nå det øvre dermis-hudlag. Fem MN-former med forskellige dimensioner blev testet i hudsimulerende hydrogeler, og udskårne hudprøver fra brune rotter (*Rattus norvegicus*) samt griseører ved at bruge en Texture Analyser til at opnå kraft-forskydningsmålinger for penetrationen. MN-form og dimensioner blev optimeret til at minimere penetrationskraften men samtidig være mekanisk stabil. Induceret hudbeskadigelse blev evalueret ved brug af histologi, og de trekantformede MN forårsagede mindst mulig hudbeskadigelse. De optimerede MN var en hybrid mellem en trekants- og blyantsform, der udviste god mekanisk stabilitet og penetrationsevne samtidig med, at de havde et passende overfladeareal til coating og fremtidige elektrokemiske målinger. Disse optimerede MN blev testet for deres mekaniske stabilitet og penetrationsevne i grise- og menneskebryst-hud. De optimerede MN endte med at være 1000 µm lange, 400 µm brede og 180 µm tykke. Det andet mål med Ph.d.-projektet var at levere allergener ved brug af MN-penetration til at igangsætte en allergisk reaktion. MN blev coatet ved brug af dip-coating med fluorescensmærkede molekyler for visualisering og kvantificering af leveringen. Det blev påvist, at MN kunne blive coatet med fluorescensmærkede molekyler, og levering blev bekræftet ved brug af cryostat-histologi og fluorescensmikroskopi. Ved måling af den resterende fluorescensmærkede coating på MN efter penetration blev det konstateret, at leveringsmængderne var meget små og svære at kvantificere. Det sidste mål med Ph.d.-projektet var at levere allergener i sensibiliserede brune rotter ved brug af allergen-coatede MN og bekræfte en lokal allergisk reaktion. *In vivo* forsøg blev udført, hvor ét inkluderede peanut-protein-ekstrakt (PPE)-sensibiliserede brune rotter og et andet birkepollenekstrakt (BPE)-sensibiliserede brune rotter. MN blev coatet med peanut-allergenet Ara h 2 ved forskellige koncentrationer for levering i PPE-sensibiliserede rotter, mens andre MN blev coatet med BPE eller birkepollenekstrakt-allergenet Bet v 1 ved forskellige koncentrationer til levering i BPE-sensibiliserede rotter. Coating med stof 48/80 blev inkluderet som positiv kontrol og fysiologisk saltvandsopløsning som negativ kontrol. Intradermal (i.d.) injektion af de samme allergenopløsningskoncentrationer blev inkluderet som en sekundær kontrol til de coatede MN. Den allergiske respons i huden blev evalueret ved brug af intravenøs injektion af Evans blue i halevenen til at visualisere blodophobning. Det var ikke muligt at måle en signifikant respons i sensibiliserede brune rotter ved MN levering. Dog var der nogle lovende, men ikke optimale målinger i sensibiliserede brune rotter, der fik i.d. injektioner. Som et sidste trin blev den leverede Ara h 2 forsøgt genfundet ved at homogenisere hudvævsprøverne fra rotterne. Ara h 2 kunne genfindes for homogeniserede hudprøver ved den højeste koncentration af i.d. injektion, men ikke fra MN.

### III) List of abbreviations

| Abbreviation | Meaning                                    |
|--------------|--|
| APC          | Antigen-presenting cell                    |
| BAT          | Basophil activation test                   |
| BN           | Brown Norway                               |
| BPE          | Birch pollen extract                       |
| CD           | Cluster of differentiation                 |
| CLSM         | Confocal laser scanning microscopy         |
| CMC          | Carboxymethyl cellulose                    |
| CRD          | Component-resolved diagnosis               |
| ELISA        | enzyme-linked immunosorbent assay          |
| FACS         | Fluorescence-activated single cell sorting |
| GMP          | Good manufacturing practice                |
| GRAS         | Generally regarded as safe                 |
| HPMC         | Hydroxypropylmethylcellulose               |
| i.d.         | Intradermal                                |
| i.p.         | Intraperitoneal                            |
| i.v.         | Intravenous                                |
| Ig           | Immunoglobulin                             |
| IHC          | Immunohistochemistry                       |
| IL           | Interleukin                                |
| ISF          | Interstitial fluid                         |
| MAT          | Mast cell activation test                  |
| MC           | Mast cell                                  |
| MHC          | Major histocompatibility complex           |
| MN           | Microneedle                                |
| MW           | Molecular weight                           |
| OCT          | Optical coherence tomography               |
| PBS          | Phosphate buffered saline                  |
| PE           | Phycoerythrin                              |
| PLGA         | Poly(lactic-co-glycolic acid)              |
| PPE          | Peanut protein extract                     |
| PVA          | Polyvinyl alcohol                          |
| PVP          | Polyvinyl pyrrolidone                      |
| RAST         | Radioallergosorbant allergen test          |
| SEM          | Scanning electron microscopy               |
| SPT          | Skin prick test                            |
| TA           | Texture Analyser                           |
| TEWL         | Trans-epidermal water loss                 |
| TH2          | T helper 2                                 |
| WAO          | World Allergy Organization                 |
| YM           | Young's modulus                            |

## **IV) Preface**

This PhD was performed in the Biomaterial Microsystems Group at the National Centre for Nano Fabrication and Characterization and the Research Group for Food Allergy at the National Food Institute as a collaboration. The project was conducted from 1<sup>st</sup> of December 2019 to 31<sup>st</sup> of March 2023 including a four-month extension due to COVID-19. It was supervised by Professor Stephan Sylvest Keller, Head of Biomaterial Microsystems Group, and co-supervised by Senior Researcher Katrine Lindholm Bøgh, Head of Research Group for Food Allergy. This project was funded by Independent Research Fund Denmark (DFF-FTP).

## V) Acknowledgements

Many people have contributed to this PhD project over the past three years, but I would first and foremost like to thank my supervisors Professor Stephan Sylvest Keller and Senior Researcher Katrine Lindholm Bøgh for giving me the opportunity to carry out the PhD project and for guiding me throughout the journey. It has been a pleasure being part of the two research groups Biomaterial Microsystems Group and the Research group for Food Allergy.

From the Biomaterial Microsystems Group, I would like to thank Long Quang Nguyen, Gerardo Garcia Zavaleta, and Mohammad Ramezannezhad for providing me with microneedles even if it was sometimes on a short notice. A special thank you to Sheida Esmail Tehrani for great company and excellent scientific discussions while working on the InstaPatch project together, and to Jitka Urbankova, Shahana Bishnoi, and Swetha Vasudevan Kanakkottu for a great time together whether we were getting together for some creative activities or at a conference, I really enjoyed your company. Additionally, a thank you to Babak Rezaei for helping me get started in the lab with CAD designing and 3D printing. Truthfully speaking, the list could go on forever, so I will simply say thank you to all former and present members of the group. It was a pleasure meeting you all, working alongside you in the labs, and getting to know you at social events outside of work.

From the Research Group for Food Allergy, I would like to thank lab technicians Juliane Margrethe Gregersen and Kresten Hermansen for training and help in the laboratory. Sarah Grundt Simonsen for the many(!) hours we spent together in the stables performing animal experiments. Even though it was hard work we had fun together. Jeppe Madura for helping with statistics and the homogenization process in the laboratory. Also thank you to my fellow PhD students Natalia Zofia Maryniak and Tiffany K. S. Sztuk for all the scientific (and sometimes personal) conversations and discussions. Also thank you to the DTU animal facilities, Bio Facility, for taking excellent care of the animals and the great cooperation. A big thank you to all former and present members – it has been a great pleasure working together with you and I made friends along the way.

I would like to thank Professor James Birchall for giving me the opportunity to come abroad to Cardiff University, Wales. I learned many new laboratory techniques and had what felt like a once in a lifetime opportunity to work with fresh human skin samples which was an interesting experience. I would in particular like to thank Emma Baczkowski for guiding me on a daily basis and being ready for any questions that I might have. Benedetta Gualeni for teaching me how to prepare skin samples and getting me started in the laboratory within just a couple of days after arriving. Ahmad Moukachar for helping me work with fluorescence in the laboratory and showing me how to operate the fluorescence microscope and work with the images in ImageJ. I would also like to thank Matthew Ivory for guiding me in working with immunohistochemistry and spending a day with me in the laboratory and being available for any guidance needed the first time working with immunohistochemistry. A very big thank you to the entire research group in Cardiff for making me feel welcome and showing me the ropes at the university and introducing me to Welsh cakes – I am still practicing on making them myself back home in Denmark.



The final thank you is for my whole family for always being supportive. My parents have always tried their very best to guide and help me and laid the foundation for the path I chose to take in life. A thank you to our cat, Albus, for participating in the writing process by sleeping next to the computer where the heat comes out and making sure I always had company. A very special thank you to my husband, Emil Ludvigsen, who not only supported me throughout the entire project, but also endured the everyday lives and everything that entailed while doing a PhD. I am eternally grateful for everything he did (also while doing his own PhD) – from having scientific discussions while watching television shows at home to making sure I ate during periods where time was limited.

## Table of contents

|  |      |
|--|------|
| I) Abstract (English) .....                                      | I    |
| II) Resumé (dansk).....  | II   |
| III) List of abbreviations.....                                  | III  |
| IV) Preface.....   | IV   |
| V) Acknowledgements .....  | V    |
| VI) List of manuscripts and study reports .....                  | VIII |
| VII) My contributions to the manuscripts and study reports ..... | IX   |
| Chapter 1: Motivation.....                                       | 1    |
| Chapter 2: Allergy .....   | 4    |
| Chapter 3: Allergy diagnostics .....                             | 10   |
| Chapter 4: Microneedles.....                                     | 17   |
| Chapter 5: Microneedle coating for intradermal delivery .....    | 29   |
| Chapter 6: Skin models for microneedle testing .....             | 39   |
| Chapter 7: Conclusions and outlook .....                         | 48   |
| Bibliography .....   | 51   |
| Appendix A: Manuscript I .....                                   |      |
| Appendix B: Study report I .....                                 |      |
| Appendix C: Manuscript II .....                                  |      |
| Appendix D: Study report II .....                                |      |

## **VI) List of manuscripts and study reports**

### **Manuscript I**

Dermal Tissue Penetration of In-plane Silicon Microneedles Evaluated in Skin-Simulating Hydrogel, Rat Skin and Pig Skin. Stephanie Ingemann Bisgaard, Long Quang Nguyen, Katrine Lindholm Bøgh, Stephan Sylvest Keller, *submitted to Advanced Healthcare Materials*.

### **Study report I**

Evaluation of In-plane Silicon Microneedle Insertion and Delivery of Compound 48/80 in Porcine and Human Breast Skin Samples. Stephanie Ingemann Bisgaard, Long Quang Nguyen, Mohammad Ramezannezhad, Emma Baczkowski, James Birchall, Katrine Lindholm Bøgh, Stephan Sylvest Keller.

### **Manuscript II**

Peanut allergen Ara h 2 Delivery with In-plane Silicon Microneedles for Test of Allergic Response. Stephanie Ingemann Bisgaard, Long Quang Nguyen, Ana Isabel Sancho, Sarah Grundt Simonsen, Gerardo Garcia Zavaleta, Mohammad Ramezannezhad, Emma Baczkowski, James Birchall, Stephan Sylvest Keller, Katrine Lindholm Bøgh, *manuscript in preparation*.

### **Study report II**

Birch Pollen Extract and Bet v 1 Allergen Delivery with In-plane Silicon Microneedles for Test of Allergic Response. Stephanie Ingemann Bisgaard, Long Quang Nguyen, Sarah Grundt Simonsen, Gerardo García Zavaleta, Mohammad Ramezannezhad, Stephan Sylvest Keller, Katrine Lindholm Bøgh.

## **VII) My contributions to the manuscripts and study reports**

### **Manuscript I**

Planned and executed experiments for testing microneedle penetration and mechanical stability in skin-simulating hydrogels. Performed all data analysis with discussions and guidance from main supervisor, Professor Stephan Sylvest Keller. *Ex vivo* experiments were planned in collaboration with co-supervisor, Senior Researcher Katrine Lindholm Bøgh. Performed all practical work regarding histology cutting and data analysis with guidance and discussions from co-supervisor. Planned and executed experiments with pig ear and performed all data analysis. Wrote the first draft of manuscript I and revised it, by implementing feedback from main and co-supervisor.

### **Study report I**

Planned all experiments in collaboration with Dr. Emma Baczkowski and Professor James Birchall at Cardiff University. Executed all experiments either in collaboration with or supervised by Dr. Emma Baczkowski. Performed all data analysis with discussion and guidance from Dr. Emma Baczkowski and Professor Stephan Sylvest Keller. Wrote the first draft of the study report I and revised it, by implementing feedback from main supervisor and co-supervisor, Senior Researcher Katrine Lindholm Bøgh.

### **Manuscript II**

Planned all animal experiments in collaboration with co-supervisor, Senior Researcher Katrine Lindholm Bøgh and executed all said animal experiments together with laboratory technician, Sarah Grundt Simonsen. Performed all data analysis with discussions and guidance from co-supervisor. Conducted all laboratory work regarding enzyme-linked immunosorbent assays with guidance from laboratory technician, Juliane Gregersen and also developed the homogenization procedure for skin samples with guidance from Senior Researcher, Jeppe Madura Larsen. Wrote the first draft of manuscript II and revised it according to feedback from co-supervisor.

### **Study report II**

Planned all animal experiments in collaboration with co-supervisor, Senior Researcher Katrine Lindholm Bøgh and executed all said animal experiments together with laboratory technician, Sarah Grundt Simonsen. Performed all data analysis with discussions and guidance from co-supervisor. Conducted all laboratory work regarding enzyme-linked immunosorbent assays with guidance from laboratory technician, Juliane Gregersen. Wrote the first draft of study report II and revised it according to feedback from co-supervisor.

# Chapter 1: Motivation

This chapter gives an introduction to the PhD project and the motivation behind it as well as the overall project named the InstaPatch. Aims and objectives are presented and elaborated, and the structure of the thesis is explained.

## 1.1 Allergy and diagnostics

There is an increasing prevalence of allergies worldwide and while some allergies are manageable, others substantially impact quality of life and can even be life-threatening by causing anaphylaxis [1]. The current way of treating allergy symptoms is dependent on the type of allergy, some such as pollen allergies can be treated with antihistamine [2] while for others such as food allergies no treatment currently exists other than avoiding being exposed to the allergens [3], [4].

The current methods for diagnostics are either based on visual interpretation, as is the case for the skin prick test (SPT) and/or assay-based where a blood sample is required [5]. The SPT method is based on the simple idea of eliciting an allergic response in the skin on the forearm of the patient in a controlled manner. Based on the wheal and flare reaction a healthcare professional can make an evaluation and determine whether the patient is likely to be allergic or not [6]. This also means that for an affirmative answer a blood sample is necessary to confirm the presence of antibodies or biomarkers involved in the allergic response.

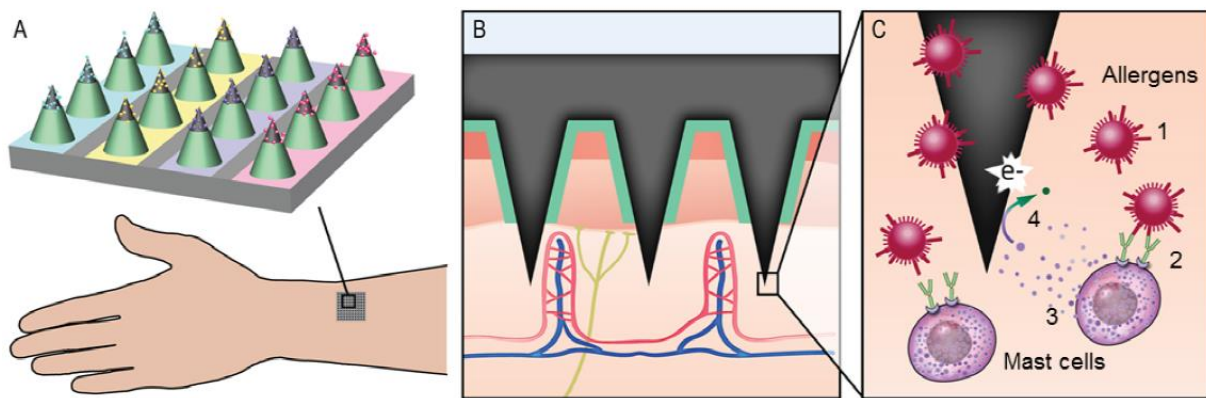
The SPT is a commonly applied method, but it has some drawbacks:

- It is non-quantitative, as it can only confirm a clinical response or suggests an allergic reaction to be tested with an assay [6].
- It can provide false positives, if the SPT needle itself causes some distress in the skin thereby irritating the skin and causing redness [7].
- It can provide false negatives, if the allergen extract dose is too low to cause a visible reaction [5].
- It is invasive, as a standard SPT requires the entire forearm since the testing sites have to be placed  $\geq 2$  cm apart [6].
- It can be considered time-consuming, as a reaction typically takes 15-20 min to arise and become visible [6].
- It requires the presence of a healthcare professional to do a manual readout and evaluate the response [6].

## 1.2 Instantaneous monitoring of allergic reactions in the skin (InstaPatch)

This PhD project is part of the research project, “Instantaneous monitoring of allergic reactions in the skin” (InstaPatch), led by Prof. Stephan Sylvest Keller at The National Centre for Nanofabrication and Characterization (DTU Nanolab). The aim is to develop a novel allergy test using a microneedle (MN) patch, which can perform electrochemical sensing of histamine released from activated mast cells (MCs) due to an allergic response. The basic idea is that the final device should be less invasive, only requiring 1 cm<sup>2</sup> of

the forearm, and perform the measurements faster and more accurately compared to the SPT. Specifically, the device should be able to give a quantitative measurement of each particular allergic reaction and inform the patient about *how* allergic they are rather than providing a yes/no answer. Figure 1.1 illustrates the general idea behind the InstaPatch. It consists of a pyrolytic carbon MN patch, which are inserted into the skin and release allergens. The released allergens stimulate MCs causing them to degranulate and release histamine. The histamine is then measured quantitatively using an electrochemical biosensor with the carbon MNs acting as biocompatible electrodes. The project was performed in collaboration with The National Food Institute (DTU Food) and Gentofte Hospital and was funded by Independent Research Fund Denmark (DFF-FTP).



**Figure 1.1: The conceptualization of the InstaPatch.** A-B) A schematic drawing of the microneedles (MNs) being inserted into an arm. C) Allergens are subsequently released from the MNs thereby activating the mast cells and causing them to degranulate. During degranulation histamine is released and measured electrochemically by the pyrolytic carbon MNs. Kindly provided by Prof. S. S. Keller from the funding application.

The InstaPatch project consisted of two PhD projects, including this one, and a post.doc. position. The first PhD project was carried out by Dr. Sheida Esmail Tehrani on developing the electrochemical biosensor assay while the post.doc. position was undertaken by Dr. Long Quang Nguyen, who worked on the fabrication side by developing the cleanroom fabrication process for the MNs and afterwards provided MNs in different dimensions and shapes for testing. The second PhD project, which is the subject of this thesis, focused on testing the MNs *ex vivo* and *in vivo* for the development of the allergy diagnostic tool.

### 1.3 Aim and objectives of the PhD thesis

The overall aim of this PhD thesis was to contribute to the development of a new allergy test by testing the MNs. This required the implementation of testing methods for skin models and analysis methods for obtaining quantitative results from designed animal experiments.

The main objectives were:

1. Develop an experimental setup and artificial skin model that allowed easy and reproducible testing of the insertion force and mechanical stability of the microfabricated MNs.

2. Confirm the obtained results for insertion force and mechanical stability from the artificial skin model in *ex vivo* skin models for a more realistic outlook.
3. Develop an intradermal (i.d.) delivery system for the allergen to be delivered i.d.
4. Perform *in vivo* animal studies to test the device.

The first research activity was to investigate the penetration force and mechanical stability of MNs with different designs in terms of tip shapes and MN dimensions. This was accomplished using hydrogel skin-simulating models, as well as excised skin samples from Brown Norway (BN) rats and pigs. The tissue damage caused by the MNs was investigated using histology and optical coherence tomography (OCT) of BN rat, pig, and human skin. Allergen delivery was formulated as a coating of the MNs, which was visualized using various, fluorescent-labeled model molecules. As the electrochemistry was not fully functional for *in vivo* testing yet, an alternative method using Evans Blue was utilized as a visualization and quantification tool in the animal studies as it should behave similarly to the wheal and flare in the SPT method.

## **1.4 Structure of the thesis**

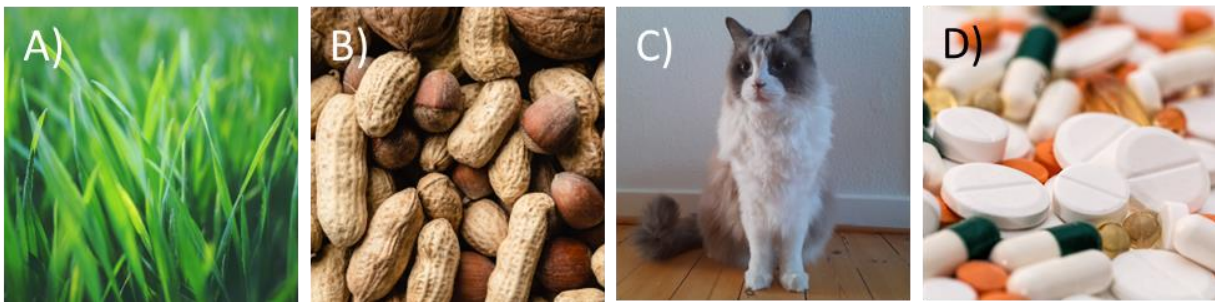
This thesis consists of seven chapters and four research projects resulting in two manuscripts, and two study reports. [Chapter 1](#) introduces the overall InstaPatch project with special emphasis on the parts covered by this PhD project. [Chapter 2](#) provides an introduction to allergy and the immunological mechanisms of how allergy is developed and what happens during an ongoing allergic reaction. [Chapter 3](#) presents a more detailed description of the various diagnostic tools either currently available or under development. [Chapter 4](#) defines the concept of MNs, elaborating on their purposes and designs found in the literature and how their mechanical stability and penetration ability are usually tested. [Chapter 5](#) highlights how MNs can be applied for delivery, looking into typical materials for solutions and the different methods for coating used in the literature. [Chapter 6](#) dives into which models can be used for testing MNs including *ex vivo* skin samples, *in vivo* models, and artificial skin models. An important factor to consider when using artificial skin models is how to validate them, which is also presented in this chapter. Finally, [chapter 7](#) sums up the entire thesis giving an overall conclusion and outlook for the future. Manuscripts I and II and the study reports I and II follow as appendices after chapter 7 and the bibliography list.

## Chapter 2: Allergy

This chapter introduces the main concepts of allergy with focus on type I hypersensitivity. Type I hypersensitivity is immunoglobulin (Ig)E-mediated allergy which is what the InstaPatch will be able to measure. MCs and their role in allergy are presented along with biomarkers for detection of MC degranulation with a focus on the biomarker tryptase.

### 2.1 What is allergy?

The term “allergy” was defined by Clemens von Pirquet in 1906 as the abnormal immune response of some individuals towards certain harmless substances [8]. Allergy is one of the most common chronic diseases, recording a worldwide increase in people who are diagnosed with an allergy [1]. Allergy is an immunological reaction towards in principle harmless allergens such as pollen, food, animal dander, and drugs (examples illustrated in Figure 2.1) and is caused by hypersensitivity of the immune system. This means that the immune system responds to these allergens as if they were a threat instead of exhibiting tolerance as would be normal for harmless allergens [3].



**Figure 2.1: Illustration of potential allergen sources.** A) grass pollen, B) peanut proteins (food allergy), C) animal dander (private picture of Albus), and D) drugs. Picture A, B and D are from Pexels.com.

The umbrella term for diseases associated with allergies is atopic diseases. These include several allergic disorders such as food allergies, atopic dermatitis, allergic rhinitis, and asthma [9], [10]. Atopy is defined as the tendency of patients to become sensitized towards allergens, i.e., develop an allergy towards the allergen [11].

There are two types of allergies, namely the IgE-mediated and non-IgE-mediated. IgE-mediated responses involve the antibody IgE and activation of MCs [12] which is elaborated further in section 2.3. Non-IgE-mediated responses are less understood and involve other components of the immune system such as T cells [13] and IgG antibodies [14]. Many of the effects associated with an IgE-mediated response are similar to those expected with enteric helminths or ectoparasites. It is believed that the increased living standards in the Western world with less exposure to such parasitic attacks makes the immune system respond in the same manner to harmless substances. This observation is the basis of the hygiene hypothesis [3], [15], [16].



## 2.2 The prevalence of allergy

According to the World Allergy Organization (WAO) white book from 2013 there has been a global prevalent increase in allergic diseases which includes asthma, rhinitis (irritation of eye, nose and throat mucus membranes), drug allergy, food allergy, eczema, urticaria (skin rash), and anaphylaxis (severe allergic reaction which can be life-threatening) [5]. Approx. 10-30% of the population in Western countries are affected by allergic diseases and in Europe approx. 11-26 million people are suffering from some kind of food allergy [5].

During the last three decades there has been a worldwide increase to 3.5-8% of children having food allergies [17], and it has been demonstrated that having an atopic disease can make a person inclined to developing another atopic disease [18]. Food allergy has been suggested to lead to the development of asthma, which is one of the most common allergies for children where approximately 9% of all children are affected [19]. Furthermore, climate changes have been suggested to also impact allergic disease by e.g., increasing the concentration of air pollutants and pollen, extending the pollen seasons, and increasing mold growth in damped houses due to flooding from tropical cyclones [20]. In short, allergy is a global burden and a health issue that must be addressed [5].

## 2.3 Type I hypersensitivity sensitization and response

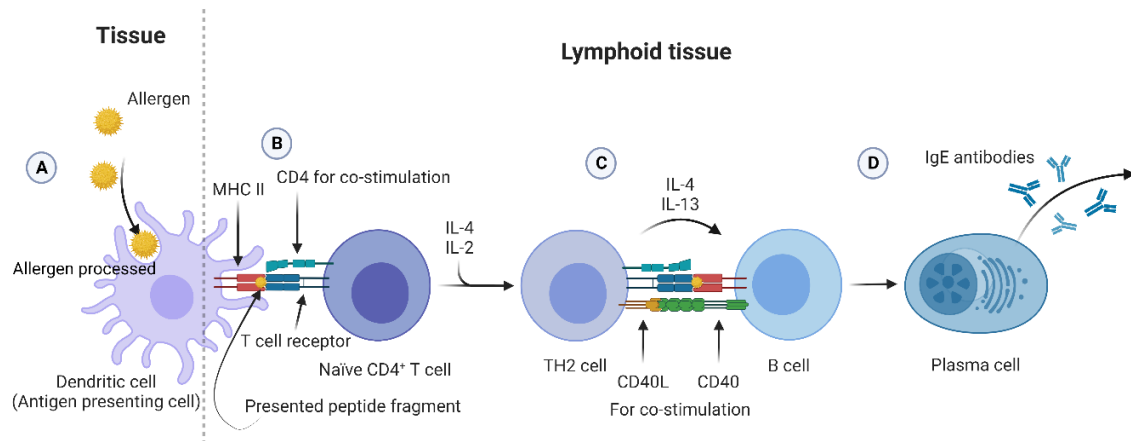
Four hypersensitivity reactions were classified by Gell and Coombs based on the immunological response [21], [22]:

- Type I hypersensitivity reactions are immediate allergic reactions mediated through IgE antibodies.
- Type II hypersensitivity reactions are cytotoxic or IgG/IgM responses.
- Type III hypersensitivity reactions are driven by IgG/IgM immune complexes.
- Type IV hypersensitivity reactions are driven by T cell responses.

In the context of this PhD, the most relevant response is type I, which will be discussed in further details. Type I hypersensitivity can be divided into two steps of i) exposure to an allergen which causes sensitization and ii) re-exposure to the same or similar (cross-reactive [23]) allergen causing an allergic reaction in the sensitized individual [3]. An allergen is a substance that is capable of inducing sensitization and causing an allergic reaction [24]. Allergens are most often proteins [3] which can be proteases that are capable of reducing the epithelial barrier function for easier intrusion [25]. However, not all allergens are proteins as some of them can also be lipids [26] or carbohydrates [27].

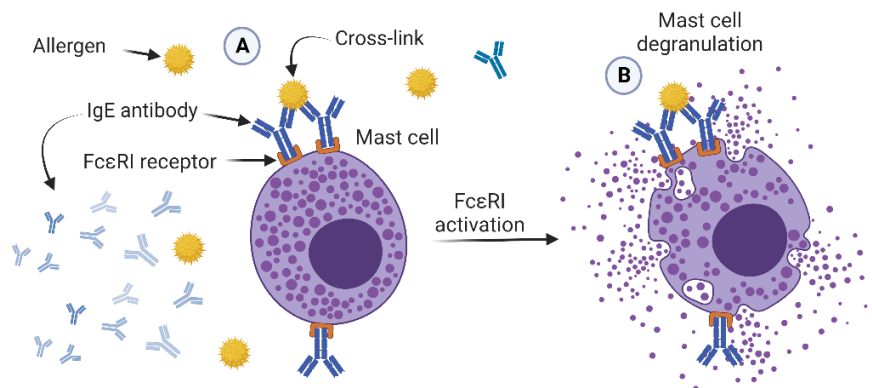
Sensitization is the process where an individual becomes allergic towards a harmless substance. The immune system encounters an allergen, e.g., grass pollen, which is in principle harmless, but is perceived by the immune system as being harmful [3], [4]. The allergen is collected by dendritic cells, B cells or macrophages that are antigen-presenting cells (APCs). The APCs engulf the allergen, and the collected allergen is carried by the APC to lymphoid tissue. Here, the engulfed allergen is processed within the cell and broken down into peptide fragments which can be presented on the cell surface [28], [29]. The peptide fragments are presented on the major histocompatibility complex (MHC) II of the cell surface to

naïve CD4<sup>+</sup> T cells for activation and differentiation of the T cell to a T helper 2 (TH2) cell by secretion of interleukin (IL)-4 and IL-2 [30]. When the TH2 cell encounters a B cell presenting a peptide fragment from the same allergen the TH2 cell secretes IL-4 and IL-13 [31] differentiating the B cell into a plasma cell and causing class-switching of the B cell [32]. This means that the B cell changes from producing only IgM and IgD antibodies to producing allergen-specific IgE antibodies which are secreted by the plasma cell [33], [34]. This process is illustrated in Figure 2.2. The produced IgE antibodies are released into the lymphatic vessels and are distributed throughout the blood circulation [35], [36].



**Figure 2.2: Allergic sensitization.** A) The allergen is collected by an antigen-presenting cell (APC) (e.g., a dendritic cell) where the allergen is processed into peptide fragments and B) these are presented on the major histocompatibility complex (MHC) II on the cell surface. MHC II can interact with naïve CD4<sup>+</sup> T cells, activating these and differentiating them to T helper 2 (TH2) cells. C) The TH2 cell activates a B cell carrying the same or similar allergen-peptide fragment and promotes this to become a D) plasma cell for allergen-specific IgE antibody production. Created with BioRender.com.

When the person is later re-exposed to the allergen a reaction is initiated where MCs are activated [3]. MCs have FcεRI receptors on their surface which bind the allergen-specific IgE antibodies [37]. When these antibodies cross-link an allergen by bivalent or multivalent binding while bound to the FcεRI receptor the MC is activated and degranulates as illustrated in Figure 2.3 [3], [38]. During degranulation two classes of inflammatory mediators are released: Mediators stored in cytoplasmic granules and newly synthesized mediators. These mediators cause vasodilation which is the widening of blood vessels, bronchoconstriction where the airways are narrowed, and endothelial retraction which makes the vessels leak and creates edema [3]. Released mediators are further elaborated in section 2.4 and 2.5. Continuous re-exposure to a certain allergen will lead to an increased production of the specific IgE antibodies [39]. These IgE-mediated responses usually happen within minutes of the re-exposure [3].



**Figure 2.3: Mast cell activation and degranulation.** A) IgE antibodies bind to the FcεRI receptor on mast cells (MCs) and cross-link with allergens causing the MC to B) degranulate and release the inflammatory mediators. Created with BioRender.com.

## 2.4 Mast cells

MCs were first discovered by Paul Ehrlich and contain the FcεRI receptor which has a strong affinity for IgE binding [38]. They are involved in the TH2 and IgE-mediated response where the MC undergoes activation dependent on IgE and FcεRI binding [40]. Upon activation several mediators are released for inflammatory responses [41].

The organelles of a MC are prone to exocytosis and extracellular release of the mediators. This release can be induced by chemicals [42], endogenous mediators [38] or immune mechanisms that may be IgE dependent or independent [43], [44]. Upon allergen cross-linking the IgE triggers an increase of Ca<sup>2+</sup> influx which increases the Ca<sup>2+</sup> content in the cytoplasm and promotes the degranulation [45]. The released lipid mediators and cytokines along with preformed histamine have an important effect on the vascular endothelium. They alter the permeability and adhesiveness allowing circulating inflammatory cells to adhere to the endothelium and migrate to the surrounding tissue [38].

The released mediators from MCs can be divided into pre-formed mediators and mediators formed upon activation. The pre-formed mediators include histamine, heparin, tryptase, chymase, cathepsin, and carboxypeptidase. The mediators formed and released upon activation include several cytokines, chemokines, prostaglandins, leukotrienes, and free radicals [40], [46]. The released mediators from MCs can contribute to the damage caused during an allergic reaction. Histamine, leukotrienes, and prostaglandins are involved in recruitment of eosinophils and increase the vascular permeability [47]. Several released cytokines affect other immune cells such as causing class switching in B cells to produce IgE antibodies [32], inducing histamine release in basophils [47], recruiting neutrophils [47], and further promoting a TH2 cell response [48], thus, enhancing the allergic reaction. MCs have been found to be present in mucosal sites and in the skin [49] with the highest concentration in the upper dermis layer just below the dermis-epidermis junction [50]. They are often located around blood vessels, nerves and appendages and are not found in the epidermis in normal skin [3].

Janssens *et al.* examined the MC distribution in normal adult skin, and it ascertained to be 108 MCs/mm<sup>2</sup> for distal body parts such as the forearm and lower legs and 77 MC/mm<sup>2</sup> for proximal body parts such as trunk and upper arm and leg. The forearm was included under the distal body parts and made up for 101 MC/mm<sup>2</sup>. Together with the lower leg (113 MC/mm<sup>2</sup>), it was one of the two sites with the highest density of MCs [50]. According to Weber *et al.* it was observed that the highest amount of MC/mm<sup>2</sup> was in various parts of the head such as the back of the head, chin, nose, and cheek. The second highest location was hand and foot with the third highest location being the upper and lower arm and leg. The lower arm was found to contain 64 MC/mm<sup>2</sup> in the upper skin layers [51]. A higher presence of MCs can be correlated to a higher probability and larger impact of an allergic reaction.

## 2.5 Biomarkers for detection of mast cell degranulation

Several biomarkers can be targeted to confirm the activation and degranulation of MCs. These biomarkers can be surface-bound, or they can be released mediators. The best surface-bound biomarkers for detection of activated MCs are cluster of differentiation (CD)63 or CD203 as these are expressed on the cell surface upon activation. Because CD63 is one of the surface-bound biomarkers associated with most allergies, this biomarker seems promising [52], [53].

As mentioned above, there are two main types of mediators released from degranulating MCs, preformed mediators (e.g., histamine, proteoglycans,  $\beta$ -hexosaminidase, and neutral peptides) and newly synthesized mediators (e.g., leukotrienes, prostaglandins, cytokines, TNF, and ILs) [46], [54].

Preformed mediators are made up of histamine, heparin, and tryptase [55]–[57]. Histamine has a quick release within 5 min [58], [59] with a half-life of 10–30 min [46], [60] whereas tryptase has a slow release which peaks after 15–120 min with a half-life of 1.5–2.5 hours [61]. Tryptase has a consistent baseline level of 1–11 ng/mL [46], [62]. Heparin levels do not increase enough after an allergic response to be a viable biomarker [46], [63]. The function of  $\beta$ -hexosaminidase in MCs is not fully known, but research suggests that it is involved in the defense against bacterial infection [64].

Newly synthesized mediators are released more slowly than preformed mediators [3], [56] and these are made up of lipid mediators, chymase, carboxypeptidase A, cytokine, and chemokines [65], [66]. Lipid mediators are released shortly after activation as part of the immediate response [46], but these are also released by other immune cells and thus, not specific for MCs [54]. Chymase is a serine protease involved in vasculature inflammatory responses, however, an immunoassay is not currently available for MC chymase detection [46]. Carboxypeptidase A levels are elevated for longer time than tryptase [46] and cytokine and chemokine release may be determined based on the type of stimuli for MC activation [40], [67]. The most investigated biomarkers for MC degranulation are histamine [68], tryptase [69] or  $\beta$ -hexosaminidase [70]. For the purpose of this project it was decided to focus on tryptase as this biomarker frequently appeared in the literature as one of the main MC specific biomarkers with a long half-life for detection [61], [71].

Tryptase is one of the main mediators released upon degranulation and is a protein that is premade and stored in the granules for release [46], [72]. There are two types of MCs: 1) MCs that contain only tryptase and are found in alveolar walls and the small intestine and 2) MCs that contain both tryptase and chymase

and are found in the dermis of the skin, the intestinal mucosa and blood vessels [61]. There are four isoforms of tryptase with two of them considered biologically relevant, namely the  $\alpha$  and  $\beta$  forms.  $\alpha$ -tryptase is secreted continuously by the resting MCs as an inactive proenzyme [61] which makes up the baseline serum level of 1-11 ng/mL [46], [62].  $\beta$ -tryptase is released upon MC activation and levels peak after 15-120 min and has a half-life of 1.5-2.5 hours [61]. For comparison, histamine peaks after 5 min with a half-life of 10-30 min [58], [60].

In the case of our InstaPatch the target biomarker would depend on its availability. Tryptase may be a more practical biomarker for measurements since it has a longer half-life [71] and is available for detection for a longer period. On the other hand, histamine concentrations peak fast after 5 minutes [58] and can be detected earlier compared to  $\beta$ -tryptase which diffuses more slowly and has a peak-release after 15-120 minutes [61]. However, tryptase has the advantage of being measurable for several hours afterwards unlike histamine [61].

## **2.6 Summary**

This chapter introduced the basic concepts of immunology in relation to allergy sensitization and allergic reactions. MCs were presented as their activation and degranulation is one of the central aspects of an allergic reaction. MC biomarkers for degranulation were introduced with a special focus on tryptase since this biomarker was investigated for *in vivo* animal experiments conducted during this thesis.

## Chapter 3: Allergy diagnostics

This chapter introduces different methods for allergy diagnostics. Diagnostics often begin with looking at the medical history of the patient and performing a physical examination [73]. After this, further investigations can be conducted such as *in vivo* skin tests and *in vitro* assays. The presented diagnostic tools represent state-of-the-art and lay the foundation for how the InstaPatch will improve allergy diagnostics.

### 3.1 *In vivo* skin tests

Skin tests are some of the easiest tests to confirm a clinical response to allergens as they are simple, convenient, reproducible, easy, and low cost to perform. However, it requires training and experience to conduct the test, interpret the outcome, and correlate it with the medical history of the patient. Skin tests should furthermore always be performed in a clinic where professionals are available for assisting in case of a systemic reaction [5].

A well-established method for screening allergies in the clinic today is the SPT. The first *in vivo* test was described by Dr. Charles Blackley in 1867 [74] with Schick and Cooke suggesting an intracutaneous test shortly after [75]. The first SPT was done by Sir Thomas Lewis in 1924 [7], [76] and the basics of the SPT method as it is known today were introduced in the 1950s [77].

The SPT is normally done on the volar area (underside) of a patient's forearm or on the upper back [5], [6] with a sterile metal SPT needle that is 1 mm long and applied perpendicularly to the skin surface [78]. The SPT method can provide evidence of sensitization and detect type I hypersensitivities [6]. However, positive SPTs are not conclusive, but require further examination and are dependent on the degree of sensitivity, number of MCs present, and the potency of the allergen extract [5]. The SPT method is performed by placing a droplet of an allergen extract on the skin of the forearm, which afterwards is punctured through the skin using the SPT needle. Ideally, if the patient is allergic towards the allergen used, then the allergen extract will induce a local allergic response in the form of inflammation that will be visible as a wheal and flare. The induced inflammatory response of the skin is normally visible within 15-20 min after which a healthcare professional evaluates it by a manual readout [6], [79]. A positive control of histamine dihydrochloride is always incorporated for comparison as this should always elicit a visible response. Moreover, a negative control of saline solution is included to give an indication of the skin trauma caused by simply pricking which might result in false positives. This can help identify false positives in the test [7]. A SPT is shown in Figure 3.1.

The evaluation is often based on the diameter of the wheal (the swollen area) and flare (redness) area where a wheal of  $\geq 3$  mm in diameter is considered positive [6], [80]. Based on Bodtger *et al.* where birch pollen was used as a model allergen, the SPT method was reproducible when comparing results over a longer period of time [81]. The needle used for the SPT has undergone optimization in order to standardize the method [82]. Further optimization of the SPT was conducted in 1998 by Nelson *et al.* [83] and also in 2005 by Carr *et al.* [84] who investigated multi-headed devices for efficient testing.

Several methods such as 2D/3D scanners [85], blood flow analysis [86], skin impedance measurements [87], thermography [88], and photography [89] have been investigated for automating the readout process of the SPT method in an attempt to standardize the method further. However, many of these advances exhibit poor precision and require expensive equipment. These methods are furthermore unable to perform the measurements simultaneously with the pricking, but have to wait for the visual allergic response to develop [77].



**Figure 3.1: Example of a skin prick test in progress.** A skin prick test (SPT) is performed by placing a droplet of allergen extract on the skin of the forearm and pricking it into the skin using a SPT needle. The SPT requires the use of the entire forearm for testing. Picture of own arm from trying the SPT method, photo by Prof. S. S. Keller.

In continuation of the SPT test, there are several variations of this method such as the scratch test where the basic principle remains the same. However, the sample is scratched into the skin rather than pricked, but without causing bleeding [90]. This may not always be a better option as the scratch test is more difficult to standardize for inhalant and food allergies [6]. An i.d. injection test has also been used and still is in some countries today. It comprises of injecting a sample of an allergen into the skin with a hypodermic needle and waiting 15 min for a response. Nonetheless, this method is often more painful than the SPT method and associated with higher risks of adverse effects [91], [92].

For food allergies, the prick-to-prick method can be used where the allergen is fresh from the source and has not been processed into an extract. In this case the SPT needle is first pricked into the fresh food and afterwards pricked into the skin. This method can be beneficial when investigating allergens that are difficult to process into extracts such as fruits and vegetables [93], [94].

The SPT method usually provides results within 15-20 min whereas *in vitro* measurements require longer time for analysis [6]. Nonetheless, the SPT method is not always the optimal way of diagnosing allergies for all patients. If the patient has extensive eczema, urticaria which is a skin rash or is taking medication like antihistamines, the results will not be reliable, and the diagnostic method is not applicable anymore.

In such instances it is much more reliable to use *in vitro* methods such as the basophil activation test (BAT), Component-resolved diagnosis (CRD) or measure the level of histamine as described later in following sections 3.3-3.7. These methods are more time-consuming than the SPT and require collection and handling of samples. *In vitro* methods can also be used to complement the interpretation of the SPT results [6].

### **3.2 Provocation test**

For some allergens the allergy is best confirmed using a provocation test where the allergen is inhaled or ingested [5]. Here, the double-blind placebo-controlled food challenge is the golden standard for diagnosing food allergies [95], [96]. It is important that this test is only performed by a trained professional who knows how to interpret symptoms and potentially provide treatment in case of adverse effects [5]. Patch tests containing suspected allergens can be used for patients where contact dermatitis is suspected [97], [98].

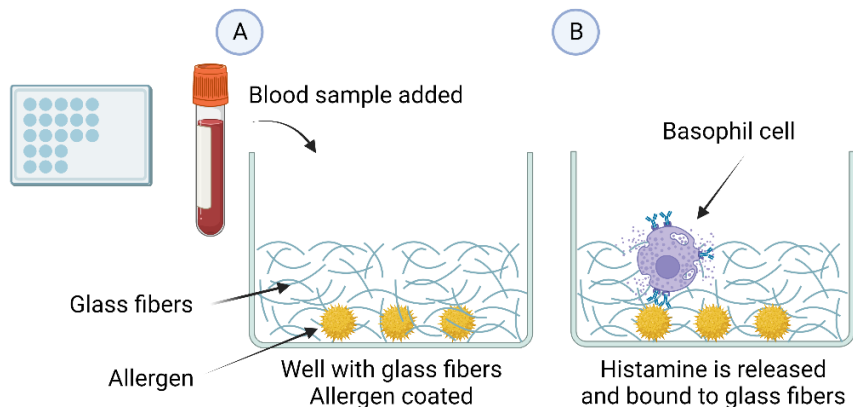
### **3.3 Histamine release test**

As mentioned above, the SPT is not always conclusive. Therefore, *in vitro* tests can provide additional results to determine a diagnosis. For the *in vitro* method of the histamine release test, the released histamine from basophils is quantified [99]. Basophil cells are like MCs capable of binding IgE and are activated once IgE antibodies crosslink with an allergen. This results in degranulation and release of mediators similar to MCs including histamine [3].

For a histamine release test, a blood sample is collected and analyzed using glass-fiber coated microtiter plates for passive separation of histamine from other components [100]. Blood samples should be analyzed within 24 hours as basophil reactivity decreases with time [101]. As illustrated in Figure 3.2A wells with glass fibers are coated with the specific allergen and a blood sample is added. In Figure 3.2B allergen-specific IgE antibodies which are surface-bound to basophils can bind to the allergen and activate these basophils. Histamine is thereby released and adsorbed on the glass fibers after which the wells are washed for removal of other components [78], [102]. The histamine collected on the glass fibers can be resuspended into the solution by a change in pH. It is then quantified by coupling to a fluorophore or radioactive isotope and comparing to a standard curve [103], [104].

A similar, but different option known as “passive sensitization” [105], [106] is to use blood obtained from non-sensitized individuals, removing IgE antibodies bound to their basophils and incubating these serum samples with allergen-specific IgE antibodies from the blood sample of the sensitized patient. This has the advantage that serum samples can be used instead of whole blood samples which makes it possible to perform the assay after the 24 hours [104]. Then the histamine release is quantified in the same manner as before, using a fluorescence- or radioimmunoassay.



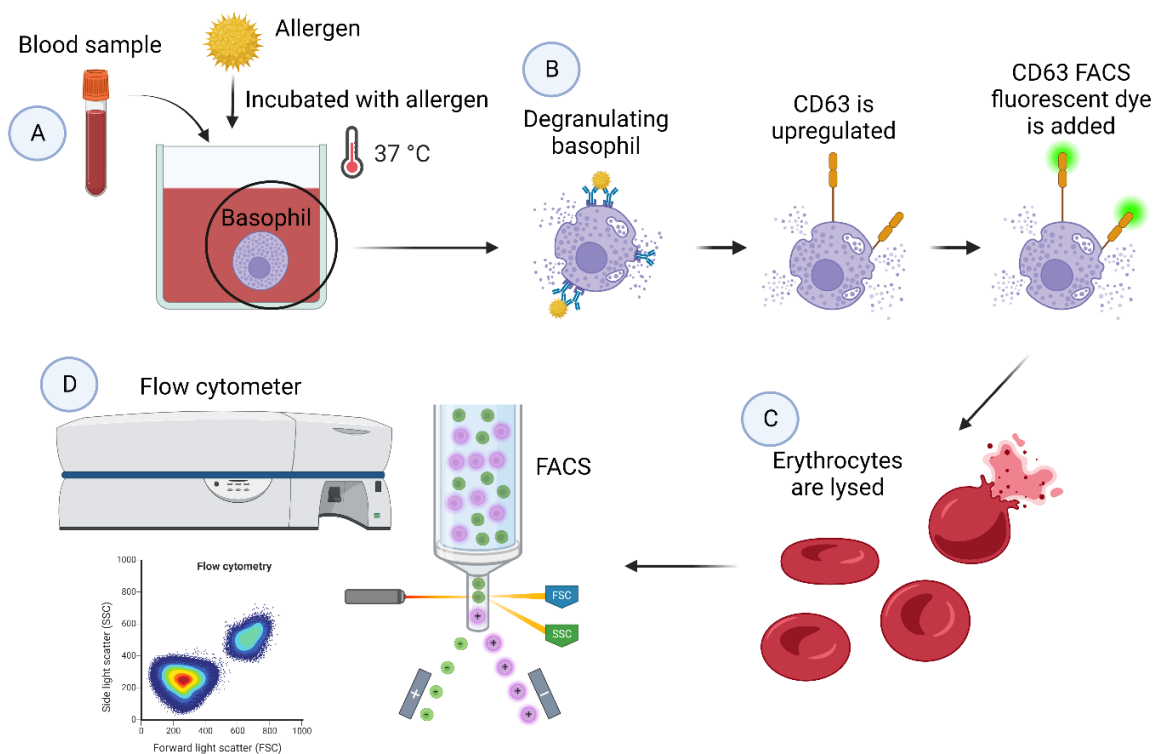


**Figure 3.2: Illustration of histamine release test.** A) Wells with glass fibers are coated with the specific allergen and a blood sample is added. B) The IgE antibodies can then bind to the allergen and activate basophils in the sample, which release histamine. The histamine is adsorbed on the glass fibers but can be released again by changing the pH and coupling the histamine to either a fluorophore or a radioactive isotope for quantification. Created with BioRender.com.

### 3.4 Basophil activation test

BAT is an *in vitro* assay that analyzes cell activation after allergen exposure in a flow cytometry setup. Biomarkers for basophil activation are CD63 and CD203c, which are surface markers that become available on sensitized basophil cells after activation [107].

As illustrated in Figure 3.3A A blood sample is collected and stimulated by incubation with an allergen at 37 °C to activate basophils. Erythrocytes are then lysed and the CD63 is labeled using e.g., phycoerythrin (PE) which is a fluorescent dye meant for fluorescence-activated single cell sorting (FACS) (Figure 3.3B-C). Using FACS which is a flow cytometry technique the sample is measured before and after stimulating with an allergen to see if the incubation with the allergen caused a significant upregulation of the basophil surface marker [108], [109] (Figure 3.3D). Based on previous studies, it was determined that the BAT should be performed within a few hours after collection of the blood sample (up to 24 hours) to ensure viability of the basophil cells [101]. Several candidates have been investigated as biomarkers for activation, in particular CD123 and CCR3 [110], but most BAT use CD63 or CD203c [111], which have been validated as acceptable markers [107]. The BAT has been shown to be particularly good for diagnosing IgE-mediated hypersensitivities, but also has the drawback that some patients have non-responding basophils thereby rendering the results inconclusive [107].



**Figure 3.3: Illustration of basophil activation test.** A) A blood sample is collected and incubated at 37°C together with an allergen. B) Basophil cells are activated and degranulated which causes an upregulation of a surface marker e.g., CD63. Flow cytometry fluorescent dye that targets CD63 is added. C) Erythrocytes (blood cells) are lysed in the blood sample. D) Flow cytometry is used to quantify the number of basophils with upregulated surface markers via fluorescence-activated cell sorting (FACS). Created with BioRender.com.

### 3.5 Mast cell activation test

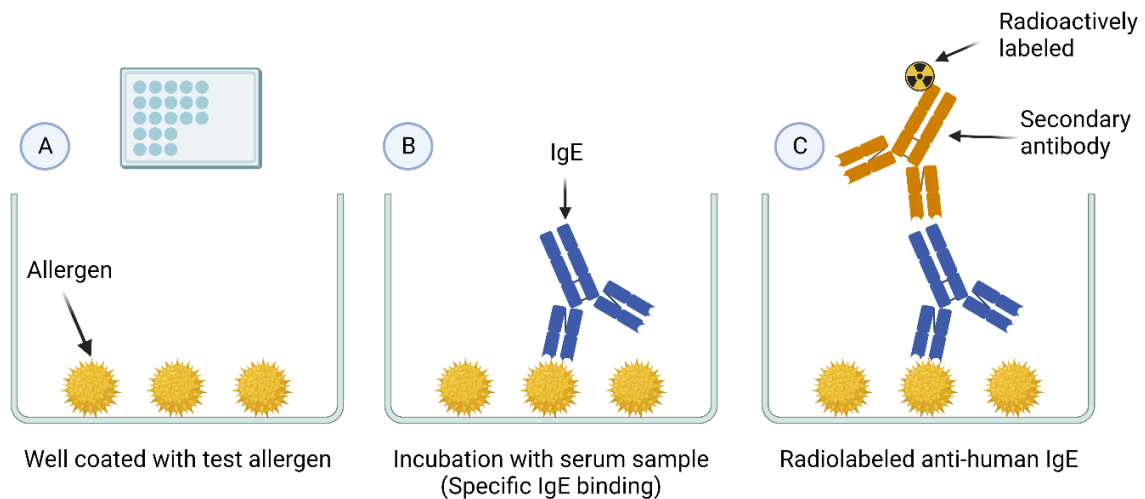
The MAT is also an *in vitro* assay similar to the above-mentioned BAT. However, instead of using a fresh blood sample it can use plasma or serum for sensitization of MCs [112], [113]. The MCs can either be obtained from the peripheral blood or tissue of the patient [114] or healthy donors [115].

The MAT is performed similarly to the BAT in the sense that the MCs are sensitized by adding the sera of the patient and sensitized MCs are activated by adding an allergen [115], [116]. Activated MCs exhibit upregulated surface markers which can be labeled using a specific fluorescent-labeled monoclonal antibody for flow cytometry analysis [117]. These surface markers are often CD63 [118], CD107a [115] or CD203c [119]. The released mediators during degranulation such as histamine [120] and chemokines [121] may also be measured using fluorescent labeling and flow cytometry.

Since flow cytometry is required for the MAT it is currently not a tool suitable for screening, but it can be used as a complementary test to the SPT or measurement of allergen-specific IgE [112].

### 3.6 Radioallergosorbant allergen test

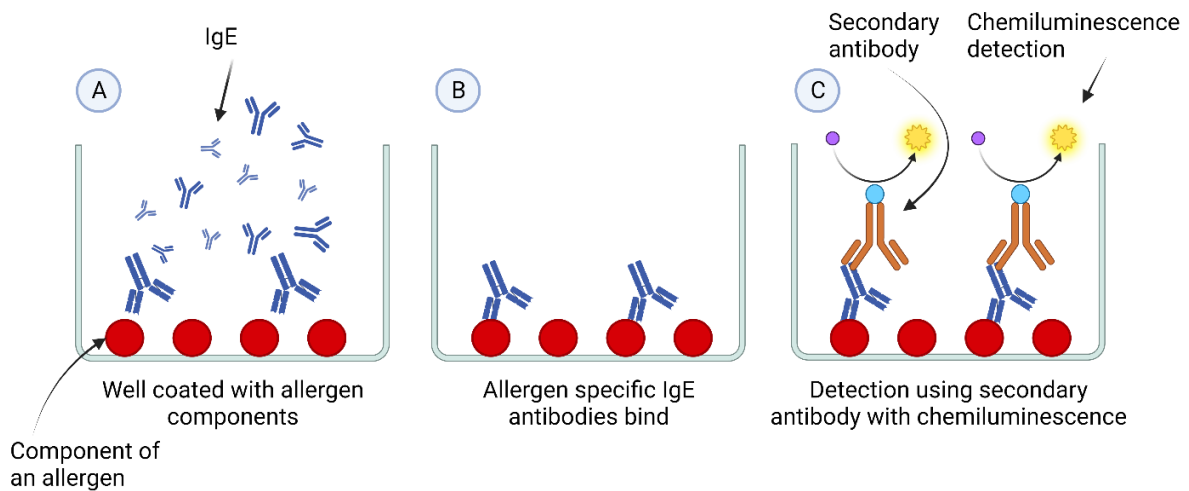
Another *in vitro* test is the radioallergosorbant allergen test (RAST) where a radiolabeled anti-IgE is used to build an immunoassay [103]. RAST detects specific IgE antibodies to determine which allergen the patient is sensitized towards [122]. As illustrated in Figure 3.4A the surface of the microtiter plate well is coated with the specific allergen and the sample serum is added to bind allergen-specific IgE (Figure 3.4B). As illustrated in Figure 3.4C a secondary radiolabeled antibody is added and binds specifically to IgE antibodies. The radioactivity can then be assessed and quantified using a standard curve [90], [103].



**Figure 3.4: Illustration of the radioallergosorbant allergen test.** A) The well is coated with the specific allergen and sample serum is added. B) Allergen-specific IgE antibodies will bind and C) a secondary antibody that is radiolabeled is added. The secondary antibody binds IgE specifically and is measurable afterwards using a radioactive label and quantifiable against a standard curve. Created with BioRender.com.

### 3.7 Component-resolved diagnosis

CRD is a method where purified allergens are used to detect IgE antibodies in blood samples. CRD was developed to improve the sensitivity of IgE diagnostic methods as it can discriminate between sensitization towards the specific allergen and cross-reactivity against other allergens [123], [124]. As illustrated in Figure 3.5A CRD is performed by using a microarray-based diagnostic solution where wells are coated with allergen components and a serum sample is added. As illustrated in Figure 3.5B allergen-specific IgE antibodies will bind and a secondary antibody with chemiluminescence is added for detection (Figure 3.5C). This can provide a more in-depth understanding of sensitization patterns in patients who suffer from several allergies as different components of the allergen can be examined. This diagnostic method has an increased specificity compared to the SPT, but less sensitivity [125], [126].



**Figure 3.5: Illustration of the component-resolved diagnosis.** A) The well is coated with the specific allergen component, and a serum sample is added. B) Allergen component specific IgE antibodies bind, and C) a secondary antibody is added which binds to the IgE antibodies. Chemiluminescence is used for detection and quantification. Created with BioRender.com.

### 3.8 Summary

This chapter introduced the current methods used for allergy diagnostics. Several methods exist and each has its advantages and disadvantages. The most popular tests remain the *in vivo* tests as they are easy, quick, and cheap to perform. However, the SPT has drawbacks, which we aim to address with the InstaPatch. By using MNs for the InstaPatch the testing area will be limited and the MNs can be fabricated for electrochemical measurements reducing the testing time while also giving a quantitative result.

## Chapter 4: Microneedles

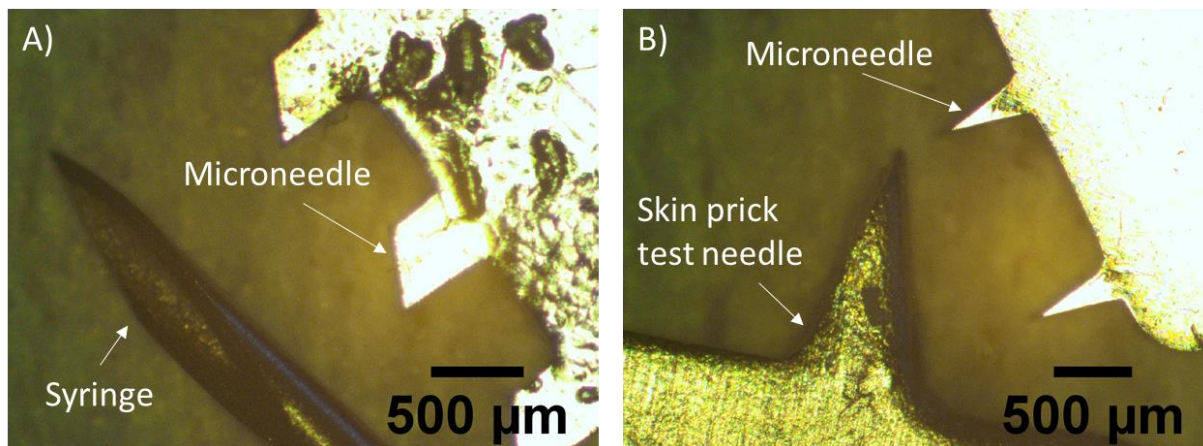
This chapter introduces the concept of MNs and how they are tested both in terms of their mechanical stability, but also their penetration ability in skin tissue. A literature study was performed on the most frequent used shapes and dimensions and the main findings are presented here. MNs with a variety of shapes and sizes have been developed depending on their purpose. Recently, MNs have also become part of allergy research in aspects of diagnostics and inducing desensitization. The chapter provides background information for research presented in manuscript I [127] and study report I [128].

### 4.1 Microneedles and their applications

The idea of fabricating MNs for skin penetration and transdermal drug delivery was introduced during the 1990's where Henry *et al.* was one of the first to report transdermal delivery using microfabricated MNs [129]. Patches of solid MNs have been investigated for delivery of desmopressin (medicine) [130], both hollow [131] and porous [132] MNs have been investigated for vaccine delivery, and controlled release of lidocaine (local anesthetic) was achieved using coated, solid polymer MNs [133]. Furthermore, Sullivan *et al.* reported on how dissolving MNs could deliver influenza vaccine to a targeted location in the skin to reach APCs for eliciting an immune response [134]. MNs have also been optimized for many different applications other than the original idea of drug delivery [135]. They have been used for extraction of samples such as interstitial fluid (ISF) [136], performing electrical measurements [137], medical diagnosis [138], and as transdermal sensors [139]. As an example, Parrilla *et al.* developed a MN-based sensor where the MNs were used as electrodes for electrochemical detection of potassium in the dermis [140]. Other examples of MNs being used as electrochemical biosensors are for monitoring uric acid and dopamine [141], glutamate [142], and glucose [143]. Lastly, MNs have started to appear within allergy research for immunotherapy and diagnostics [144], [145].

### 4.2 What are microneedles?

MNs are defined as small structures with sub-mm size that act like needles and are used to pierce an object or a body part, typically the skin [135]. Often the main purpose is delivery of a molecule, which is not in itself able to pass through the stratum corneum of the skin barrier. The MNs are capable of piercing the skin disrupting it temporarily depending on the length of the MN [146]. The most important parameters for MNs are their penetration ability and mechanical stability. MNs should be able to penetrate the epidermis and reach the dermis skin layer [147]. Furthermore, the design of the MNs (i.e., shape and dimensions) should ensure mechanical stability as the flexibility of the skin may impact the required penetration force. If the penetration force exceeds the force that the material can withstand, the MNs may break [132]. The main advantage of MNs compared to hypodermic needles is that they can be less invasive, provide a less painful insertion, and the penetration depth can be more controlled if the aim is to reach the dermis and not the blood veins [132], [148]. Figure 4.1 shows the MNs fabricated for this PhD in comparison with a 27G syringe and the SPT needle used for allergy testing in the clinic today.



**Figure 4.1: Microneedle comparison with syringe needle and skin prick test needle.** Optical microscope images for comparison between A) a 27G syringe and a hypodermic shaped microneedle (MN) (500  $\mu\text{m}$  length and 400  $\mu\text{m}$  width), and B) the skin prick test needle used in the clinic and a triangular shaped MN (500  $\mu\text{m}$  length and 200  $\mu\text{m}$  width).

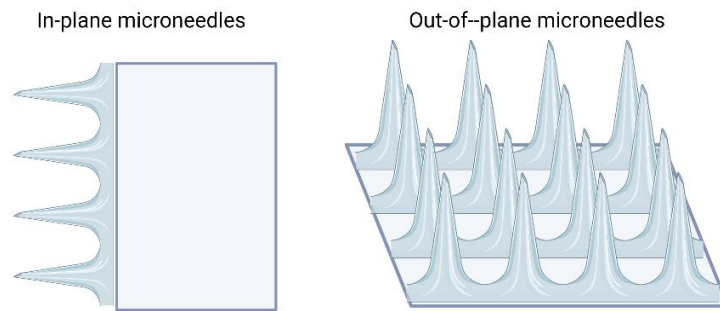
### 4.3 Microneedle materials

MNs can be processed from a variety of materials including silicon [149], metals [150], ceramics [151], silica glass [152], carbohydrates [153], and polymers [154]. Silicon has a crystalline structure and allows MNs to be produced in many shapes and sizes and makes batch production possible [155]. Nonetheless, cleanroom processing of silicon is expensive, can be time-consuming, and the produced MNs can be fragile and break [156], [157]. Silicon does, however, have the advantage of being biocompatible [158], [159]. Stainless steel and titanium alloys have been used for making MNs and have the advantages of good mechanical properties and biocompatibility [160]. Ceramic MNs are mainly used due to their excellent chemical resistance [132] and silica glass can be brittle and usually these MNs are made by hand, making the process time-consuming [146]. Carbohydrates, usually maltose, may also be used for making MNs. These MNs are often made using a template and a potential molecule for delivery is directly mixed into the carbohydrate solution, which is optimal for a controlled drug release [161]. Furthermore, many different types of polymers are used as MNs, often for dissolving or biodegradable MNs [162], [163]. MNs made from polymer are often fabricated using an inverse mold made from e.g., silicon [164]. In this PhD thesis silicon was selected as the MN material due to its biocompatibility and that the cleanroom processing allows for process control and obtaining small structures. Lastly, silicon MNs can be coated with a polymer, which can in turn be converted to carbon via pyrolysis. The pyrolytic carbon is an excellent electrode material for electrochemistry [165].

### 4.4 Microneedle configurations

MNs can be fabricated in two configurations, namely in-plane where MNs are fabricated in parallel to the surface of the material [166] and out-of-plane where MNs are fabricated orthogonally to the surface [130] (Figure 4.2). For out-of-plane MNs fabricated using silicon wafers, the achievable MN height will be limited by the thickness of the silicon wafer, as the MNs are “carved” from the wafer by removing the surrounding

material, e.g., via etching. Furthermore, it is a challenge to fabricate out-of-plane MNs with a high aspect ratio in silicon [167]. For out-of-plane MNs made by e.g., cutting into stainless steel sheets there is a higher level of flexibility for the dimensions and aspect ratio [168]. Silicon micromachining allows for fabrication of longer in-plane Silicon MNs compared to out-of-plane, as the MN shapes are etched into the wafer based on a predefined design [166]. In order to avoid the “bed of nails” effects for out-of-plane MNs [169], the density and interspacing of the MNs should always be optimized. Otherwise the MNs may not penetrate the skin as desired and will not be able to perform their application [170]–[172]. In this PhD thesis, the in-plane MN configuration was selected because of a straightforward microfabrication of in-plane silicon MN and a high design flexibility.

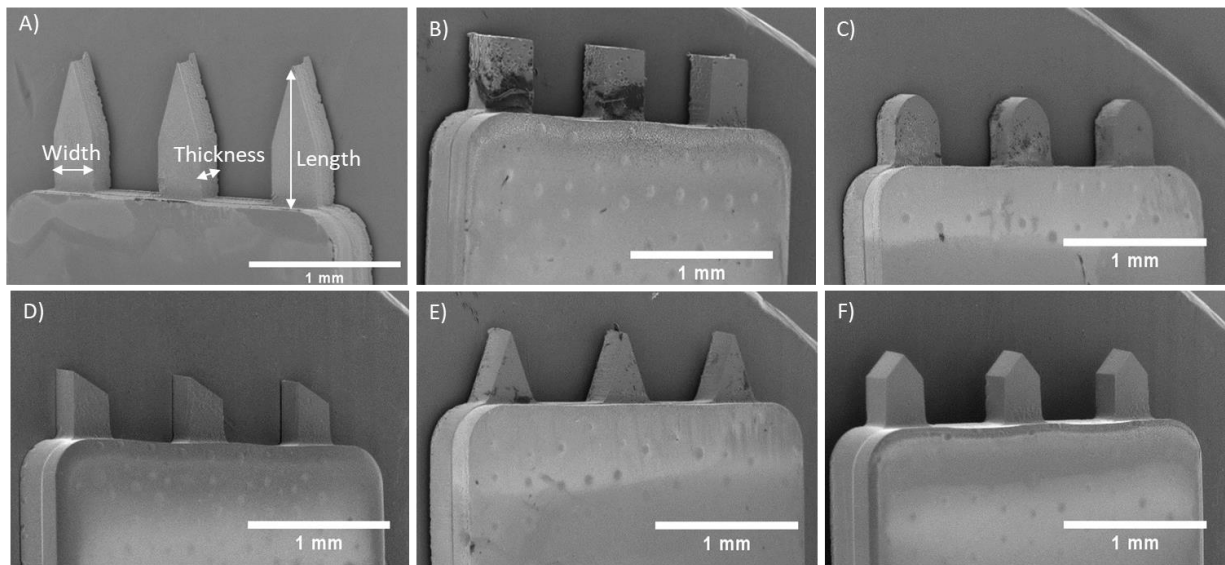


**Figure 4.2: Schematic of in-plane and out-of-plane microneedles.** Microneedles (MNs) are typically divided into two groups: In-plane and out-of-plane MNs. In-plane MNs consist of MNs placed in one line whereas out-of-plane MNs consist of an array of several MNs which can range from just a few to hundreds. Created with BioRender.com.

#### 4.5 Microneedle dimensions and shapes

The dimensions and shapes of the MNs have an impact on the ability to penetrate the skin. The elastic properties of skin affect the penetration and some MN shapes may not be able to penetrate properly as the skin simply folds around the MN [160]. Several MN shapes and dimensions have been proposed in the literature with varying lengths and widths as well as sharpness or angle of the MN tip [173]–[176]. The sharper the tip the more easily the penetration occurs i.e. the lower the penetration force [177]. Table 4.1 provides an overview of various MN shapes and their application found in the literature.

As reviewed by Waghule *et al.*, MNs are usually between 150-1500  $\mu\text{m}$  long with a 50-250  $\mu\text{m}$  width and 1-25  $\mu\text{m}$  thickness [146], but these dimensions are indicative and may vary depending on the application. For example in one study the width was 300  $\mu\text{m}$  [178] and in another one the length was 2000  $\mu\text{m}$  [166]. The parameters for MNs could be divided into single MN parameters including height, width, thickness, shape, and tip angle, whereas MN array parameters also include MN pitch (center to center spacing) and arrangement. Figure 4.3 shows in-plane silicon MNs that were employed throughout this PhD thesis where some of the potential dimensions and shapes are highlighted.

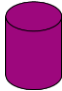

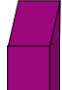





**Figure 4.3: Silicon in-plane microneedles from the PhD project.** A) Optimized microneedles (MNs) based on research project I with 1000  $\mu\text{m}$  length, 400  $\mu\text{m}$  width, and 180  $\mu\text{m}$  thickness. SEM image is to illustrate potential MN dimensions. B-F) Various MN shapes as examples: B) Flat, C) lancet, D) hypodermic, E) triangular, and F) Pencil shape. B-F) Adopted from manuscript I [127].

The MN shapes are often hypodermic [149], beveled [179], triangular [150], octagonal [180], pencil [181] or pyramid shaped [175]. MNs can be cylindrical protrusions [182] or flat like a cantilever [174] and the sharpness or tip angle of the MN vary, but is very important for efficient penetration. A general observation is that larger tip diameters require higher penetration forces [132], [177].



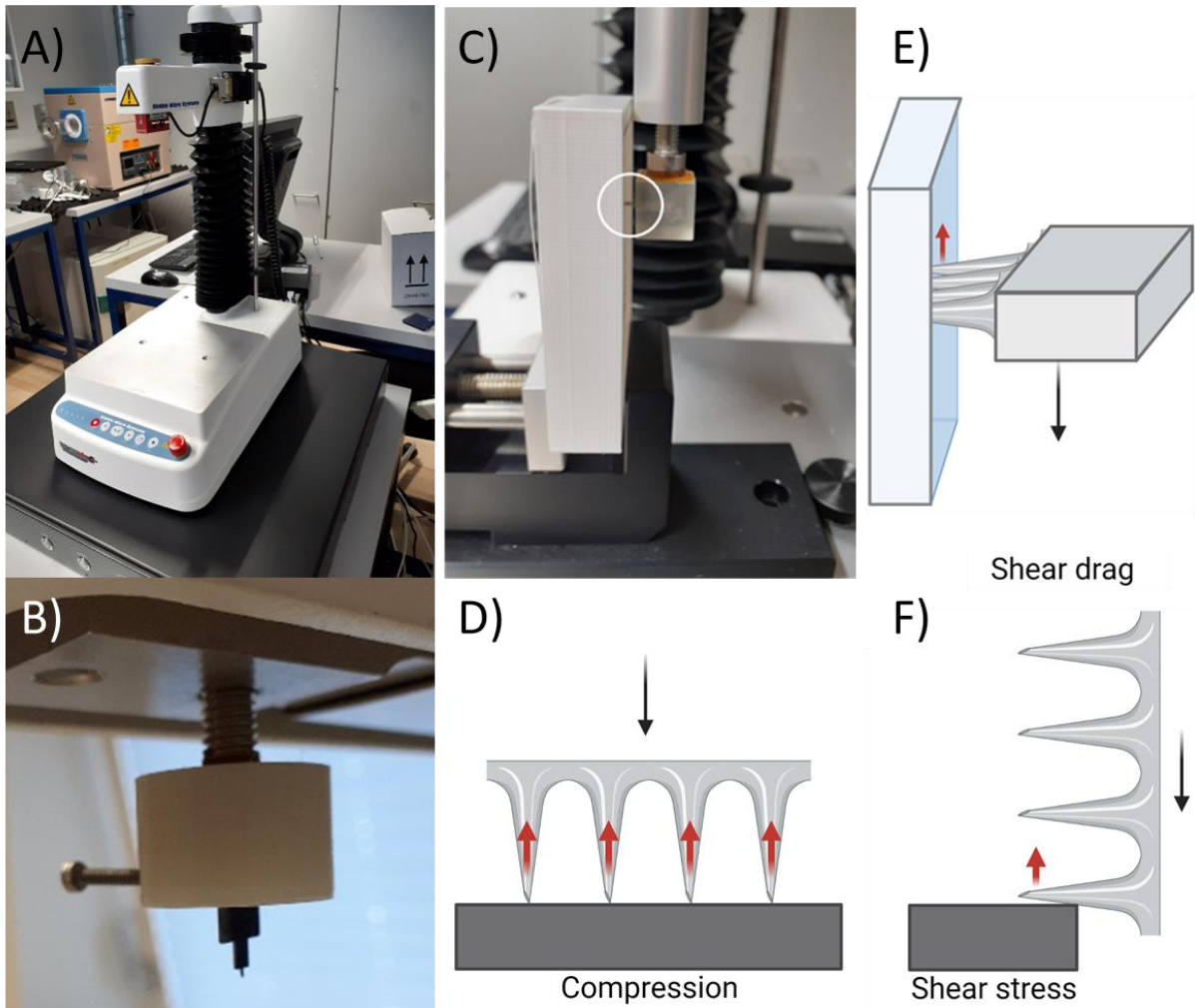
**Table 4.1: Short overview of microneedle shapes and their application.** Several different shapes of microneedles have been reported in literature. These have been used for various purposes ranging from delivery of molecules to detection of biomarkers.

| Mirconeedle shape   | Application and reference examples   |
|---|--|
| Circular/cylindrical/octagonal<br> | Cell surgery [173], [183]<br>Insertion in skin [180], [184], [185]<br>Transdermal delivery [182], [186], [187]   |
| Square/rectangular/cantilever<br>  | Delivery device [186]<br>Collecting blood samples [174]  |
| Beveled/hypodermic<br>             | Molecule delivery in cells and skin [149]<br>Facilitating diffusion of high molecular weight compounds [160]<br>Simulation of skin insertion [175]<br>Transdermal penetration [179]<br>Transdermal drug delivery [188]<br>Microneedle characterization [189]                 |
| Sharp tipped/pencil/conical<br>  | Molecule delivery in cells and skin [149]<br>Transdermal delivery [129], [168], [181], [190]–[192]<br>Simulation of skin insertion [175]<br>Transdermal penetration [179], [193]<br>Repeated insertion of microneedles [178]<br>Transdermal drug delivery (simulation) [194] |
| Pyramid<br>                      | Simulation of skin insertion [175]<br>Transdermal penetration [179]<br>Clinical administration [195]   |
| Triangular<br>                   | Transdermal delivery [162], [168], [176], [192], [196], [197]<br>Vaccine delivery and antibody extract [198]<br>Cell surgery [183]<br>Facilitating diffusion of high molecular weight compounds [150]  |

## 4.6 Mechanical stability of microneedles

For mechanical stability it is essential that the MNs can withstand the forces experienced during insertion and removal from skin. There are two main parameters to examine, namely the force which causes the MNs to fracture and the force required for skin penetration [180]. The ratio between these ( $\frac{\text{Fracture force}}{\text{Insertion force}}$ ) is known as the safety margin, which should be as high as possible [199]. The failure of MNs is most often evaluated by pressing the MN into a hard and unyielding surface, and determining the failure force in the associated force-displacement graph [184]. The failure modes are either fracture by compressive [162], [186] or shear forces [180] which means the MNs exhibit complete fracture [200], bending [173] or buckling [174], [199]. MN stability may also be determined using simulations, which can later be tested experimentally [183], [194]. It has previously been determined that the fracture force is dependent on the thickness of the MN. More specifically for hollow MNs, it was observed that increasing the wall thickness also increased the fracture force [168]. Especially for hollow MNs, high mechanical stability is required, as the cavity in the center of the MN is prone to collapse due to the reduced structural integrity [132]. Ideally, MNs should be thin and sharp for easy skin penetration and they should be strong enough not to break within the skin [177], [199].

For investigating the mechanical stability already existing equipment is commonly used, though sometimes it originally served a different purpose such as a Royce 552 Bond test system used for shear stress measurements [180] or a dynamometer used for compressive measurements [162]. Most commonly the equipment is a force-displacement machine used to test and measure the mechanical stability in terms of force required for e.g., fracture [184], [186], [199]. In two studies, as well as in our research project I (elaborated in section 4.9.2), a Texture Analyser (TA) was used [201], [202], which is essentially also a force-displacement machine. Figure 4.4 shows examples of different strategies for testing of the mechanical stability of MNs using a TA.



**Figure 4.4: Examples of testing the mechanical stability of microneedles.** A) Texture Analyser (TA) used for testing the mechanical stability of the microneedles (MNs). B) Image of mounted MNs to the arm of the TA. C) Image of how the shear drag test of the MNs in this project was performed. The MNs are marked with a white circle and dragged downwards through a skin-simulating hydrogel. D-F) Illustrations of testing mechanical stability of MNs. The black arrows indicate the movement, and the red arrows indicate the force on the MNs. D) Illustration of testing MN compression. E) Illustration of testing MN shear drag. F) Illustration of testing MN shear stress. Images D-F were created using BioRender.com.

#### 4.7 Mechanical testing of microneedle penetration

As mentioned above, evaluation of MN penetration is a part of the assessment of the mechanical stability of MNs as they should be stable enough to penetrate without fracturing inside the skin. Often this type of test can be performed quite simply by inserting the MNs into a skin model (skin models are elaborated in chapter 6) and assess if the MNs fracture [183]. MN insertion may either be manual [195] or using a machine for consistency [150]. For some studies the force can be measured simultaneously using a force-gauge [171], but most studies perform this test while the MNs are mounted to a force-displacement device which measures the applied force during insertion [172], [184]. In this way the penetration force

is measured simultaneously with testing the MNs for insertion fracture. The insertion force is influenced by the shape and dimensions of the MNs along with the angle and radius of the tip [164]. As the MN tip surface area increases so will the required displacement to achieve penetration [183]. Testing the insertion force can contribute to the optimization of the shape and dimensions [164].

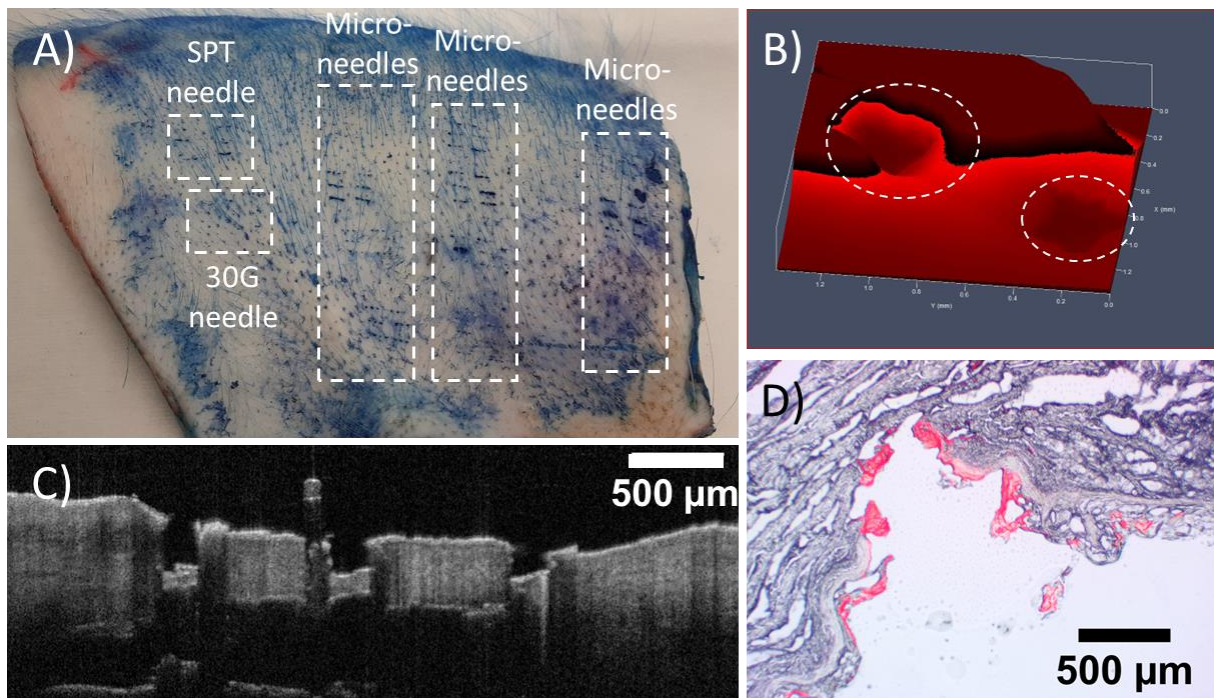
Additional to mechanical testing, MN penetration is often confirmed visually as explained in the following section 4.8, but sometimes this is done in a quantitative manner using other methods. Measuring a drop in electrical resistance across the skin barrier can confirm and quantify penetration [188], [199]. Likewise, measuring increased trans-epidermal water loss (TEWL) indicates a breach of the skin barrier and thereby confirms penetration [160], [170]. Another way of confirming penetration is if the MNs are delivering a molecule which can be measured using e.g., immunohistochemistry (IHC) [203] or after homogenization of a skin sample [204]. Penetration can also be confirmed indirectly, e.g. by delivery of insulin which has an impact on glucose levels that can be measured [168], or a vaccine delivery with measurements of specific antibodies in the blood serum afterwards [198].

#### **4.8 Visualization of microneedle penetration**

By visualizing the MN penetration their ability to penetrate the epidermis and penetration depth can be evaluated and the potential tissue damage caused by the MNs may be assessed. MN insertion in skin samples has been visualized using confocal laser scanning microscopy (CLSM) where a fluorescent dye for visualization was applied before and after skin penetration [150], [205], [206]. Other dyes such as trypan blue [160], [207] and methylene blue [180], [195] have also been used for visualization as these dyes are hydrophobic and do not stain the stratum corneum but only the areas where the skin has been damaged by the MN [150], [208]. OCT is also an option for visualization of MN penetration [185], [209] as it can provide a 3D scanning of the selected area. If the MN insertion was performed in skin, a sample may be collected for histology [207] with different options for tissue staining such as Meyer's hematoxylin and eosin (H&E) or toluidine blue. Furthermore, methods such as cryostat histology and cryo-scanning electron microscopy (SEM) have also been used. Histology is the analysis of microscopy images of biological samples where it is possible to stain for certain features such as specific cells and thereby visualize damage to the stratum corneum [186], [187]. Histology has the advantage of imaging the sample cross-sectionally [208], [210]. Cryo SEM is another method, where the sample is snap frozen in liquid nitrogen and imaged in a SEM. This imaging technique allows for a higher resolution and provides the option of breaking the sample for a cross-sectional view [160]. A general consideration when visualizing penetration holes in dermal tissue is the time it takes the skin to reseal. Depending on the time that passes between MN application to the skin and the visual analysis, the skin may start to reseal and thereby show less or maybe no visible penetration [211]. Figure 4.5 shows examples of how MN holes have been visualized throughout this project using methylene blue, CLSM, OCT, and histology.

In several studies it has been found that not the entire length of the MN penetrates into the skin due to the viscoelastic behavior of skin tissue. This has been observed using video recordings, methylene blue staining, and fluorescent dyes [193], [212]. Gittard *et al.* reported that approx. 88.5% of poly(dimethylsiloxane) MN length penetrated into porcine skin. In the same study, it was observed that the skin undergoes compression by the MN until a certain force threshold. After this the skin ruptured

and the MN was able to penetrate into the skin which rebounded onto the MNs [212]. In a different study the penetration depth of 3.3 mm solid glass MNs in *ex vivo* human skin was investigated using video frames and performing methylene blue staining. The authors found that with a maximum vertical skin displacement of 1.5 mm, the penetration depth was approx. 250  $\mu\text{m}$  for all tip diameters of 5, 15, 24, and 37  $\mu\text{m}$  [193], i.e. only 7.5% of the needle actually penetrated the skin at this displacement.



**Figure 4.5: Methods for visualizing microneedle penetration holes.** A) Porcine ear pricked with microneedles (MNs), SPT needle, and 30G needle (positive control) and afterwards stained with 1% methylene blue in de-ionized water for 1 h. The methylene blue was gently wiped off and MN holes appeared as blue dots. Adapted from manuscript I [127]. B) Agarose skin-simulating hydrogel containing rhodamine B fluorescence pricked with MNs. Visualized using a confocal laser scanning microscope where two holes are visible and indicated by two dotted white circles. C) Porcine skin sample pricked with MNs and visualized using optical coherence tomography immediately after removing the MNs. Adapted from study report I [128]. D) Cryostat histology image representing MN hole where MNs were coated with 10 mg/mL rhodamine B dextran and fluorescent-labeled coating was delivered. The image is comprised of two overlaid images, a brightfield microscope image and a fluorescence microscope image. Adopted from manuscript II [213].

## 4.9 Microneedle investigations in this project

### 4.9.1 Microneedle dimensions and shapes

The aim of this part of the PhD was to ensure the mechanical stability of selected MNs so they would not fracture during penetration. Furthermore, the MNs should penetrate the epidermis skin layer and reach the upper dermis layer where the MCs are present.

In-plane solid silicon MNs were selected for this project in the shapes of flat (control MN), hypodermic, lancet, triangular, and pencil (Figure 4.3B-F). Different MN dimensions were examined including lengths

of 500  $\mu\text{m}$  and 1000  $\mu\text{m}$ , widths of 200  $\mu\text{m}$  and 400  $\mu\text{m}$ , and thicknesses of 500  $\mu\text{m}$ , 350  $\mu\text{m}$ , and 180  $\mu\text{m}$ . This was to optimize the MN shape and dimensions for successful penetration without fracture. The ideal behavior of the MNs was excellent skin penetration with as low as possible penetration force and tissue damage while maintaining a sufficient surface area for ultimately performing the *in situ* electrochemical measurements. The optimized MNs were determined to be a hybrid between the triangular and pencil shapes with 1000  $\mu\text{m}$  length, 400  $\mu\text{m}$  width, and 180  $\mu\text{m}$  thickness (Figure 4.3A). The optimized MNs were tested for their mechanical stability and ability to penetrate skin using porcine neck and human breast skin.

The penetration results of the initial study for optimization of MN shape and dimensions are presented in manuscript I [127] and the penetration results for the optimized MNs in porcine neck and human breast skin are presented in study report I [128]. The manuscript and study report are included in the appendix of this PhD thesis. In the following sections a short summary of research project I and II will be presented.

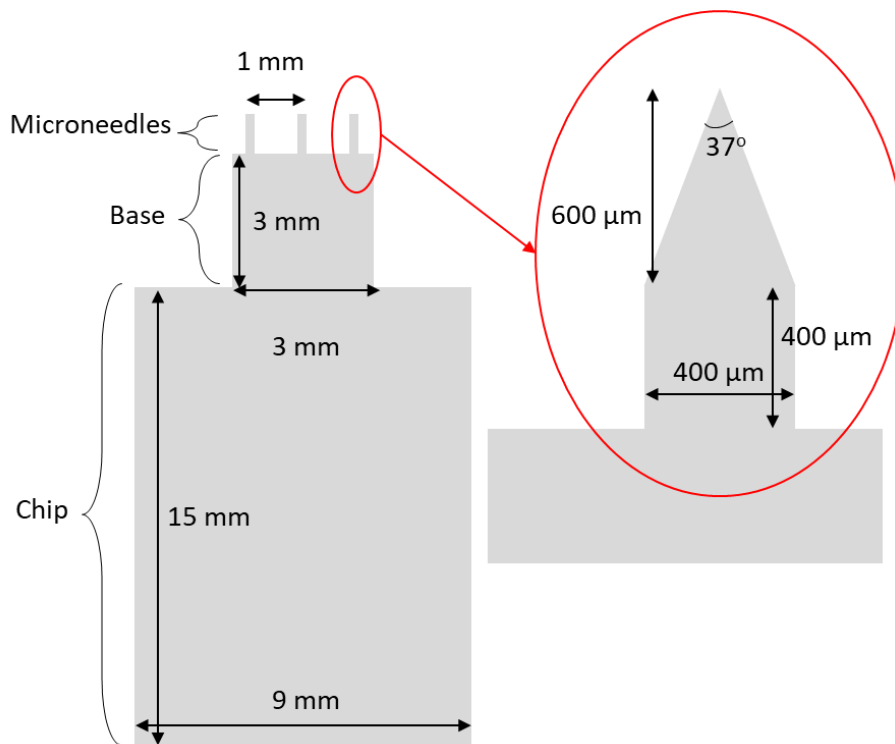
#### **4.9.2 Research project I: Evaluation of microneedle shape and dimensions for penetration in different skin models**

In the first research project, the aim was to evaluate selected MNs of varying shape and dimensions. The MNs should exhibit mechanical stability and penetration ability reaching the upper dermis skin layer. The experimental methods and results are described and discussed in detail in manuscript I [127] included in appendix A.

In brief, five different in-plane silicon MN shapes (flat, hypodermic, pencil, triangular, and lancet) were tested in research project I using different skin models, i.e. skin-simulating hydrogels, *ex vivo* skin samples of BN rats, and a porcine ear. The MN dimensions included the length, width, and thickness which were iteratively varied for optimization. An investigation of the mechanical stability, penetration force, and tissue damage was performed using the aforementioned skin models.

The MNs were found to have sufficient mechanical stability without fracturing upon penetration and the penetration force was measured using a TA for obtaining force-displacement curves. The tissue damage was evaluated using histology and it was observed that not the entire MN length penetrated into the skin, however, the MNs did penetrate the epidermis and reached the upper dermis which is the target area of the InstaPatch. The general conclusion was that the triangular shaped MN caused the least amount of damage overall and required the lowest penetration force in the skin models.

Based on the results from research project I, the selected shape for the next experimental studies in the PhD project was a hybrid between the triangular and pencil shaped MNs as shown in Figure 4.3A above. The triangular tip shape provided the abovementioned assets in terms of penetration, while the pencil shape had a larger surface area, which was judged to be more suitable for allergen delivery and ultimately performing the electrochemical measurements intended for the InstaPatch. The final optimized MN shape and dimensions are illustrated as a schematic in Figure 4.6. The pencil shaped MNs are 1000  $\mu\text{m}$  long, 400  $\mu\text{m}$  wide, and 180  $\mu\text{m}$  thick and extrude from a 3 x 3 mm base sitting on a 9 x 15 mm chip for handling.



**Figure 4.6: Illustration of optimized microneedles.** The optimized microneedles were a hybrid between the triangular and pencil shape tested in research project I. The optimized dimensions were 1000  $\mu\text{m}$  length, 400  $\mu\text{m}$  width, and 180  $\mu\text{m}$  thickness. Adopted from manuscript II [213].

#### 4.9.3 Research project II (part I): Evaluation of optimized microneedles for penetration in porcine neck skin and human breast skin samples

In a second research project the optimized MN shape and dimensions identified in research project I were tested in porcine neck and human breast skin samples during an external stay at Cardiff University. The methods and results are described in detail in study report I [128] included in appendix B.

Porcine skin was first used for testing MN insertion at 5, 10, and 15 N where 5 N was found to be sufficient for penetration without breakage of the MNs. Penetration was confirmed using cryostat histology and methylene blue staining together with OCT measurements performed immediately after retracting the MNs from the porcine skin.

Furthermore, MN arrays were tested by combining two and three rows of in-plane MNs with spacers in between and inserting these MN arrays in porcine skin. Here, penetration was also confirmed using methylene blue and OCT where it was observed that the penetration efficiency decreased with more than one row. This essentially means that the interspacing of the MNs needs further optimization and testing if several in-plane MN chips should be combined into 3D array with multiple rows of MNs.

#### **4.10 Summary**

This chapter introduced the concept of MNs and their potential applications. An overview of MNs and their materials was given where in-plane solid silicon MNs were selected for our study. Various dimensions and shapes of MNs were also presented as this literature study was the first part of the project for selection of MNs for testing. Five MN shapes: Flat, lancet, hypodermic, pencil, and triangular with varying dimensions were tested in research project I. Different methods were considered for testing mechanical stability, penetration ability, and visualization of MN holes. For mechanical stability and penetration, a TA was used to measure the fracture force of the MNs and measure the penetration force of the MNs in skin-simulating hydrogels, excised BN rat skin samples, and porcine ear skin. No breakage of the MNs was observed upon penetration of the various skin models. Visualization was achieved using methylene blue and histology in research project I, as well as using fluorescence, OCT, and cryostat histology in research project II. The outcome was the optimized hybrid MN shape of a triangular and pencil shape with dimensions of 1000  $\mu\text{m}$  length, 400  $\mu\text{m}$  width, and 180  $\mu\text{m}$  thickness.



## Chapter 5: Microneedle coating for intradermal delivery

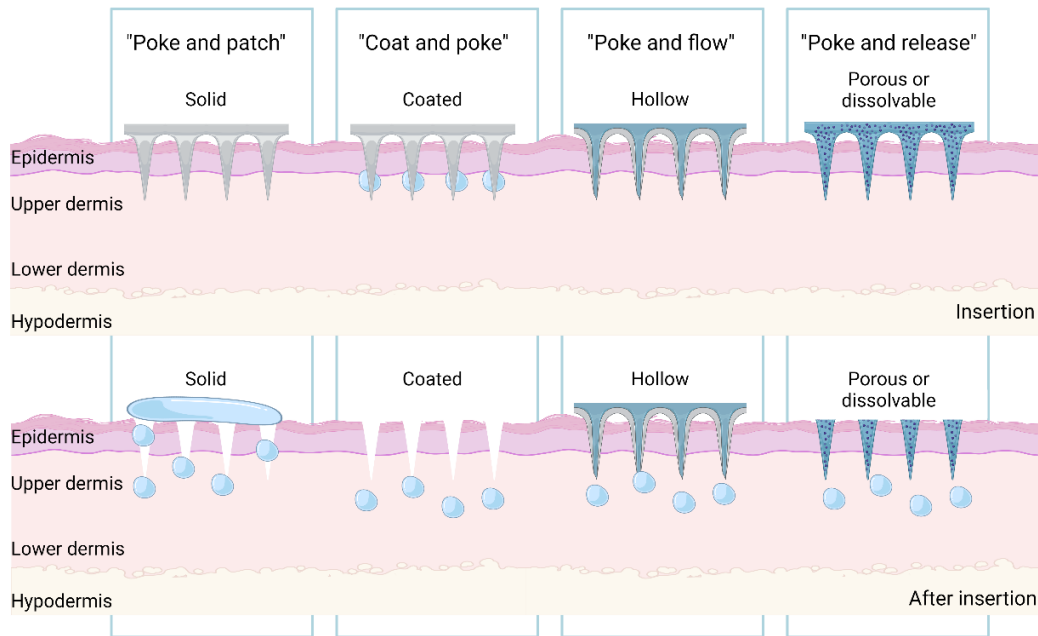
For this project the specific purpose is allergy diagnostics using the SPT as a base model for improvements. As in the SPT, a specific allergen needs to be delivered for testing to confirm a certain allergy. The MNs therefore need to not only perform the *in situ* measurements, but also to deliver the allergen together with the electrochemical measurement. This chapter introduces the different types of MNs that exist for dermal delivery and their mode of action. The focus will be on the so called “poke-and-release” delivery method where solid MNs are coated and inserted directly into the skin for delivery. The various materials of solutions will be presented alongside the methods for how to coat MNs as well as how to evaluate the coated MNs.

### 5.1 Intradermal molecule delivery using microneedles

MNs for drug delivery are typically divided into two categories namely solid and hollow MNs where the solid MNs include MNs which can generate holes (channels) within the skin, MNs that are coated, as well as dissolvable or porous MNs [214], [215]. The main parameters to consider for drug delivery is a controlled release and reaching the target area which is usually the dermis skin layer. In addition, the drug should also not be deactivated by other components included in the delivery method [190], [191]. Once the coated MNs are inserted into the skin the coating should start to dissolve thereby releasing into the ISF. The limiting factors for this approach is the available surface area of the MNs for coating and insertion, and the insertion time [216].

As reviewed by Prausnitz [214] and Van Der Maaden *et al.* [215] there are four different strategies for delivery of molecules such as drugs or vaccines as illustrated in Figure 5.1. The first one is defined as “poke and patch” where solid MNs create channels in the skin tissue for a patch or solution that is either applied before the initial poking or afterwards. For this purpose, it is essential that the channels stay open long enough for the drug to diffuse into the skin [217]. In a large sense the current SPT could be considered a “poke and patch” method. The second strategy is “coat and poke” where solid MNs are coated with coating solution containing the drug for delivery that is then released upon penetration. Ideally for this method the coating is released rapidly to ensure that the solid MNs do not have to remain within the skin for very long time [197], [218]. The third method is “poke and flow” where hollow MNs are inserted into the skin and a solution is delivered directly to the insertion site. This method has the advantage of being able to deliver the drug in pulses [188] and easily deliver significant amounts of drugs with a high molecular weight (MW) [219]. Finally, the fourth strategy is “poke and release” where the MNs must remain in the skin for some time to allow controlled release. These MNs are either porous [220] or dissolvable [221] where the drug is trapped inside the pores [132], [220], hydrogel [222], polymer [163] or other biodegradable materials that the MNs may be made of. Dissolvable MNs also have the advantage of not leaving biohazard materials afterwards [223] and some hydrogel-based MNs have the ability to swell up upon insertion and thereby creating channels which allows passage for drugs through the skin barrier [224]. In some studies, the above-mentioned categories have also been combined into hybrid versions. For example, solid silicon MNs have been designed with a dissolvable tip which would break off in the skin and slowly dissolve thereby releasing a drug [225].

This chapter will focus on the “coat and poke” strategy, as this was the method envisioned for the i.d. delivery of allergens in the InstaPatch project.



**Figure 5.1: Four different delivery strategies using microneedles.** There are four different approaches for using microneedle (MN) delivery of molecules. The first one being the “poke and patch” where solid MNs are inserted creating puncture holes where liquid afterwards can diffuse into. The second one is “coat and poke” where solid MNs are coated with a drug and then inserted for release. The third one is “poke and flow” where hollow MNs are inserted, and the drug solution can be injected directly. The last one is “poke and release” where porous or dissolvable MNs are inserted for a controlled release. Created with BioRender.com.

## 5.2 Materials for microneedle coating

For the “coat and poke” method described above, the MNs have to be coated with the molecules that should be delivered into the skin. When selecting a formulation for a MN coating solution several considerations must be made. During the coating method, it should be ensured that the solution is able to wet the MN surface and that its spreading can be controlled to obtain a uniform coating in terms of thickness and material properties. When adding a surfactant, the wettability and spreading of the coating solution is increased [196]. The MNs should dry uniformly and avoid de-wetting which is related to the surface interactions with e.g., the silicon. Silicon MNs can be treated with plasma changing the surface free energy of the surface [226]. When adding a viscosity enhancer, the thickness of the deposited coating can typically be increased and controlled by the amount of enhancer added. Increasing the viscosity also slows down the de-wetting process during drying, allowing the solution to remain on the surface long enough for the solvent to evaporate and the coating to set [227].

Many parameters related to the coating play a role for molecule delivery, such as the coating layer thickness and MN surface area [196]. After deposition, the coating should adhere to the MN during skin penetration. The mechanical properties of the coating should be optimized such that the coating remains

on the MN surface until insertion into the skin, to ensure that a minimum amount of coating is scraped off on the surface. After skin penetration, the coating should be dissolved or degraded within the ISF of the skin [227]. Finally, the materials that are included in the coating solution should generally be biocompatible and not cause distress or damage to the skin [196] – except for materials such as drugs [163] or vaccines [190], in which the delivered molecule within the solution *should* cause a specific reaction.

The components of a coating solution should ideally be generally regarded as safe (GRAS), and several GRAS surfactants and viscosity enhancers have been proposed in the literature to improve and modify the properties of the coating. Surfactants reduce the surface tension and increase wettability of the solution. Lutrol F-68 NF [196] and Tween 20 [197] are often used and in some instances Poloxamer 188 and Quil-A [192] are employed. Viscosity enhancers help to increase the thickness of the coating. For viscosity enhancers carboxymethyl cellulose (CMC) salt [227], methylcellulose [198], and hydroxypropylmethylcellulose (HPMC) [197] are often used, but also sucrose [227], hyaluronic acid [227], sodium alginate [227], polyvinylpyrrolidone (PVP) [228], polyvinyl alcohol (PVA) [162], glycerol [227], poly(lactic-co-glycolic acid) (PLGA) [227], and alginic acid [229] are commonly used. Xanthan gum [227], gum ghatti [229], and karaya gum [229] have also been employed although to a lesser degree. In addition, stabilizers can be added to stabilize bioactive components. Common stabilizers are trehalose [162], sucrose [162], glucose [190], inulin [229], and dextran [229]. The coating solutions are usually based on deionized water [162] or phosphate buffered saline (PBS) [190]. The activity of the drug in the final solution should be investigated and tested as it was observed in one study that the CMC added to the solution had deactivated the vaccine antigen. It is therefore necessary to ensure that the components of the solution do not interfere with the molecule for delivery [229].

It is often easier to deliver hydrophilic drugs than hydrophobic ones since the coating should be easily dissolved within the ISF, which is water-based. When coating MNs with hydrophobic molecules the excipients should be soluble in both an aqueous environment, which the ISF consists of, as well as an organic solvent to allow coating to dissolve [227], [230]. As an example PVP might be used in this case as it is soluble in both water and ethanol [227].

There are several examples of various types of molecules which have been incorporated into coatings. Among these are peanut extract [144], ovalbumin [198], vaccine [190], insulin [181], and anticancer agents [231]. In most cases the solution incorporated some of the above-mentioned components in different concentrations optimized for a given final application.

In this PhD it was decided to use CMC as the viscosity enhancer in aqueous coating solutions. A surfactant was purposely not included as these were found to often have an irritating effect on skin causing inflammation [232]. This would have an impact on the final *in vivo* measurements done in BN rats.

### **5.3 Methods for coating of microneedles**

As mentioned above, MNs have to be coated using a solution containing the molecule of interest for delivery, such as a drug, and in most cases additional components such as viscosity enhancers, surfactants, and stabilizers. The criteria for a good method are that it should provide a uniform coating with the

possibility of a high drug loading. Furthermore, it should be reproducible, fast, and simple [196]. If the MNs should be used for commercial purposes the coating method should be cheap and sterile following good manufacturing practices (GMP) [233]. Several different coating approaches can be found in the literature such as gas-jet drying [192], spray coating [197], inkjet printing [234], and dip-coating [227]. These four examples are illustrated in Figure 5.2.

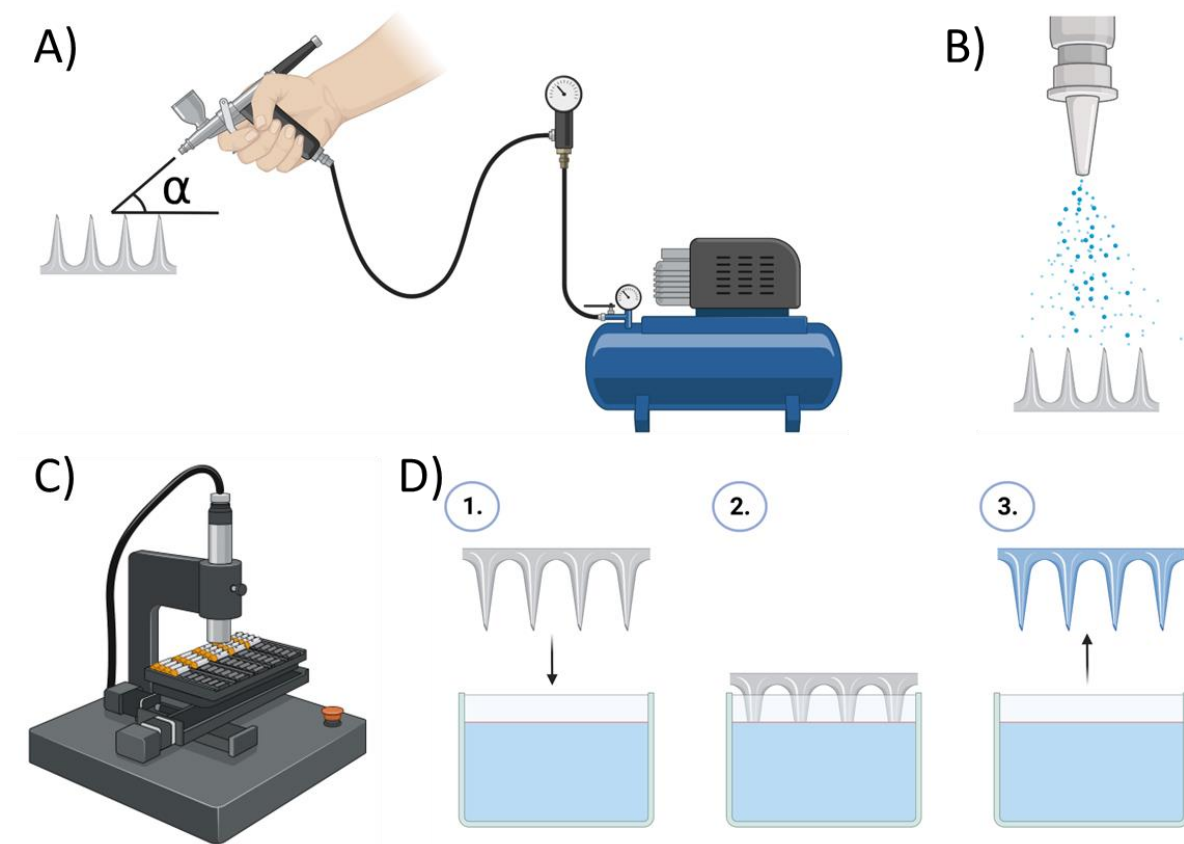
Gas-jet drying (Figure 5.2A) may be advantageous if the MNs are very small as it distributes the coating evenly on smaller MNs ( $\leq 90 \mu\text{m}$ ). In gas-jet drying, the coating solution is added to the MNs, and a gas-jet with a speed 6-8 m/s is afterwards used to dry the solution. Finally, an increased gas-jet speed of 10 m/s is used to remove excess coating [192].

For a spray coating (Figure 5.2B) process, a spray bottle with a nozzle is used. An appropriate nozzle opening is needed to accommodate the molecules in the coating solution as well as a precise control of the viscosity. The MNs are fixed and the coating procedure can be controlled using a peristaltic pump to control the rate of liquid deposition on the MNs [197].

Inkjet printing (Figure 5.2C) can be used to ensure precise coating of MNs with a known dose. The doses can be dispensed with precision in amount and location on the surface of a solid MN with very little waste. An inkjet printer works with a XYZ movable printer head that dispenses a chosen amount of liquid at a selected position [234]. Since the droplet volumes when using the inkjet printer are very low (48-524 pL [235]) the solvent evaporates quickly leaving behind the solid content of the solution-coated on the MN. When using the inkjet printer for dispensing, the quality of the coating depends on the nozzle size of the dispenser. If the nozzle of the dispenser becomes very small clogging might arise and affect the inkjet printing, and this can especially happen if the concentration of larger molecules is high within the solution [181]. Another parameter that needs optimization is the placement of the MNs. This is exemplified in a study by Ross *et al.* where the MNs were mounted at an angle of  $45^\circ$  relative to the dispenser head of an inkjet printer to ensure correct coating of only one side of solid MNs [181]. Since the droplet volume dispensed is so small, it is important to ensure that the distance between the coating area (e.g. the MN tip) and the nozzle is optimized [231].

Dip-coating (Figure 5.2D) is one of the simpler methods and more commonly used for coating MNs. In this approach, the MNs are simply dipped into a coating solution and then again retracted in a controlled manner followed by drying [227]. The dip-coating method has several variables which can also partake in defining the amount delivered [228]. These parameters are the number of times the MNs are dipped into the solution, the insertion and removal speed in the solution, and duration the MNs are immersed in the solution [196]. The dip-coating method can be done manually or using a customized machine with controlled movement [196]. The coating method impacts the composition of the coating solution as e.g., the nozzles from the above-mentioned method inkjet printing usually require lower concentrations of larger molecules to prevent clogging [181] whereas dip-coating does not have this constraint.

For the purpose of this PhD the dip-coating method was selected for coating of in-plane solid silicon MNs. It was simple and easy to perform and using a TA it was possible to control the speed of moving the MNs into and out of the solution.



**Figure 5.2: Illustration of four different coating methods of microneedles.** A) Gas-jet drying. B) Spray coating. C) Inkjet printing where droplets of solution is dispersed on the microneedles (MNs). D) Dip-coating where 1. The MNs are lowered into the solution, 2. The MNs are in the solution, and 3. The MNs are retracted out of the solution. Created with BioRender.com.

## 5.4 Evaluation of microneedle coating and delivery

In most cases the MN coating and delivery are linked, and it is easiest to evaluate the coating through delivery. The most commonly used method for evaluation of MN coatings, whether to confirm its presence on the MN or conduct quantitative measurements of delivery, is using fluorescence. Fluorescent-labeled coatings have been used to visually confirm their presence on MNs before and after insertion [196], [227]. Fluorescence measurements have also been used as a quantitative tool to determine the amount of fluorescent-labeled molecules on the MNs and also the amount delivered after insertion [144], [236]. In some instances, fluorescence is combined with other methods such as histology. Cryostat histology allows skin samples to be cut and viewed without staining making it possible to easily observe and confirm fluorescent-labeled molecules delivered inside MN holes and/or on top of the surface of the skin [187]. As mentioned in section 4.7, tissue penetration may also be evaluated via the coating, such as measuring the quantity of the molecule delivered [204] or measuring on the outcome of the delivered molecule e.g., an increase in antibodies found in blood serum [198].

## 5.5 Microneedles in allergy research

MNs have recently emerged within allergy research and subjected to an investigation for their potential use to either diagnose allergies or induce tolerance or desensitization. In allergen immunotherapy, desensitization is induced by a gradual increased exposure of individuals to allergens until they become non-allergic or have less symptoms. The ability of coated MNs to deliver allergen extract for desensitization and inducing tolerance has been tested in mice for peanut allergy. In these studies a water-based coating solution containing the allergen extract and CMC was utilized and promising results were obtained in regards to desensitization [144], [236], [237]. As an improvement on the current SPT method, MNs have also been examined as a potential diagnostic tool for allergy in two particular studies both using dissolvable MNs [145], [238]. Since MNs are likely less invasive and have a low risk of adverse effects, they have been tested in mice with the aim of diagnosing specific allergen allergies. While delivery of allergen was confirmed in one study neither of the two studies presented a fully developed allergy test [145], [238].

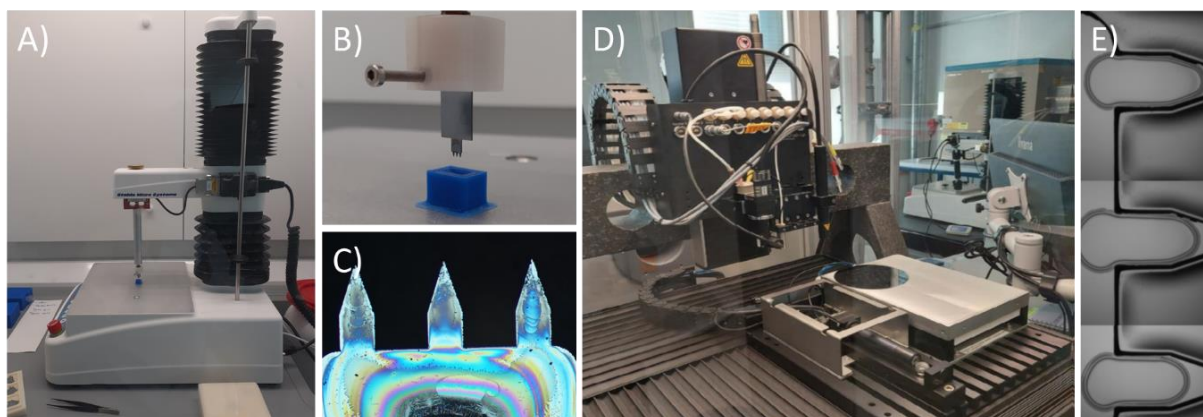
## 5.6 Investigations of coating and macromolecule delivery in this project

### 5.6.1 Intradermal delivery with silicon microneedles

As mentioned above, the “coat and poke” strategy was selected for the i.d. delivery of allergens in this PhD. Basically, the allergen-coated in-plane solid silicon MNs with integrated electrodes will be inserted in the skin, the allergen will be released, and the activation of the MCs will be measured electrochemically by measuring histamine or another redox-active biomarker. For dissolvable MNs used in the case of the poke and release method, integration of electrodes would not be possible and another method than electrochemistry should be developed for measuring the MC activation. For hollow MNs the fabrication process would be further complicated as opposed to fabricating solid MNs.

One of the main objectives of this PhD was to develop a simple and reproducible method for coating MNs with allergens. Ideally, the resulting coating should be delivered with the insertion of the MNs to enable *in situ* electrochemical measurements. The dip-coating method was selected as it was a simple method. It was furthermore possible to perform this dip-coating method using the TA already applied in research project I. Figure 5.3A-C shows how the dip-coating process was done as well as an example of MNs coated using the dip-coating method. Inkjet printing was also investigated using an AutoDrop Inkjet printing system from MicroDrop Technologies shown in Figure 5.3D and an example of droplet deposition on MNs with the inkjet printer is presented in Figure 5.3E. However, it was ultimately decided to continue with the dip-coating method as the inkjet printing would require more optimization before it was viable for use compared to dip-coating.

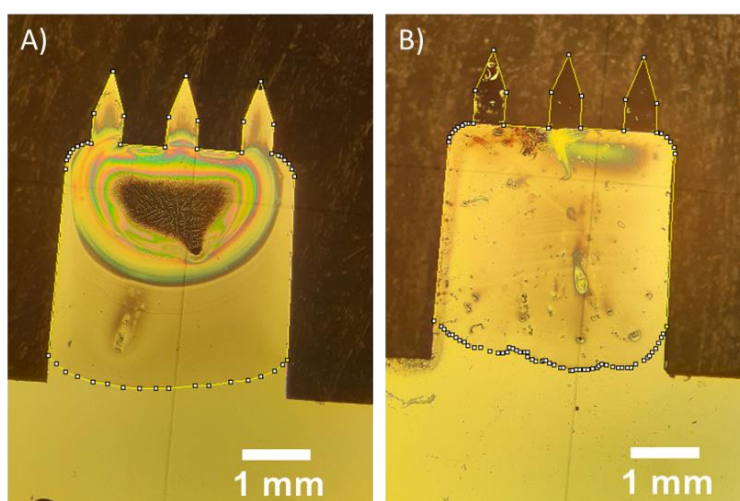
Based on previous studies using peanut extract-coated MNs [144], [237], it was also decided to use a PBS-based solution containing the peanut allergen Ara h 2 [239], [240] and CMC. A surfactant was purposely left out as these are often found to have an irritable effect on skin, which would have interfered with our detection method using Evans blue (elaborated in section 5.6.4). The CMC was necessary to include to enhance the solution viscosity. Without CMC the solution would be too water-like and potentially not much allergen would be deposited on the MNs.



**Figure 5.3: Coating methods used in this PhD.** A) Dip-coating performed inside a fume hood for a controlled environment using a Texture Analyser. B) Close-up image of microneedles (MNs) moving into the solution inside the blue well. C) Example of coated MNs using the dip-coating method. D-E) Inkjet printer images kindly provided by Isabel Fontán Arrizabalaga. D) Image of the inkjet printer which was also investigated as a potential coating method. E) Example of MNs coated using droplet dispersion from the inkjet printer.

### 5.6.2 Preliminary testing of dip-coating

During dip-coating, both the MNs and the base were immersed into the solution and coated. However, during *in vivo* experiments only the coating deposited on the MNs could dissolve into the skin. To estimate the amount of coating covering the MNs, three replicates of MNs with three different coating concentrations were evaluated by measuring the coated surface area. The total coated surface area and the actual coated MN area were estimated from optical microscope images on the front and reverse side of the MN chip using ImageJ. The approx. percentage of coating covering the three MNs was calculated to be 12% of the total coating. Figure 5.4 depicts the above estimation.



**Figure 5.4: Coated microneedles to provide an example of how the estimated coating coverage of the microneedles was determined.** Using ImageJ, the coated surface area of the microneedles' (MNs') A) front and B) reverse side were estimated. The amount of coating only covering the MNs was calculated to be 12% of the total coating.

### 5.6.3 Visualization of coating delivery

In this PhD, fluorescence measurements were used to confirm the presence of coatings on the MNs, measure the fluorescence quantitatively, and confirm fluorescent-labeled molecule delivery within the skin. FITC-dextran was selected as the model molecule due to its MW of 20 kDa which is very similar to the MW of 16-18 kDa for the peanut allergen Ara h 2 [241], [242]. Ara h 2 was selected for MN coating and i.d. delivery *in vivo* as it is one of the main peanut proteins associated with peanut allergy together with Ara h 1, 3, and 6 [239], [240]. During the initial experiments with dip-coating, it was observed that the delivery molecule and its concentration had an impact on the coating release. FITC-BSA with a MW of 66 kDa was included in the study to investigate the potential impact of higher MW molecules on the coating solution. This was relevant because some allergens are larger molecules than Ara h 2. It was established that the formulation of the coating solution requires optimization for each individual molecule that is to be delivered.

While FITC was used as the fluorescence on MNs, Rhodamine B dextran (MW of 10 kDa) was chosen as the model molecule for visualization of fluorescent-labeled coating delivery in skin samples to avoid autofluorescence. Skin may fluoresce at the same wavelength as FITC unlike the rhodamine B, which fluoresces at a different wavelength [243], [244].

### 5.6.4 Research project III (part 1): Ara h 2 allergen-coated in-plane silicon microneedles for intradermal delivery

In a third research project, the aim was to test MN delivery using peanut protein Ara h 2-coated MNs. Here, a brief summary of the study is included. A detailed description of the experimental methods and results are presented and discussed in manuscript II [213] which is included in appendix C.

Rat experiments were carried out in the animal facility at the Technical University of Denmark. Ethical approval was given by the Danish Animal Experiments Inspectorate with the authorization number (2020-15-0201-00732-C1). The experiments were overseen by the University's in-house Animal Welfare Committee for animal care and use.

It was first proved that MNs could be coated with fluorescent-labeled molecules, and these could be released directly from the MNs and measured. Coating delivery was investigated using porcine skin and human breast skin samples where MNs with fluorescent-labeled coating (Fluorescein isothiocyanate-dextran, Albumin-fluorescein isothiocyanate conjugate, Rhodamine B isothiocyanate-Dextran, and Rhodamine B-conjugated Ara h 2) were inserted for 60 s and the remaining, fluorescent-labeled coating on the MNs was measured. The skin samples were subject to cryostat histology thereby making the delivery of fluorescent-labeled coating visible. It was not possible to determine accurately the amount of fluorescent-labeled coating delivered by measuring the remaining coating on the MNs after insertion. However, it was possible to confirm delivery using the cryostat histology images.

MNs coated with the peanut allergen Ara h 2 were tested in peanut protein extract (PPE)-sensitized BN rats to investigate if they would elicit a local allergic response. The allergic response was made visible using Evans blue which was injected intravenously (i.v.) through the tail vein. Evans blue binds to albumin



thereby staining the blood blue [245]. Allergic responses have previously been visualized using Evans blue [246]–[248] and the technique of staining blood to make blood accumulations visible has been used for several years [249], [250]. Compound 48/80 was used as a positive control as it causes degranulation of MCs [42] and PBS was used as a negative control. As a control to the BN rats receiving allergen delivery by MNs, BN rats receiving an i.d. injection of the same allergen solution concentrations were included as it was expected that a local allergic response would be visible for these. For the rats receiving i.d. injection some responses could be observed, though, the Evans blue method was found not to be optimal. No measurable reaction different from negative control reactions was observed in rats receiving the allergen or compound 48/80 by MN insertion.

As a final attempt to quantify the delivered amount of Ara h 2, skin samples were collected from i.d. injection sites and MN insertion sites and homogenized. Using an Ara h 2 specific enzyme-linked immunosorbent assay (ELISA), it was only possible to measure Ara h 2 in the skin homogenates that had received the highest concentration of i.d. injection.

#### **5.6.5 Research project IV: Birch pollen extract and Bet v 1 allergen-coated in-plane silicon microneedles for intradermal delivery**

In a fourth research project, the aim was to test MN delivery using birch pollen extract (BPE) and Bet v 1 allergen-coated MNs. Here, a brief summary of the study is included. A detailed description of the experimental methods and results are given and discussed in study report II [251] which is included in appendix D.

In a final study conducted over the course of this PhD, an animal experiment was conducted similar to the above-mentioned research project III, but instead of having MNs coated with peanut protein Ara h 2, the MNs were coated with BPE or the birch pollen allergen Bet v 1. The BN rats were sensitized with the BPE. The rats receiving an i.d. injection exhibited more promising responses; however, the MN insertion did not provide a measurable reaction compared to the negative control reactions as was observed in the above research project III.

#### **5.6.6 Research project II (part II): Immunohistochemistry to confirm mast cell degranulation after compound 48/80 delivery by optimized microneedles**

In the second research project previously presented in section 4.9.3, the optimized MN shape and dimensions were also investigated for their delivery ability as described within this chapter. MNs were coated with compound 48/80 which should activate MCs and cause degranulation [42]. This was investigated using IHC to stain for CD63, which is a surface-bound marker of MC activation. A confirmation of MC degranulation using this method was not observed. The experiment and results are further discussed in study report I [128] in appendix B.

### **5.7 Summary**

This chapter introduced the concept of solutions and methods for coating MNs for delivery. An overview of solutions and methods was presented where the dip-coating and inkjet printing methods were

investigated in the PhD. A water- and CMC-based solution was selected together with a dip-coating method for the “poke and poke” strategy and MNs were shown to be coated with fluorescent-labeled molecules.

Delivery of fluorescent-labeled molecules was confirmed using cryostat histology on porcine and human breast skin samples. Peanut allergen Ara h 2-coated MNs were tested in an *in vivo* animal experiment with PPE-sensitized BN rats as part of research project III. As an extension to research project III, BPE and Bet v 1 allergen-coated MNs were also tested in BPE-sensitized BN rats in research project IV. The conclusion from research project III and IV was that the delivered amount of allergen or positive control compound 48/80 was either too small to elicit an allergic response or the allergic response was too small to be measured using Evans blue.

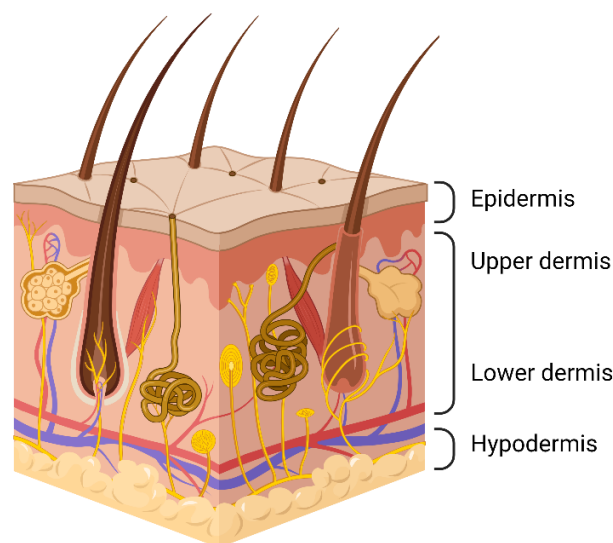
Once the optimized MN shape and dimensions have been selected and a solution and method for coating have been chosen, the MNs should be tested. For the purpose of testing, there is a variety of different skin and animal models to choose from depending on what should be investigated.

## Chapter 6: Skin models for microneedle testing

This chapter introduces what skin is and what kinds of skin models are available. These models are available as *in vitro*, *ex vivo*, and *in vivo* models. For the purpose of this PhD the focus will be on the hydrogel-based artificial skin models as this was used in research project I and BN rats since these were used in research project I, III, and IV.

### 6.1 Layers of the skin

The skin is the largest organ of the body and is vital for protection against water loss and potentially harmful substances from the environment. The advantage of delivery via the skin is the bypassing of degradation by the gastrointestinal tract and the hepatic metabolism [252]. The skin is comprised of three major layers: Epidermis, dermis, and hypodermis (Figure 6.1). The epidermis consists of keratinocytes in four layers: Stratum basale, stratum spinosum, stratum granulosum, and stratum corneum where the last one is the outermost layer. The thickness of the stratum corneum is approx. 10-20  $\mu\text{m}$ , 50-100  $\mu\text{m}$  for the epidermis, and 1000-2000  $\mu\text{m}$  for the dermis [253], [254]. Stratum corneum plays an important role in the skin barrier function as it controls the permeability of the skin and is mechanically resistant [255]. The dermis is a fibrous tissue consisting of collagen and elastic fibers forming the extracellular matrix [256], [257]. This layer contains capillary and lymphatic vessels and is most often the target of molecule delivery. Below the dermis layer is the subcutaneous tissue, hypodermis, which is comprised mainly of fat [255]. The thickness of skin varies depending on age, anatomical location, gender, ethnicity, and pathological differences [258]. One study found that human skin on the dorsal region (the front side) of the forearm had a stratum corneum of approx. 18.3  $\mu\text{m} \pm 4.9 \mu\text{m}$  and an epidermis of approx. 56.6  $\mu\text{m} \pm 11.5 \mu\text{m}$  thick [259]. Adult skin has an average pH of 5.07 [260] and exhibits linear elasticity and anisotropic characteristics meaning that its mechanical behavior is dependent on the direction in which the stress is applied [261]. Several immune cells are present within the skin either residing there or passing through while looking for pathogens. In the epidermis there are Langer cells which are a special type of APCs that reside in between the keratinocytes [262]. The dermis contains several immune cells such as dendritic cells, macrophages, and MCs, which assist in fighting infections and foreign bodies, as well as summoning more immune cells to locations displaying inflammatory stimulation [263]–[265].



**Figure 6.1: Illustration of the skin layers.** The skin is comprised of the three main layers: Epidermis, dermis (upper and lower dermis), and hypodermis. The main target for the InstaPatch is the lower epidermis and upper dermis where mast cells are located. Created with BioRender.com.

## 6.2 Ex vivo skin samples

*Ex vivo* skin samples may be the closest option to real life without using *in vivo* testing and provide the researchers with a wider range of possibilities such as testing harmful substances on skin and breakage of skin. Often skin samples are collected from either animals or humans, where the skin can be excised during surgery or obtained from a cadaver [150]. Skin samples can be collected from animals such as rabbits [266], mice, rats [201], and pigs [212]. The porcine skin has the highest similarity to human skin [208], [267] and the ear of a pig should be representative for the forearm skin of a human [268]–[270]. Human skin samples can be used as reference for comparing results but are usually more difficult to obtain [171], [208]. Skin from smaller species like rats and mice exhibit more viscoelastic properties than skin from larger species such as humans. This is likely due to the higher thickness of the epidermis layer relative to the dermis in smaller species [271]. When using *ex vivo* skin samples the skin thickness and composition will vary between species and anatomical location, which should be taken into consideration. Due to this, it is difficult to compare results obtained across different species [272].

### 6.2.1 Skin storage

One main disadvantage of using excised skin samples is that they often must be stored between collecting and using the sample and once it has been excised it no longer retains its original shape and size and becomes difficult to handle [273], [274]. Typically, human skin samples are stored at either -20 °C [176], [195] or -80 °C [150], [160], [186], [275]. Storage for three weeks at -20 °C has been found to have little impact on the integrity of the skin. However, significant damage may occur to skin stored at -80 °C [276]. In some studies the excised skin samples (both human and porcine) were stored using moist paper at 4 °C until testing [261], [277] and in another study, PBS was applied to the skin every 5 min to prevent

dehydration and retain the integrity and pH of the skin until use [181], [184]. Skin samples such as porcine skin are also stored at -20 °C [209] or -80 °C [207].

### **6.2.2 Experimental procedures**

Several different types of experimental setups have been developed and used for testing MNs *ex vivo*. Usually a supportive layer such as styrofoam [150], soft polymer clay [184], and paper clay as a hard substrate or PDMS as a soft substrate [171] have been used to simulate the dermis or hypodermis layer below the excised skin. Fatty areas and muscle tissue are normally removed from the skin sample before conducting the experiment as these often add further variables and affect the reproducibility of the results [181]. The skin layers in human skin samples may be separated if the aim of the investigation is focused on a specific layer [176], [275]. Some studies developed their own equipment for insertion of MNs into skin samples [150] and in one study a human skin sample was strapped to a loading block [177]. When performing insertion experiment the *in vivo* state of the skin should be resembled as close as possible including the stretching of the skin [193], [230].

### **6.3 *In vivo* models**

Often when MNs are tested in *in vivo* settings it is to evaluate a biological outcome not possible in *ex vivo*. This includes delivery of vaccine [190], immunotherapy disease treatment [278], *in situ* measurement of glucose [143] or simply testing tissue damage/MN insertion using TEWL [160]. Often mice, rats or pigs are used for *in vivo* studies [170]. Repeated MN insertion was examined in one study which found that repeated insertion did not alter the skin appearance or barrier function over time based on TEWL measurements. They also found that inflammatory biomarkers were not significantly overexpressed after MN insertion [178].

### **6.4 Artificial skin models**

Several different types of artificial models have been used to simulate skin. Some of them have been liquid suspensions [279], [280], gelatinous substances [281], polymers [272], [282], elastomers [283], epoxy resin [284], metals [285], textiles [286], and layered parafilm [287]. Each of the models was developed for its own purpose and type of investigation. Artificial skin models may prove to be a good alternative to *ex vivo* and *in vivo* tests as they can be more reproducible, but it should be noted that they cannot replace *in vivo* models [288], [289].

#### **6.4.1 Cell-based skin models**

*In vitro* cells cultures can be used to produce an artificial skin layer as a membrane. As reviewed by Choudhury *et al.* it is difficult to include the complexity of cells if they are grown in a 2D monolayer rather than a 3D stack. By growing the cells on a 3D scaffold the cells are more likely to differentiate and allow the relevant expression of receptors, proteins and so forth within the native tissue. Several cell-based skin models are available at present time for different types of tissues. Great technical advances have made it possible to culture systems that are very close to real life tissue [290].

Commercially available and “ready-to-use” cell-based skin models are also an option; however, these can be expensive. Examples of commercially available models are the Vitroskin® (IMS Empowering Product Development, FL, USA) [291], [292] and Bio Skin Plate #30 (Beaulax, Co. LTD, Tokyo, Japan) [293]. In a review by Eudier *et al.*, these two models were selected for testing as they are meant to be easy to handle and affordable. The authors found that Vitroskin® needed hydration before use following a company protocol but had very similar surface properties to the ones of real skin on a human forearm. Bio Skin Plate #30 could be used immediately as-is and exhibited good mechanical properties mimicking those of real human skin [294].

#### **6.4.2 Biologically inactive skin models**

Artificial skin models which are biologically inactive, i.e., meaning that they do not contain living cells, can be reproduced several times and be adapted to exhibit the physical properties of various types of tissue [286]. While *ex vivo* skin samples may provide a more realistic outcome, a polymer-based artificial skin model is sometimes more favorable in research as it can provide more reliable and reproducible results. When discussing reliability, it is worth noting that while measurements performed in these setups can be compared within the same artificial model, the model might not be directly transferable to a real biological system [286], [289]. In the context of this thesis the focus will be on gelatinous substances as these are the primary ones found in literature for MN testing.

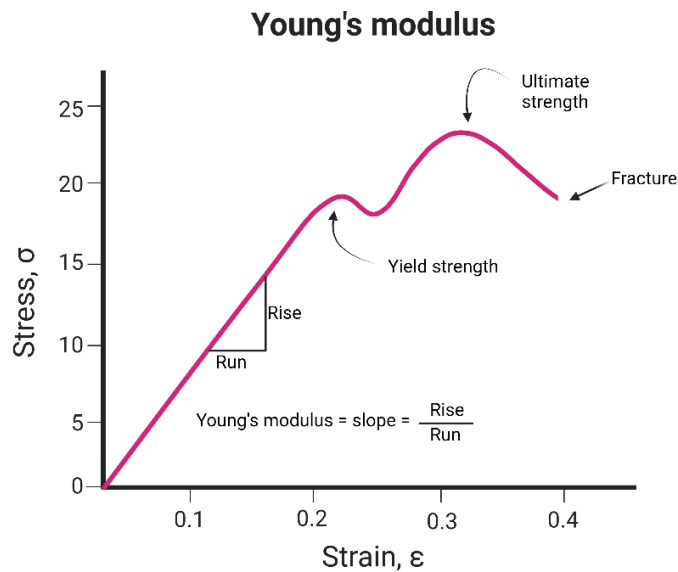
Gelatinous models are water-based, and their mechanical and chemical properties can be controlled. The most often used models within this category are gelatin [281], agar [295], and agarose [296]. Gelatin is a protein obtained from partial hydrolysis of collagen and is present in skin and bones. Dried gelatin has the advantage of a long shelf-life [281] and these types of hydrogels are often used to mimic skin in ballistics tests [297]. Agarose hydrogels have been used as a skin model [298] for testing MNs [189], [299]. Studies have also been performed with multilayered skin-simulating hydrogels where gelatin and agarose were mixed [266] and agar/agarose skin simulants are routinely used [296], [300]. Based on the concentration of agarose added to the water-based solution, the mechanical properties of the hydrogel can be altered [301] and the final hydrogel can simulate various types of tissue such as skin [300] or brain [302], [303].

### **6.5 Validation of artificial and *ex vivo* skin models**

#### **6.5.1 Young’s modulus**

Validation of artificial and *ex vivo* skin models is important when comparing the results to the ones obtained with *in vivo* measurements. Skin models can be validated by investigating their deformation behavior. For example, the elastic modulus, also known as Young’s modulus (YM), can be determined. YM is equal to the slope of the linear region in the stress-strain curve of a solid material as illustrated in Figure 6.2 [304]. The stress-strain curve can be obtained by either compression or tension [305]. YM is a parameter often used for comparison of materials and can be applied to *in vivo* and *ex vivo* skin as well as skin models [306]. YM is defined as stress divided by strain for small strains, i.e., strains that are still within the linear elastic deformation regime where the strained material will return to its original size and shape when the stress is relieved. In other words, YM tells how much a material will elastically deform when a certain stress is applied. If the material does not return to its original form after the stress is relieved, a

permanent residual deformation has occurred. The yield strength is a measure of the stress or strain required to induce a permanent deformation, whereas the breakage or fracture strength is a measure of the stress or strain required for breakage of the material. In the case of skin, the YM is dependent on the resistance of skin to elastic elongation as defined by Hooke's law. Within the elastic range the stress-strain relationship is linear and YM expresses the factor of proportionality [307], [308]. YM may be measured *in vivo* [309], [310], but it can also be measured *ex vivo* on either full-thickness skin (consisting of all skin layers) [150], [195] or separated skin layers [311].



**Figure 6.2: Schematic of a Young's modulus measurement.** Young's modulus (YM) is calculated by measuring the stress/strain relationship and finding the slope of the first (linear) part of the graph. YM can be used for comparing *in vitro* or *ex vivo* skin models with *in vivo* skin. Created with BioRender.com.

### 6.5.2 Validation tests

Studies often compare the YM of the artificial skin model with the one of *ex vivo* or *in vivo* skin [189], [296]. However, there is no golden standard for measuring the YM of skin as it is dependent on several factors such as gender and age [312]–[314]. It has been observed that the physical properties of skin change with age and that the thickness of the skin increases until maturity and then starts to decrease again [315].

There are four main methods for testing the YM of skin, which are indentation [316], torsion [317], tension [261], and suction tests [318]. For the indentation method, a known force is applied to deform the skin, after which the mechanical properties of the skin may be determined. In this case the YM is dependent on the contact dimensions and indentation depth. In the torsion method a constant rotation or torque is applied through an intermediary disk. The tension method is based on loading the skin parallel to its surface and stretching it while measuring the force. Suction is done by applying a circular vacuum to the skin and the deformation can be quantified using ultrasound devices [274], [306].

Pailler-Mattei *et al.* proposed an indentation method for determining the mechanical properties of skin using the stress-strain relationship of *in vivo* skin. While this method is close to the real world, it raises some questions about the influence of the subcutaneous layer and muscle tissue beneath the skin. They therefore suggested using a two-layer elastic skin model to improve the mechanical properties of the skin model [316]. Ahearne *et al.* also used the indentation method to determine YM of hydrogel skin models [296] while Koelmans *et al.* did their compression study using a two-layer model based on agarose gel with a commercially available foil on top to simulate the stratum corneum. They found that the characterization methods complemented *in vivo* experiments well [189]. Simulations are also an option based on experimental results and knowledge about the thickness of skin, water content, and other mechanical properties to predict YM of e.g., the separate skin layers [319], [320].

### 6.5.3 Validation results

Measurements for determining the YM are dependent on both the test method and skin location and due to these variances, the YM reported for human skin varies between 0.42-0.85 MPa for torsion tests [316], [317], 4.6-20 MPa for tension and torsion tests [321], and 0.05-0.15 MPa for suction tests [313], [316], [317]. Wei *et al.* illustrated how much impact just the tip radius of a probe for indentation test has as the YM varied for the studies in humans between 50.3 kPa  $\pm$  19.3 kPa for tip radius 0.18 mm to 2.0 kPa  $\pm$  1.1 kPa for tip radius 3.15 mm [271]. Kalra *et al.* reviewed the four methods for mechanical testing of skin and found that the YM was within the range of 5-100 kPa for indentation tests, within 25-140 kPa for torsion and tension testing, and within 25-260 kPa for suction testing [306]. Table 6.1 provides an overview of YM values found in the literature for the human forearm *in vivo* using the described methods.

The value of YM is not only dependent on the type of testing performed, but also on the structure of the skin. Langer *et al.* mapped the natural lines of skin tension [322] and it was observed by surgeons that incisions done along these lines resulted in little to no scarring. During tensile testing in 1966 it was observed that the characteristics of deformed skin are dependent on the orientation of the skin sample i.e., the Langer lines. YM is thereby dependent on the sample orientation whether it is measured parallel or orthogonal to Langer lines [261].



**Table 6.1: Values of *in vivo* Young's modulus found in literature for the human arm.** Due to the application of the InstaPatch the following table is focused on *in vivo* Young's modulus (YM) values associated with the arm obtained using either indentation, torsion, tension or suction test as described above. The table is meant to give an overview of YM values and their variance.

| Method                    | Young's modulus          |
|---------------------------|--------------------------|
| Indentation test          | 1.11 kPa [323]           |
|                           | 1.09 kPa [323]           |
|                           | 1.51 kPa [323]           |
|                           | 14.0 kPa [324]           |
|                           | 5.1 – 13.3 kPa [325]     |
|                           | 10.7 ± 2.6 kPa [326]     |
|                           | 7.2 ± 2.1 kPa [326]      |
|                           | 14.38 ± 3.61 kPa [327]   |
|                           | 6.20 ± 1.45 kPa [327]    |
|                           | 4.5 – 8 kPa [316]        |
|                           | 12.3 kPa ± 2.6 kPa [309] |
|                           | 7.7kPa ± 1.6 kPa [309]   |
|                           | 5.4 kPa ± 1.2 kPa [309]  |
|                           | 5.67 kPa [328]           |
| 19.46 ± 0.54 kPa [329]    |                          |
| 0,0504 ± 0,0144 kPa [330] |                          |
| 0,0662 ± 0,0107 kPa [330] |                          |
| Torsion test              | 10-100 kPa [314]         |
|                           | 20-50 kPa [314]          |
|                           | 420 kPa [317]            |
|                           | 850 kPa [317]            |
|                           | 1120 kPa [331]           |
| Tension test              | 130 – 657 kPa [332]      |
| Suction test              | 110 – 120 kPa [315]      |
|                           | 80 – 260 kPa [315]       |

Essentially, artificial skin models can be validated by comparison to the YM value obtained from either *in vivo* or *ex vivo* skin measurements to estimate how close the resemblance of the mechanical properties are. Nonetheless, it is worth noting that the method of measuring YM and the sample location should be as similar as possible for the skin simulant and the *ex vivo/in vivo* sample that it is being compared to. This has e.g., been done in hydrogels [296], [333], [334] to ensure as close a comparison as possible even if the YM is not yet optimal.

## 6.6 *In vivo* models for allergy testing

Animal studies are often used within allergy research with rats as one of the most common animal models [145] and the BN rat (*rattus norvegicus*) is particularly suitable as it exhibits excellent IgE sensitization [335]. Other rat strains have been investigated, but seem to fail in the IgE production [336], [337]. The BN rat is commonly used in immunological studies [338] such as allergy studies as their oral sensitization is easily developed [339].

The BN rats have been found to be sensitized when an allergen is provided either orally [340] or by intraperitoneal (i.p.) injection [341]. Sensitization is usually confirmed by determining antigen dose-response and assessing IgE and IgG levels in blood serum. To induce sensitization, the BN rats are given e.g., a food protein regularly and often adjuvants are included which are substances that help create a stronger immune response. In one study they were given ovalbumin with a carrageenan adjuvant twice a week for six weeks to induce sensitization with great success [335].

## **6.7 Selection of skin models for microneedle testing in this project**

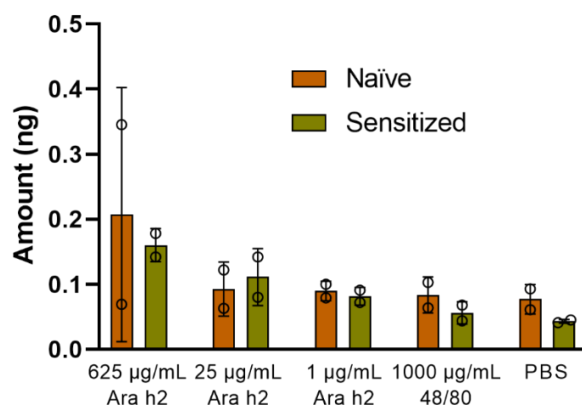
### **6.7.1 Models used in this project**

An agarose skin-simulating hydrogel was selected for testing mechanical stability and penetration ability of MNs in research project I. It had been reported within the literature to be a stable and reproducible model that was simple to set up in the laboratory. A detailed description of the hydrogel skin tissue-simulant is included in manuscript I [127]. Two agarose concentrations were considered, 1.5% and 2% w/v. The resulting hydrogels were tested using compression tests and these results were compared to measurements performed on a volunteer's forearm where the InstaPatch is meant for application. The 1.5% agarose skin-simulating hydrogel was selected as the skin model for MN testing as it had the lowest YM values and was closer to the YM of the forearm.

For *ex vivo* experiments BN rats, porcine ear and neck, and human breast skin samples were used as part of research projects II and III. For *in vivo* experiments BN rats were used as part of research projects III and IV. The BN rat animal model for allergies had already been developed and used in previous studies [342], [343].

### **6.7.2 Research project III (part 2): Preliminary experiments on biomarker detection for mast cell degranulation**

Skin samples were collected at the i.d. injection sites and MN insertion sites of Ara h 2 delivery as part of research project III described in section 5.6.4. To confirm that an allergic response had occurred tryptase was measured in homogenized skin samples using rat tpsab1 ELISA kit (EKR864, Nordic BioSite AB, Täby, Sweden), since tryptase is expected to be released from the MCs during degranulation [61]. For a preliminary study, MNs coated with Ara h 2 solution concentrations ranging from 1 µg/mL to 625 µg/mL were inserted into the skin samples for 60 s and biopsies were taken, snap frozen using liquid nitrogen, and later homogenized. Then it was attempted to quantify the released tryptase in the skin biopsy by performing the ELISA on the homogenate. It was not possible to observe a difference in tryptase response between naïve and sensitized animals (Figure 6.3). As this was only preliminary data and only the skin tissue homogenates from four animals (two naïve and two sensitized) were analyzed more samples should be prepared and tested before drawing too many conclusions.



**Figure 6.3: Recovered tryptase in skin samples from microneedle insertion in animals.** Experiment conducted as a part of research project III with homogenized skin samples after Ara h 2 delivery by microneedles (MNs). MNs were coated with different coating solution concentrations of Ara h 2 (1, 25, 625 µg/mL) and the positive control compound 48/80 (1000 µg/mL) (mean ± SD, n=2).

## 6.8 Summary

This chapter introduced skin models used for testing MNs. These ranged from artificial skin models through *ex vivo* skin samples to *in vivo* models. Skin-simulating hydrogels, excised BN rat skin, porcine skin, and human breast skin samples were used for testing the mechanical stability and penetration of MNs in research projects I and II. Sensitized BN rats were used for *in vivo* animal experiments in research projects III and IV. The most commonly used method for validating skin models is measurement and comparison of YM. YM was used in research project I to compare the skin-simulating hydrogel (artificial skin model) with YM of *in vivo* forearm skin for initial testing of the mechanical stability and penetration ability of the MNs. While YM comparisons are not optimal, they are arguably the best measure of comparison between models at the moment. A standardization of the YM measuring method for skin would be very valuable for future studies using skin models.

## Chapter 7: Conclusions and outlook

This PhD project provided a thorough testing of the penetration ability and mechanical stability of MNs and also investigated coating and delivery using MNs. MN dimensions and shapes were investigated and thoroughly tested, and a simple coating method was established using dip-coating. The final combination of dip-coated MNs with optimized dimensions and shape was tested in *in vivo* animal experiments using sensitized BN rats.

Results from manuscript I showed that the penetration force of MNs could be measured using skin-simulating hydrogels, BN rat skin, and pig ear skin samples. Depending on the selected skin model the force measurements varied, however, for comparison between MN dimensions and tip shapes each of these skin models were shown to function. The MNs did not break during testing in these skin models, thus, showing good mechanical stability. The fracture force was furthermore measured and found to be much higher than the penetration force for all MNs. Tissue damage was estimated using histology of the BN rat and pig ear skin samples. It was generally observed that the triangular shaped MN required the lowest penetration force and caused the least amount of tissue damage. The required penetration force and surface damage induced by these MNs were even shown to be lower than for the SPT needle used in the clinic today. The optimized MN became a hybrid between a triangular and pencil shape to increase the surface area for electrochemistry measurements while minimizing penetration force. The length of the optimized MN was determined to be 1000  $\mu\text{m}$  with a width of 400  $\mu\text{m}$  for increased surface area. Additional surface area was sacrificed by reducing the thickness of the MNs in order to improve the penetration ability. The MNs had a final thickness of 180  $\mu\text{m}$ , which proved to be mechanically stable enough for skin penetration.

Based on study report I, the optimized MNs were tested for their ability to penetrate skin using pig neck and human breast skin and the mechanical stability was further confirmed. MN insertion at 5 N was found to be sufficient for penetration in skin samples, and OCT measurements made it possible not only to confirm the penetration in skin, but the MN holes could also be measured more precisely compared to the histology analysis presented in manuscript I, as these OCT scans were done immediately after retracting the MNs from the skin without having to wait for additional processing steps of the skin which is required for histology. It was found that the penetration depth was dependent on the applied force and that manual insertion had much more variation than when the applied force was controlled by a force gauge. Rows of in-plane MNs were assembled in a 2D-array format and were investigated in terms of the array effect on penetration ability. It was confirmed that the penetration efficiency decreased as more rows were added and therefore that the design of the InstaPatch should be further optimized if the MNs are to go from the single row in-plane format to an out-of-plane 2D-array patch format. Finally, delivery of compound 48/80 was tested in fresh human breast skin to activate MCs and upregulate surface marker CD63, which could then be stained for using IHC. However, the results showed only unspecific binding of the secondary antibody. The IHC would have needed more optimization in order to work and ideally, the coating release should also be further optimized.

The results presented in manuscript II showed that the amount of delivered coating was very small and thus, could not be quantified accurately by measuring the remaining, fluorescent-labeled coating on the

MNs. The delivery was confirmed by cryostat histology where the delivered fluorescent-labeled coating was visible under a fluorescence microscope. It was observed that the delivery molecule influenced the coating, and the coating solution should therefore always be optimized for the individual molecule to be delivered. The coating method should also be further optimized to ensure only coating on the MNs to obtain a more exact measure of the delivered dose. This would also provide a more accurate estimation of delivery efficiency using the fluorescence quantification method.

Using PPE-sensitized BN rats with i.v. injection of Evans blue for visualization of reactions, gave a few clear dose-response curves for rats receiving Ara h 2 i.d. injections, while rats receiving Ara h 2-coated MN insertions gave no measurable reaction compared to the negative controls. Study report II functioned as an extension of manuscript II where both the BPE and Bet v 1 was applied instead of Ara h 2. Rats were sensitized using BPE and similar results were obtained from this study where no significant measurable reaction against BPE or Bet v 1 could be achieved using the MNs even if the results from i.d. injection in the rats were better than in manuscript II for Ara h 2.

The dip-coating method used in this study coated not only the MNs, but also the base from which the MNs extrude. This meant that due to the large background fluorescence coming from the coating on the base, the small decrease in remaining fluorescence signal became difficult to quantify. It would therefore be ideal to optimize the dip-coating method to only coat the MNs. It was estimated in section 5.6.2 that the combined amount of coated surface area on the three MNs was only 12% of the total coated area. This estimation assumed that the coating had the same thickness over all coated surfaces.

Tryptase which is released during MC activation and degranulation was measured using an ELISA kit on homogenized skin samples obtained in research project III (see section 6.7.2). The preliminary data suggested no measurable difference between the tryptase found in naïve and sensitized rats. Nonetheless, only four rats were included in this preliminary study, and hence, it is recommendable to run this ELISA again with more samples and rats.

As an overall conclusion, the MNs were shown to possess sufficient mechanical stability and be able to penetrate skin-simulating hydrogels, rat, pig, and human skin samples using very low penetration forces. The MNs could be coated with various molecules and small amounts delivered. It was not possible to get a significant measurable allergic response in sensitized BN rats using coated MNs.

## 7.1 Outlook

As some of the results from the research projects conducted within this PhD thesis were inconclusive due to limited time further investigations into these subjects would be of utmost relevance. The outlooks for the various subjects are outlined below.

### Coating solution and method:

The dip-coating method should be further optimized so only the MNs are coated, and more coating methods should be investigated and potentially optimized. Inkjet printing could be promising and provide a more controlled coating strategy as a droplet, or a series of droplets can be applied to each individual MN. This would also ease the process of coating several different allergens on separate MNs later on. The delivery efficiency needs to be improved by optimizing the solution of the coating for the individual allergen to be delivered. For this purpose, fluorescent-labeled molecules or fluorescent-conjugated allergens could be applicable to measure delivery efficiency. The delivered dose should be quantified as it was not possible to accurately quantify this in research project III. This may be possible once the coating method is optimized to only coat MNs, otherwise the amount of molecules for delivery could be measured by other means – the MNs could e.g., be weighed on a sensitive weight before and after coating and delivery. It could be interesting further to confirm delivery by IHC targeting the specific allergen (e.g., Ara h 2) or CD63 after compound 48/80 delivery as attempted in research project II when the delivery has been optimized.

### *In vivo* animal experiments:

It would be good to complement the image analysis of Evans blue with quantitative measurements as Evans blue can be measured using a spectrophotometer. Homogenized skin samples to which the allergen was delivered after i.v. injection of Evans blue could be used for the purpose of quantifying the Evans blue reaction using spectrophotometry. A local allergic reaction after MN insertion with allergen-coating should be confirmed by other means such as detecting biomarkers strongly associated with an allergic response. This was attempted using a tryptase ELISA kit on homogenized skin samples, however, the preliminary data did not provide any firm conclusions. The test should therefore be repeated with more samples from more rats and potentially, the ELISA would need some optimization too. As described in section 2.5 there are some potential biomarkers specifically for MC degranulation, which could be targeted such as surface marker CD63 or the biomarkers tryptase, histamine or  $\beta$ -hexosaminidase. The *in vivo* animal experiments could also be designed to include an allergen that the animals should not respond to as a second negative control.

All things considered; much optimization is still needed in order to realize the InstaPatch.

## Bibliography

- [1] R. Pawankar, "Allergic diseases and asthma: A global public health concern and a call to action," *World Allergy Organ. J.*, vol. 7, no. 1, pp. 1–3, 2014.
- [2] P. Kuna *et al.*, "The role and choice criteria of antihistamines in allergy management - expert opinion," *Postep. Dermatologii i Alergol.*, vol. 33, no. 6, pp. 397–410, 2016.
- [3] S. J. Galli, M. Tsai, and A. M. Piliponsky, "The development of allergic inflammation," *Nature*, vol. 454, no. July, pp. 445–454, 2008.
- [4] S. Kumar, A. K. Verma, M. Das, and P. D. Dwivedi, "Molecular mechanisms of IgE mediated food allergy," *Int. Immunopharmacol.*, vol. 13, no. 4, pp. 432–439, 2012.
- [5] R. Pawankar, T. Holgate, Stephen, G. W. Canonica, R. Lockey, and M. S. Blaiss, *WAO - White Book on Allergy*, vol. 30, no. 4. 2013.
- [6] L. Heinzerling *et al.*, "The skin prick test - European standards," *Clin. Transl. Allergy*, vol. 3, no. 1, pp. 1–10, 2013.
- [7] J. Antunes, L. Borrego, A. Romeira, and P. Pinto, "Skin prick tests and allergy diagnosis," vol. 37, no. 3, pp. 155–164, 2009.
- [8] A. M. Silverstein, "Clemens Freiherr von Pirquet : Explaining immune complex disease in 1906," vol. 1, no. 6, pp. 453–455, 2000.
- [9] E. H. Tham and D. Y. M. Leung, "Mechanisms by which atopic dermatitis predisposes to food allergy and the atopic March," *Allergy, Asthma Immunol. Res.*, vol. 11, no. 1, pp. 4–15, 2019.
- [10] D. A. Hill, R. W. Grundmeier, G. Ram, and J. M. Spergel, "The epidemiologic characteristics of healthcare provider-diagnosed eczema, asthma, allergic rhinitis, and food allergy in children: A retrospective cohort study," *BMC Pediatr.*, vol. 16, no. 1, pp. 1–8, 2016.
- [11] *Oxford Concise Medical Dictionary*, 9th ed. Oxford Quick Reference, 2015.
- [12] S. S. Deo, K. J. Mistry, A. M. Kakade, and P. V. Niphadkar, "Role played by Th2 type cytokines in IgE mediated allergy and asthma," *Lung India*, vol. 27, no. 2, pp. 66–71, 2010.
- [13] F. Savino *et al.*, "Analysis of Serum Th2 Cytokines in Infants with Non-IgE Mediated Food Allergy Compared to Healthy Infants," *Nutrients*, vol. 14, no. 8, pp. 1–9, 2022.
- [14] L. Merras-Salmio, K. L. Kolho, A. S. Pelkonen, M. Kuitunen, M. J. Mäkelä, and E. Savilahti, "Markers of gut mucosal inflammation and cow's milk specific immunoglobulins in non-IgE cow's milk allergy," *Clin. Transl. Allergy*, vol. 4, no. 1, pp. 1–8, 2014.
- [15] S. Romagnani, "Coming back to a missing immune deviation as the main explanatory mechanism for the hygiene hypothesis," *J. Allergy Clin. Immunol.*, vol. 119, no. 6, pp. 1511–1513, 2007.
- [16] D. P. Strachan, "Hay fever, hygiene, and household size," *J. Fam. Hist.*, vol. 299, no. 3, pp. 1259–1260, 1989.
- [17] R. X. Foong, G. du Toit, and A. T. Fox, "Asthma, food allergy, and how they relate to each other," *Front. Pediatr.*, vol. 5, no. May, pp. 1–6, 2017.

- [18] S. M. Tariq, S. M. Matthews, E. A. Hakim, and S. H. Arshad, "Egg allergy in infancy predicts respiratory allergic disease by 4 years of age," *Pediatr. Allergy Immunol.*, vol. 11, no. 3, pp. 162–167, 2000.
- [19] C. Caffarelli, M. Garrubba, C. Greco, C. Mastroilli, and C. P. Dascola, "Asthma and food allergy in children: Is there a connection or interaction?," *Front. Pediatr.*, vol. 4, no. APR, pp. 1–7, 2016.
- [20] C. H. Katelaris and P. J. Beggs, "Climate change: allergens and allergic diseases," *Intern. Med. J.*, vol. 48, no. 2, pp. 129–134, 2018.
- [21] T. V. Rajan, "The Gell-Coombs classification of hypersensitivity reactions: A re-interpretation," *Trends Immunol.*, vol. 24, no. 7, pp. 376–379, 2003.
- [22] M. C. Dispenza, "Classification of hypersensitivity reactions," *Allergy Asthma Proc.*, vol. 40, no. 6, pp. 470–473, 2019.
- [23] S. McClain, "Bioinformatic screening and detection of allergen cross-reactive IgE-binding epitopes," vol. 1600676, pp. 1–14, 2017.
- [24] E. Jarolim *et al.*, "IgE and IgG antibodies of patients with allergy to birch pollen as tools to define the allergen profile of *Betula verrucosa*\*," *Allergy*, vol. 44, no. 6, pp. 385–395, 1989.
- [25] S. K. Jeong *et al.*, "Mite and cockroach allergens activate protease-activated receptor 2 and delay epidermal permeability barrier recovery," *J. Invest. Dermatol.*, vol. 128, no. 8, pp. 1930–1939, 2008.
- [26] V. Leduc, D. A. Moneret-Vautrin, J. T. C. Tzen, M. Morisset, L. Guerin, and G. Kanny, "Identification of oleosins as major allergens in sesame seed allergic patients," *Allergy Eur. J. Allergy Clin. Immunol.*, vol. 61, no. 3, pp. 349–356, 2006.
- [27] F. Holzweber *et al.*, "Inhibition of IgE binding to cross-reactive carbohydrate determinants enhances diagnostic selectivity," *Allergy Eur. J. Allergy Clin. Immunol.*, vol. 68, no. 10, pp. 1269–1277, 2013.
- [28] E. K. Lakey, E. Margoliash, and S. K. Pierce, "Identification of a peptide binding protein that plays a role in antigen presentation," *Proc. Natl. Acad. Sci. U. S. A.*, vol. 84, no. 6, pp. 1659–1663, 1987.
- [29] B. Eiz-Vesper and H. M. Schmetzer, "Antigen-presenting cells: Potential of proven und new players in immune therapies," *Transfus. Med. Hemotherapy*, vol. 47, no. 6, pp. 429–431, 2020.
- [30] Z. Liu *et al.*, "IL-2 and Autocrine IL-4 Drive the In Vivo Development of Antigen-Specific Th2 T Cells Elicited by Nematode Parasites," *J. Immunol.*, vol. 174, no. 4, pp. 2242–2249, 2005.
- [31] C. L. Sokol, G. M. Barton, A. G. Farr, and R. Medzhitov, "A mechanism for the initiation of allergen-induced T helper type 2 responses," vol. 9, no. 3, pp. 310–318, 2008.
- [32] M. A. Berkowska, J. J. Heeringa, E. Hajdarbegovic, and M. Van Der Burg, "Human IgE 1 B cells are derived from T cell – dependent and T cell – independent pathways," *J. Allergy Clin. Immunol.*, vol. 134, no. 3, pp. 688-697.e6, 2014.
- [33] R. S. Geha, H. H. Jabara, and S. R. Brodeur, "The regulation of immunoglobulin E class-switch recombination," *Nature Reviews Immunology*, vol. 3, no. 9, pp. 721–732, 2003.
- [34] P. D. Hodgkin, J. H. Lee, and A. B. Lyons, "B cell differentiation and isotype switching is related to



- division cycle number," *J. Exp. Med.*, vol. 184, no. 1, pp. 277–281, 1996.
- [35] K. Murphy and C. Weaver, *Janeway's Immunobiology*, 9th editio. 2016.
- [36] W. Yu, D. M. H. Freeland, and K. C. Nadeau, "Food allergy: Immune mechanisms, diagnosis and immunotherapy," *Nat. Rev. Immunol.*, vol. 16, no. 12, pp. 751–765, 2016.
- [37] M. Swieter, C. Rimmere, K. Mcneillo, A. Froeseo, and D. Befus, "Isolation and characterization of IgE receptors from rat intestinal mucosal mast cells," *Eur. J. Immunol.*, pp. 1879–1885, 1989.
- [38] K. Amin, "The role of mast cells in allergic inflammation," *Respir. Med.*, vol. 106, no. 1, pp. 9–14, 2012.
- [39] M. H. Shamji *et al.*, "The role of allergen-specific IgE, IgG and IgA in allergic disease," *Allergy Eur. J. Allergy Clin. Immunol.*, vol. 76, no. 12, pp. 3627–3641, 2021.
- [40] S. J. Galli, S. Nakae, and M. Tsai, "Mast cells in the development of adaptive immune responses," *Nat. Immunol.*, vol. 6, no. 2, pp. 135–142, 2005.
- [41] S. Wernersson and G. Pejler, "Mast cell secretory granules : armed for battle," vol. 14, no. JULY, 2014.
- [42] W. D. Paton, "Compound 48/80: A potent histamine liberator," *Br. J. Pharmacol. Chemother.*, vol. 6, no. 3, pp. 499–508, 1951.
- [43] K. Tatemoto *et al.*, "Endogenous protein and enzyme fragments induce immunoglobulin E-independent activation of mast cells via a G protein-coupled receptor, MRGPRX2," *Scand. J. Immunol.*, vol. 87, no. 5, 2018.
- [44] S. I. Mayr *et al.*, "IgE-Dependent Mast Cell Activation Potentiates Airway Responses in Murine Asthma Models," *J. Immunol.*, vol. 169, no. 4, pp. 2061–2068, 2002.
- [45] E. Shumilina *et al.*, "Blunted IgE-Mediated Activation of Mast Cells in Mice Lacking the Ca<sup>2+</sup>-Activated K<sup>+</sup> Channel KCa3.1," *J. Immunol.*, vol. 180, no. 12, pp. 8040–8047, 2008.
- [46] D. D. Metcalfe *et al.*, "Biomarkers of the involvement of mast cells, basophils and eosinophils in asthma and allergic diseases," *World Allergy Organ. J.*, vol. 9, no. 1, pp. 1–15, 2016.
- [47] J. M. Brown, T. M. Wilson, and D. D. Metcalfe, "The mast cell and allergic diseases : role in pathogenesis and implications for therapy Clinical and Experimental Allergy," pp. 4–18, 2007.
- [48] W. E. Paul and J. Zhu, "How are TH2-type immune responses initiated and amplified?," *Nat Rev Immunol*, vol. 10, no. 4, pp. 225–235, 2010.
- [49] K. Amin *et al.*, "Inflammation and Structural Changes in the Airways of Patients with Atopic and Nonatopic Asthma," vol. 162, no. 8, pp. 2295–2301, 2000.
- [50] A. S. Janssens, R. Heide, J. C. Den Hollander, P. G. M. Mulder, B. Tank, and A. P. Oranje, "Mast cell distribution in normal adult skin," *J. Clin. Pathol.*, vol. 58, no. 3, pp. 285–289, 2005.
- [51] A. Weber, J. Knop, and M. Maurer, "Pattern analysis of human cutaneous mast cell populations by total body surface mapping," *Br. J. Dermatol.*, vol. 148, no. 2, pp. 224–228, 2003.
- [52] T. Schäfer, P. Starkl, C. Allard, R. M. Wolf, and T. Schweighoffer, "A granular variant of CD63 is a regulator of repeated human mast cell degranulation," *Allergy Eur. J. Allergy Clin. Immunol.*, vol.

- 65, no. 10, pp. 1242–1255, 2010.
- [53] Z. Orinska, P. M. Hagemann, I. Halova, and P. Draber, “Tetraspanins in the regulation of mast cell function,” *Med. Microbiol. Immunol.*, vol. 209, no. 4, pp. 531–543, 2020.
- [54] K. Kabashima *et al.*, “Biomarkers for evaluation of mast cell and basophil activation,” *Immunol. Rev.*, vol. 282, no. 1, pp. 114–120, 2018.
- [55] L. B. Schwartz, R. A. Lewis, D. Seldin, and K. F. Austen, “Acid hydrolases and tryptase from secretory granules of dispersed human lung mast cells,” *J. Immunol.*, vol. 126, no. 4, pp. 1290–1294, 1981.
- [56] L. B. Schwartz, A. M. Irani, K. Roller, M. C. Castells, and N. M. Schechter, “Quantitation of histamine, tryptase, and chymase in dispersed human T and TC mast cells,” *J. Immunol.*, vol. 138, no. 8, pp. 2611–2615, 1987.
- [57] J. S. Miller, E. H. Westin, and L. B. Schwartz, “Cloning and characterization of complementary DNA for human tryptase,” *J. Clin. Invest.*, vol. 84, no. 4, pp. 1188–1195, 1989.
- [58] T. P. Waalkes, H. Weissbach, J. Bozicevich, and S. Udenfriend, “Serotonin and histamine release during anaphylaxis in the rabbit,” *J. Clin. Invest.*, vol. 36, no. 7, pp. 1115–1120, 1957.
- [59] Y. Nakamura, K. Ishimaru, S. Shibata, and A. Nakao, “Regulation of plasma histamine levels by the mast cell clock and its modulation by stress,” *Sci. Rep.*, vol. 7, no. November 2016, pp. 1–12, 2017.
- [60] I. Pollock, R. D. Murdoch, and M. H. Lessof, “Plasma histamine and clinical tolerance to infused histamine in normal, atopic and urticarial subjects,” *Agents Actions*, vol. 32, no. 3–4, pp. 359–365, 1991.
- [61] V. Payne and P. C. A. Kam, “Mast cell tryptase: A review of its physiology and clinical significance,” *Anaesthesia*, vol. 59, no. 7, pp. 695–703, 2004.
- [62] A. Sverrild *et al.*, “Genetic factors account for most of the variation in serum tryptase - A twin study,” *Ann. Allergy, Asthma Immunol.*, vol. 111, no. 4, pp. 286–289, 2013.
- [63] R. L. Stevens, C. C. Fox, L. M. Lichtenstein, and K. F. Austen, “Identification of chondroitin sulfate E proteoglycans and heparin proteoglycans in the secretory granules of human lung mast cells,” *Proc. Natl. Acad. Sci. U. S. A.*, vol. 85, no. 7, pp. 2284–2287, 1988.
- [64] N. Fukuishi *et al.*, “Does  $\beta$ -Hexosaminidase Function Only as a Degranulation Indicator in Mast Cells? The Primary Role of  $\beta$ -Hexosaminidase in Mast Cell Granules,” *J. Immunol.*, vol. 193, no. 4, pp. 1886–1894, 2014.
- [65] J. Kalesnikoff *et al.*, “Monomeric IgE stimulates signaling pathways in mast cells that lead to cytokine production and cell survival,” *Immunity*, vol. 14, no. 6, pp. 801–811, 2001.
- [66] R. Greene *et al.*, “Sensory Neurons in Vitro Excite Vagal Sensory Neurons in Vitro,” pp. 2249–2253, 2013.
- [67] C. Gonzalez-Espinosa *et al.*, “Preferential signaling and induction of allergy-promoting lymphokines upon weak stimulation of the high affinity IgE receptor on mast cells,” *J. Exp. Med.*, vol. 197, no. 11, pp. 1453–1465, 2003.

- [68] J. A. Price, "Microplate assay for measurement of histamine release from mast cells," *Biotechniques*, vol. 22, no. 5, pp. 958–962, 1997.
- [69] L. B. Schwartz *et al.*, "Development of a new, more sensitive immunoassay for human tryptase: Use in systemic anaphylaxis," *J. Clin. Immunol.*, vol. 14, no. 3, pp. 190–204, 1994.
- [70] R. M. Z. G. Naal, J. Tabb, D. Holowka, and B. Baird, "In situ measurement of degranulation as a biosensor based on RBL-2H3 mast cells," *Biosens. Bioelectron.*, vol. 20, no. 4, pp. 791–796, 2004.
- [71] J. Vitte, "Human mast cell tryptase in biology and medicine," *Mol. Immunol.*, vol. 63, no. 1, pp. 18–24, 2015.
- [72] M. Pallaoro, M. S. Fejzo, L. Shayesteh, J. L. Blount, and G. H. Caughey, "Characterization of genes encoding known and novel human mast cell tryptases on chromosome 16p13.3," *J. Biol. Chem.*, vol. 274, no. 6, pp. 3355–3362, 1999.
- [73] J. A. Boyce *et al.*, *Guidelines for the diagnosis and management of food allergy in the United States: Report of the NIAID-sponsored expert panel*, vol. 126, no. 6 SUPPL. Elsevier Ltd, 2010.
- [74] P. Comtois, "The experimental research of Charles H. Blackley," *Aerobiologia (Bologna)*, vol. 11, no. 1, pp. 63–68, 1995.
- [75] O. Coetzee *et al.*, "Allergy Diagnostic Testing: An Updated Practice Parameter," *Ann. ALLERGY, ASTHMA Immunol.*, vol. 100, p. 15, 2008.
- [76] "Vascular reactions of the skin to injury," *Lancet*, pp. 279–280, 1924.
- [77] X. Justo, I. Díaz, J. J. Gil, and G. Gastaminza, "Prick test: evolution towards automated reading," *Allergy: European Journal of Allergy and Clinical Immunology*, vol. 71, no. 8, pp. 1095–1102, 2016.
- [78] P. A. Østergaard, F. Ebbesen, H. Nolte, and P. S. Skov, "Basophil histamine release in the diagnosis of house dust mite and dander allergy of asthmatic children: Comparison between prick test, RAST, basophil histamine release and bronchial provocation," *Allergy*, vol. 45, no. 3, pp. 231–235, 1990.
- [79] J. Cannon and P. Cullinan, "Skin prick testing," *Occup. Med. (Chic. Ill)*, vol. 69, no. 4, pp. 298–299, 2019.
- [80] J. P. M. Van Der Valk, R. G. Van Wijk, E. Hoorn, L. Groenendijk, I. M. Groenendijk, and N. W. De Jong, "Measurement and interpretation of skin prick test results," *Clin. Transl. Allergy*, pp. 6–10, 2016.
- [81] U. Bodtger, C. R. Jacobsen, L. K. Poulsen, and H. J. Malling, "Long-term repeatability of the skin prick test is high when supported by history or allergen-sensitivity tests: A prospective clinical study," *Allergy Eur. J. Allergy Clin. Immunol.*, vol. 58, no. 11, pp. 1180–1186, 2003.
- [82] O. Østerballe and B. Weeke, "A New Lancet for Skin Prick Testing," *Allergy*, vol. 34, no. 4, pp. 209–212, 1979.
- [83] H. S. Nelson, J. Lahr, A. Buchmeier, and D. McCormick, "Clinical aspects of allergic disease: Evaluation of devices for skin prick testing," *J. Allergy Clin. Immunol.*, vol. 101, no. 2 I, pp. 153–156, 1998.

- [84] W. W. Carr, B. Martin, R. S. Howard, L. Cox, and L. Borish, "Comparison of test devices for skin prick testing," *J. Allergy Clin. Immunol.*, vol. 116, no. 2, pp. 341–346, 2005.
- [85] S. Wöhrl, K. Vigl, M. Binder, G. Stingl, and M. Prinz, "Automated measurement of skin prick tests: An advance towards exact calculation of wheal size," *Exp. Dermatol.*, vol. 15, no. 2, pp. 119–124, 2006.
- [86] T. C. Li Kam Wa, N. E. Almond, E. D. Cooke, and P. Turner, "Skin blood flow changes following intradermal bradykinin injections measured by laser doppler flowmetry: Comparison with weal and flare," *J. Med. Eng. Technol.*, vol. 14, no. 5, pp. 190–193, 1990.
- [87] M. Nyrén, S. Ollmar, I. Nicander, and L. Emtestam, "An electrical impedance technique for assessment of wheals," *Allergy Eur. J. Allergy Clin. Immunol.*, vol. 51, no. 12, pp. 923–926, 1996.
- [88] E. Rokita, T. Rok, and G. Tatoń, "Application of thermography for the assessment of allergen-induced skin reactions," *Med. Phys.*, vol. 38, no. 2, pp. 765–772, 2011.
- [89] O. Bulan, "Improved wheal detection from skin prick test images," *Image Process. Mach. Vis. Appl. VII*, vol. 9024, no. March 2014, p. 90240J, 2014.
- [90] B. Chinoy, E. Yee, and S. L. Bahna, "Skin testing versus radioallergosorbent testing for indoor allergens," *Clin. Mol. Allergy*, vol. 3, no. Id, pp. 1–7, 2005.
- [91] S. G. O. Johansson, "for research and routine allergy diagnosis ImmunoCAP® Specific IgE test : an objective tool for research," vol. 7159, 2014.
- [92] M. M. D. Fisher and C. J. Bowey, "Intradermal compared with prick testing in the diagnosis of anaesthetic allergy," *Br. J. Anaesth.*, vol. 79, no. 1, pp. 59–63, 1997.
- [93] R. Asero *et al.*, "IgE-mediated food allergy diagnosis: Current status and new perspectives," *Mol. Nutr. Food Res.*, vol. 51, no. 1, pp. 135–147, 2007.
- [94] F. Rancé, A. Juchet, F. Brémont, and G. Dutau, "Correlations between skin prick tests using commercial extracts and fresh foods, specific IgE, and food challenges," *Allergy Eur. J. Allergy Clin. Immunol.*, vol. 52, no. 10, pp. 1031–1035, 1997.
- [95] C. D. May, "Objective clinical and laboratory studies of immediate hypersensitivity reactions to foods in asthmatic children," *J. Allergy Clin. Immunol.*, vol. 58, no. 4, pp. 500–515, 1976.
- [96] H. A. Sampson *et al.*, "Standardizing double-blind, placebo-controlled oral food challenges: American Academy of Allergy, Asthma & Immunology-European Academy of Allergy and Clinical Immunology PRACTALL consensus report," *J. Allergy Clin. Immunol.*, vol. 130, no. 6, pp. 1260–1274, 2012.
- [97] H. Majamaa, P. Moisio, K. Holm, H. Kautiainen, and K. Turjanmaa, "Cow's milk allergy: Diagnostic accuracy of skin prick and patch tests and specific IgE," *Allergy Eur. J. Allergy Clin. Immunol.*, vol. 54, no. 4, pp. 346–351, 1999.
- [98] B. Y. Chung, H. O. Kim, C. W. Park, and C. H. Lee, "Diagnostic usefulness of the serum-specific IgE, the skin prick test and the atopy patch test compared with that of the oral food challenge test," *Ann. Dermatol.*, vol. 22, no. 4, pp. 404–411, 2010.
- [99] P. Stahl Skov, S. Norn, and B. Weeke, "A new method for detecting histamine release," *Agents Actions*, vol. 14, no. 3–4, pp. 414–416, 1984.

- [100] P. Stahl Skov, H. Mosbech, S. Norn, and B. Weeke, "Sensitive Glass Microfibre-Based Histamine Analysis for Allergy Testing in Washed Blood Cells: Results Compared with Conventional Leukocyte Histamine Release Assay," *Allergy*, vol. 40, no. 3, pp. 213–218, 1985.
- [101] K. Mukai *et al.*, "Assessing basophil activation by using flow cytometry and mass cytometry in blood stored 24 hours before analysis," *J. Allergy Clin. Immunol.*, vol. 139, no. 3, pp. 889-899.e11, 2017.
- [102] H. Nolte, K. Storm, and P. O. Schiøtz, "Diagnostic value of a glass fibre-based histamine analysis for allergy testing in children," *Allergy*, vol. 45, no. 3, pp. 213–223, 1990.
- [103] B. Nayak, Z. Li, I. Ahmed, and H. Lin, "Removal of Allergens in Some Food Products Using Ultrasound," in *Ultrasound: Advances in Food Processing and Preservation*, no. 1, Elsevier Inc., 2017, pp. 267–292.
- [104] L. K. Poulsen, "In vivo and in vitro techniques to determine the biological activity of food allergens," *J. Chromatogr. B Biomed. Sci. Appl.*, vol. 756, no. 1–2, pp. 41–55, 2001.
- [105] L. F. Larsen *et al.*, "A comparative study on basophil activation test, histamine release assay, and passive sensitization histamine release assay in the diagnosis of peanut allergy," *Allergy Eur. J. Allergy Clin. Immunol.*, vol. 73, no. 1, pp. 137–144, 2018.
- [106] M. Iversen and S. Norn, "Examination of serum IgE specific to pig protein in pig farmers by histamine release test," *Ann. Agric. Environ. Med.*, vol. 7, no. 2, pp. 85–88, 2000.
- [107] E. C. McGowan and S. Saini, "Update on the performance and application of basophil activation tests," *Curr. Allergy Asthma Rep.*, vol. 13, no. 1, pp. 101–109, 2013.
- [108] M. L. Sanz *et al.*, "Allergen-induced basophil activation: CD63 cell expression detected by flow cytometry in patients allergic to *Dermatophagoides pteronyssinus* and *Lolium perenne*," *Clin. Exp. Allergy*, vol. 31, no. 7, pp. 1007–1013, 2001.
- [109] A. F. Santos *et al.*, "Basophil activation test discriminates between allergy and tolerance in peanut-sensitized children," *J. Allergy Clin. Immunol.*, vol. 134, no. 3, pp. 645–652, 2014.
- [110] O. V. Hausmann, T. Gentinetta, M. Fux, S. Ducrest, W. J. Pichler, and C. A. Dahinden, "Robust expression of CCR3 as a single basophil selection marker in flow cytometry," *Allergy Eur. J. Allergy Clin. Immunol.*, vol. 66, no. 1, pp. 85–91, 2011.
- [111] D. MacGlashan Jr., "Expression of CD203c and CD63 in Human Basophils: Relationship to Differential Regulation of Piecemeal and Anaphylactic Degranulation Processes," *Clin Exp Allergy*, vol. 40, no. 9, pp. 1365–1377, 2010.
- [112] A. F. Santos, M. D. Kulis, and H. A. Sampson, "Bringing the Next Generation of Food Allergy Diagnostics Into the Clinic," *J. Allergy Clin. Immunol. Pract.*, vol. 10, no. 1, pp. 1–9, 2022.
- [113] A. F. Santos, N. Couto-Francisco, N. Bécares, M. Kwok, H. T. Bahnson, and G. Lack, "A novel human mast cell activation test for peanut allergy," *J. Allergy Clin. Immunol.*, vol. 142, no. 2, pp. 689-691.e9, 2018.
- [114] I. Y. S. Tam, H. Y. A. Lau, S. Y. Tam, and T. H. Lee, "Mast cell activation test using patient-derived mast cells exhibits distinct combinatorial phenotypic profiles among allergic patients," *Allergy Eur. J. Allergy Clin. Immunol.*, vol. 75, no. 7, pp. 1796–1799, 2020.

- [115] R. Bahri *et al.*, "Mast cell activation test in the diagnosis of allergic disease and anaphylaxis," *J. Allergy Clin. Immunol.*, vol. 142, no. 2, pp. 485-496.e16, 2018.
- [116] D. G. Ebo *et al.*, "Flow-based allergen testing: Can mast cells beat basophils?," *Clin. Chim. Acta*, vol. 532, no. March, pp. 64–71, 2022.
- [117] J. Elst *et al.*, "Mast cell activation tests by flow cytometry: A new diagnostic asset?," *Clin. Exp. Allergy*, vol. 51, no. 11, pp. 1482–1500, 2021.
- [118] J. Elst *et al.*, "Mast cell activation test in chlorhexidine allergy: a proof of concept," *Br. J. Anaesth.*, vol. 125, no. 6, pp. 970–975, 2020.
- [119] N. Cop *et al.*, "Influence of IL-6, IL-33, and TNF- $\alpha$  on human mast cell activation: Lessons from single cell analysis by flow cytometry," *Cytom. Part B - Clin. Cytom.*, vol. 94, no. 3, pp. 405–411, 2018.
- [120] N. Cop *et al.*, "Phenotypic and functional characterization of in vitro cultured human mast cells," *Cytom. Part B - Clin. Cytom.*, vol. 92, no. 5, pp. 348–354, 2017.
- [121] R. Joulia, F. E. L'Faqihi, S. Valitutti, and E. Espinosa, "IL-33 fine tunes mast cell degranulation and chemokine production at the single-cell level," *J. Allergy Clin. Immunol.*, vol. 140, no. 2, pp. 497-509.e10, 2017.
- [122] R. A. Wood, W. Phipatanakul, R. G. Hamilton, and P. A. Eggleston, "A comparison of skin prick tests , intradermal skin tests , and RASTs in the diagnosis of cat allergy," pp. 773–779, 1999.
- [123] E. Calamelli, L. Liotti, I. Beghetti, V. Piccinno, L. Serra, and P. Bottau, "Component-Resolved Diagnosis in Food Allergies," pp. 1–20, 2019.
- [124] C. Panaitescu *et al.*, "Precision medicine in the allergy clinic: the application of component resolved diagnosis," *Expert Rev. Clin. Immunol.*, vol. 18, no. 2, pp. 145–162, 2022.
- [125] A. S. Miguel-rod ríguez *et al.*, "Clinica Chimica Acta Component-resolved diagnosis in allergic disease : Utility and limitations," *Clin. Chim. Acta*, vol. 489, no. August 2018, pp. 219–224, 2019.
- [126] D. G. Ebo *et al.*, "Component-resolved diagnosis from latex allergy by microarray Clinical & Experimental Allergy," no. Ccd, pp. 348–358, 2009.
- [127] S. I. Bisgaard, L. Q. Nguyen, K. L. B gh, and S. S. Keller, "Dermal Tissue Penetration of In-plane Silicon Microneedles Evaluated in Skin-simulating Hydrogel, Rat Skin, and Porcine Skin," 2023.
- [128] S. I. Bisgaard *et al.*, "Evaluation of In-plane Silicon Microneedle Insertion and Delivery of Compound 48/80 in Porcine and Human Breast Skin Samples," 2023.
- [129] D. V. McAllister, S. Henry, M. G. Allen, and M. R. Prausnitz, "Microfabricated microneedles: A novel approach to transdermal drug delivery," *Proc. Control. Release Soc.*, vol. 87, no. 25, pp. 30–31, 1998.
- [130] M. Cormier *et al.*, "Transdermal delivery of desmopressin using a coated microneedle array patch system," *J. Control. Release*, vol. 97, no. 3, pp. 503–511, 2004.
- [131] N. Ogai *et al.*, "Enhanced immunity in intradermal vaccination by novel hollow microneedles," *Ski. Res. Technol.*, vol. 24, no. 4, pp. 630–635, 2018.
- [132] K. van der Maaden, R. Luttge, P. J. Vos, J. Bouwstra, G. Kersten, and I. Ploemen, "Microneedle-

- based drug and vaccine delivery via nanoporous microneedle arrays," *Drug Deliv. Transl. Res.*, vol. 5, no. 4, pp. 397–406, 2015.
- [133] Y. Zhang, K. Brown, K. Siebenaler, A. Determan, D. Dohmeier, and K. Hansen, "Development of lidocaine-coated microneedle product for rapid, safe, and prolonged local analgesic action," *Pharm. Res.*, vol. 29, no. 1, pp. 170–177, 2012.
- [134] P. M. Sullivan SP, Koutsonanos DG, Del Pilar Martin M, Lee JW, Zarnitsyn V, Choi SO, Murthy N, Compans RW, Skountzou I, "Dissolving Polymer Microneedle Patches for Influenza Vaccination," *Nat. Med.*, vol. 16, no. 18, pp. 915–920, 2010.
- [135] Y. C. Kim, J. H. Park, and M. R. Prausnitz, "Microneedles for drug and vaccine delivery," *Adv. Drug Deliv. Rev.*, vol. 64, no. 14, pp. 1547–1568, 2012.
- [136] J. Zhu *et al.*, "Gelatin Methacryloyl Microneedle Patches for Minimally Invasive Extraction of Skin Interstitial Fluid," *Small*, vol. 16, no. 16, pp. 1–9, 2020.
- [137] K. Y. Chen, L. Ren, Z. P. Chen, C. F. Pan, W. Zhou, and L. L. Jiang, "Fabrication of micro-needle electrodes for bio-signal recording by a magnetization-induced self-assembly method," *Sensors (Switzerland)*, vol. 16, no. 9, pp. 1–15, 2016.
- [138] P. R. Miller, R. J. Narayan, and R. Polsky, "Microneedle-based sensors for medical diagnosis," *J. Mater. Chem. B*, vol. 4, no. 8, pp. 1379–1383, 2016.
- [139] A. A. Tarar, U. Mohammad, and S. K. Srivastava, "Wearable skin sensors and their challenges: A review of transdermal, optical, and mechanical sensors," *Biosensors*, vol. 10, no. 6, 2020.
- [140] M. Parrilla *et al.*, "Wearable All-Solid-State Potentiometric Microneedle Patch for Intradermal Potassium Detection," *Anal. Chem.*, vol. 91, no. 2, pp. 1578–1586, 2019.
- [141] S. A. Skoog, P. R. Miller, R. D. Boehm, A. V. Sumant, R. Polsky, and R. J. Narayan, "Nitrogen-incorporated ultrananocrystalline diamond microneedle arrays for electrochemical biosensing," *Diam. Relat. Mater.*, vol. 54, no. 1, pp. 39–46, 2015.
- [142] J. R. Windmiller *et al.*, "Bicomponent Microneedle Array Biosensor for Minimally-Invasive Glutamate Monitoring," *Electroanalysis*, vol. 23, no. 10, pp. 2302–2309, 2011.
- [143] L. Zhao, Z. Wen, F. Jiang, Z. Zheng, and S. Lu, "Silk/polyols/GOD microneedle based electrochemical biosensor for continuous glucose monitoring," *RSC Adv.*, vol. 10, no. 11, pp. 6163–6171, 2020.
- [144] A. K. Shakya *et al.*, "Microneedles coated with peanut allergen enable desensitization of peanut sensitized mice," *J. Control. Release*, vol. 314, no. October, pp. 38–47, 2019.
- [145] Y. Ito *et al.*, "Dissolving microneedles as skin allergy test device," *Biol. Pharm. Bull.*, vol. 40, no. 4, pp. 531–534, 2017.
- [146] T. Waghule *et al.*, "Microneedles: A smart approach and increasing potential for transdermal drug delivery system," *Biomed. Pharmacother.*, vol. 109, no. July 2018, pp. 1249–1258, 2019.
- [147] R. K. Sivamani, B. Stoeber, D. Liepmann, and H. I. Maibach, "Microneedle penetration and injection past the stratum corneum in humans," *J. Dermatolog. Treat.*, vol. 20, no. 3, pp. 156–159, 2009.

- [148] G. Ma and C. Wu, "Microneedle, bio-microneedle and bio-inspired microneedle: A review," *J. Control. Release*, vol. 251, pp. 11–23, 2017.
- [149] D. V. McAllister *et al.*, "Microfabricated needles for transdermal delivery of macromolecules and nanoparticles: Fabrication methods and transport studies," *Proc. Natl. Acad. Sci. U. S. A.*, vol. 100, no. SUPPL. 2, pp. 13755–13760, 2003.
- [150] F. J. Verbaan *et al.*, "Improved piercing of microneedle arrays in dermatomed human skin by an impact insertion method," *J. Control. Release*, vol. 128, no. 1, pp. 80–88, 2008.
- [151] B. Cai, W. Xia, S. Bredenberg, H. Li, and H. Engqvist, "Bioceramic microneedles with flexible and self-swelling substrate," *Eur. J. Pharm. Biopharm.*, vol. 94, pp. 404–410, 2015.
- [152] J. Gupta, E. I. Felner, and M. R. Prausnitz, "Minimally invasive insulin delivery in subjects with type 1 diabetes using hollow microneedles," *Diabetes Technology and Therapeutics*, vol. 11, no. 6, pp. 329–337, 2009.
- [153] P. Mukhopadhyay, K. Sarkar, M. Chakraborty, S. Bhattacharya, R. Mishra, and P. P. Kundu, "Oral insulin delivery by self-assembled chitosan nanoparticles: In vitro and in vivo studies in diabetic animal model," *Mater. Sci. Eng. C*, vol. 33, no. 1, pp. 376–382, 2013.
- [154] Y. Ido *et al.*, "Conducting polymer microelectrodes anchored to hydrogel films," *ACS Macro Lett.*, vol. 1, no. 3, pp. 400–403, 2012.
- [155] M. A. Hopcroft, W. D. Nix, and T. W. Kenny, "What is the Young's modulus of silicon?," *J. Microelectromechanical Syst.*, vol. 19, no. 2, pp. 229–238, 2010.
- [156] P. Makvandi *et al.*, *Engineering Microneedle Patches for Improved Penetration: Analysis, Skin Models and Factors Affecting Needle Insertion*, vol. 13, no. 1. Springer Singapore, 2021.
- [157] S. D. Gittard, A. Ovsianikov, B. N. Chichkov, A. Doraiswamy, and R. J. Narayan, "Two-photon polymerization of microneedles for transdermal drug delivery," *Expert Opinion on Drug Delivery*, vol. 7, no. 4, pp. 513–533, 2010.
- [158] L. A. Ferrara, A. J. Fleischman, D. Togawa, T. W. Bauer, E. C. Benzel, and S. Roy, "An in vivo biocompatibility assessment of MEMS materials for spinal fusion monitoring," *Biomed. Microdevices*, vol. 5, no. 4, pp. 297–302, 2003.
- [159] G. Voskerician *et al.*, "Biocompatibility and biofouling of MEMS drug delivery devices," *Biomaterials*, vol. 24, no. 11, pp. 1959–1967, 2003.
- [160] F. J. Verbaan *et al.*, "Assembled microneedle arrays enhance the transport of compounds varying over a large range of molecular weight across human dermatomed skin," *J. Control. Release*, vol. 117, no. 2, pp. 238–245, 2007.
- [161] C. S. Kolli and A. K. Banga, "Characterization of solid maltose microneedles and their use for transdermal delivery," *Pharm. Res.*, vol. 25, no. 1, pp. 104–113, 2008.
- [162] Y. Chen, B. Z. Chen, Q. L. Wang, X. Jin, and X. D. Guo, "Fabrication of coated polymer microneedles for transdermal drug delivery," *J. Control. Release*, vol. 265, no. March, pp. 14–21, 2017.
- [163] J. Park, M. G. Allen, and M. R. Prausnitz, "Biodegradable polymer microneedles : Fabrication , mechanics and transdermal drug delivery," vol. 104, pp. 51–66, 2005.



- [164] B. Ahn, "Optimal Microneedle Design for Drug Delivery Based on Insertion Force Experiments with Variable Geometry," *Int. J. Control. Autom. Syst.*, vol. 18, no. 1, pp. 143–149, 2020.
- [165] R. L. McCreery, "Advanced carbon electrode materials for molecular electrochemistry," *Chem. Rev.*, vol. 108, no. 7, pp. 2646–2687, 2008.
- [166] S. J. Paik *et al.*, "In-plane single-crystal-silicon microneedles for minimally invasive microfluid systems," *Sensors Actuators, A Phys.*, vol. 114, no. 2–3, pp. 276–284, 2004.
- [167] M. W. Ashraf *et al.*, "Design, fabrication and analysis of silicon hollow microneedles for transdermal drug delivery system for treatment of hemodynamic dysfunctions," *Cardiovasc. Eng.*, vol. 10, no. 3, pp. 91–108, 2010.
- [168] W. Martanto, S. P. Davis, N. R. Holiday, J. Wang, H. S. Gill, and M. R. Prausnitz, "Transdermal delivery of insulin using microneedles in vivo," *Pharm. Res.*, vol. 21, no. 6, pp. 947–952, 2004.
- [169] M. S. Lhernould, C. Gobillon, and P. Lambert, "Microneedle array penetration tests: Understanding the 'bed of nails' phenomenon," *ONdrugDelivery*, no. 40, pp. 29–32, 2013.
- [170] G. Yan, K. S. Warner, J. Zhang, S. Sharma, and B. K. Gale, "Evaluation needle length and density of microneedle arrays in the pretreatment of skin for transdermal drug delivery," *Int. J. Pharm.*, vol. 391, no. 1–2, pp. 7–12, 2010.
- [171] J. S. Kochhar, T. C. Quek, W. J. Soon, J. Choi, S. Zou, and L. Kang, "Effect of microneedle geometry and supporting substrate on microneedle array penetration into skin," *J. Pharm. Sci.*, vol. 102, no. 11, pp. 4100–4108, 2013.
- [172] O. Olatunji, D. B. Das, M. J. Garland, L. Belaid, and R. F. Donnelly, "Influence of array interspacing on the force required for successful microneedle skin penetration: Theoretical and practical approaches," *J. Pharm. Sci.*, vol. 102, no. 4, pp. 1209–1221, 2013.
- [173] E. M. T. Shibata, A. Nakanishi, T. Sakai, N. Kato, T. Kawashima, T. Mineta, "Fabrication and mechanical characterization of microneedle array for cell surgery," *TRANSDUCERS 2007 - 2007 Int. Solid-State Sensors, Actuators Microsystems Conf.*, pp. 3–3, 2007.
- [174] P. Aggarwal and C. R. Johnston, "Geometrical effects in mechanical characterizing of microneedle for biomedical applications," *Sensors Actuators, B Chem.*, vol. 102, no. 2, pp. 226–234, 2004.
- [175] C. Y. Chiu, H. C. Kuo, Y. Lin, J. L. Lee, Y. K. Shen, and S. J. Kang, "Optimal design of microneedles inserts into skin by numerical simulation," *Key Eng. Mater.*, vol. 516, pp. 624–628, 2012.
- [176] F. Chabri *et al.*, "Microfabricated silicon microneedles for nonviral cutaneous gene delivery," *Br. J. Dermatol.*, vol. 150, no. 5, pp. 869–877, 2004.
- [177] P. Khanna, K. Luongo, J. A. Strom, and S. Bhansali, "Sharpening of hollow silicon microneedles to reduce skin penetration force," *J. Micromechanics Microengineering*, vol. 20, no. 4, 2010.
- [178] E. M. Vicente-Perez *et al.*, "Repeat application of microneedles does not alter skin appearance or barrier function and causes no measurable disturbance of serum biomarkers of infection, inflammation or immunity in mice in vivo," *Eur. J. Pharm. Biopharm.*, vol. 117, pp. 400–407, 2017.
- [179] K. T. Chang, Y. K. Shen, F. Y. Fan, Y. Lin, and S. C. Kang, "Optimal design and fabrication of a microneedle arrays patch," *J. Manuf. Process.*, vol. 54, no. March, pp. 274–285, 2020.

- [180] C. O'Mahony, "Structural characterization and in-vivo reliability evaluation of silicon microneedles," *Biomed. Microdevices*, vol. 16, no. 3, pp. 333–343, 2014.
- [181] S. Ross, N. Scoutaris, D. Lamprou, D. Mallinson, and D. Douroumis, "Inkjet printing of insulin microneedles for transdermal delivery," *Drug Deliv. Transl. Res.*, vol. 5, no. 4, pp. 451–461, 2015.
- [182] Y. Xie, B. Xu, and Y. Gao, "Controlled transdermal delivery of model drug compounds by MEMS microneedle array," *Nanomedicine Nanotechnology, Biol. Med.*, vol. 1, no. 2, pp. 184–190, 2005.
- [183] T. Kawashima, "Mechanical characterization and insertion performance of hollow microneedle array for cell surgery," *J. Micro/Nanolithography, MEMS, MOEMS*, vol. 8, no. 3, pp. 1–7, 2009.
- [184] S. Kim, S. Shetty, D. Price, and S. Bhansali, "Skin penetration of silicon dioxide microneedle arrays," *Annu. Int. Conf. IEEE Eng. Med. Biol. - Proc.*, pp. 4088–4091, 2006.
- [185] J. Enfield, M.-L. O'Connell, K. Lawlor, E. Jonathan, C. O'Mahony, and M. Leahy, "In-vivo dynamic characterization of microneedle skin penetration using optical coherence tomography," *J. Biomed. Opt.*, vol. 15, no. 4, p. 046001, 2010.
- [186] P. Khanna, B. R. Flam, B. Osborn, J. A. Strom, and S. Bhansali, "Skin penetration and fracture strength testing of silicon dioxide microneedles," *Sensors Actuators, A Phys.*, vol. 170, no. 1–2, pp. 180–186, 2011.
- [187] L. Wei-Ze *et al.*, "Super-short solid silicon microneedles for transdermal drug delivery applications," *Int. J. Pharm.*, vol. 389, no. 1–2, pp. 122–129, 2010.
- [188] N. Roxhed, P. Griss, and G. Stemme, "Membrane-sealed hollow microneedles and related administration schemes for transdermal drug delivery," *Biomed. Microdevices*, vol. 10, no. 2, pp. 271–279, 2008.
- [189] W. W. Koelmans, G. Krishnamoorthy, A. Heskamp, J. Wissink, S. Misra, and N. Tas, "Microneedle Characterization Using a Double-Layer Skin Simulant," *Mech. Eng. Res.*, vol. 3, no. 2, pp. 51–63, 2013.
- [190] Y. C. Kim, F. S. Quan, R. W. Compans, S. M. Kang, and M. R. Prausnitz, "Formulation and coating of microneedles with inactivated influenza virus to improve vaccine stability and immunogenicity," *J. Control. Release*, vol. 142, no. 2, pp. 187–195, 2010.
- [191] H. S. Gill and M. R. Prausnitz, "Pocketed microneedles for drug delivery to the skin," *J. Phys. Chem. Solids*, vol. 69, no. 5–6, pp. 1537–1541, 2008.
- [192] X. Chen *et al.*, "Dry-coated microprojection array patches for targeted delivery of immunotherapeutics to the skin," *J. Control. Release*, vol. 139, no. 3, pp. 212–220, 2009.
- [193] A. M. Römgers, D. L. Bader, J. A. Bouwstra, F. P. T. Baaijens, and C. W. J. Oomens, "Monitoring the penetration process of single microneedles with varying tip diameters," *J. Mech. Behav. Biomed. Mater.*, vol. 40, pp. 397–405, 2014.
- [194] C. Radhika and B. K. Gnanavel, "Buckling analysis of polymer microneedle for transdermal drug delivery," *Mater. Today Proc.*, vol. 46, pp. 3538–3541, 2020.
- [195] M. I. Haq *et al.*, "Clinical administration of microneedles: Skin puncture, pain and sensation," *Biomed. Microdevices*, vol. 11, no. 1, pp. 35–47, 2009.

- [196] H. S. Gill and M. R. Prausnitz, "Coated microneedles for transdermal delivery," *J. Control. Release*, vol. 117, no. 2, pp. 227–237, 2007.
- [197] M. G. McGrath, A. Vrdoljak, C. O'Mahony, J. C. Oliveira, A. C. Moore, and A. M. Crean, "Determination of parameters for successful spray coating of silicon microneedle arrays," *Int. J. Pharm.*, vol. 415, no. 1–2, pp. 140–149, 2011.
- [198] D. Jenkins, S. Corrie, C. Flaim, and M. Kendall, "High density and high aspect ratio solid micro-nanoprojection arrays for targeted skin vaccine delivery and specific antibody extraction," *RSC Adv.*, vol. 2, no. 8, pp. 3490–3495, 2012.
- [199] S. P. Davis, B. J. Landis, Z. H. Adams, M. G. Allen, and M. R. Prausnitz, "Insertion of microneedles into skin: Measurement and prediction of insertion force and needle fracture force," *J. Biomech.*, vol. 37, no. 8, pp. 1155–1163, 2004.
- [200] P. Khanna, K. Luongo, J. A. Strom, and S. Bhansali, "Axial and shear fracture strength evaluation of silicon microneedles," *Microsyst. Technol.*, vol. 16, no. 6, pp. 973–978, 2010.
- [201] Z. Zhu *et al.*, "Rapidly dissolvable microneedle patches for transdermal delivery of exenatide," *Pharm. Res.*, vol. 31, no. 12, pp. 3348–3360, 2014.
- [202] Á. Cárcamo-Martínez, Q. K. Anjani, A. D. Permana, A. S. Cordeiro, E. Larrañeta, and R. F. Donnelly, "Coated polymeric needles for rapid and deep intradermal delivery," *Int. J. Pharm. X*, vol. 2, no. March, p. 100048, 2020.
- [203] G. Li, A. Badkar, S. Nema, C. S. Kolli, and A. K. Banga, "In vitro transdermal delivery of therapeutic antibodies using maltose microneedles," *Int. J. Pharm.*, vol. 368, no. 1–2, pp. 109–115, 2009.
- [204] A. A. Dandekar, H. T. Garimella, C. L. German, and A. K. Banga, "Microneedle Mediated Iontophoretic Delivery of Tofacitinib Citrate," *Pharm. Res.*, pp. 735–747, 2022.
- [205] S. Bal *et al.*, "In vivo visualization of microneedle conduits in human skin using laser scanning microscopy," *Laser Phys. Lett.*, vol. 7, no. 3, pp. 242–246, 2010.
- [206] R. Alvarez-Román, A. Naik, Y. N. Kalia, H. Fessi, and R. H. Guy, "Visualization of skin penetration using confocal laser scanning microscopy," *Eur. J. Pharm. Biopharm.*, vol. 58, no. 2, pp. 301–316, 2004.
- [207] J. S. Kochhar, W. J. Goh, S. Y. Chan, and L. Kang, "A simple method of microneedle array fabrication for transdermal drug delivery," *Drug Dev. Ind. Pharm.*, vol. 39, no. 2, pp. 299–309, 2013.
- [208] K. Moronkeji, S. Todd, I. Dawidowska, S. D. Barrett, and R. Akhtar, "The role of subcutaneous tissue stiffness on microneedle performance in a representative in vitro model of skin," *J. Control. Release*, vol. 265, pp. 102–112, 2017.
- [209] T. Rattanapak *et al.*, "Transcutaneous immunization using microneedles and cubosomes: Mechanistic investigations using Optical Coherence Tomography and Two-Photon Microscopy," *J. Control. Release*, vol. 172, no. 3, pp. 894–903, 2013.
- [210] L. K. Vora, R. F. Donnelly, E. Larrañeta, P. González-Vázquez, R. R. S. Thakur, and P. R. Vavia, "Novel bilayer dissolving microneedle arrays with concentrated PLGA nano-microparticles for targeted intradermal delivery: Proof of concept," *J. Control. Release*, vol. 265, no. September, pp.

93–101, 2017.

- [211] J. Gupta, H. S. Gill, S. N. Andrews, and M. R. Prausnitz, “Kinetics of skin resealing after insertion of microneedles in human subjects,” *J. Control. Release*, vol. 154, no. 2, pp. 148–155, 2011.
- [212] S. D. Gittard *et al.*, “The effects of geometry on skin penetration and failure of polymer microneedles,” *J. Adhes. Sci. Technol.*, vol. 27, no. 3, pp. 227–243, 2013.
- [213] S. I. Bisgaard *et al.*, “Peanut Allergen Ara h 2 Delivery with In-plane Silicon Microneedles for Test of Allergic Response,” 2023.
- [214] M. R. Prausnitz, “Microneedles for transdermal drug delivery,” *Adv. Drug Deliv. Rev.*, vol. 56, no. 5, pp. 581–587, 2004.
- [215] K. Van Der Maaden, W. Jiskoot, and J. Bouwstra, “Microneedle technologies for (trans)dermal drug and vaccine delivery,” *J. Control. Release*, vol. 161, no. 2, pp. 645–655, 2012.
- [216] X. He, J. Sun, J. Zhuang, H. Xu, Y. Liu, and D. Wu, “Microneedle System for Transdermal Drug and Vaccine Delivery: Devices, Safety, and Prospects,” *Dose-Response*, vol. 17, no. 4, pp. 1–18, 2019.
- [217] S. M. Bal *et al.*, “Influence of microneedle shape on the transport of a fluorescent dye into human skin in vivo,” *J. Control. Release*, vol. 147, no. 2, pp. 218–224, 2010.
- [218] A. K. Shakya, C. H. Lee, and H. S. Gill, “Coated microneedle-based cutaneous immunotherapy prevents Der p 1–induced airway allergy in mice,” *J. Allergy Clin. Immunol.*, vol. 142, no. 6, pp. 2007–2011.e3, 2018.
- [219] N. Wonglertnirant, H. Todo, P. Opanasopit, T. Ngawhirunpat, and K. Sugibayashi, “Macromolecular delivery into skin using a hollow microneedle,” *Biol. Pharm. Bull.*, vol. 33, no. 12, pp. 1988–1993, 2010.
- [220] A. Sadeqi, G. Kiaee, W. Zeng, H. Rezaei Nejad, and S. Sonkusale, “Hard polymeric porous microneedles on stretchable substrate for transdermal drug delivery,” *Sci. Rep.*, vol. 12, no. 1, pp. 1–10, 2022.
- [221] K. Migalska, D. I. J. Morrow, M. J. Garland, R. Thakur, A. D. Woolfson, and R. F. Donnelly, “Laser-engineered dissolving microneedle arrays for transdermal macromolecular drug delivery,” *Pharm. Res.*, vol. 28, no. 8, pp. 1919–1930, 2011.
- [222] N. G. Oh, S. Y. Hwang, and Y. H. Na, “Fabrication of a PVA-Based Hydrogel Microneedle Patch,” *ACS Omega*, vol. 7, no. 29, pp. 25179–25185, 2022.
- [223] J. W. Lee, J. H. Park, and M. R. Prausnitz, “Dissolving microneedles for transdermal drug delivery,” *Biomaterials*, vol. 29, no. 13, pp. 2113–2124, 2008.
- [224] R. F. Donnelly *et al.*, “Hydrogel-forming microneedle arrays exhibit antimicrobial properties: Potential for enhanced patient safety,” *Int. J. Pharm.*, vol. 451, no. 1–2, pp. 76–91, 2013.
- [225] B. Chen, J. Wei, F. E. H. Tay, Y. T. Wong, and C. Iliescu, “Silicon microneedle array with biodegradable tips for transdermal drug delivery,” *Microsyst. Technol.*, vol. 14, no. 7, pp. 1015–1019, 2008.
- [226] A. U. Alam, M. M. R. Howlader, and M. J. Deen, “Oxygen Plasma and Humidity Dependent Surface Analysis of Silicon, Silicon Dioxide and Glass for Direct Wafer Bonding,” *ECS J. Solid State*

- Sci. Technol.*, vol. 2, no. 12, pp. P515–P523, 2013.
- [227] H. S. Gill and M. R. Prausnitz, “Coating formulations for microneedles,” *Pharm. Res.*, vol. 24, no. 7, pp. 1369–1380, 2007.
- [228] S. Li, W. Li, and M. Prausnitz, “Individually coated microneedles for co-delivery of multiple compounds with different properties,” *Drug Deliv. Transl. Res.*, vol. 8, no. 5, pp. 1043–1052, 2018.
- [229] Y. C. Kim, F. S. Quan, R. W. Compans, S. M. Kang, and M. R. Prausnitz, “Formulation of microneedles coated with influenza virus-like particle vaccine,” *AAPS PharmSciTech*, vol. 11, no. 3, pp. 1193–1201, 2010.
- [230] X. Zhao, S. A. Coulman, S. J. Hanna, F. S. Wong, C. M. Dayan, and J. C. Birchall, “Formulation of hydrophobic peptides for skin delivery via coated microneedles,” *J. Control. Release*, vol. 265, pp. 2–13, 2017.
- [231] M. J. Uddin, N. Scoutaris, P. Klepetsanis, B. Chowdhry, M. R. Prausnitz, and D. Douroumis, “Inkjet printing of transdermal microneedles for the delivery of anticancer agents,” *Int. J. Pharm.*, vol. 494, no. 2, pp. 593–602, 2015.
- [232] I. Effendy and H. I. Maibach, “Surfactants and experimental irritant contact dermatitis,” *Contact Dermatitis*, vol. 33, no. 4, pp. 217–225, 1995.
- [233] “Good Manufacturing Practice,” *European Medicines Agency*, 2022. [Online]. Available: <https://www.ema.europa.eu/en/human-regulatory/research-development/compliance/good-manufacturing-practice>.
- [234] P. Marizza, S. S. Keller, and A. Boisen, “Inkjet printing as a technique for filling of micro-wells with biocompatible polymers,” *Microelectron. Eng.*, vol. 111, pp. 391–395, 2013.
- [235] “USER MANUAL - Printing System Autodrop Professional,” *microdrop Technol.*, p. 40, 2020.
- [236] J. J. Landers *et al.*, “Targeted allergen-specific immunotherapy within the skin improves allergen delivery to induce desensitization to peanut,” *Immunotherapy*, 2022.
- [237] A. K. Shakya and H. S. Gill, “A comparative study of microneedle-based cutaneous immunization with other conventional routes to assess feasibility of microneedles for allergy immunotherapy,” *Vaccine*, vol. 33, no. 33, pp. 4060–4064, 2015.
- [238] L. G. Tran and W. T. Park, “Rapid biodegradable microneedles with allergen reservoir for skin allergy test,” *Micro and Nano Systems Letters*, vol. 8, no. 1. Springer Singapore, pp. 0–4, 2020.
- [239] S. J. Koppelman, M. Wensing, M. Ertmann, A. C. Knulst, and E. F. Knol, “Relevance of Ara h1, Ara h2 and Ara h3 in peanut-allergic patients, as determined by immunoglobulin E Western blotting, basophil-histamine release and intracutaneous testing: Ara h2 is the most important peanut allergen,” *Clin. Exp. Allergy*, vol. 34, no. 4, pp. 583–590, 2004.
- [240] A. K. Kukkonen, A. S. Pelkonen, S. Mäkinen-Kiljunen, H. Voutilainen, and M. J. Mäkelä, “Ara h 2 and Ara 6 are the best predictors of severe peanut allergy: A double-blind placebo-controlled study,” *Allergy Eur. J. Allergy Clin. Immunol.*, vol. 70, no. 10, pp. 1239–1245, 2015.
- [241] J. S. Stanley *et al.*, “Identification and mutational analysis of the immunodominant IgE binding epitopes of the major peanut allergen Ara h 2,” *Arch. Biochem. Biophys.*, vol. 342, no. 2, pp. 244–

253, 1997.

- [242] J. M. Chatel, H. Bernard, and F. M. Orson, "Isolation and characterization of two complete Ara h 2 isoforms cDNA," *Int. Arch. Allergy Immunol.*, vol. 131, no. 1, pp. 14–18, 2003.
- [243] R. Na, I. M. Stender, L. Ma, and H. C. Wulf, "Autofluorescence spectrum of skin: Component bands and body site variations," *Ski. Res. Technol.*, vol. 6, no. 3, pp. 112–117, 2000.
- [244] E. V. Salomatina and A. B. Pravdin, "Fluorescence dynamics of human epidermis (ex vivo) and skin (in vivo)," no. October 2003, 2020.
- [245] O. Jacobson, D. O. Kiesewetter, and X. Chen, "Albumin-Binding Evans Blue Derivatives for Diagnostic Imaging and Production of Long-Acting Therapeutics," *Bioconjug. Chem.*, vol. 27, no. 10, pp. 2239–2247, 2016.
- [246] E. Jensen-Jarolim *et al.*, "Allergen mimotopes in food enhance type I allergic reactions in mice," *FASEB J.*, vol. 13, no. 12, pp. 1586–1592, 1999.
- [247] I. Schöll *et al.*, "Allergen-loaded biodegradable poly(D,L-lactic-co-glycolic) acid nanoparticles down-regulate an ongoing Th2 response in the BALB/c mouse model," *Clin. Exp. Allergy*, vol. 34, no. 2, pp. 315–321, 2004.
- [248] U. Baranyi *et al.*, "Tolerization of a Type I Allergic Immune Response through Transplantation of Genetically Modified Hematopoietic Stem Cells," *J. Immunol.*, vol. 180, no. 12, pp. 8168–8175, 2008.
- [249] Z. Ovary, "Immediate Reactions in the Skin of Experimental Animal Provoked by Antibody-Antigen Interaction," *Progr. Allergy*, vol. 5, pp. 459–508, 1958.
- [250] M. W. Chase, "Studies on the Sensitization of Animals With Simple Chemical Compounds: X. Antibodies inducing immediate-type skin reactions," *J. Exp. Med.*, vol. 86, no. 6, pp. 489–514, 1947.
- [251] S. I. Bisgaard *et al.*, "Birch Pollen Extract and Bet v 1 Allergen Delivery with In-plane Silicon Microneedles for Test of Allergic Response," 2023.
- [252] N. A. Monteiro-Riviere, "Structure and function of skin," *Toxicol. Ski.*, pp. 1–18, 2010.
- [253] M. Foldvari *et al.*, "Topical delivery of interferon alpha by biphasic vesicles: Evidence for a novel nanopathway across the stratum corneum," *Mol. Pharm.*, vol. 7, no. 3, pp. 751–762, 2010.
- [254] J. Torin Huzil, S. Sivaloganathan, M. Kohandel, and M. Foldvari, "Drug delivery through the skin: Molecular simulations of barrier lipids to design more effective noninvasive dermal and transdermal delivery systems for small molecules, biologics, and cosmetics," *Wiley Interdiscip. Rev. Nanomedicine Nanobiotechnology*, vol. 3, no. 5, pp. 449–462, 2011.
- [255] C. Hwa, E. A. Bauer, and D. E. Cohen, "Skin Biology," *Dermatol. Ther.*, vol. 24, pp. 464–470, 2011.
- [256] H. Y. Chang *et al.*, "Diversity, topographic differentiation, and positional memory in human fibroblasts," *Proc. Natl. Acad. Sci. U. S. A.*, vol. 99, no. 20, pp. 12877–12882, 2002.
- [257] D. J. Tobin, "Biochemistry of human skin—our brain on the outside," *Chem. Soc. Rev.*, vol. 35, no. 1, pp. 52–67, 2005.
- [258] R. Wong, S. Geyer, W. Weninger, J. C. Guimberteau, and J. K. Wong, "The dynamic anatomy and

- patterning of skin," *Exp. Dermatol.*, vol. 25, no. 2, pp. 92–98, 2016.
- [259] J. Sandby-Møller, T. Poulsen, and H. C. Wulf, "Epidermal Thickness at Different Body Sites: Relationship to Age, Gender, Pigmentation, Blood Content, Skin Type and Smoking Habits," *Acta Derm. Venereol.*, vol. 83, no. 6, pp. 410–413, 2003.
- [260] J. W. Fluhr, S. Pfisterer, and M. Gloor, "Direct comparison of skin physiology in children and adults with bioengineering methods," *Pediatr. Dermatol.*, vol. 17, no. 6, pp. 436–439, 2000.
- [261] A. N. Annaidh, M. Ottenio, K. Bruyère, M. Destrade, and M. D. Gilchrist, "Mechanical properties of excised human skin," *IFMBE Proc.*, vol. 31 IFMBE, pp. 1000–1003, 2010.
- [262] F. Ginhoux *et al.*, "Langerhans cells arise from monocytes in vivo," *Nat. Immunol.*, vol. 7, no. 3, pp. 265–273, 2006.
- [263] L. K. Mackay *et al.*, "Long-lived epithelial immunity by tissue-resident memory T (TRM) cells in the absence of persisting local antigen presentation," *Proc. Natl. Acad. Sci. U. S. A.*, vol. 109, no. 18, pp. 7037–7042, 2012.
- [264] S. Tamoutounour *et al.*, "Origins and functional specialization of macrophages and of conventional and monocyte-derived dendritic cells in mouse skin," *Immunity*, vol. 39, no. 5, pp. 925–938, 2013.
- [265] K. Kabashima, T. Honda, F. Ginhoux, and G. Egawa, "The immunological anatomy of the skin," *Nat. Rev. Immunol.*, vol. 19, no. 1, pp. 19–30, 2019.
- [266] A. I. Chen *et al.*, "Multilayered tissue mimicking skin and vessel phantoms with tunable mechanical, optical, and acoustic properties," *Med. Phys.*, vol. 43, no. 6, pp. 3117–3131, 2016.
- [267] R. Kong and R. Bhargava, "Characterization of porcine skin as a model for human skin studies using infrared spectroscopic imaging," *Analyst*, vol. 136, no. 11, pp. 2359–2366, 2011.
- [268] U. Jacobi *et al.*, "Porcine ear skin: An in vitro model for human skin," *Ski. Res. Technol.*, vol. 13, no. 1, pp. 19–24, 2007.
- [269] S. Debeer *et al.*, "Comparative histology and immunohistochemistry of porcine versus human skin," *Eur. J. Dermatology*, vol. 23, no. 4, pp. 456–466, 2013.
- [270] N. Sekkat, Y. N. Kalia, and R. H. Guy, "Biophysical study of porcine ear skin in vitro and its comparison to human skin in vivo," *J. Pharm. Sci.*, vol. 91, no. 11, pp. 2376–2381, 2002.
- [271] J. C. J. Wei, G. A. Edwards, D. J. Martin, H. Huang, M. L. Crichton, and M. A. F. Kendall, "Allometric scaling of skin thickness, elasticity, viscoelasticity to mass for micro-medical device translation: From mice, rats, rabbits, pigs to humans," *Sci. Rep.*, vol. 7, no. 1, pp. 1–17, 2017.
- [272] S. A. Ranamukhaarachchi *et al.*, "Development and Validation of an Artificial Mechanical Skin Model for the Study of Interactions between Skin and Microneedles," *Macromol. Mater. Eng.*, vol. 301, no. 3, pp. 306–314, 2016.
- [273] A. S. Caro-Bretelle *et al.*, "Effect of sample preservation on stress softening and permanent set of porcine skin," *J. Biomech.*, vol. 48, no. 12, pp. 3135–3141, 2015.
- [274] H. Joodaki and M. B. Panzer, "Skin mechanical properties and modeling: A review," *Proc. Inst. Mech. Eng. Part H J. Eng. Med.*, vol. 232, no. 4, pp. 323–343, 2018.

- [275] S. Henry, D. V. McAllister, M. G. Allen, and M. R. Prausnitz, "Microfabricated microneedles: A novel approach to transdermal drug delivery," *Proc. Control. Release Soc.*, vol. 87, no. 25, pp. 30–31, 1998.
- [276] J. B. Nielsen, I. Plasencia, J. A. Sørensen, and L. A. Bagatolli, "Storage conditions of skin affect tissue structure and subsequent in vitro percutaneous penetration," *Skin Pharmacol. Physiol.*, vol. 24, no. 2, pp. 93–102, 2011.
- [277] M. A. Kosoglu, R. L. Hood, Y. Chen, Y. Xu, M. N. Rylander, and C. G. Rylander, "Fiber optic microneedles for transdermal light delivery: Ex vivo porcine skin penetration experiments," *J. Biomech. Eng.*, vol. 132, no. 9, pp. 1–7, 2010.
- [278] A. K. Shakya, C. H. Lee, and H. S. Gill, "Microneedle-Mediated Allergen-Specific Immunotherapy for the Treatment of Airway Allergy in Mice," *Mol. Pharm.*, vol. 17, no. 8, pp. 3033–3042, 2020.
- [279] E. L. Hull, M. G. Nichols, and T. H. Foster, "Quantitative broadband near-infrared spectroscopy of tissue-simulating phantoms containing erythrocytes," *Phys. Med. Biol.*, vol. 43, no. 11, pp. 3381–3404, 1998.
- [280] M. Lualdi, A. Colombo, B. Farina, S. Tomatis, and R. Marchesini, "A phantom with tissue-like optical properties in the visible and near infrared for use in photomedicine," *Lasers Surg. Med.*, vol. 28, no. 3, pp. 237–243, 2001.
- [281] A. Dąbrowska *et al.*, "A water-responsive, gelatine-based human skin model," *Tribol. Int.*, vol. 113, no. July 2016, pp. 316–322, 2017.
- [282] S. Makode, G. Singh, and A. Chanda, "Development of novel anisotropic skin simulants," *Phys. Scr.*, vol. 96, no. 12, 2021.
- [283] J. Jachowicz, R. McMullen, and D. PrettyPaul, "Indentometric analysis of in vivo skin and comparison with artificial skin models," *Ski. Res. Technol.*, vol. 13, no. 3, pp. 299–309, 2007.
- [284] D. R. White, R. J. Martin, and R. Darlison, "Epoxy resin based tissue substitutes," *Br. J. Radiol.*, vol. 50, no. 599, pp. 814–821, 1977.
- [285] A. Psikuta, M. Richards, and D. Fiala, "Single-sector thermophysiological human simulator," *Physiol. Meas.*, vol. 29, no. 2, pp. 181–192, 2008.
- [286] A. K. Dabrowska *et al.*, "Materials used to simulate physical properties of human skin," *Ski. Res. Technol.*, vol. 22, no. 1, pp. 3–14, 2016.
- [287] E. Larrañeta *et al.*, "A proposed model membrane and test method for microneedle insertion studies," *Int. J. Pharm.*, vol. 472, no. 1–2, pp. 65–73, 2014.
- [288] C. Lotte, C. Patouillet, M. Zanini, A. Messenger, and R. Roguet, "Permeation and skin absorption: Reproducibility of various industrial reconstructed human skin models," *Skin Pharmacol. Appl. Skin Physiol.*, vol. 15, no. SUPPL. 1, pp. 18–30, 2002.
- [289] E. Abd *et al.*, "Skin models for the testing of transdermal drugs," *Clin. Pharmacol. Adv. Appl.*, vol. 8, pp. 163–176, 2016.
- [290] S. Choudhury and A. Das, "Advances in generation of three-dimensional skin equivalents: pre-clinical studies to clinical therapies," *Cytotherapy*, vol. 23, no. 1, pp. 1–9, 2021.



- [291] M. Douguet, C. Picard, G. Savary, F. Merlaud, N. Loubat-bouleuc, and M. Grisel, "Spreading properties of cosmetic emollients: Use of synthetic skin surface to elucidate structural effect," *Colloids Surfaces B Biointerfaces*, vol. 154, pp. 307–314, 2017.
- [292] S. Chen and B. Bhushan, "Nanomechanical and nanotribological characterization of two synthetic skins with and without skin cream treatment using atomic force microscopy," *J. Colloid Interface Sci.*, vol. 398, pp. 247–254, 2013.
- [293] F. Eudier, D. Hirel, M. Grisel, C. Picard, and G. Savary, "Prediction of residual film perception of cosmetic products using an instrumental method and non-biological surfaces: The example of stickiness after skin application," *Colloids Surfaces B Biointerfaces*, vol. 174, no. October 2018, pp. 181–188, 2019.
- [294] F. Eudier, G. Savary, M. Grisel, and C. Picard, "Skin surface physico-chemistry: Characteristics, methods of measurement, influencing factors and future developments," *Adv. Colloid Interface Sci.*, vol. 264, pp. 11–27, 2019.
- [295] S. Nebuya, M. Noshiro, B. H. Brown, R. H. Smallwood, and P. Milnes, "Detection of emboli in vessels using electrical impedance measurements - phantom and electrodes," *Physiol. Meas.*, vol. 26, no. 2, 2005.
- [296] M. Ahearne, Y. Yang, A. J. El Haj, K. Y. Then, and K. K. Liu, "Characterizing the viscoelastic properties of thin hydrogel-based constructs for tissue engineering applications," *J. R. Soc. Interface*, vol. 2, no. 5, pp. 455–463, 2005.
- [297] J. Jussila, A. Leppäniemi, M. Paronen, and E. Kulomäki, "Ballistic skin simulant," *Forensic Sci. Int.*, vol. 150, no. 1, pp. 63–71, 2005.
- [298] G. Busco, A. V. Omran, L. Ridou, J. M. Pouvesle, E. Robert, and C. Grillon, "Cold atmospheric plasma-induced acidification of tissue surface: Visualization and quantification using agarose gel models," *J. Phys. D. Appl. Phys.*, vol. 52, no. 24, 2019.
- [299] D. Zhang, D. B. Das, and C. D. Rielly, "Microneedle Assisted Micro-Particle Delivery from Gene Guns: Experiments using skin-mimicking agarose gel," *J. Pharm. Sci.*, vol. 103, no. 2, pp. 613–627, 2014.
- [300] Y. Deng, G. Winter, and J. Myschik, "Preparation and validation of a skin model for the evaluation of intradermal powder injection devices," *Eur. J. Pharm. Biopharm.*, vol. 81, no. 2, pp. 360–368, 2012.
- [301] V. Normand, D. L. Lootens, E. Amici, K. P. Plucknett, and P. Aymard, "New insight into agarose gel mechanical properties," *Biomacromolecules*, vol. 1, no. 4, pp. 730–738, 2000.
- [302] D. Singh, S. Boakye-Yiadom, and D. S. Cronin, "Comparison of porcine brain mechanical properties to potential tissue simulant materials in quasi-static and sinusoidal compression," *J. Biomech.*, vol. 92, pp. 84–91, 2019.
- [303] F. Pervin, W. S. Avenue, W. Lafayette, W. W. Chen, W. S. Avenue, and W. Lafayette, "Mechanically Similar Gel Simulants for Brain Tissues," *Dyn. Behav. Mater.*, vol. 1, pp. 9–13, 2010.
- [304] M. Nachman and S. E. Franklin, "Artificial Skin Model simulating dry and moist in vivo human skin friction and deformation behaviour," *Tribol. Int.*, vol. 97, pp. 431–439, 2016.

- [305] J. G. Williams and C. Gamonpilas, "Using the simple compression test to determine Young's modulus, Poisson's ratio and the Coulomb friction coefficient," *Int. J. Solids Struct.*, vol. 45, no. 16, pp. 4448–4459, 2008.
- [306] A. Kalra, A. Lowe, and A. M. Al-Jumaily, "Mechanical Behaviour of Skin: A Review," *J. Mater. Sci. Eng.*, vol. 5, no. 4, 2016.
- [307] M. Pawlaczyk, M. Lelonkiewicz, and M. Wieczorowski, "Age-dependent biomechanical properties of the skin," *Postep. Dermatologii i Alergol.*, vol. 30, no. 5, pp. 302–306, 2013.
- [308] B. Lautrup, *Physics of Continuous Matter*, 2nd ed. .
- [309] C. Pailler-Mattei, R. Debret, R. Vargiolu, P. Sommer, and H. Zahouani, "In vivo skin biophysical behaviour and surface topography as a function of ageing," *J. Mech. Behav. Biomed. Mater.*, vol. 28, pp. 474–483, 2013.
- [310] Y. A. Kvistedal and P. M. F. Nielsen, "Estimating material parameters of human skin in vivo," *Biomech. Model. Mechanobiol.*, vol. 8, no. 1, pp. 1–8, 2009.
- [311] M. Geerligs, L. van Breemen, G. Peters, P. Ackermans, F. Baaijens, and C. Oomens, "In vitro indentation to determine the mechanical properties of epidermis," *J. Biomech.*, vol. 44, no. 6, pp. 1176–1181, 2011.
- [312] A. Kalra, A. Lowe, and A. Al Jumaily, "An Overview of Factors Affecting the Skins Youngs Modulus," *J. Aging Sci.*, vol. 4, no. 2, 2016.
- [313] S. Diridollou *et al.*, "In vivo model of the mechanical properties of the human skin under suction," *Ski. Res. Technol.*, vol. 6, no. 4, pp. 214–221, 2000.
- [314] R. Sanders, "Torsional elasticity of human skin in vivo," *Pflügers Arch. Eur. J. Physiol.*, vol. 342, no. 3, pp. 255–260, 1973.
- [315] S. Diridollou *et al.*, "Skin ageing: Changes of physical properties of human skin in vivo," *Int. J. Cosmet. Sci.*, vol. 23, no. 6, pp. 353–362, 2001.
- [316] C. Pailler-Mattei, S. Bec, and H. Zahouani, "In vivo measurements of the elastic mechanical properties of human skin by indentation tests," *Med. Eng. Phys.*, vol. 30, no. 5, pp. 599–606, 2008.
- [317] P. G. Agache, C. Monneur, J. L. Leveque, and J. De Rigal, "Mechanical Properties and Young's Modulus of Human Skin in Vivo," *Arch. Dermatol. Res.*, vol. 269, pp. 221–232, 1980.
- [318] F. Khatyr, C. Imberdis, D. Varchon, J.-M. Lagarde, and G. Josse, "Measurement of the mechanical properties of the skin using the suction test. Comparison between three methods: geometric, Timoschenko and finite elements," *Ski. Res. Technol.*, vol. 12, pp. 24–31, 2007.
- [319] Y. Hara, Y. Masuda, T. Hirao, and N. Yoshikawa, "The relationship between the Young's modulus of the stratum corneum and age: A pilot study," *Ski. Res. Technol.*, vol. 19, no. 3, pp. 339–345, 2013.
- [320] K. H. Lim *et al.*, "New extensometer to measure in vivo uniaxial mechanical properties of human skin," *J. Biomech.*, vol. 41, no. 5, pp. 931–936, 2008.
- [321] J. F. M. Manschot and A. J. M. Brakkee, "The measurement and modelling of the mechanical

- properties of human skin in vivo-I. The measurement," *J. Biomech.*, vol. 19, no. 7, pp. 511–515, 1986.
- [322] K. Langer, "On the anatomy and physiology of the skin," *Br. J. Plast. Surg.*, 1862.
- [323] D. L. Bader and P. Bowker, "Mechanical characteristics of skin and underlying tissues in vivo," *Biomaterials*, vol. 4, no. 4, pp. 305–308, 1983.
- [324] K. Elleuch, R. Elleuch, and H. Zahouani, "Comparison of Elastic and Tactile Behavior of Human Skin and Elastomeric Materials Through Tribological Tests," *Polym. Eng. Sci.*, pp. 1715–1720, 2006.
- [325] G. Boyer, H. Zahouani, A. Le Bot, and L. Laquieze, "In vivo characterization of viscoelastic properties of human skin using dynamic micro-indentation," *J. Biomed. Heal. Informatics*, pp. 4584–4587, 2007.
- [326] G. Boyer, L. Laquière, A. Le Bot, S. Laquière, and H. Zahouani, "Dynamic indentation on human skin in vivo: Ageing effects," *Ski. Res. Technol.*, vol. 15, no. 1, pp. 55–67, 2009.
- [327] G. Boyer, C. Pailler Mattei, J. Molimard, M. Pericoi, S. Laquieze, and H. Zahouani, "Non contact method for in vivo assessment of skin mechanical properties for assessing effect of ageing," *Med. Eng. Phys.*, vol. 34, no. 2, pp. 172–178, 2012.
- [328] A. Delalleau, G. Josse, J. M. Lagarde, H. Zahouani, and J. M. Bergheau, "Characterization of the mechanical properties of skin by inverse analysis combined with the indentation test," *J. Biomech.*, vol. 39, no. 9, pp. 1603–1610, 2006.
- [329] Y. Zheng and A. F. T. Mak, "Effective elastic properties for lower limb soft tissues from manual indentation experiment," *IEEE Trans. Rehabil. Eng.*, vol. 7, no. 3, pp. 257–267, 1999.
- [330] T. Virén, J. T. Iivarinen, J. K. Sarin, I. Harvima, and H. N. Mayrovitz, "Accuracy and reliability of a hand-held in vivo skin indentation device to assess skin elasticity," *Int. J. Cosmet. Sci.*, vol. 40, no. 2, pp. 134–140, 2018.
- [331] C. Escoffier, J. De Rigal, A. Rochefort, R. Vassalet, J.-L. Lèvêque, and P. G. Agache, "Age-related mechanical: an in vivo study," *J. Invest. Dermatol.*, vol. 93, no. 3, pp. 353–357, 1989.
- [332] F. Khatyr, C. Imberdis, P. Vescovo, D. Varchon, and J. Lagarde, "Model of the viscoelastic behaviour of skin in vivo and study of anisotropy," *Ski. Res. Technol.*, pp. 96–103, 2004.
- [333] J. A. Stammen, S. Williams, D. N. Ku, and R. E. Guldberg, "Mechanical properties of a novel PVA hydrogel in shear and unconfined compression," *Biomaterials*, vol. 22, no. 8, pp. 799–806, 2001.
- [334] T. J. Koob and D. J. Hernandez, "Mechanical and thermal properties of novel polymerized NDGA-gelatin hydrogels," *Biomaterials*, vol. 24, no. 7, pp. 1285–1292, 2003.
- [335] H. A. C. Atkinson, I. T. Johnson, J. M. Gee, F. Grigoriadou, and K. Miller, "Brown Norway rat model of food allergy: Effect of plant components on the development of oral sensitization," *Food Chem. Toxicol.*, vol. 34, no. 1, pp. 27–32, 1996.
- [336] J. L. Van Gramberg, M. J. de Veer, R. E. O'Hehir, E. N. T. Meeusen, and R. J. Bischof, "Use of Animal Models to Investigate Major Allergens Associated with Food Allergy," *J. Allergy*, vol. 2013, pp. 1–10, 2013.

- [337] L. M. J. Knippels, A. H. Penninks, M. Van Meeteren, and G. F. Houben, "Humoral and cellular immune responses in different rat strains on oral exposure to ovalbumin," *Food Chem. Toxicol.*, vol. 37, no. 8, pp. 881–888, 1999.
- [338] K. Modlinska and W. Pisula, "The natural history of model organisms the norway rat, from an obnoxious pest to a laboratory pet," *Elife*, vol. 9, pp. 1–13, 2020.
- [339] L. M. J. Knippels and A. H. Penninks, "Assessment of the allergic potential of food protein extracts and proteins on oral application using the Brown Norway rat model," *Environ. Health Perspect.*, vol. 111, no. 2, pp. 233–238, 2003.
- [340] L. M. J. Knippels, G. F. Houben, S. Spanhaak, and A. H. Penninks, "An oral sensitization model in Brown Norway rats to screen for potential allergenicity of food proteins," *Methods A Companion to Methods Enzymol.*, vol. 19, no. 1, pp. 78–82, 1999.
- [341] M. Pérez *et al.*, "Development and characterization of an allergic asthma rat model for interventional studies," *Int. J. Mol. Sci.*, vol. 21, no. 11, 2020.
- [342] A. S. R. Ballegaard, C. B. Madsen, and K. L. Bøgh, "An Animal Model for Wheat Allergy Skin Sensitisation: A Comparative Study in Naive versus Tolerant Brown Norway Rats," *Int. Arch. Allergy Immunol.*, vol. 178, no. 2, pp. 106–118, 2019.
- [343] K. L. Bøgh, V. Barkholt, and C. B. Madsen, "Characterization of the Immunogenicity and Allergenicity of Two Cow's Milk Hydrolysates - A Study in Brown Norway Rats," *Scand. J. Immunol.*, vol. 81, no. 5, pp. 274–283, 2015.

## Appendix A: Manuscript I

### Manuscript I

Dermal Tissue Penetration of In-plane Silicon Microneedles Evaluated in Skin-Simulating Hydrogel, Rat Skin and Pig Skin. Stephanie Ingemann Bisgaard, Long Quang Nguyen, Katrine Lindholm Bøgh, Stephan Sylvest Keller, *submitted to Advanced Healthcare Materials*.

# Dermal Tissue Penetration of In-plane Silicon Microneedles Evaluated in Skin-simulating Hydrogel, Rat Skin, and Porcine Skin

Stephanie Ingemann Bisgaard<sup>a,b</sup>, Long Quang Nguyen<sup>a</sup>, Katrine Lindholm Bøgh<sup>b</sup>, Stephan Sylvest Keller<sup>a,\*</sup>

<sup>a</sup> National Centre for Nano Fabrication and Characterization, DTU Nanolab, Technical University of Denmark, Ørstedes Plads, Building 347, 2800 Kgs. Lyngby, Denmark.

<sup>b</sup> The National Food Institute, DTU Food, Technical University of Denmark, Kemitorvet, Building 202, 2800 Kgs. Lyngby, Denmark.

\* Corresponding author: [suke@dtu.dk](mailto:suke@dtu.dk)

Keywords: Microneedles, transdermal drug delivery, intradermal sensing, tissue penetration, skin-simulating hydrogel

## Abstract

In the past decade, microneedle-based sensors have been introduced as a novel strategy for in situ monitoring of biomarkers in the skin. Here, in-plane silicon microneedles with different dimensions and shapes are fabricated and their ability to penetrate skin is evaluated. Arrays with flat, triangular, hypodermic, lancet-shaped and pencil-shaped microneedles, and a length of 500-1000  $\mu\text{m}$  are considered. The fracture force is higher than 20 N for all microneedle arrays (MNA) confirming a high mechanical stability of the microneedles. The penetration force in skin-simulating hydrogels, excised abdominal rat skin and porcine ear skin is at least five times lower than the fracture force for all MNA designs. The lowest force for skin penetration is required for triangular microneedles with a low width and thickness. Skin tissue staining and histological analysis of rat abdominal skin and porcine ear skin confirm successful penetration of the epidermis for all MNA designs. However, the penetration depth is between 100-300  $\mu\text{m}$ , which is considerably lower than the microneedle length. Tissue damage estimated by visual analysis of the penetration hole is smallest for triangular microneedles. Penetration ability and tissue damage are compared to the skin prick test (SPT) needle applied for allergy testing in the skin.

## 1. Introduction

A main challenge for transdermal drug delivery is that many drugs are not capable of crossing the skin barrier to induce a therapeutic effect [1]. In the past two decades, microneedles have been introduced addressing this issue and demonstrating delivery of different compounds such as drugs or vaccines to the skin [2], [3]. More recently, microneedles have also been proposed as intradermal sensors for measuring glucose [4], [5], glutamate [6] and other biomarkers in the skin [7], [8]. Microneedle-based sensors are typically designed to penetrate the epidermis and reach the interstitial fluid (ISF) in the dermis, where biomarkers are readily accessible for analysis. Microneedles have been fabricated with many different shapes, sizes, and materials which are usually optimized for the specific purpose they serve. Microneedle materials include for example ceramics [9], polymers [10], silicon [11], and metals [12]. The microneedles can be nano-porous [13], hollow [14], or solid [15], and these formats have all been used for transdermal delivery of compounds from either within or on the microneedles. In most cases, microneedles are

designed as out-of-plane arrays where several hundred microneedles penetrate the skin at the same time. Alternatively, they are placed in a single row in an in-plane configuration [2], [16].

The overall aim for microneedles is to minimize invasiveness while ensuring that a drug is delivered at the correct location or that the microneedle-based sensor reaches the desired site for performing specific measurements. Therefore, several aspects should be considered for tissue penetration when designing microneedles for a specific application. Firstly, the mechanical stability of the microneedles should be sufficiently high to allow penetration of the epidermis and avoid fracture inside the skin. For mechanical characterization, microneedles are exposed to compressive, or shear stress and their mechanism of failure is observed [17] to evaluate if they fracture, bend [18] or buckle [19]. Additionally, the fracture force is measured as the force the microneedles can withstand before breaking [20]. For quantitative analysis, force displacement curves have been recorded with custom made equipment [21] or using a texture analyzer (TA) [22]. Secondly, the force required for skin tissue penetration with the microneedles should be as low as possible and preferably orders of magnitude lower than their fracture force. The penetration ability of microneedles can be quantified by analysis of the penetration force. Microneedle geometry has a large impact on the penetration force and should therefore be optimized. The geometrical parameters include the center-to-center spacing (pitch) between the microneedles in the array, their base [23], [24] and tip diameters [25], as well as the shape of the microneedle tip [15], [26]. Thirdly, the penetration depth has been identified as the most influential factor when determining delivery efficiency [26]. Finally, the microneedles should cause minimal injury to the surrounding tissue. Therefore, it is relevant to compare the local tissue damage caused by microneedles as an indication of the invasiveness.

For evaluation of these parameters, various strategies have been considered. Skin samples and skin simulants are widely employed for testing of the mechanical stability and penetration ability of microneedles [27]. Hydrogels such as gelatin and agarose are most commonly used as materials for skin tissue simulants because they are easy to prepare and their specific composition can be adapted to simulate different tissues [28]–[32]. There, when optimizing the skin-simulating model, it is relevant to compare the Young's modulus of the simulant and the type of tissue that it should mimic [33], [34]. As an alternative to skin simulants, excised skin samples from humans [13], [27] or animals [23], [35] have been used as *ex vivo* models. Kochhar *et al.* compared several skin models based on excised rat or porcine skin mounted on hard or soft substrates serving as tissue-like mechanical supports, and with human skin as a reference [23]. The study concluded that a soft polydimethylsiloxane (PDMS) substrate better mimics skin tissue than a hard material such as clay. The skin layers vary depending on the species and on the location the tissue sample was removed from. Porcine skin has been established as an excellent model for human skin [36] and specifically porcine ear skin has high similarity with human forearm skin [37], [38]. For visual confirmation of skin penetration, staining with methylene blue or Trypan blue has often been used. These compounds stain the skin where it has been damaged resulting in blue dots where microneedles have penetrated the skin sample [39] [21]. Measurements of the Trans-epidermal water loss (TEWL) measurements before and after microneedle insertion can provide an indication of the overall tissue damage caused by the microneedles [40]. However, these methods are unable to provide insight into the actual local effect of individual microneedles on the dermal tissue or quantitative information about the penetration depth.

The aim of this study was to evaluate in-plane silicon microneedles for dermal tissue penetration with the future perspective of microneedle-based sensing in the ISF. The ideal microneedles for this application require a low force for penetration of the epidermis, reach the dermis, and cause minimal tissue damage. For the systematic investigation of these aspects, in-plane silicon microneedles with various shapes and

dimensions were fabricated with conventional Si microfabrication methods. The penetration force, penetration depth, and local tissue damage were evaluated using skin-simulating hydrogels, excised abdominal rat skin, and porcine ear skin, combining force-distance measurements, optical microscopy and skin tissue staining. For direct comparison with a clinical application, the lancet needle used for skin prick testing (SPT) in allergy diagnostics was included in this study since it is specifically designed to reach the dermis [41]. Finally, the detailed investigation of Si microneedle penetration allowed for a comparative discussion of the three different skin tissue models employed in terms of their ease of use and biological relevance.

## 2. Results

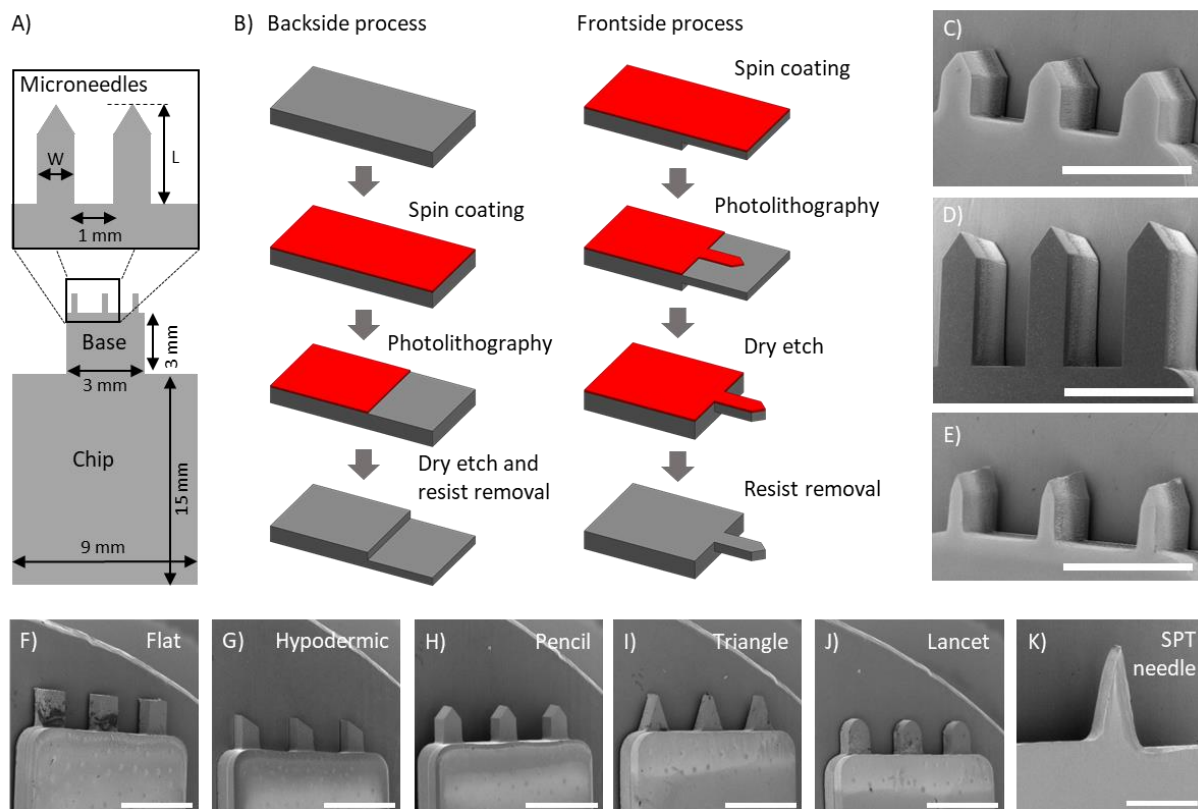
### 2.1. Microfabrication of in-plane Si microneedles

First, microneedle chips with in-plane Si microneedle arrays (MNA) were designed and fabricated. The design of the microneedle chips is illustrated in **Figure 1A**. The main chip had dimensions of 9 mm x 15 mm facilitating handling during application of the microneedles. A base of 3 mm x 3 mm extruded from the main chip and an array of three in-plane microneedles extruded from the base. The base was included to act as a physical barrier during insertion of the microneedles into the skin and to prevent damage of the tissue by the main chip.

The microneedle chips were fabricated by Si micromachining as illustrated in **Figure 1B**. In brief, two consecutive iterations of photolithography and etching from the back- and frontside of a 4-inch Si wafer were performed to define the thickness of the microneedles and the microneedle shape, respectively. On each wafer, 16 microneedle chips were fabricated.

For a systematic evaluation of skin penetration, MNA with different dimensions and shapes were designed. The length  $L$  of microneedle-based intradermal sensors reported in the literature varies quite significantly with values ranging from 150-1500  $\mu\text{m}$  [42]. Therefore, MNA with  $L=500\ \mu\text{m}$  (L500) and  $L=1000\ \mu\text{m}$  (L1000) (**Figure 1C-D**) were fabricated for this study. For further investigation of the effect of dimensional parameters, microneedles with two different widths  $W=200\ \mu\text{m}$  (W200) and  $W=400\ \mu\text{m}$  (W400) (**Figure 1C and 1E**) and three different thicknesses  $T=180\ \mu\text{m}$  (T180),  $T=350\ \mu\text{m}$  (T350), and  $T=500\ \mu\text{m}$  (T500) were prepared. Finally, MNA with five different shapes were fabricated including flat, hypodermic, pencil-shaped, triangular, and lancet microneedles (**Figure 1F-J**). These shapes represent the most reported microneedle geometries while the flat MNA served as a control. **Figure 1K** shows the SPT needle with a length of approximately 1100  $\mu\text{m}$ , width of 700  $\mu\text{m}$  and a thickness of 270  $\mu\text{m}$  used for comparison.





**Figure 1:** MNA design and fabrication. A) Schematic illustration of the Si chip with the array of three microneedles.  $W$  = microneedle width and  $L$  = microneedle length; B) Schematic overview of the microfabrication method with backside and frontside processes defining the thickness and shape of the in-plane Si microneedles; C-E): SEM images of MNA with different length  $L$ , width  $W$  and thickness  $T$ : C)  $(L500, W400, T500)$ ; D)  $(L1000, W400, T500)$ ; E)  $(L500, W200, T500)$ ; F-K): SEM images showing the different microneedle shapes (flat (control), hypodermic, pencil, triangular, and lancet) used in this study  $(L500, W400, T500)$ , along with the skin prick test (SPT) needle for comparison. Scalebars = 1 mm.

## 2.2. Mechanical stability of in-plane Si microneedles

After fabrication, the mechanical stability of the MNA was investigated. The measurements of the fracture force upon compression demonstrated excellent mechanical stability of the in-plane Si microneedles. Even for the MNA with three microneedles of  $(L1000, W200, T180)$  the fracture force was  $24.9 \pm 11.3$  N (Figure S1A, SI). For evaluation of the mechanical stability towards shear stress after insertion in the skin, the MNA were dragged through a vertically placed skin-simulating hydrogel (Figure S1B-C, SI). The microneedles did not break when exposed to the shear stress and were able to withstand a shear force of  $0.15 \pm 0.02$  N. These results indicate a high mechanical stability for application in the skin for all the MNA designs used in this study.

## 2.3. Microneedle penetration in skin-simulating hydrogel

### 2.3.1. Penetration force measurements in agarose hydrogels

A skin-simulating model was established for initial evaluation of penetration ability of the microneedles. The main advantage of using skin simulants was that material properties could more easily be controlled than for real skin samples facilitating comparative measurements. Penetration force measurements in a well-established skin-simulating model should allow for systematic investigation of the influence of the different microneedle dimensions and shapes on skin penetration.

Here, agarose hydrogel was chosen as the skin model since it has been shown previously to be a good skin simulant [1,2,3]. A method for reproducible preparation of agarose hydrogels in a 3D printed mold was developed (Figure S2A-D, SI). The agarose content in the hydrogel determines the viscoelastic properties of the gel [44]. According to literature, a skin tissue model typically requires 2-3% w/v of agarose [45]–[47] while a 0.6% w/v agarose hydrogel is more appropriate for brain tissue models [48], [49]. In preliminary experiments, hydrogels with concentrations of 1.5% and 2% w/v agarose were prepared. The Young's modulus, indicating the material stiffness, was determined by compression tests and compared with skin tissue (Figure S2E-F, SI). Based on these results, 1.5% w/v agarose hydrogel was chosen as the skin-simulating model and used immediately after preparation.

For the evaluation of their ability to penetrate the skin-simulating hydrogel, MNA chips with different microneedle dimensions and shapes were mounted on a texture analyzer (TA) (**Figure 2A** and S2G-I, SI). During the measurements, the force was recorded while vertically approaching the hydrogel with a constant speed of 2 mm s<sup>-1</sup> (Figure S2J, SI). In the resulting force-displacement curves, typically two force peaks were identified (**Figure 2B**). The origin of these peaks was determined by correlating the vertical probe movement with the lengths of the microneedles and the MNA base. The first peak was assigned to the penetration of the microneedles into the hydrogel while the second peak was attributed to the consecutive penetration of the MNA base.

Figure 2B shows two force-displacement curves recorded for pencil-shaped MNA with a length of 500 μm and 1000 μm, respectively. After an initial stage of gel compression (step 3), approximately the same force was required to penetrate the hydrogel (step 4) independently of the microneedle length. However, Figure 2B illustrates that it was more difficult to identify the penetration peak for the shorter microneedles due to the subsequent contact between the base and the hydrogel (step 5). Therefore, all force-displacement curves were differentiated for easier identification of the force peaks. The most relevant parameter extracted from these recordings was the penetration force corresponding to the force value of the first peak ( $F_p$  in Figure 2B).

### *2.3.2. Influence of microneedle dimensions on penetration force*

First, the influence of the MNA dimensions on the penetration force was investigated. **Figure 2C** confirms, using a two-way ANOVA with Tukey's multiple comparisons test, that there is no significant difference between the required penetration force for the same MNA when the length is changed between 500 and 1000 μm. Thus, the length of the MNA had no effect on the force required for penetration of the hydrogel. However, a statistically significant difference was found when increasing the width from 200 μm to 400 μm for the same microneedle shape, thus indicating that the microneedle width impacts the force required for penetration of the hydrogel. Comparing the penetration force between W200 and W400, an increase of approximately 40% for the L1000 and 44% for L500 was found, respectively. A similar impact on the penetration force was confirmed for all the different MNA shapes (L500, T500) when increasing the width from 200 μm to 400 μm as shown in **Figure 2D**. The difference between the two widths was statistically significant for all MNA designs except for the triangle shape. In general, an increase of the

penetration force between 48-62% was observed for the wider microneedles compared to the narrow ones, which was nicely correlated with an increase of the cross-sectional area of the microneedles by 50%. Considering the third dimensional parameter, the thickness of the microneedles was varied from 180  $\mu\text{m}$  to 350  $\mu\text{m}$  and 500  $\mu\text{m}$  and the results of the penetration force measurements are summarized in **Figure 2E**. The force required for penetration of the hydrogels was significantly different for T180 vs. T350 and T180 vs. T500 for all microneedle shapes. The lower thickness of the microneedles clearly resulted in a decrease of the penetration force. The decrease was approximately 50-66% changing from T500 to T180, which again was very well correlated with a decrease in the cross-sectional area of the microneedles by 64%. The combined results for MNA with different dimensions indicate that the cross-sectional area of the microneedles was the main parameter influencing the penetration force for MNA with a given microneedle shape.

### *2.3.3. Influence of microneedle shape on penetration force*

Next, the influence of the microneedle shape on the penetration force was investigated. As indicated in Figure 2D-E, the trends were similar for all microneedle dimensions. The triangular microneedles resulted in the lowest penetration force, followed by pencil-shaped, hypodermic, and lancet microneedles having similar values, whereas the flat control required the highest force for penetration of the hydrogel. **Figure 2F** compares microneedles with different shapes (L500, W400, T180) with a SPT needle used in the clinic for allergy testing in the dermis. These MNA dimensions were selected because they were closest to the ones of the SPT needle. Multiple statistically significant differences were identified among the different microneedle shapes and the SPT needle. The results showed that the microneedle shape had an impact on the penetration force and confirmed that the MNA with a triangular shape required the lowest force of  $24 \pm 1$  mN for hydrogel penetration. When comparing the MNA with the SPT needle it is important to note that the SPT needle was a single microneedle whereas the MNA consisted of three microneedles. Multiplying the penetration force measured for the SPT needle with a factor of three results in a value comparable to the one for the triangular microneedles.

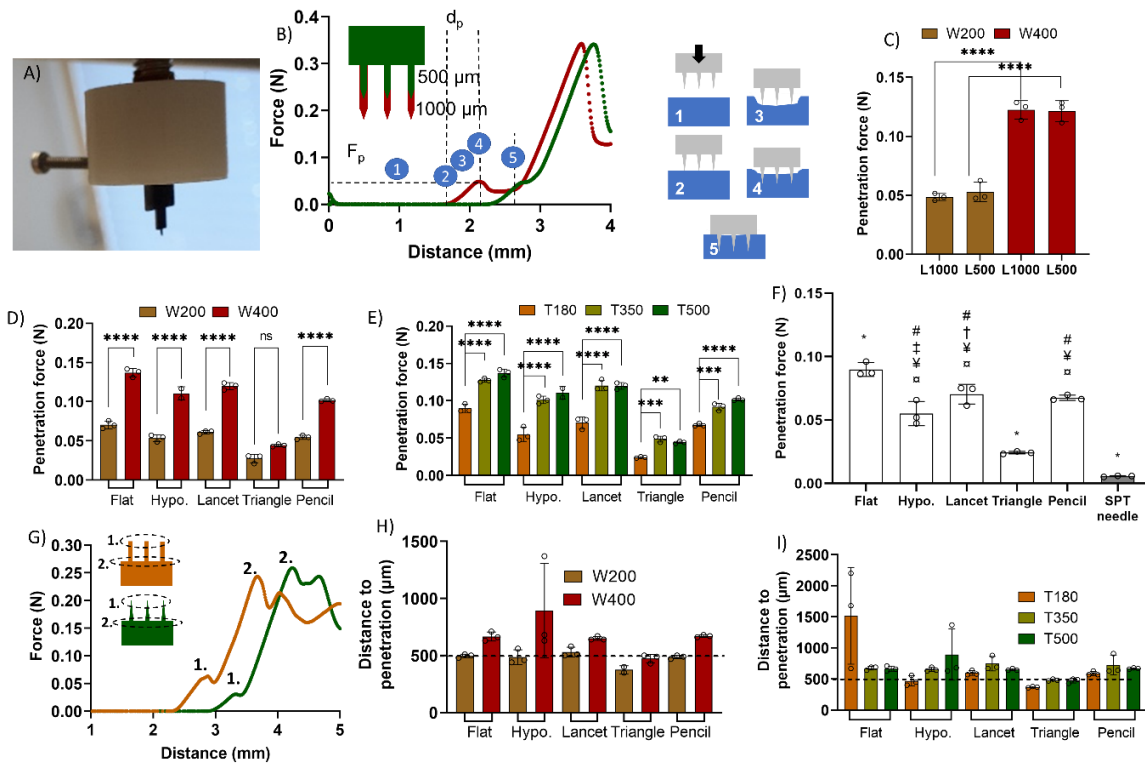
**Figure 2G** is an example of two force-displacement curves measured for a MNA with flat (L500, W200, T500) and triangular microneedles (L500, W200, T500), respectively. For the flat microneedles, a steep and clearly visible peak was measured. Apparently, the skin-simulating hydrogel bounced back up after penetration of the flat microneedle resulting in a decline of the force and yielding a very distinct peak. In comparison, microneedles with the triangular shape were inserted more gradually into the hydrogel, thus merely causing a plateauing of the force measured after initial penetration.

### *2.3.4. Influence of microneedle geometry on hydrogel compression before penetration*

As an additional parameter for evaluation of hydrogel penetration, the vertical compression of the skin-simulating hydrogel by the MNA before measurable penetration occurred was considered. More specifically, the vertical distance travelled from the first detectable contact of the MNA with the hydrogel until the penetration peak was defined as the distance to penetration  $d_p$  (Figure 2B).

**Figure 2H-I** indicates that the distance to penetration was larger for microneedles with a larger width or a higher thickness although differences were less evident than for the penetration force. Furthermore, the results show that for almost all the MNA the distance to penetration was larger than 500  $\mu\text{m}$  (black dotted line), which was the actual length of the microneedles. This was attributed to the elastic properties and compressibility of the skin-simulating hydrogel. For most of the MNA, this also means that eventually

the MNA base (Figure 2A) might have been in contact with the hydrogel before actual microneedle penetration occurred. Figure 2H-I shows that only the triangular microneedles with the lowest thickness and width were able to penetrate the hydrogel after a distance lower than or equal to the microneedle length of 500  $\mu\text{m}$ . On the one hand, an eventual contact of the MNA base before penetration might be a drawback preventing the microneedles from entering the skin and causing damage of the epidermis. On the other hand, the microneedle base might be employed to regulate penetration depth and minimize tissue damage in the dermis. The simplest strategy avoiding contact between the skin-simulating hydrogel and the MNA base before penetration was to increase the microneedle length to 1000  $\mu\text{m}$ .



**Figure 1:** Microneedle penetration in skin-simulating hydrogel. A) Image of MNA chip mounted on texture analyzer; B) Force-displacement curves recorded for pencil-shaped MNA (L1000, W200, T500) (red) and (L500, W200, T500) (green): 1 - MNA approaching the skin-simulating hydrogel, 2 - Initial contact of microneedles with the hydrogel, 3 - Compression of the elastic hydrogel due to the applied force, 4 - Microneedles penetrating the hydrogel, 5 - Microneedles fully inserted and physical contact between MNA base and hydrogel;  $F_p$  = penetration force correlated with microneedle penetration in step 4;  $d_p$  = distance to penetration; C) Penetration force for pencil-shaped MNA with different lengths and widths (T500); Penetration force for MNA with five different microneedle shapes with D) (L500, T500) and two different widths, E) (L500, W400) and varying thicknesses, and F) (L500, W400, T180) compared with SPT needle. # Significant difference ( $\alpha = 0.05$ ) from flat, † Significant difference from hypodermic, ‡ Significant difference from lancet, ¥ Significant difference from triangle, ¢ Significant difference from pencil, ¤ Significant difference from SPT needle, \*Significant difference from all other shapes and SPT needle (One-way ANOVA with Tukey's multiple comparisons test); G) Force-displacement curves recorded for flat (orange) and triangular (green) MNA (L500, W200, T500); Distance to penetration for MNA with five different microneedle shapes with H) (L500, T500) and two different widths, and I) (L500, W400) and varying thicknesses. The black dotted line indicates the actual length of the microneedles; All values are mean  $\pm$

SD. For statistical analyses (except in F) a two-way ANOVA with Tukey's multiple comparisons test was used, and the significant differences are marked as: \*\*  $p \leq 0.01$ , \*\*\*  $p \leq 0.001$ , \*\*\*\*  $p \leq 0.0001$ .

## 2.4. Ex vivo penetration of rat abdominal skin

### 2.4.1. Penetration force measurements in excised rat abdominal skin

The penetration experiments in the hydrogel skin model provided an excellent indication of the penetration behavior of different in-plane Si microneedles. However, it is imperative to investigate penetration ability of the microneedles in real skin samples. Based on the results obtained with the skin-simulating hydrogel model, the triangular and pencil-shaped microneedles as well as the flat control were selected for further investigation in ex vivo studies. The thickness of all microneedles was 180  $\mu\text{m}$  while the width was varied between 200  $\mu\text{m}$  and 400  $\mu\text{m}$  and the length between 500  $\mu\text{m}$  and 1000  $\mu\text{m}$ . The SPT needle was again included for comparison. Abdominal skin samples of six rats, three males, and three females, were used for this ex vivo animal study. After sacrificing the animals, the excised abdominal skin samples for penetration force measurements were fixed to their original size using a custom-built 3D-printed tissue fixture (**Figure 3A-B**). According to literature, a supporting layer placed beneath the skin sample provides a better approximation of real skin tissue [23], [39], [50]. Therefore, a 1.5% w/v skin-simulating hydrogel was placed beneath the excised rat skin as a supporting tissue layer. In a similar setup as for the skin-simulating model, the TA was used for skin penetration (Figure S3A, SI). Penetration force measurements were done in duplicates on each skin sample and placed either at the edge or in the center resulting in a total of 12 measurements for each MNA design. No significant difference between the penetration force measured in the center and at the edge of the skin sample was observed (Figure S3B, SI).

For the penetration force measurements in the skin-simulating hydrogels, a penetration force could be extracted for all the MNA using differentiation of the force-displacement curves. However, for the rat abdominal skin samples detection of skin penetration with the same method was clearly more challenging and not possible for all MNA designs. **Figure 3C** shows force-displacement curves recorded for triangular microneedles with different dimensions representative for the three main categories of penetration measurements observed in rat abdominal skin: 1) The presence of a penetration peak with a low force < 1 N for (L1000, W200), 2) the presence of a penetration peak with a high force > 1 N for (L1000, W400) and 3) the absence of a penetration force peak for (L500, W200). To ensure that the extracted penetration force in fact was the one of the microneedles and not the one of MNA base, the first peak in the force-displacement curves was only analyzed if a second peak was present. If only one peak was identified, it was impossible to determine with certainty whether it corresponded to penetration of the microneedles or the base, and such measurements were therefore not considered.

### 2.4.2. Influence of microneedle dimensions on rat skin penetration

**Figure 3D** reports the percentage of force-displacement measurements with successful detection of a penetration peak for the investigated MNA. For all microneedles with a length of 500  $\mu\text{m}$  and for MNA with a flat tip less than 25% of the measurements allowed to extract a penetration force. In comparison, the success rate for the triangular microneedles with a length of 1000  $\mu\text{m}$  and the pencil-shaped MNA with (L1000, W200) was close to 100%. The results indicate that a microneedle length of 500  $\mu\text{m}$  was insufficient for reliable detection of skin penetration, while it was facilitated for the longer microneedles

with a pointed shape. For the shorter MNA, the base (Figure 1A) probably encountered the skin sample well before penetration of the microneedles, which impacted the force measurement. The longer MNA travelled a longer distance before the base encountered the skin sample, which allowed for easier penetration and distinction of the force peaks.

In **Figure 3E** the penetration forces successfully extracted from the measurements in excised rat skin are summarized for the different MNA. These results show that in the few successful measurements with MNA having a length of 500  $\mu\text{m}$  and for flat microneedles, penetration forces were high (category 2 above). In comparison, the penetration force for triangular and pencil-shaped microneedles with a length of 1000  $\mu\text{m}$  was below 1 N in almost all measurements (category 1 above). Nevertheless, the penetration force for all microneedles was more than 10 times lower than the fracture force (Figure S1A, SI) and no damage of the MNA was observed after penetration of rat abdominal skin. Considering the width of the microneedles, no influence on the penetration force was observed. **Figure 3F** presents the distance to penetration for the same measurements. The black dotted line marks the distance equivalent to the respective microneedle lengths. Essentially, these measurements indicate that after first detectable contact with the skin all the MNA were travelling longer than their respective microneedle lengths before penetration occurred. The fact that the penetration distance was longer than the length of the microneedles showcases the high degree of elasticity of the rat abdominal skin. In summary, only the MNA with a length of 1000  $\mu\text{m}$  and triangular or pencil-shaped microneedles provided sufficient data for further statistical analysis of skin penetration.

#### *2.4.3. Microneedle penetration in skin from male and female rats*

First, individual rats of the same sex were compared to obtain an indication of the reproducibility of the microneedle testing and the eventual influence of animal-to-animal variations. For this analysis, the inclusion criterium was at least duplicate measurements for two different rats, and only three MNA fulfilled this criterion (triangular, L1000, W200; triangular, L1000, W400; pencil-shaped, L1000, W200).

**Figure 3G** shows the statistical comparison between the individual males and females. No significant differences between individual rats within the same sex were identified using a one-way ANOVA with Tukey's multiple comparisons test except for the triangular MNA with (L1000, W400) in male rats. This indicates that the excised rat skin from different animals within the same sex is likely similar.

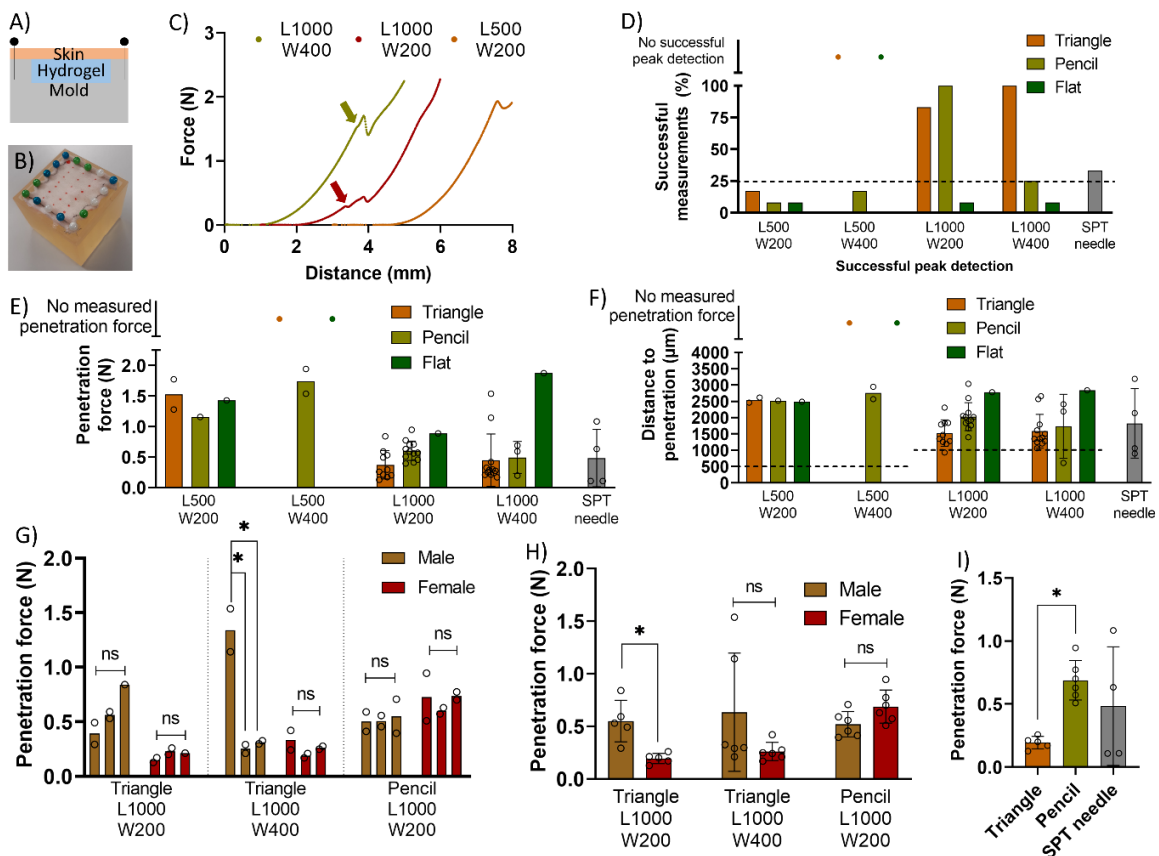
Secondly, penetration force measurements in male and female rats were compared to evaluate potential influence of rat abdominal skin properties depending on the sex. **Figure 3H** is a comparison between the same MNA designs tested in male and female rat skin samples. It appears that the female rat skins tend to require less penetration force than the male rat skins considering the mean values obtained with triangular microneedles. For the statistical analysis, the inclusion criterium was at least three force measurements for male and female rats, respectively. An unpaired T-test with Bonferroni correction ( $\alpha=0.016$ ) demonstrated that significantly higher forces were required for penetration of the skin of male rats compared to female rats considering the triangular MNA with (L1000, W200). This suggests that there are differences between microneedle penetration in male and female skin samples, probably due to a higher skin thickness for male rats (Figure 3C, SI). On a more qualitative level, the skin samples from females were generally easier to handle as they appeared to be more elastic. This means that the sex of the rats had to be considered when comparing dermal tissue penetration with microneedles.

#### *2.4.4. Influence of microneedle shape on rat skin penetration*

Based on the findings above, the penetration forces measured in the female rat skin were pooled for each of the two different microneedle shapes and compared with the SPT needle. **Figure 3I** shows a comparison of the triangular and pencil-shaped MNA (L1000, W200) with the SPT needle. The mean penetration force is lower for the triangular microneedles than for the pencil-shaped microneedles and the SPT needles. The difference between the triangular and pencil-shaped MNA was statistically significant considering a one-way ANOVA with Tukey's multiple comparisons test. These findings on the microneedle shape are in line with the results obtained with the skin-simulating hydrogels where the triangular shape in general displayed the lowest measured penetration force.

#### 2.4.5. Comparison of penetration forces in skin simulating hydrogel and excised rat abdominal skin

Comparing the penetration forces measured in the hydrogels (Figure 2) and rat skin samples (Figure 3), it is evident that the rat skin samples required more than ten times higher force for penetration by the microneedles. This may be attributed to the fact that the hydrogel skin model is not able to simulate the presence of the epidermis and the stratum corneum [51], which are the most robust dermal tissue layers to be penetrated. Furthermore, the distance to penetration is considerably higher for excised rat skin samples compared to hydrogel skin-simulants probably because they are more elastic than agarose hydrogels when mounted above the supporting layer in the tissue fixture.



**Figure 3:** Ex vivo penetration of rat abdominal skin. A) Schematic cross-sectional view of a pinned down excised rat abdominal skin sample with the 1.5% w/v skin-simulating hydrogel placed beneath as support

mimicking the flesh. B) Image of the experimental setup with the pinned down excised rat abdominal skin sample on the 3D printed mold. C) Force-displacement curve recorded for three triangular MNA with different dimensions. The arrows indicate the penetration force peak position identified by differentiation of the curve. Red – successful measurement with a low penetration force, green – successful measurement with a high penetration force, and orange – no detectable penetration force; D) Percentage of successful penetration force peak detection for a total of 12 measurements with each MNA design (6 rats, 2 measurements). The black dotted line indicates at least three measurements with peak detection; E) Penetration force and F) distance to penetration (mean  $\pm$  SD) extracted from successful measurements in D) for MNA with different shapes and dimensions. The black dotted lines in F) indicate the distance corresponding to the microneedle length; G) Individual penetration forces for abdominal skin samples from 3 male and 3 female rats (one-way ANOVA with Tukey's multiple comparisons test,  $\alpha=0.05$ ); H) Comparison of penetration force (mean  $\pm$  SD) for skin from males and females (Unpaired T-test using Bonferroni correction,  $\alpha=0.016$ ); I) Penetration force (mean  $\pm$  SD) for triangular and pencil-shaped MNA (L1000, W200) compared with the SPT needle in female rats (two-way ANOVA with Tukey's multiple comparisons test,  $\alpha=0.05$ ). For all statistical analyses the significant differences are marked as: \*  $p \leq 0.05$ .

## 2.5. Penetration hole depth and tissue damage in rat abdominal skin

### 2.5.1. Tissue staining for visualization of penetration holes in rat abdominal skin

For a visual investigation of dermal tissue penetration by the in-plane Si microneedles, the same MNA designs as the ones used for the ex vivo penetration experiments in excised rat skin were manually applied to the abdominal skin of six euthanized rats (three male and three female). Skin samples with penetration holes were collected for paraffin histology to visually evaluate skin penetration and tissue damage. For histology, the skin samples were cut into 5  $\mu\text{m}$  thick slices and stained with Mayer's hematoxylin and eosin for visualization of the skin layers and penetration holes. **Figure 4A-D** shows examples of scanned images of histology slices containing a microneedle penetration hole. The thickness of the stratum corneum and the epidermis for abdominal rat skin prepared in paraffin has been reported as 5  $\mu\text{m}$  and 12  $\mu\text{m}$ , respectively[52]. In all images, the microneedles penetrated through the stratum corneum and the epidermis (dark layer), and into the dermis.

Visual identification of penetration holes in the rat abdominal skin tissue slices was challenging and more difficult for some MNA designs than for others. There was a clear tendency that it was easier to identify penetration holes caused by pencil-shaped microneedles compared to the other shapes (Figure S4A, SI). However, it should be noted that for all investigated MNA designs at least six penetration holes could be found using histology, demonstrating that the microneedles were able to penetrate the skin. This was the case even though it was impossible to identify penetration force peaks in TA measurements on excised rat abdominal skin for some of the MNA designs (Figure 3D). This might indicate that skin penetration with the microneedles was more difficult with a gradual slow approach in excised skin compared to manual application on the rat skin before it was excised. Another explanation could be that the TA method was not sensitive enough to measure penetration forces for some of the MNA.

### 2.5.2. Influence of microneedle design on penetration hole depth in rat skin

The tissue staining and histological identification of the penetration holes allowed for analysis of the penetration hole depth and width, and the estimation of the overall tissue damage caused by the MNA with different dimensions and shapes. For statistical comparisons six microneedle penetration holes were



considered for each MNA design, which had to originate from at least three different animals, and where both female and male animals had to be represented.

**Figure 4E** summarizes the maximum depth of the penetration holes identified for different MNA. All MNA including the SPT needle penetrated through the stratum corneum and the epidermis, and into the dermis. However, the measured hole depth was considerably lower than the actual microneedles. This means that either the microneedles were incompletely inserted into the skin tissue (Figure S4B, SI) or that the penetration hole depth visible in the stained tissue slices was smaller than the actual penetration depth of the microneedles due to partial closure of the skin tissue after retracting the MNA. For the penetration hole depth, no statistically significant differences were found between microneedles with different shapes and dimensions, and when comparing the in-plane Si MNA with the SPT needle. However, the mean values in Figure 4E indicate that the penetration depth for pencil-shaped > triangular > flat MNA. This is also observed when comparing Figure 4A representing a hole caused by a pencil-shaped microneedle with Figure 4B representing a hole caused by a flat microneedle with the same dimensions (L1000, W400). There, the hole for the pencil-shaped microneedle was deeper than for the flat microneedle. Most surprisingly, the penetration hole depth in Figure 4E seemed to be independent of the length for flat and triangular microneedles. Only for pencil-shaped microneedles the mean values indicate that longer needles penetrated deeper into the skin as it would be expected.

### *2.5.3. Influence of microneedle design on tissue damage in rat skin*

For a first assessment of tissue damage, the width of the penetration holes at the stratum corneum (top of the dark layer in Figure 4A-D) was measured and the results are summarized in **Figure 4F**. For all MNA including the SPT needle, the measured hole width was lower than the actual width of the microneedles. This supports the hypothesis of partial recovery of the skin tissue after removal of the microneedles discussed above for the penetration depth. Similar to the penetration hole depth, no significant differences for the penetration hole width between the MNA designs could be identified. However, the mean values for the hole width for pencil-shaped and triangular microneedles with a width of 400  $\mu\text{m}$  were higher than for the microneedles with a width of 200  $\mu\text{m}$ . This follows the expectation that wider microneedles should cause wider holes upon penetration of the skin than more narrow ones.

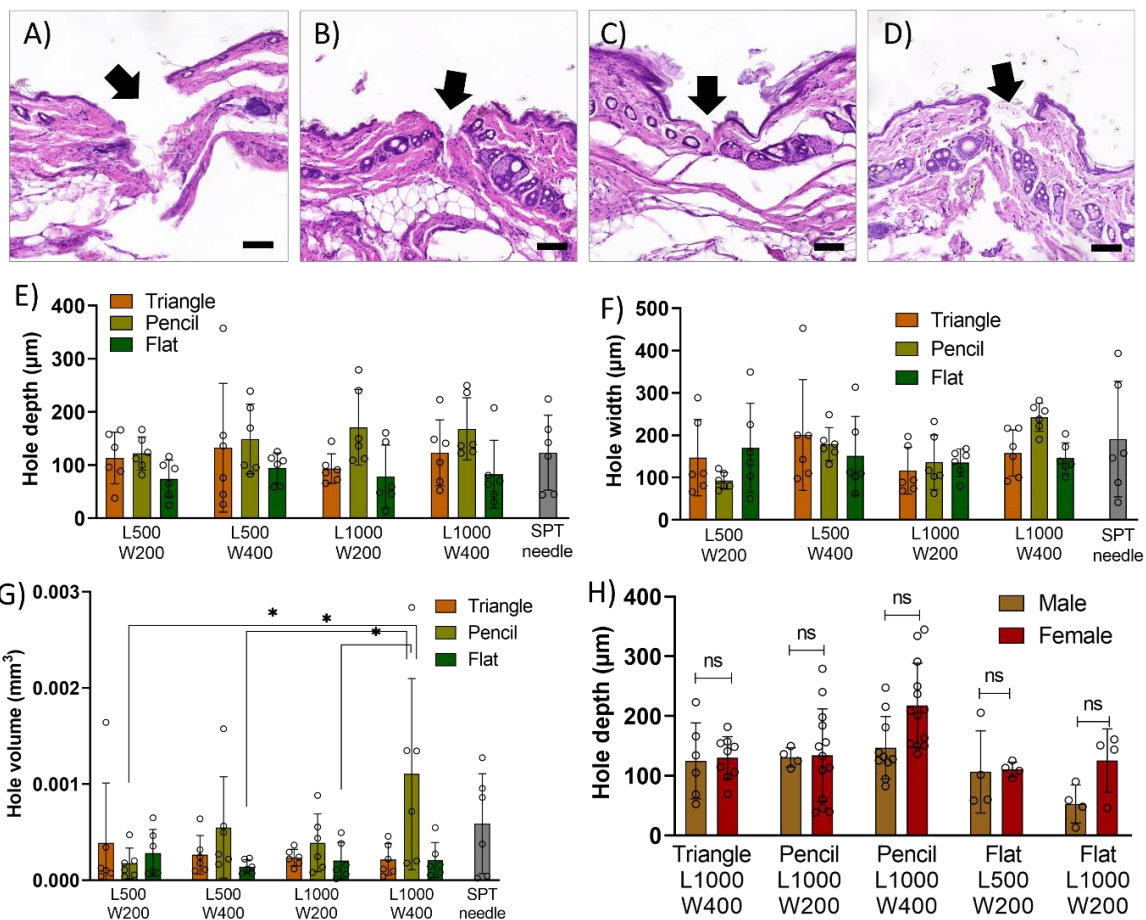
For a more generic comparative analysis of tissue damage, the volume of the penetration holes was estimated using the hole width and the hole depth (S5 – SI). **Figure 4G** shows the hole volume for the different MNA designs. As a general observation on the microneedle shape, pencil-shaped microneedles seemed to cause larger tissue damage than flat and triangular ones. Figure 4B and Figure 4D represent a penetration hole caused by a flat and a triangular microneedle, respectively, displaying less tissue damage compared to Figure 4A showing the rat skin with a penetration hole caused by a pencil-shaped microneedle with the same dimensions. Interestingly, skin penetration with the flat MNA resulted in relatively low mean hole volumes (Figure 4G), while it was expected that this design would cause most tissue damage.

When analyzing the influence of microneedle dimensions on the penetration hole volume, less tissue damage was observed for pencil-shaped microneedles with shorter length and smaller width compared to longer and wider ones. Figure 4C represents a penetration hole caused by a pencil-shaped microneedle with (L500, W200) having less volume than the one for the microneedle with (L1000, W400) shown in Figure 4A. The pencil-shaped microneedles with (L1000, W400) had the largest mean value for the hole volume with large standard deviations, indicating a large variation in tissue damage with this MNA design.

The mean values in Figure 4G suggest that the hole volume for the triangular, flat, and most pencil-shaped microneedles was smaller compared to the one for the SPT needle, which means that the in-plane Si microneedles are not causing more tissue damage than the SPT needle applied for allergy testing in the clinic.

#### 2.5.4. Penetration hole depth and tissue damage in skin from male and female rats

Finally, eventual differences in the penetration hole depth and tissue damage between male and female rats were investigated. The inclusion criterium for the different MNA designs was the identification of at least three holes for male and female rats each. **Figure 4H** is a comparison of the penetration hole depth for male and female rats. Using unpaired T-tests with Bonferroni correction ( $\alpha=0.01$ ) no significant differences were found between male and female rats, meaning that the tissue damage caused by the MNA was similar for both sexes. However, it is worth noting that penetration holes were more easily identified in female skin samples during histological analysis. In total, 41% more holes in skin samples from females than in tissue from males. This indicates that even if the individual microneedles did not cause significantly different tissue damage there was still very likely a difference between the properties of male and female skin. This is in line with the observations during penetration force measurements, where male rat skin proved to be more difficult to penetrate than female rat skin.



**Figure 4:** Histological analysis of penetration depth and tissue damage in rat abdominal skin. A-D) Scanned images of histology slices (scale bar = 100  $\mu\text{m}$ ) containing a penetration hole caused by A) pencil-shaped (L1000, W400), B) flat (L1000, W400), C) pencil-shaped (L500, W200) and D) triangular (L1000, W400) microneedles; E-G) Analysis of skin slices with penetration holes for different MNA dimensions and shapes ( $n=6$ ): E) Hole depth, F) hole width and G) estimated hole volume; H) Comparison of the microneedle hole depth in the skin of male and female rats for different MNA designs and dimensions ( $n=4-13$ ). All values are mean  $\pm$  SD. For the statistical analyses in E)-G) a three-way ANOVA with Tukey's multiple comparisons test was used and in H) unpaired T-tests with Bonferroni correction ( $\alpha=0.01$ ); the significant differences are marked as: \*  $p \leq 0.05$ .

## 2.6. Ex vivo penetration of porcine ear skin

### 2.6.1. Penetration force measurements in porcine ear skin

In previous studies, the skin of the porcine ear was reported to closely resemble the skin on a human forearm [37], [38]. Therefore, for easier translation to human skin, a porcine ear was excised and the penetration force measurements conducted on the rat abdominal skin samples were repeated on the porcine ear skin using the TA (**Figure 5A**). The penetration forces were evaluated for flat, triangular, and pencil-shaped MNA with the same dimensions as for the rat abdominal skin experiments and with at least three replicate measurements for each MNA design. The value of the penetration force was extracted using differentiation as mentioned previously for rat abdominal skin and hydrogel skin models.

The force-displacement curves recorded in porcine ear skin largely resembled the ones for rat abdominal skin (Figure 3C) and the same three categories of measurements were observed as exemplified in **Figure 5B**: 1) The presence of a penetration peak with a low force  $< 2$  N (triangular, L1000, W200) clearly identifiable in the differentiated curve (Figure S6A, SI), 2) the presence of a penetration peak with a high force  $> 2$  N (flat, L1000, W200) that was difficult to identify and 3) the absence of a penetration force peak (flat, L1000, W400). It should be noted that all MNA were perfectly intact after the penetration measurements.

### 2.6.2. Influence of microneedle design on porcine skin penetration

Similar to the study with rat skin samples, detection of penetration force peaks was challenging for many of the MNA designs (Figure S6B, SI). Particularly for the shorter microneedles with a length of 500  $\mu\text{m}$ , penetration force peaks could only be identified in a few measurements and the penetration force was  $> 2$  N (Figure S6C, SI). In comparison, peak detection was clearly facilitated for the microneedles with a length of 1000  $\mu\text{m}$  with up to 100% successful measurements for the pencil-shaped microneedles (L1000, W400) and flat (L1000, W200) (Figure S6B, SI). These results are in line with the findings for rat abdominal skin, confirming that a microneedle length of 500  $\mu\text{m}$  was not enough for reliable measurements of skin penetration.

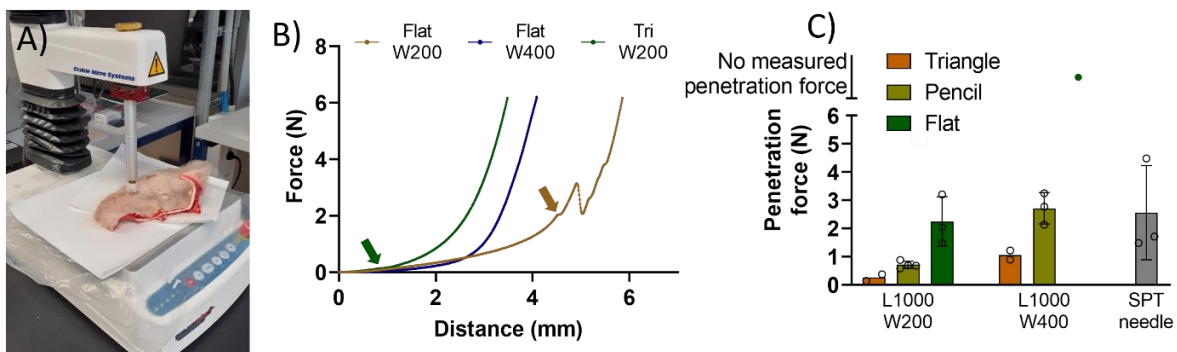
Therefore, only the long microneedles were considered for further statistical analysis and discussion. **Figure 5C** presents the penetration forces measured in porcine ear skin for MNA with a length of 1000  $\mu\text{m}$ . The microneedles with triangular shape required the lowest force for skin penetration followed by pencil-shaped MNA and the flat control. Furthermore, penetration force was lower for the microneedles with a width of 200  $\mu\text{m}$  compared to the ones with a width of 400  $\mu\text{m}$ . These findings are in good agreement with the measurements in skin-simulating hydrogels, while the measurements in rat abdominal skin were less conclusive. Notably, the penetration forces for the triangular MNA measured

in porcine ear skin were considerably lower than for the SPT needle, despite the fact that the MNA consisted of three microneedles.

Furthermore, considering the distance to penetration (Figure S6D, SI), it was evident that the vertical movement of the TA probe between first skin contact and microneedle penetration was larger than the microneedle length for almost all MNA designs. This is in line with the observations for the rat abdominal skin and probably implies that the MNA base encountered the skin sample prior to penetration. The only exception was the triangular MNA with (L1000, W200) where the distance to penetration was equal to the microneedle length. This confirms that this MNA was most optimal for penetration of porcine ear skin.

### 2.6.3. Comparison of penetration forces in excised rat abdominal skin and porcine ear skin

The results for the ex vivo penetration studies conducted in rat abdominal skin and porcine ear skin were comparable. In both skin models analysis of the penetration force based on force-distance measurements with the TA was not very successful for microneedles with a length of 500  $\mu\text{m}$ . For the longer microneedles, in both tissue models triangular MNA with a width of 200  $\mu\text{m}$  required the lowest force for skin penetration of all investigated MNA designs, with 194 mN and 254 mN in female rat and porcine skin, respectively. For most of the other MNA designs and the SPT needles, penetration forces measured in porcine skin were slightly higher than in rat skin. This might be explained by a higher thickness of porcine ear skin compared to rat skin [51]. Furthermore, hard tissue layers such as cartilage were present below the porcine skin while the excised rat abdominal skin was mounted above soft hydrogels during the measurements. Similarly, the distance to penetration for all MNA designs was higher in porcine ear skin (Figure S6D, SI) compared to the values for the rat abdominal skin samples (Figure 3F). This indicates that more tissue compression was required to penetrate the slightly thicker porcine ear skin compared to the rat skin.



**Figure 5:** Ex vivo penetration of rat abdominal skin. A) Image showing the setup for performing penetration force measurements on porcine ear skin. B) Force-displacement curves recorded for flat (L1000, W200), triangular (L1000, W200) and flat (L1000, W400) MNA. The penetration force peak positions identified by differentiation of the force-displacement curve are indicated by arrows. C) Penetration force (mean  $\pm$  SD) for microneedles with a length of 1000  $\mu\text{m}$  compared to the SPT needle.

## 2.7. Penetration hole depth and tissue damage in porcine ear skin

### 2.7.1. Tissue staining for visualization of penetration holes in porcine ear skin

A histological analysis in porcine ear skin was conducted to complement the force measurements, visually confirm skin penetration and analyze tissue damage. In an identical procedure as for the rat abdominal

skin samples, MNA with different designs were manually applied to porcine skin, dermal tissue samples were collected and stained, and histology was performed. For these experiments, flat, triangular and pencil-shaped MNA with dimensions (L1000, W400, T180) were selected because these microneedles caused most tissue damage in rat abdominal skin (Figure 4I). **Figure 6A-D** shows representative images of scanned histology slices with penetration holes caused by four different MNA designs. The thickness of porcine ear skin prepared in paraffin has been reported as 10  $\mu\text{m}$  and 51  $\mu\text{m}$  for stratum corneum and epidermis, respectively [52]. The images demonstrate that the microneedles were able to successfully penetrate the skin layers of stratum corneum and epidermis, and reach down into the upper dermis. For additional confirmation of MNA penetration, the porcine ear was stained with methylene blue. This is a hydrophilic, low molecular weight molecule, which usually cannot be absorbed through the hydrophobic stratum corneum unless the tissue has been damaged [39]. The blue dots in **Figure 6E** show that the MNA penetrated through the stratum corneum. With an optical microscope blue-stained penetration holes could be observed for all the MNA designs confirming that all the microneedles penetrated the skin.

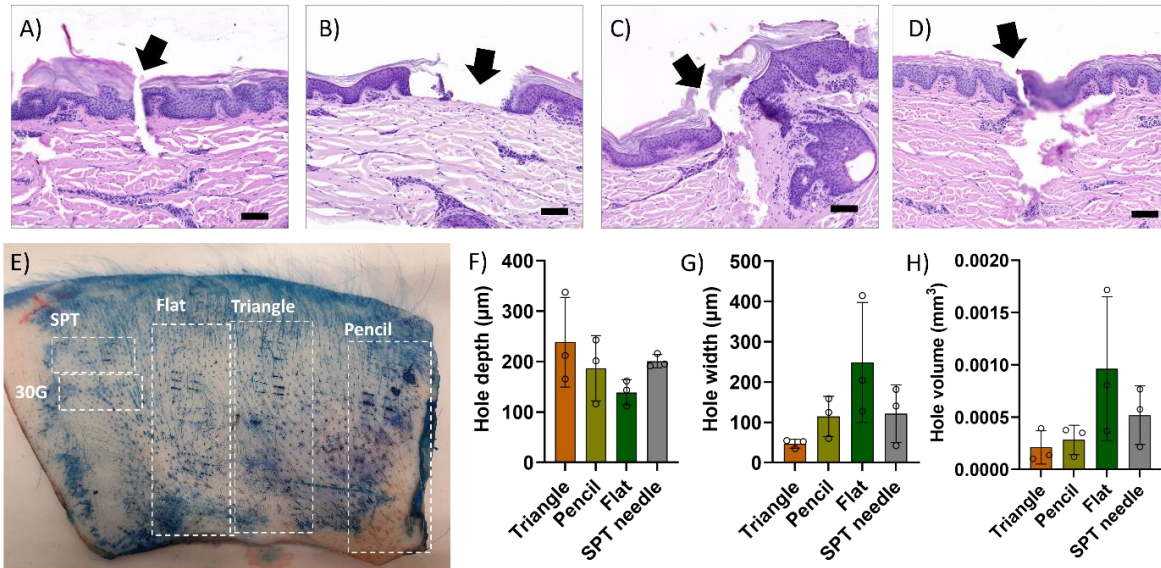
### *2.7.2. Influence of microneedle design on hole depth and tissue damage*

As previously for the rat abdominal skin, the stained skin slices allowed to characterize penetration hole depth, hole width and tissue damage. **Figure 6F-G** shows the maximum penetration hole depths and widths for different microneedle shapes and the SPT measured in the histology slices. The depth of the penetration holes was significantly lower than the actual microneedle length of 1000  $\mu\text{m}$ , which is in line with the results observed for rat skin samples (Figure 4E). Either the microneedles were not completely inserted into the porcine skin, or the skin tissue partially recovered after physical removal of the MNA.

**Figure 6H** presents the penetration hole volume estimated using the hole depth and width for different microneedle shapes and the SPT as a measure for tissue damage ( $S5 - S1$ ). Using a one-way ANOVA with Tukey's multiple comparisons test no significant differences were found in Figure 6F-H. However, the results indicate that the triangular microneedles caused deeper penetration holes with a lower width compared to the flat microneedles generating wider holes and penetrating less deep into the tissue, while the pencil-shaped microneedles were in between. This is also visible in Figure 6A-C showing images of penetration holes caused by triangular, flat and pencil-shaped microneedles, respectively. The lower mean values for the penetration hole volume of triangular and pencil-shaped microneedles (Figure 6H) compared to flat microneedles and SPT needles indicate that these MNA cause least tissue damage. The histological analysis of penetration holes confirmed the results from the penetration force measurements where the triangular microneedles were identified as most suitable for penetration of porcine ear skin.

### *2.7.3. Comparison of penetration depth and tissue damage in rat abdominal skin and porcine ear skin*

A comparison of the histological analysis of rat abdominal skin (Figure 4E-G) with the one for porcine skin (Figure 6F-H) shows that the penetration hole depth and the tissue damage for identical MNA designs was very similar in both skin models. In both cases, the measured penetration hole depth was significantly lower than what was expected based on the microneedle length. In general, the width of the penetration holes seemed to be slightly lower in porcine ear skin compared to rat skin, which might be attributed to higher recovery of the porcine skin after removal of the MNA.



**Figure 6:** Histological analysis of penetration depth and tissue damage in porcine ear skin; A-D) Scanned images of histology slices (scale bar = 100  $\mu\text{m}$ ) containing a penetration hole caused by A) triangular, B) flat, C) pencil-shaped microneedles with (L1000, W400, T180) and D) a SPT needle; E) Image of porcine ear skin stained with methylene blue. The blue dots indicate microneedle penetration holes. The SPT needle and a 30G hypodermic needle were included for comparison; F-H) Analysis of porcine skin slices with penetration holes for microneedle with (L1000, W400, T180) and different shapes: F) Hole depth, G) hole width and H) estimated hole volume; all values are (mean  $\pm$  SD) (n=3).

### 3. Discussion

In-plane Si microneedles with different shapes and dimensions were fabricated for the systematic investigation of skin tissue penetration as a first step towards the vision of microneedle-based sensing in the dermis. More specifically, flat, hypodermic, pencil-shaped, lancet-shaped, and triangular microneedles with variable lengths, widths and thicknesses were compared. The penetration ability of the MNA was assessed in 1.5% w/v agarose-based skin-simulating hydrogel, excised abdominal rat skin and porcine ear skin serving as three distinct skin models.

The method implemented for microfabrication of in-plane Si microneedles provides high flexibility with respect to the MNA design. The length, width, shape and number of the Si microneedles in the array are fully defined by the mask design in the photolithography steps, and the microneedle thickness is solely determined by the duration of the etching process from the backside. Furthermore, the microfabrication method readily allows future integration of sensing modalities required for detection of biomarkers in the skin. For example, electrodes and optical components have been integrated on Si-based neural probes prepared with a similar method [53]. These are advantages compared to typical strategies for microfabrication out-of-plane microneedles such as micromoulding [54], metal micromachining [55] or additive manufacturing [56].

The most important requirement for safe intradermal sensing with microneedles is sufficient mechanical stability to prevent fracture during skin penetration. For this purpose, the force resulting in fracture of the microneedles must be compared with the force required for penetration of the target tissue. In this study, the measured penetration forces for all MNA designs were at least five times lower than the lowest

fracture force and no physical damage of the microneedles was observed after testing. In all three skin models, penetration forces for triangular microneedles were lowest compared to the other shapes. In porcine ear skin, microneedles with triangular shape, a width of 200  $\mu\text{m}$ , a thickness of 180  $\mu\text{m}$  and a length of 1000  $\mu\text{m}$  displayed penetration forces approximately 100 times lower than the fracture force. The thickness and properties of porcine ear skin are similar to human skin, which should leave a reasonable margin for safe application of the in-plane Si microneedles in human skin. Furthermore, the penetration forces for these MNA were lower than for the SPT needle applied for intradermal allergy testing in the clinic.

Following the expectations, the cross-sectional area of the microneedles was the main geometric parameter influencing the penetration force in skin-simulating hydrogels. This means that both reducing thickness and decreasing the width can be considered to reduce the penetration force if needed. There, the preferred strategy might depend on the final application of the MNA. For microneedle-based sensing, a larger width might be preferred compared to a higher thickness because this facilitates integration of sensing modalities on the top surface of the microneedles. The length had no apparent effect on penetration force in skin-simulating hydrogels. However, reliable penetration force measurements in rat abdominal skin were only possible with microneedles having a length of 1000  $\mu\text{m}$ , which was attributed to the high elasticity of real skin samples.

The histological analysis of penetration holes in rat abdominal skin and porcine ear skin, and methylene blue staining, demonstrated successful penetration of the epidermis and into the dermis with all investigated in-plane Si microneedles. However, the measured depth of the penetration holes was between 100-300  $\mu\text{m}$ , which was significantly less than the actual length of the microneedles. This was attributed to incomplete insertion of the microneedles due to the high elasticity of the skin combined with partial recovery of the tissue after physical removal of the MNA from the skin. Nevertheless, the MNA reached the dermis and potentially could be used for microneedle-based sensing in the ISF. Furthermore, tissue damage was assessed through estimation of the penetration hole volume. The results indicated that triangular microneedles caused less damage compared to flat and pencil-shaped microneedles, and the SPT needle in both rat abdominal skin and porcine ear skin.

As an additional outcome, the three skin models employed in this study can be compared. Hydrogel skin-simulant, rat abdominal skin and porcine ear skin are all viable options for systematic evaluation of microneedles and certainly can complement each other. Penetration forces were one order of magnitude lower than in real skin tissue samples. Nevertheless, the fact that the trends for the penetration force were similar for all three tissue models confirms that skin-simulating hydrogels are an excellent non biological model for initial comparative testing of microneedles due to a simple preparation method and higher reproducibility of the measurements. The results for the ex vivo penetration studies conducted in rat abdominal skin and porcine ear skin were comparable. While it seems that both skin tissue models are suitable for systematic evaluation of microneedle penetration, other aspects could be relevant if only one of them should be selected. For example, measurements on porcine ear skin might be advantageous due to the availability of porcine ears as byproduct from pig slaughter while experiments with excised rat skin require access to dedicated animal facilities. The differences in penetration forces measured in rat abdominal skin from males and females emphasize the importance of parameters such as sex, age, tissue location and species on results from ex vivo and in vivo testing of microneedles. Therefore, comparison with values reported in literature is often challenging.

## 4. Conclusions

The in-plane Si microneedles fabricated in this study were able to penetrate the stratum corneum and the epidermis of rat abdominal skin and porcine ear skin. The microneedles were inserted a few 100  $\mu\text{m}$  into the dermis, which should allow for future microneedle-based detection of biomarkers in the interstitial fluid. The results demonstrate that the microneedle shape matters both with respect to the force required for penetration of different skin models and tissue damage. Triangular microneedles seemed to be optimal for dermal tissue penetration. The Si microneedles demonstrated high mechanical stability, no fracture or physical damage was observed after skin penetration.

## 5. Experimental section

### 5.1. Microfabrication of in-plane Si microneedles

For 500  $\mu\text{m}$  thick microneedles, a 17  $\mu\text{m}$  thick film of SU-8 2035 (Kayaku Advanced Materials, Westborough, MA, USA) was deposited on 500  $\mu\text{m}$  thick double side polished (DSP) 4-inch Si wafers (Siegert Wafers, Aachen, Germany) using a RCD8 T spin coater from Süss MicroTec (Garching, Germany) and soft-baked on a hotplate for 30 min at 50°C. The pattern of the microneedles was designed in CleWin 5 layout editor (WeWin software, Hengelo, The Netherlands). UV exposure of the resist was performed at a wavelength of 375 nm on a maskless aligner MLA150 from Heidelberg Instruments (Heidelberg, Germany) with a dose of 200  $\text{mJ cm}^{-2}$  and a defocus value  $\text{DF}=0$ . A post exposure bake was conducted for 2 h at 50 °C followed by development in mr-Dev 600 (Microresist Technologies, Berlin, Germany) for 2x5 min. The Si wafers were mounted on another Si carrier substrate with Crystalbond 555 (SPI Supplies, West Chester, PA, USA) using a hotplate at 90°C for 60 s. The photoresist pattern was transferred into the Si by deep reactive ion etching (DRIE) in an STS ICP Advanced Silicon Etcher (SPTS Technologies, Newport, UK) for 500 cycles using the BOSCH process. The etch process was divided in subsets of approximately 50 cycles with waiting periods of 5 min in between to reduce heating of the Crystalbond and prevent delamination of the etched Si wafer from the underlying Si carrier substrate. This process resulted in complete etching through the Si wafer and definition of the outline of the microneedles. Finally, the photoresist was removed during 30 min in a Plasma Asher 300 from PVA TePla (Wettenberg, Germany) with 400 sccm  $\text{O}_2$ , 70 sccm  $\text{N}_2$  and a power of 1000 W. The microneedle chips were collected from the underlying carrier substrate by heating the Crystalbond to 90°C on a hotplate.

For 350  $\mu\text{m}$  thick microneedles, a 20  $\mu\text{m}$  thick layer of AZ4562 photoresist (Merck KgaA, Darmstadt, Germany) was spin coated on 350  $\mu\text{m}$  DSP Si wafers with a Gamma 4M spin coater from Süss MicroTec and soft-baked at 110°C for 10 min. UV exposure on the MLA was performed with a dose of 1100  $\text{mJ cm}^{-2}$  and  $\text{DF}=-2$ . Robot puddle development in TMAH was performed using 10 steps with AZ726 MIF Developer (Merck KgaA, Darmstadt, Germany) for 60 s each. DRIE etching was performed as described above using 300 etch cycles. For fabrication of 180  $\mu\text{m}$  thick Si microneedles, two iterations of photolithography with AZ4562 and DRIE were implemented. First, the 350  $\mu\text{m}$  thick DSP 4-inch Si wafers were etched from the backside with 150 cycles to thin down the needles and then the outline of the Si microneedles was etched from the topside with 175 cycles.

### 5.2. Mechanical stability of in-plane Si microneedles



For testing of the mechanical stability of the microneedles a texture analyser (TA) (Stable Microsystems, Godalming, UK) was used. First, compression tests were performed with the microneedle chip mounted in a vertical position. For this purpose, custom-made microneedle holders were prepared using fused filament fabrication (FFF) with poly(lactic acid) (PLA) on a Felix Pro Series printer (FELIX Printers, IJsselstein, The Netherlands) (Figure S2I, SI). The TA probe was moved down onto the TA platform with a speed of 2 mm/s and the force required for microneedle fracture was determined. Only flat MNA (L1000, W200, T180) were tested. The mechanical stability towards shear stress was evaluated using a 3D-printed shear stress holder where the MNA were attached horizontally (Figure S1B-C). The skin-simulating hydrogel was mounted vertically while still in its mold and the microneedles were inserted into the hydrogel. Then, the MNA were dragged downwards through the hydrogel using the TA and subsequently inspected to identify structural damage. MNA with (T180, W200 and W400) and three different lengths of L500, L750 and L1000 were tested.

### 5.3. Preparation of skin-simulating hydrogels

Agarose powder type I (low electroendosmosis (EEO)), CAS: 9012-36-6, Sigma-Aldrich, St. Louis, MO, USA), (1, 1.5 and 2 % w/v) was mixed with de-ionized water in a beaker and placed on a hot plate with a magnetic stirrer (Figure S2A, SI). The hydrogel solution was heated to 80 °C while being slowly stirred until it became transparent. 3D-printed molds were designed using Fusion 360 (Autodesk, CA, USA, V2.0.14793) and sliced using Simplify3D (Simplify3D, OH, USA, version 4.1.2). These were printed using FFF. The hydrogel solution was then poured into the 3D-printed molds and placed in a desiccator for around 20-30 min to slowly remove the air bubbles (Figure S2A, SI). The 3D-printed mold comprised two parts (Figure S2B-C, SI). The top part of the mold was removed once the air bubbles had escaped, and the solution had gelled. The protruding part of the hydrogel was cut to provide a smooth surface for the microneedle testing (Figure S2D, SI). The degassing step was very important for obtaining reproducible measurements of penetration forces. The compressive Young's modulus of the skin-simulating hydrogels was measured using the TA fitted with a large disc-probe vertically compressing the entire hydrogel at once. The compressive Young's modulus value was then calculated using the Exponent Connect software (version 8.0.3.0, Stable Microsystems, Godalming, UK) based on the initial, linear increase in force upon compressing the hydrogel. All skin-simulating hydrogels were used immediately after preparation because storage for >24 h resulted in high variability of the hydrogel properties (Figure S2F, SI).

### 5.4. Penetration force measurements in agarose hydrogels

The penetration force was measured using the TA where the MNA was mounted vertically using the same custom-made 3D-printed microneedle holder as described above for compression testing. The skin-simulating hydrogel was placed horizontally on the TA platform beneath the MNA. The MNA was moved down into the hydrogel at a test speed of 2 mm s<sup>-1</sup> and the force was measured simultaneously. Initial measurements of the penetration force at various insertion speeds were conducted with the TA and an insertion speed of 2 mm s was found to provide the most reproducible penetration force results (Figure 2Sj).

In the recorded force-displacement curves  $F(x)$ , the noise level of baseline was determined by measuring the average force recorded by the TA at a distance of 0.5 mm prior to initial contact of the MNA with the gel. The first point of contact between the hydrogel and the MNA was defined as the distance at which the recorded force exceeded the average value of the baseline + 3 x SD ensuring that the recorded force was above the noise level of the baseline measurement. The penetration force was determined

graphically by plotting the differential of the measured force vs. the vertically moved distance of the microneedles, i.e., plotting  $dF/dx(x)$ . The x-value from the first data point for which  $dF/dx$  was closest to zero ( $\geq 0$ ) was used to determine the penetration force in the  $F(x)$  plot. To ensure that the data point was not background noise, the drop should be higher than the mean value of baseline + 3 x SD. A parameter called “distance to penetration” was defined as the distance between the initial contact between gel and MNA and actual penetration. All statistical analyses were made using GraphPad Prism V9.5.0 (San Diego, CA, USA).

### **5.5. Penetration force measurements in excised rat abdominal skin**

Sample preparation for ex vivo penetration measurements in rat abdominal skin was carried out at the animal facility of the Technical University of Denmark (DTU). Ethical approval was given by the Danish Animal Experiments Inspectorate with the authorization number (2020-15-0201-00732-C1). Brown Norway (BN) rats were from in-house breeding colony of the National Food Institute, DTU. Rats were housed in macrolon cages with aspen bedding at  $22^{\circ}\text{C} \pm 1^{\circ}\text{C}$  with a relative humidity of  $55 \pm 5\%$ . The air was changed 50-55 times/h and electric lights were on from 9.00 a.m. to 9.00 p.m. Before skin excision, the rats were sacrificed by decapitation using carbon dioxide as anesthesia.

From six rats (three male and three female) with an age of 8-9 weeks old, an abdominal skin sample of 30 mm x 30 mm was excised and placed between two tissue papers wetted with PBS preventing drying of the skin. For penetration measurements, the skin samples were stretched to their original size and mounted on a custom-built 3D-printed tissue fixture using pins (Figure 3A). A 1.5% w/v agarose type I powder skin-simulating hydrogel was used as a supporting layer beneath the skin samples during the penetration force measurements (Figure 3A-B). The force measurements were conducted using a TA with a custom-built 3D-printed probe with an identical procedure as for the skin-simulating hydrogels (Figure S3A, SI).

### **5.6. Tissue staining for visualization of penetration holes in rat abdominal skin**

After sacrificing six of the BN rats (three male and three female), the abdominal skin of each rat was pierced manually with three MNA of each design before the skin was excised for histological analysis. For histology, the skin samples were embedded in paraffin blocks and cut into 5  $\mu\text{m}$  thick tissue slices. In each histology session, 111 slices were cut. Every 4<sup>th</sup> slice was stained with Mayer’s hematoxylin and eosin (H&E) for visualization of the skin layers and microneedle penetration holes. All stained tissue slices were scanned using the Panoramic MIDI 3DHISTECH (3DHISTECH Ltd., Budapest, Hungary), CaseViewer software where data was generated through accessing research infrastructure at DTU National Food Institute, including FOODHAY (Food and Health Open Innovation Laboratory, Danish Roadmap for Research Infrastructure). MN penetration holes were identified based on the following criteria: 1) Clear visual disruption of the stratum corneum, 2) the penetration hole appeared on more than one tissue slice, and 3) the tissue slices included initial appearance of a penetration hole and final disappearance ensuring that the complete hole was included. Multiple histology sessions were conducted until at least 6 penetration holes were identified for each MNA design. Using the scanned images, the depth of the holes and the hole-width at stratum corneum was measured using the CaseViewer software (version 2.4.0.119028 provided by 3DHISTECH, Budapest, Hungary). Based on these measurements and the total number of tissue slices where the same hole appeared, the hole volume was calculated (S5, SI).

### 5.7. Penetration force measurements in porcine ear skin

Porcine ears were collected from a pork at The Panum Institute, University of Copenhagen immediately after sacrifice. Thereafter, they were placed in re-sealable plastic bags containing PBS (pH = 7.1-7.5, p15425, Sigma Aldrich, St. Louis, MO, USA) and transported in a polystyrene box containing cooling elements. The porcine ears were used as-is and the MNA penetration force was measured using the TA as described for the rat skin samples. However, the porcine ear skin was not excised to maintain the original stretchability and the penetration force measurements were performed directly on the ear.

### 5.8. Tissue staining for visualization of penetration holes in porcine ear skin

Porcine ears were manually pierced with the MNA and histological analysis of the excised porcine ear skin was performed as described above for rat abdominal skin. Additionally, the porcine ear was manually penetrated with the MNA in known locations and afterwards placed for 1 h in 1% methylene blue (CAS: 122965-43-9, Sigma-Aldrich, St. Louis, MO, USA) diluted in de-ionized water. The skin sample was wiped with a tissue to remove excess methylene blue. The stained penetration holes were observed with an optical microscope (Leica INM100, Leica Microsystems, Wetzlar, Germany).

## 6. Acknowledgements

The authors would like to acknowledge funding from the Independent Research Fund Denmark (grant no. 8022-00215B), and the LEO Foundation (grant no. LF17046). The authors would also like to thank Associate Professor Line Hagner Nielsen from DTU Health Tech for assistance in retrieving the porcine ears and laboratory technician Sarah Grundt Simonsen for helping with ex vivo experiments. Further thanks to the DTU Animal Facility (BioFacility) for taking care of the rats.

## 7. Conflict of interest

The authors declare no conflict of interest.

## 8. Data availability statement

Data can be made available upon request.

## References

- [1] D. V. McAllister, S. Henry, M. G. Allen, and M. R. Prausnitz, "Microfabricated microneedles: A novel approach to transdermal drug delivery," *Proceedings of the Controlled Release Society*, vol. 87, no. 25, pp. 30–31, 1998, doi: 10.1021/js980042.
- [2] K. Van Der Maaden, W. Jiskoot, and J. Bouwstra, "Microneedle technologies for (trans)dermal drug and vaccine delivery," *Journal of Controlled Release*, vol. 161, no. 2, pp. 645–655, 2012, doi: 10.1016/j.jconrel.2012.01.042.

- [3] H. Jun, M. H. Ahn, I. J. Choi, S. K. Baek, J. H. Park, and S. O. Choi, "Immediate separation of microneedle tips from base array during skin insertion for instantaneous drug delivery," *RSC Adv*, vol. 8, no. 32, pp. 17786–17796, 2018, doi: 10.1039/c8ra02334d.
- [4] P. R. Miller, R. J. Narayan, and R. Polsky, "Microneedle-based sensors for medical diagnosis," *J Mater Chem B*, vol. 4, no. 8, pp. 1379–1383, 2016, doi: 10.1039/c5tb02421h.
- [5] L. Zhao, Z. Wen, F. Jiang, Z. Zheng, and S. Lu, "Silk/polyols/GOD microneedle based electrochemical biosensor for continuous glucose monitoring," *RSC Adv*, vol. 10, no. 11, pp. 6163–6171, 2020, doi: 10.1039/c9ra10374k.
- [6] J. R. Windmiller *et al.*, "Bicomponent Microneedle Array Biosensor for Minimally-Invasive Glutamate Monitoring," *Electroanalysis*, vol. 23, no. 10, pp. 2302–2309, 2011, doi: 10.1002/elan.201100361.
- [7] P. Dardano, I. Rea, and L. De Stefano, "Microneedles-based electrochemical sensors: New tools for advanced biosensing," *Curr Opin Electrochem*, vol. 17, pp. 121–127, 2019, doi: 10.1016/j.coelec.2019.05.012.
- [8] M. Dervisevic, M. Alba, B. Prieto-Simon, and N. H. Voelcker, "Skin in the diagnostics game: Wearable biosensor nano- and microsystems for medical diagnostics," *Nano Today*, vol. 30, p. 100828, 2020, doi: 10.1016/j.nantod.2019.100828.
- [9] M. A. Boks, W. W. J. Unger, S. Engels, M. Ambrosini, Y. Van Kooyk, and R. Luttge, "Controlled release of a model vaccine by nanoporous ceramic microneedle arrays," *Int J Pharm*, vol. 491, no. 1–2, pp. 375–383, 2015, doi: 10.1016/j.ijpharm.2015.06.025.
- [10] D. V. McAllister *et al.*, "Microfabricated needles for transdermal delivery of macromolecules and nanoparticles: Fabrication methods and transport studies," *Proc Natl Acad Sci U S A*, vol. 100, no. SUPPL. 2, pp. 13755–13760, 2003, doi: 10.1073/pnas.2331316100.
- [11] E. M. T. Shibata, A. Nakanishi, T. Sakai, N. Kato, T. Kawashima, T. Mineta, "FABRICATION AND MECHANICAL CHARACTERIZATION OF MICRONEEDLE ARRAY FOR CELL SURGERY," *TRANSDUCERS 2007 - 2007 International Solid-State Sensors, Actuators and Microsystems Conference*, pp. 3–3, 2007.
- [12] M. R. Prausnitz, "Microneedles for transdermal drug delivery," *Adv Drug Deliv Rev*, vol. 56, no. 5, pp. 581–587, 2004, doi: 10.1016/j.addr.2003.10.023.
- [13] K. van der Maaden, R. Luttge, P. J. Vos, J. Bouwstra, G. Kersten, and I. Ploemen, "Microneedle-based drug and vaccine delivery via nanoporous microneedle arrays," *Drug Deliv Transl Res*, vol. 5, no. 4, pp. 397–406, 2015, doi: 10.1007/s13346-015-0238-y.
- [14] I. Mansoor, Y. Liu, U. O. Hafeli, and B. Stoeber, "Fabrication of hollow microneedle arrays using electrodeposition of metal onto solvent cast conductive polymer structures," *2013 Transducers and Eurosensors XXVII: The 17th International Conference on Solid-State Sensors, Actuators and Microsystems, TRANSDUCERS and EUROSENSORS 2013*, no. June, pp. 373–376, 2013, doi: 10.1109/Transducers.2013.6626780.

- [15] D. Jenkins, S. Corrie, C. Flaim, and M. Kendall, "High density and high aspect ratio solid micro-nanoprojection arrays for targeted skin vaccine delivery and specific antibody extraction," *RSC Adv*, vol. 2, no. 8, pp. 3490–3495, 2012, doi: 10.1039/c2ra20153d.
- [16] P. Aggarwal and C. R. Johnston, "Geometrical effects in mechanical characterizing of microneedle for biomedical applications," *Sens Actuators B Chem*, vol. 102, no. 2, pp. 226–234, 2004, doi: 10.1016/j.snb.2004.04.024.
- [17] C. O'Mahony, "Structural characterization and in-vivo reliability evaluation of silicon microneedles," *Biomed Microdevices*, vol. 16, no. 3, pp. 333–343, 2014, doi: 10.1007/s10544-014-9836-6.
- [18] P. Khanna, B. R. Flam, B. Osborn, J. A. Strom, and S. Bhansali, "Skin penetration and fracture strength testing of silicon dioxide microneedles," *Sens Actuators A Phys*, vol. 170, no. 1–2, pp. 180–186, 2011, doi: 10.1016/j.sna.2010.09.024.
- [19] C. Radhika and B. K. Gnanavel, "Buckling analysis of polymer microneedle for transdermal drug delivery," *Mater Today Proc*, vol. 46, pp. 3538–3541, 2020, doi: 10.1016/j.matpr.2020.12.397.
- [20] S. P. Davis, B. J. Landis, Z. H. Adams, M. G. Allen, and M. R. Prausnitz, "Insertion of microneedles into skin: Measurement and prediction of insertion force and needle fracture force," *J Biomech*, vol. 37, no. 8, pp. 1155–1163, 2004, doi: 10.1016/j.jbiomech.2003.12.010.
- [21] F. J. Verbaan *et al.*, "Improved piercing of microneedle arrays in dermatomed human skin by an impact insertion method," *Journal of Controlled Release*, vol. 128, no. 1, pp. 80–88, 2008, doi: 10.1016/j.jconrel.2008.02.009.
- [22] Z. Zhu *et al.*, "Rapidly dissolvable microneedle patches for transdermal delivery of exenatide," *Pharm Res*, vol. 31, no. 12, pp. 3348–3360, 2014, doi: 10.1007/s11095-014-1424-1.
- [23] J. S. Kochhar, T. C. Quek, W. J. Soon, J. Choi, S. Zou, and L. Kang, "Effect of microneedle geometry and supporting substrate on microneedle array penetration into skin," *J Pharm Sci*, vol. 102, no. 11, pp. 4100–4108, 2013, doi: 10.1002/jps.23724.
- [24] O. Olatunji, D. B. Das, M. J. Garland, L. Belaid, and R. F. Donnelly, "Influence of array interspacing on the force required for successful microneedle skin penetration: Theoretical and practical approaches," *J Pharm Sci*, vol. 102, no. 4, pp. 1209–1221, 2013, doi: 10.1002/jps.23439.
- [25] A. M. Römgens, D. L. Bader, J. A. Bouwstra, F. P. T. Baaijens, and C. W. J. Oomens, "Monitoring the penetration process of single microneedles with varying tip diameters," *J Mech Behav Biomed Mater*, vol. 40, pp. 397–405, 2014, doi: 10.1016/j.jmbbm.2014.09.015.
- [26] A. Davidson, B. Al-Qallaf, and D. B. Das, "Transdermal drug delivery by coated microneedles: Geometry effects on effective skin thickness and drug permeability," *Chemical Engineering Research and Design*, vol. 86, no. 11, pp. 1196–1206, 2008, doi: 10.1016/j.cherd.2008.06.002.
- [27] S. Kim, S. Shetty, D. Price, and S. Bhansali, "Skin penetration of silicon dioxide microneedle arrays," *Annual International Conference of the IEEE Engineering in Medicine and Biology - Proceedings*, pp. 4088–4091, 2006, doi: 10.1109/IEMBS.2006.260142.

- [28] R. Pomfret, G. Miranpuri, and K. Sillay, "The substitute brain and the potential of the gel model," *Ann Neurosci*, vol. 20, no. 3, pp. 118–122, 2013, doi: 10.5214/ans.0972.7531.200309.
- [29] M. Ahearne, Y. Yang, A. J. El Haj, K. Y. Then, and K. K. Liu, "Characterizing the viscoelastic properties of thin hydrogel-based constructs for tissue engineering applications," *J R Soc Interface*, vol. 2, no. 5, pp. 455–463, 2005, doi: 10.1098/rsif.2005.0065.
- [30] T. Kawashima, "Mechanical characterization and insertion performance of hollow microneedle array for cell surgery," *Journal of Micro/Nanolithography, MEMS, and MOEMS*, vol. 8, no. 3, p. 033014, 2009, doi: 10.1117/1.3206971.
- [31] A. K. Dabrowska *et al.*, "Materials used to simulate physical properties of human skin," *Skin Research and Technology*, vol. 22, no. 1, pp. 3–14, 2016, doi: 10.1111/srt.12235.
- [32] K. Moronkeji, S. Todd, I. Dawidowska, S. D. Barrett, and R. Akhtar, "The role of subcutaneous tissue stiffness on microneedle performance in a representative in vitro model of skin," *Journal of Controlled Release*, vol. 265, pp. 102–112, 2017, doi: 10.1016/j.jconrel.2016.11.004.
- [33] C. Pailler-Mattei, S. Bec, and H. Zahouani, "In vivo measurements of the elastic mechanical properties of human skin by indentation tests," *Med Eng Phys*, vol. 30, no. 5, pp. 599–606, 2008, doi: 10.1016/j.medengphy.2007.06.011.
- [34] Y. Deng, G. Winter, and J. Myschik, "Preparation and validation of a skin model for the evaluation of intradermal powder injection devices," *European Journal of Pharmaceutics and Biopharmaceutics*, vol. 81, no. 2, pp. 360–368, 2012, doi: 10.1016/j.ejpb.2012.03.008.
- [35] A. P. Raphael, C. A. Primiero, A. B. Ansaldo, H. L. Keates, H. P. Soyer, and T. W. Prow, "Elongate microparticles for enhanced drug delivery to ex vivo and in vivo pig skin," *Journal of Controlled Release*, vol. 172, no. 1, pp. 96–104, 2013, doi: 10.1016/j.jconrel.2013.07.025.
- [36] R. Kong and R. Bhargava, "Characterization of porcine skin as a model for human skin studies using infrared spectroscopic imaging," *Analyst*, vol. 136, no. 11, pp. 2359–2366, 2011, doi: 10.1039/c1an15111h.
- [37] U. Jacobi *et al.*, "Porcine ear skin: An in vitro model for human skin," *Skin Research and Technology*, vol. 13, no. 1, pp. 19–24, 2007, doi: 10.1111/j.1600-0846.2006.00179.x.
- [38] N. Sekkat, Y. N. Kalia, and R. H. Guy, "Biophysical study of porcine ear skin in vitro and its comparison to human skin in vivo," *J Pharm Sci*, vol. 91, no. 11, pp. 2376–2381, 2002, doi: 10.1002/jps.10220.
- [39] K. Moronkeji, S. Todd, I. Dawidowska, S. D. Barrett, and R. Akhtar, "The role of subcutaneous tissue stiffness on microneedle performance in a representative in vitro model of skin," *Journal of Controlled Release*, vol. 265, pp. 102–112, 2017, doi: 10.1016/j.jconrel.2016.11.004.
- [40] F. J. Verbaan *et al.*, "Assembled microneedle arrays enhance the transport of compounds varying over a large range of molecular weight across human dermatomed skin," *Journal of Controlled Release*, vol. 117, no. 2, pp. 238–245, 2007, doi: 10.1016/j.jconrel.2006.11.009.

- [41] L. Heinzerling *et al.*, "The skin prick test - European standards," *Clin Transl Allergy*, vol. 3, no. 1, pp. 1–10, 2013, doi: 10.1186/2045-7022-3-3.
- [42] T. Waghule *et al.*, "Microneedles: A smart approach and increasing potential for transdermal drug delivery system," *Biomedicine and Pharmacotherapy*, vol. 109, no. September 2018, pp. 1249–1258, 2019, doi: 10.1016/j.biopha.2018.10.078.
- [43] W. W. Koelmans, G. Krishnamoorthy, A. Heskamp, J. Wissink, S. Misra, and N. Tas, "Microneedle Characterization Using a Double-Layer Skin Simulant," *Mechanical Engineering Research*, vol. 3, no. 2, pp. 51–63, 2013, doi: 10.5539/mer.v3n2p51.
- [44] V. Normand, D. L. Lootens, E. Amici, K. P. Plucknett, and P. Aymard, "New insight into agarose gel mechanical properties," *Biomacromolecules*, vol. 1, no. 4, pp. 730–738, 2000, doi: 10.1021/bm005583j.
- [45] M. Ahearne, Y. Yang, A. J. El Haj, K. Y. Then, and K. K. Liu, "Characterizing the viscoelastic properties of thin hydrogel-based constructs for tissue engineering applications," *J R Soc Interface*, vol. 2, no. 5, pp. 455–463, 2005, doi: 10.1098/rsif.2005.0065.
- [46] Y. Deng, G. Winter, and J. Myschik, "Preparation and validation of a skin model for the evaluation of intradermal powder injection devices," *European Journal of Pharmaceutics and Biopharmaceutics*, vol. 81, no. 2, pp. 360–368, 2012, doi: 10.1016/j.ejpb.2012.03.008.
- [47] W. W. Koelmans, G. Krishnamoorthy, A. Heskamp, J. Wissink, S. Misra, and N. Tas, "Microneedle Characterization Using a Double-Layer Skin Simulant," *Mechanical Engineering Research*, vol. 3, no. 2, pp. 51–63, 2013, doi: 10.5539/mer.v3n2p51.
- [48] D. Singh, S. Boakye-Yiadom, and D. S. Cronin, "Comparison of porcine brain mechanical properties to potential tissue simulant materials in quasi-static and sinusoidal compression," *J Biomech*, vol. 92, pp. 84–91, Jul. 2019, doi: 10.1016/j.jbiomech.2019.05.033.
- [49] A. Kozana, T. Boursianis, G. Kalaitzakis, M. Raissaki, and T. G. Maris, "Neonatal brain: Fabrication of a tissue-mimicking phantom and optimization of clinical T1w and T2w MRI sequences at 1.5 T," *Physica Medica*, vol. 55, pp. 88–97, Nov. 2018, doi: 10.1016/j.ejmp.2018.10.022.
- [50] A. K. Dabrowska *et al.*, "Materials used to simulate physical properties of human skin," *Skin Research and Technology*, vol. 22, no. 1, pp. 3–14, 2016, doi: 10.1111/srt.12235.
- [51] J. C. J. Wei, G. A. Edwards, D. J. Martin, H. Huang, M. L. Crichton, and M. A. F. Kendall, "Allometric scaling of skin thickness, elasticity, viscoelasticity to mass for micro-medical device translation: From mice, rats, rabbits, pigs to humans," *Sci Rep*, vol. 7, no. 1, pp. 1–17, 2017, doi: 10.1038/s41598-017-15830-7.
- [52] N. A. Monteiro-Riviere, D. G. Bristol, T. O. Manning, R. A. Rogers, and J. E. Riviere, "Interspecies and interregional analysis of the comparative histologic thickness and laser doppler blood flow measurements at five cutaneous sites in nine species," *J Invest Dermatol*, vol. 95, no. 5, pp. 582–586, 1990.

- [53] S. Vasudevan, J. Kajtez, A. Heiskanen, J. Emnéus, and S. S. Keller, "Leaky opto-electrical neural probe for optical stimulation and electrochemical detection of dopamine exocytosis," in *Proc. IEEE MEMS 2020*, IEEE, 2020, pp. 388–391.
- [54] Z. Wang *et al.*, "Microneedle patch for the ultrasensitive quantification of protein biomarkers in interstitial fluid," *Nat Biomed Eng*, vol. 5, no. 1, pp. 64–76, Jan. 2021, doi: 10.1038/s41551-020-00672-y.
- [55] S. A. Skoog, P. R. Miller, R. D. Boehm, A. V. Sumant, R. Polsky, and R. J. Narayan, "Nitrogen-incorporated ultrananocrystalline diamond microneedle arrays for electrochemical biosensing," *Diam Relat Mater*, vol. 54, no. 1, pp. 39–46, 2015, doi: 10.1016/j.diamond.2014.11.016.
- [56] R. K. Mishra, V. M. A. M., F. Soto, R. Chrostowski, and J. Wang, "Microneedle Biosensor for Minimally-Invasive Transdermal Detection of Nerve Agents," *Analyst*, pp. 918–924, 2017, doi: 10.1039/C6AN02625G.



# Dermal Tissue Penetration of In-plane Silicon Microneedles Evaluated in Skin-simulating Hydrogel, Rat Skin and Porcine Skin – Supporting Information

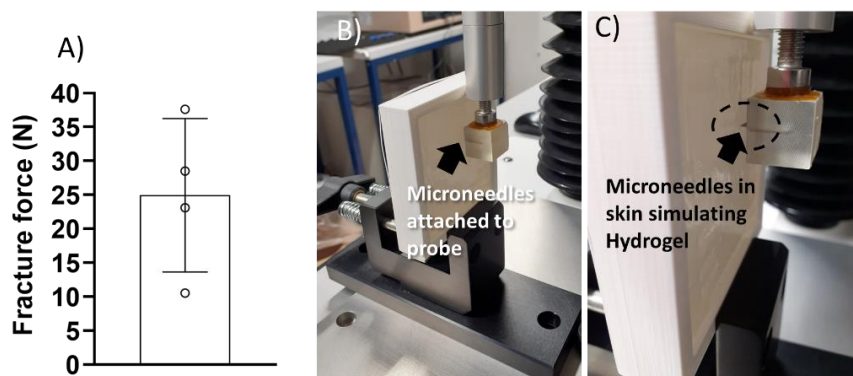
Stephanie Ingemann Bisgaard<sup>a,b</sup>, Long Quang Nguyen<sup>a</sup>, Katrine Lindholm Bøgh<sup>b</sup>, Stephan Sylvest Keller<sup>a,\*</sup>

<sup>a</sup> National Centre for Nano Fabrication and Characterization, DTU Nanolab, Technical University of Denmark, Ørsteds Plads, Building 347, 2800 Kgs. Lyngby, Denmark.

<sup>b</sup> The National Food Institute, DTU Food, Technical University of Denmark, Kemitorvet, Building 202, 2800 Kgs. Lyngby, Denmark.

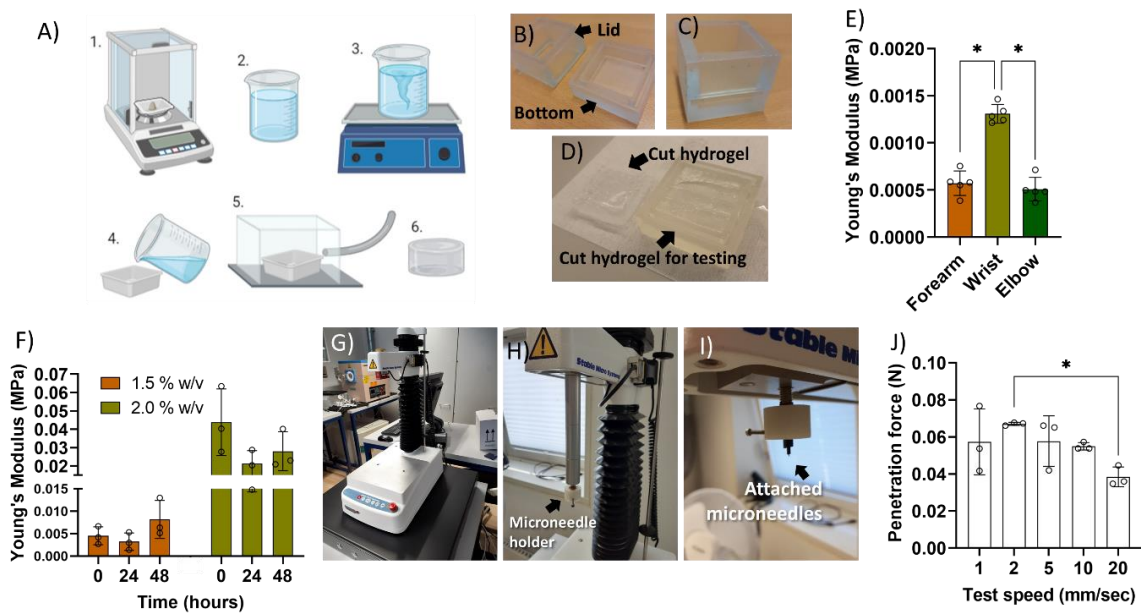
\* Corresponding author: [suke@dtu.dk](mailto:suke@dtu.dk)

## S1 – Mechanical testing of in-plane Si microneedles



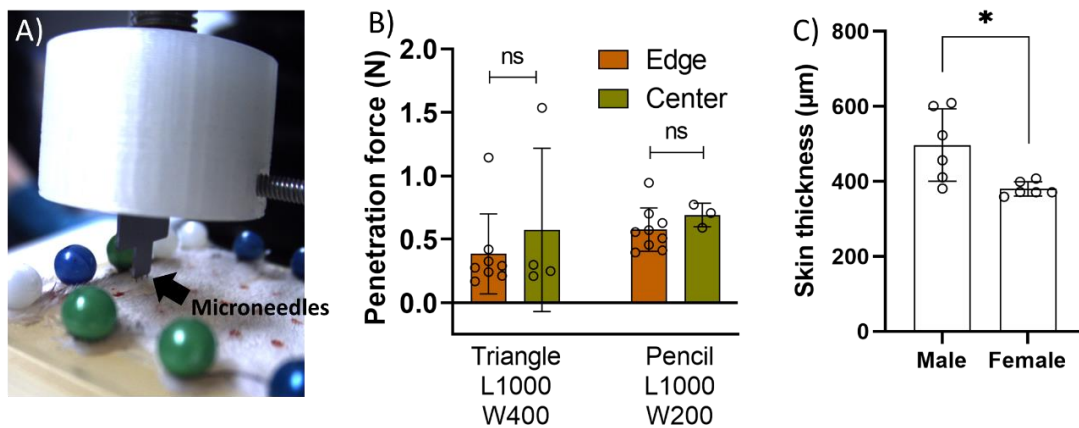
**Figure S1:** Mechanical testing of microneedles: A) Fracture force (mean  $\pm$  SD) measured for flat microneedles (L1000, W200, T180) upon compression onto a hard substrate using the texture analyzer indicating good mechanical stability; B) Image showing the attachment of the custom-made 3D printed TA probe with a MNA for shear stress testing. The black arrow indicates where the MNA is attached; C) Close-up image showing how the attached MNA is inserted into the skin simulating hydrogel for shear stress testing as indicated with black arrow.

## S2 – Penetration force measurements in skin-simulating hydrogel



**Figure S2:** Preparation of skin simulating hydrogel and preliminary validation experiments. A) Schematic overview of preparation method for the skin simulating hydrogel: 1. Weighing of agarose powder, 2. Addition of de-ionized water, 3. Heating of solution to 80°C while stirring with a magnetic stirrer, 4. Casting of agarose solution into 3D printed mold, 5. Removal of bubbles from solution in mold using a desiccator, 6. Cool down of the solution. Created with BioRender.com; B-D) Images showing a custom-made 3D-printed mold for preparation of the skin simulating agarose hydrogels: B) Lid and bottom of the mold; C) assembled mold ready for casting of hydrogel solution, degassing and solidification; D) After degassing and solidification, the lid was removed and the top layers of the skin-simulating hydrogel were cut off to achieve a smooth hydrogel surface without bubbles; E) Compressive Young's modulus measurements (mean  $\pm$  SD) performed with the texture analyzer (TA) on a human arm at three different locations: Forearm, wrist and elbow; F) Compressive Young's modulus measurements (mean  $\pm$  SD) for 1.5 % w/v and 2.0 % w/v agarose hydrogels after storage for 0, 24 and 48 h at 4°C; G) Image of the TA used for penetration force measurements; H) Image of the custom-made 3D-printed MNA probe holder attached to the TA; I) Close-up view of attached MNA; J) Penetration force measurements (mean  $\pm$  SD) for flat MNA (L500, W200, T500) measured at different test speeds of 1, 2, 5, 10 and 20 mm/s.

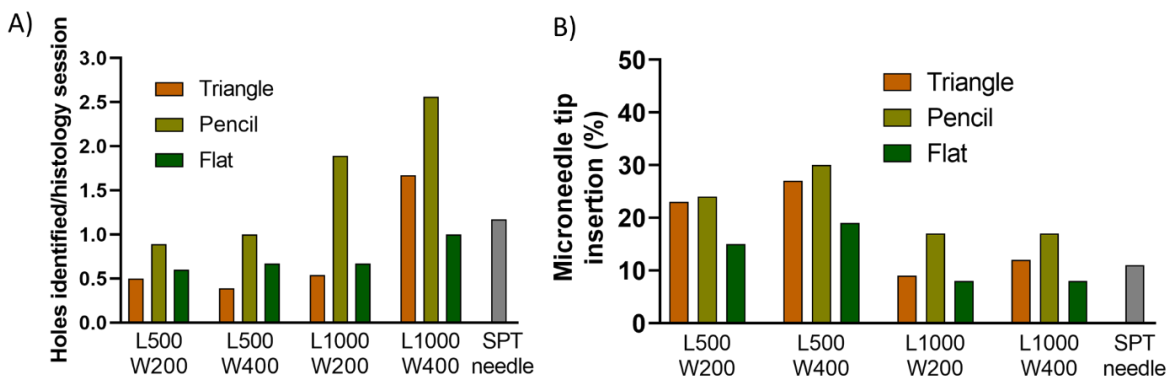
### S3 – Ex vivo penetration of rat abdominal skin



**Figure S3:** A) Picture showing a close-up of the custom-made 3D-printed holder mounted on the TA probe with a MNA being inserted into an excised rat abdominal skin sample. B) Penetration force (mean  $\pm$  SD) for triangular and pencil-shaped MNA measured at the edge and in the center of a pinned down excised rat skin sample. A paired T-test was performed, and no significant differences were found. C) Skin thickness measurements (mean  $\pm$  SD) conducted by excising six male and six female rat skin samples and measuring the thickness with a caliper. An unpaired T-test identified significant differences between the thickness of male and female rats.

### S4 – Analysis of penetration holes in rat abdominal skin

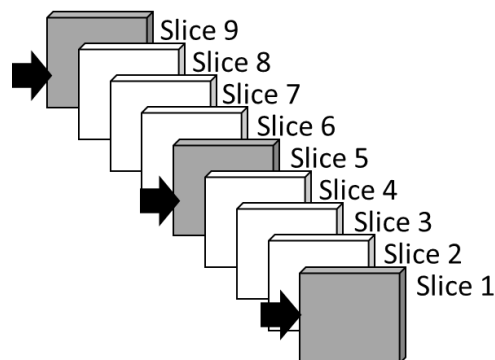
The total number of manually applied MNA for each design was 18 (6 rats, 3 MNA in each). Each MNA had 3 microneedles, which potentially would result in 54 penetration holes. In each histology session, 111 tissue slices were cut. Every 4<sup>th</sup> slice was stained and analyzed to identify penetration holes. Additional histology sessions were conducted until at least 6 penetration holes were identified for each MNA design. Figure S4A presents the average number of penetration holes identified per histology session for each MNA design. Low values are indicative for challenges in finding holes for a specific design. As a tendency, holes caused by pencil-shaped microneedles could more easily be found compared to the other shapes.



**Figure S4:** A) Average number of penetration holes identified in each session of histological analysis of the rat abdominal skin samples after manual application of MNA with different designs; B) Estimated percentage of microneedle length inserted into the rat abdominal skin calculated as the ratio of the penetration hole depth and the actual microneedle length.

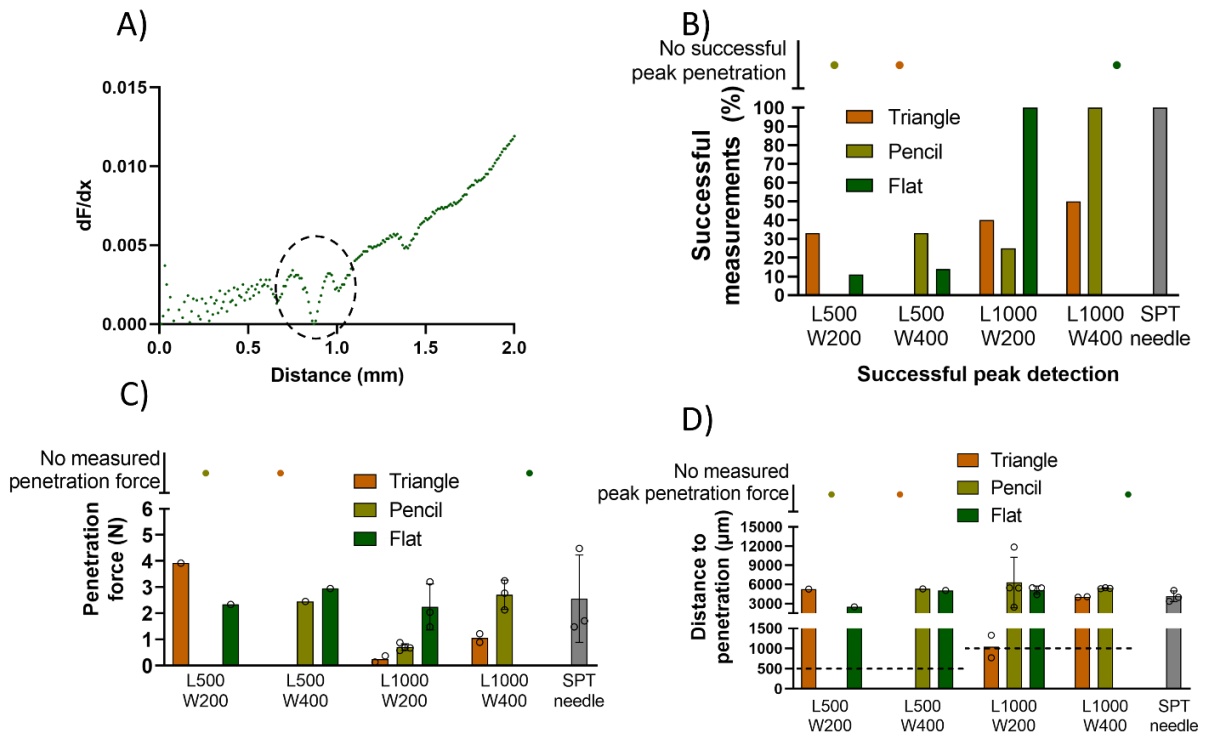
### S5 – Analysis of tissue damage in ex vivo penetration studies

For the analysis of the permanent damage caused by the microneedles in rat abdominal skin and porcine ear skin, the excised tissue was prepared for histological analysis as described in the methods section. Skin samples from the rats and the pig were embedded in paraffin blocks and cut into 5  $\mu\text{m}$  thick slices. Every 4<sup>th</sup> slice was stained and analyzed as illustrated in Figure S6 (slice 1, slice 5, slice 9, ...). If a penetration hole was identified, the penetration hole volume was estimated assuming that every slice was 5  $\mu\text{m}$  thick. First, the penetration hole in the histology slice was categorized as either having a rectangular or a triangular shape. This categorization was done blinded without knowing which type of MNA had caused the hole. Secondly, it was assumed that the penetration holes in the slices which were not collected had the same shape and dimensions as the previous collected slice. In the example illustrated in Figure S5, this would be assuming that the holes in slice 2-4 had the same shape and dimensions as the holes in slice 1, and the holes in slice 6-8 have same shape and dimensions as the hole in slice 5 and so forth. Finally, the penetration hole volume  $V$  was calculated as  $V = \frac{1}{2}dwt$  for triangular holes and  $V = dwt$  for rectangular holes, where  $d$  is the maximum measured depth of the penetration hole,  $w$  is the maximum width of the hole and  $t$  is the thickness of the hole, calculated as  $t = 4NT$  where  $N$  is the number of histology slices the hole appears on,  $T = 5 \mu\text{m}$  is the thickness of each histology slice, and 4 is included because only every fourth slice was collected for Mayer's hematoxylin and eosin staining.



**Figure S5:** Schematic illustration of skin tissue slice selection for histology staining. Each slice has a thickness of 5  $\mu\text{m}$ . Every fourth slice is selected for staining and subsequent histological analysis as indicated by the black arrow.

**S6 – Ex vivo penetration of porcine skin**



**Figure S6:** A) Differentiated force-displacement curve for a triangular MNA (L1000, W200, T180) recorded in porcine ear skin (corresponding to figure 5B in the main paper). The circle indicates the position of the penetration force peak; B) Percentage of successful penetration force peak detection for a total of  $n=3-9$  measurements with each MNA design; C) Penetration force and D) distance to penetration (mean  $\pm$  SD) extracted from successful measurements in A) for MNA with different shapes and dimensions. The black dotted lines in D) indicate the distance corresponding to the microneedle length.

## **Appendix B: Study report I**

### **Study report I**

Evaluation of In-plane Silicon Microneedle Insertion and Delivery of Compound 48/80 in Porcine and Human Breast Skin Samples. Stephanie Ingemann Bisgaard, Long Quang Nguyen, Mohammad Ramezannezhad, Emma Baczkowski, James Birchall, Katrine Lindholm Bøgh, Stephan Sylvest Keller.

# Evaluation of In-plane Silicon Microneedle Insertion and Delivery of Compound 48/80 in Porcine and Human Breast Skin Samples

Stephanie Ingemann Bisgaard<sup>a,b</sup>, Long Quang Nguyen<sup>a</sup>, Mohammad Ramezannezhad<sup>a</sup>, Emma Baczkowski<sup>c</sup>, James Birchall<sup>c</sup>, Katrine Lindholm Bøgh<sup>b</sup>, Stephan Sylvest Keller<sup>a,\*</sup>

<sup>a</sup> National Centre for Nano Fabrication and Characterization, DTU Nanolab, Technical University of Denmark, Ørstedes Plads, Building 347 East, 2800 Kgs. Lyngby, Denmark.

<sup>b</sup> National Food Institute, DTU Food, Technical University of Denmark, Kemitovet, Building 202, 2800 Kgs. Lyngby, Denmark.

<sup>c</sup> Welsh School of Pharmacy and Pharmaceutical Sciences, Cardiff University, Redwood Building, King Edward VII Ave, Cardiff CF10 3NB, Great Britain.

\* E-mail of corresponding author: [suke@dtu.dk](mailto:suke@dtu.dk)

## Abstract

Microneedles (MNs) are being explored for various purposes. We envision using MNs for developing an improved allergy diagnostics method based on a patch of MNs which will both deliver the allergen intradermally and measure the allergic reaction. The first aim was to test the mechanical stability and penetration ability of in-plane silicon MNs optimized in a previous study. Furthermore, the penetration efficiency of the in-plane MNs was tested when the MNs were configured in 2D-arrays to investigate the penetration ability of a patch. The second aim was to test delivery of compound 48/80 (48/80) using coated MNs. The mechanical stability and penetration of the MNs was tested using excised porcine and human breast skin samples with insertion forces of 5, 10, and 15 N. In-plane MNs arranged in 2D-arrays were tested using excised porcine skin samples and methylene blue staining for visualization of penetration holes. Delivery of compound 48/80 was investigated using excised fresh human breast skin to test for mast cell (MC) degranulation. For this purpose, immunohistochemistry staining for the CD63 surface marker was used. The MNs were found to be mechanically stable during insertion at 5 N and the penetration depth depended on the insertion force. It was found that not all the MNs penetrated when the MNs were arranged in a 2D-array with more than one row of MNs. IHC staining of fresh human breast skin samples with delivery of 48/80 did not reveal any MC activation and degranulation. In conclusion, the developed MNs are sufficiently stable to penetrate the skin, however, further optimization is needed if the MNs are to be arranged in a patch format. The delivered 48/80 amount was either too small to cause MC degranulation or the induced degranulation was insufficient to be detected using the IHC staining.

## 1. Introduction

The Welsh School of Pharmacy at Cardiff University provided the possibility of conducting experiments with human skin samples for a more realistic evaluation of the penetration ability of optimized MNs. The

optimization of the microneedles (MNs) were presented in manuscript I [1] and investigation of allergen delivery using the MNs is presented in manuscript II [2].

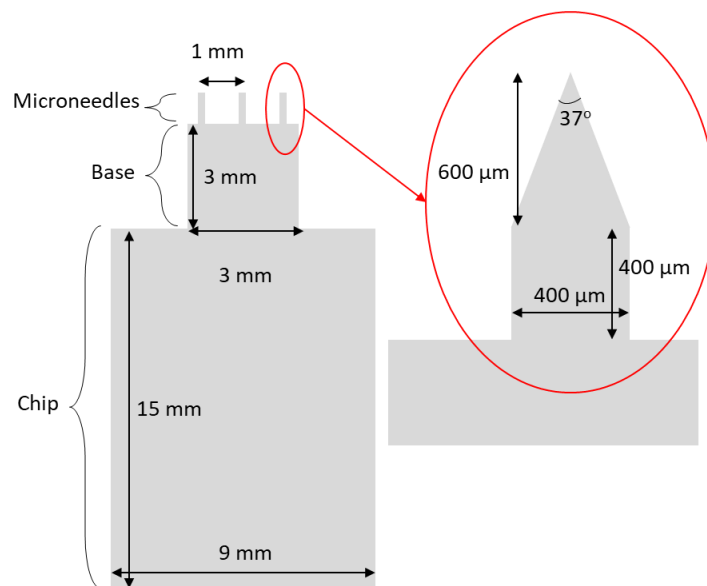
The first aim of the study presented here was to further investigate the mechanical stability and penetration of the optimized MNs. For this purpose, the impact of applied force upon insertion into porcine skin was investigated along with the impact of having the MNs configured in a 2D-array, as the final configuration of the improved diagnostic device is intended as a patch of MNs.

The second aim of the study was to test the coating delivery of compound 48/80-coated MNs in excised fresh human breast skin samples. Compound 48/80 is a molecule which initiates mast cell (MC) degranulation [3] and is used as a positive control for the *in vivo* animal experiments presented in manuscript II [2] and study report II [4]. Upon activation and degranulation of MCs surface bound markers become upregulated and available for detection, among these is CD63 [5], [6], which in theory can be stained for using immunohistochemistry (IHC).

## 2. Materials and methods

### 2.1 Fabrication of in-plane silicon microneedles

Cleanroom fabrication of in-plane silicon MNs is described in manuscript I [1]. In brief, the MNs were fabricated using photolithography and dry etching to define the MN shape and dimensions. The MN shape was a pencil shape with 1000  $\mu\text{m}$  length, 400  $\mu\text{m}$  width, and 180  $\mu\text{m}$  thickness as illustrated in Figure 1.



**Figure 1: Shape and dimensions of the optimized in-plane silicon microneedles.** Three microneedles (MNs) extrude at the end of the base which is extruding from the chip used for handling. The final MN shape was a pencil shape with 1000  $\mu\text{m}$  length, 400  $\mu\text{m}$  width, and 180  $\mu\text{m}$  thickness. Adopted from manuscript II [2].



## **2.2 Skin sample preparation**

Human skin explants were collected from surgical procedures under informed patient consent and local ethical committee approval (South East Wales Research Ethics Committee Ref: 08/WSE03/55).

The preparation of porcine and human breast skin samples is described in detail in manuscript II [2]. In brief, the skin samples were allowed to thaw at room temperature for 30 min before processing. All skin samples were prepared inside a sterile fume hood where fat and muscle tissue were removed on the dermis side of the sample. To keep the skin sample hydrated it was dapped with phosphate buffered saline (PBS) every 5-10 min.

## **2.3 Cryosectioning of skin samples**

The procedure for cryosectioning skin samples was as described in manuscript II [2]. In short, biopsy samples were frozen using optimal cutting temperature embedding matrix (OCTEM, Carl Roth, Karlsruhe, Germany) at -20 °C and stored at -80 °C until cryosectioning. The frozen samples were cryosectioned using a Cryotome FSE cryostat (Thermo Scientific, Waltham, Massachusetts, USA). The cryosectioned slices were 10 µm thick and collected on Thermo Scientific™ SuperFrost™ Microscope Slides, Cut (Fischer Scientific, Waltham, MA, USA).

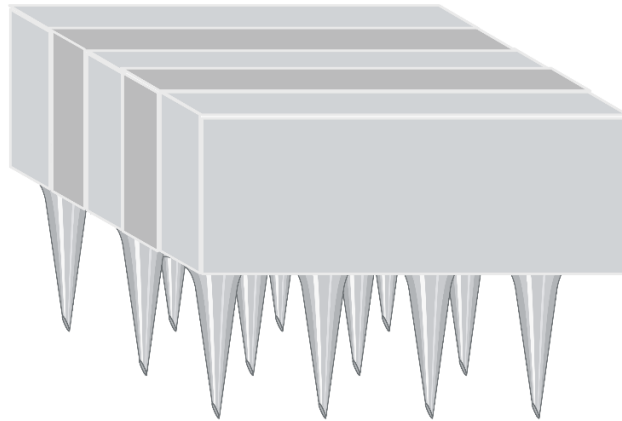
All biopsy skin samples were fixed using formaldehyde prior to freezing, except for the fresh human skin that was used for compound 48/80 (48/80, Sigma-Aldrich, St. Louis, MO, USA) coating delivery and IHC as it was unknown how fixing of the skin would affect the IHC.

## **2.4 Microneedle insertion force in porcine skin sample**

MNs were inserted into a porcine shoulder skin sample for 60 s at forces of 5, 10, and 15 N using a Sauter force gauge (model FH 100, Sauter, Basel, Schweiz). Immediately after removing the MNs, the location of insertion was scanned by optical coherence tomography (OCT) using VivoSight (Michelson Diagnostics Ltd., Kent, UK). The OCT files were analyzed using ImageJ 1.52a (Wayne Rasband, National Institutes of Health, USA). For visualizing skin penetration, 1% methylene blue (Sigma-Aldrich) in PBS was added to the skin surface for 3 min, whereafter it was gently wiped off. Biopsies were afterwards collected from each insertion site, fixed using formaldehyde, frozen in OCTEM at -20 °C and stored at -80 °C for later cryosectioning.

## **2.5 Insertion of microneedle array in porcine skin sample**

In-plane MN chips with 3 MNs per chip were stacked on top of each other, using 350 µm thick silicon chips as spacers, to create a 2 x 3 and a 3 x 3 array of MNs as illustrated in Figure 2. The MN arrays were inserted into a porcine neck skin sample with an applied force of 5 N using a Sauter force gauge. Afterwards the sample was stained with 1% methylene blue in PBS for 3 min to make the penetration holes visible. Based on this, the penetration yield was calculated as the ratio between the number of observable penetration holes and the number of MNs in the array.



**Figure 2: Illustration of in-plane silicon microneedle array.** In-plane silicon microneedles (MNs, light gray) were placed together in rows with spacers (dark gray) in between to form 2 x 3 and 3 x 3 MN arrays. Created with BioRender.com.

## 2.6 Coating solution

The formulation of the coating solution was as described in manuscript II [2]. In brief, 48/80 and carboxymethyl cellulose (CMC) sodium salt (low viscosity) (Sigma-Aldrich) were added to de-ionized water. CMC was added to an end concentration of 1% w/v and 48/80 to an end concentration of 1000  $\mu\text{g}/\text{mL}$ . The amount of 48/80 on the MNs after coating is unknown.

## 2.7 Dip-coating

Dip-coating was done as described in manuscript II [2]. In a few words, the MN chip was mounted vertically on a Texture Analyser (TA, Stable Microsystems, Godalming, UK) using a 3D printed probe. The probe was moved downwards with a speed of 0.50 mm/s into the coating solution and remained there for 10 s. The MN chip was then retracted from the coating solution with a speed of 0.50 mm/s and left to dry for a few minutes.

## 2.8 Immunohistochemistry on human breast skin samples

IHC was performed on cryosectioned samples of fresh human breast skin. MNs coated with 1000  $\mu\text{g}/\text{mL}$  48/80, as well as MNs without coating, were pricked into the skin sample manually for 60 s. Biopsies were collected at the MN insertion locations, as well as at pristine locations where MNs had not been inserted as controls. Biopsy samples were not fixed in formaldehyde, but frozen in OCTEM at  $-20\text{ }^{\circ}\text{C}$  and stored at  $-80\text{ }^{\circ}\text{C}$  until use. Samples were cryosectioned as described in section 2.3 (see also manuscript II [2] for further details).

The primary antibody Recombinant Anti-CD63 antibody [ERP5702] – Late Endosome Marker (ab134045) (Abcam, Cambridge, UK) and IHC kit Rabbit specific HRP/DAP (ABC) Detection IHC Kit (ab64261) (Abcam, Cambridge, UK) were used for IHC staining according to the manufacturer's instructions.

## 2.9 Statistics

All statistical analyses were conducted using one-way ANOVA with Tukey's multiple comparisons test at a significance level of  $\alpha=0.05$ .

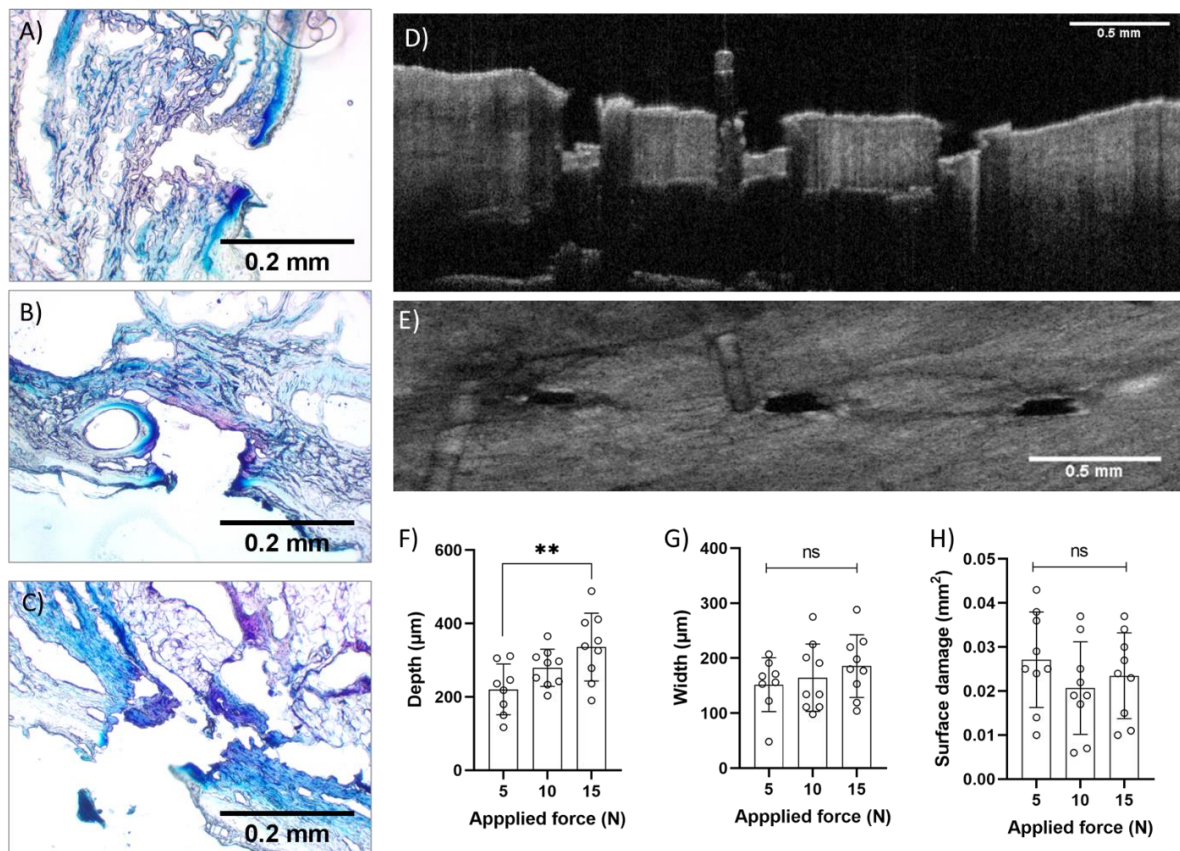
## 3. Results and discussion

### 3.1 The impact of applied force on microneedle insertion in porcine skin

MNs were inserted in porcine shoulder skin samples at different forces (5, 10, and 15 N) to evaluate penetration of the skin and determine the optimal insertion force. It was found that 5 N force was sufficient for skin penetration, while also having the lower risk of accidentally breaking the MNs (Figure 3A-C). To visualize the penetration holes, the skin sample was scanned using OCT immediately after penetration. This provided a 3D scan of the sample with the MN holes, giving both a cross-sectional and a top-view (Figure 3D-E).

Based on the OCT scans it was possible to measure the hole depth and hole width and calculate the surface damage using ImageJ (Figure 3F-H). There was found one significant difference (one-way ANOVA with Tukey's multiple comparisons test) for the hole depth between 5 N and 15 N applied force. This illustrates that the applied force had an impact on the hole depth, which follows the expectations (Figure 3F). Based on the mean values obtained for the MN penetration depths the insertion percentages of the MNs were 22% for 5 N, 28% for 10 N, and 34% for 15 N meaning that the full length (1000  $\mu\text{m}$ ) of the MNs did not penetrate. This was expected based on the outcome of manuscript I [1] where the same partial insertion of the MNs was observed in Brown Norway rat skin samples and porcine ear skin samples. For hole width and surface damage no statistically, significant differences were identified between the various tested insertion forces (Figure 3G-H).

The mean values of penetration hole widths were compared with the calculated width of the MN at the mean penetration depth for each applied force of 5, 10, and 15 N, respectively. The mean penetration hole widths (152, 164, and 185  $\mu\text{m}$ ) were similar to the calculated MN widths (140, 177, 213  $\mu\text{m}$ ) at the respective mean insertion depths (140, 177, and 213  $\mu\text{m}$ ). This confirms that the penetration holes had not begun to close before conducting the OCT measurement, and hence the reported mean depths are likely a true indicator of how deep the MNs went at each force.



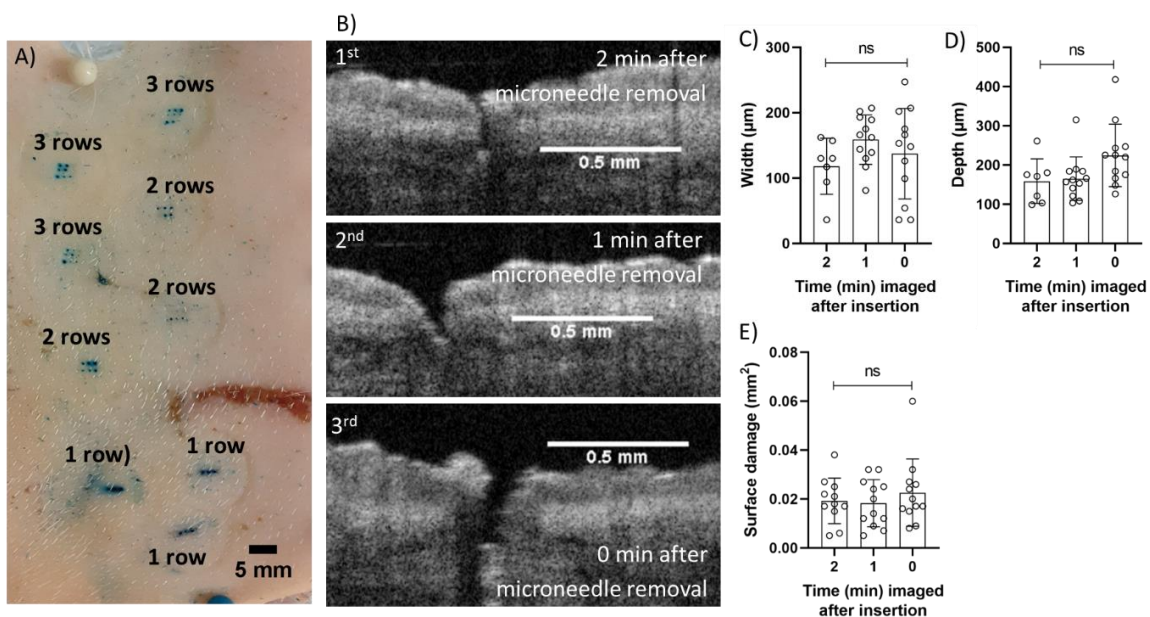
**Figure 3: The impact of applied force on microneedle insertion in porcine shoulder skin samples.** A-C) Histology slices representing microneedle (MN) holes in porcine shoulder skin sample stained with 1% methylene blue in PBS for 3 min at A) 5 N insertion force, B) 10 N insertion force, C) 15 N insertion force. D) OCT image of porcine shoulder skin sample representing three MN holes in a row (cross-sectional view). E) OCT image of porcine shoulder skin sample representing three MN holes in a row (top-view). F-H) Dimensions of MN penetration holes measured using OCT and ImageJ. F) Hole depth (mean  $\pm$  SD). G) Hole width (mean  $\pm$  SD). H) Surface damage (mean  $\pm$  SD). Statistically significant difference is marked as \*\* =  $p \leq 0.01$ .

### 3.2 Inserting arrays of microneedles in porcine skin

The MNs used in this study have an in-plane configuration, comprised of three MNs in a single row. However, for the final application it would be ideal with an array containing more than just one row. Thus, it was investigated how the MNs would behave if arranged in a 2 x 3 or 3 x 3 matrix. Insertion of in-plane MNs in a 2D-array format was tested using porcine neck skin. For one row (three MNs) the yield was 100%  $\pm$  0%, for two rows (six MNs) the yield was 61%  $\pm$  19%, and for three rows (nine MNs) the yield was 85%  $\pm$  6% (Figure 4A). This indicated that if the MNs of the improved diagnostic device are to be in an array format, the placement of the individual MNs should be optimized to minimize the bed-of-nails-effect and ensure a 100% successful penetration.

### 3.2.1 Manual insertion of microneedles in human breast skin

Manual insertion of MNs for 60 s in human breast skin was investigated using OCT and it was observed that the MN holes closed quickly. This is shown in Figure 4B, where the hole was almost closed 2 min after retraction of the MN from the skin. Based on the OCT images and ImageJ the hole width (Figure 4C), depth (Figure 4D), and surface damage (Figure 4E) at different times after retraction of the MN from the tissue were determined. No statistically significant differences (one-way ANOVA with Tukey's multiple comparisons test) were found. This is interesting, since the holes, during visual assessment, seemed to be closing rapidly, cf. Figure 4B. The measurements from manual insertion appear to have a larger variance compared to the data recorded for the MN insertions using a force gauge (Figure 3F-H), thus illustrating that manual insertion is less reproducible.

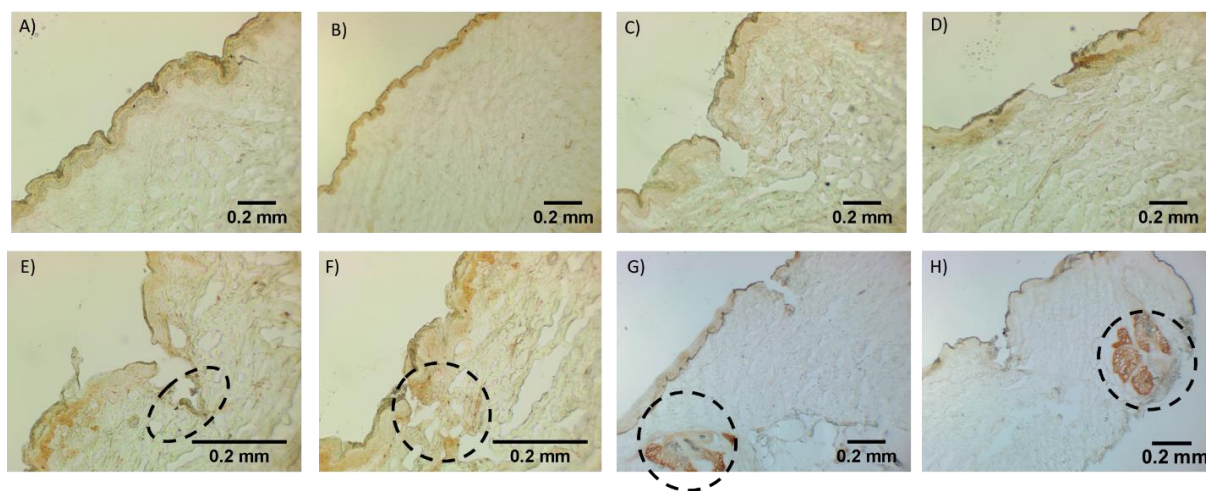


**Figure 4: Applying arrays of microneedles and investigating manual insertion.** A) Porcine neck skin sample stained with 1% methylene blue in PBS for 3 min after microneedle (MN) insertions with one, two or three rows of MN chips assembled in an array (corresponding to 1 x 3, 2 x 3, and 3 x 3 arrays of MNs). B) OCT images of human breast skin sample at different times (0, 1, and 2 min) after manual insertion of MNs for 60 s. C-E) MN hole dimensions measured using OCT and ImageJ in human breast skin samples at different times after manual insertion. C) Hole width (mean  $\pm$  SD). D) Hole depth (mean  $\pm$  SD). E) Surface damage (mean  $\pm$  SD).

### 3.3 Delivery of compound 48/80 for mast cell degranulation and immunohistochemistry on human breast skin

Compound 48/80 was used as a positive control in the animal studies in manuscript II [2] as it stimulates MCs to degranulate. In theory, it should be possible to confirm MC activation by releasing 48/80 from the MN coating and staining the human breast skin sample with IHC for CD63 detection. CD63 is a receptor that is upregulated upon MC degranulation and can therefore be used as a surface marker for MC activation [7].

For this purpose, plain intact human breast skin samples without MN insertion (Figure 5A-B) were stained together with skin where un-coated (Figure 5C-D) and 48/80-coated MNs (Figure 5E-F) had been inserted. Initially, the results seemed promising as some darker areas appeared in the staining of histology slices from 48/80-coated MNs as seen in Figure 5E-F. These dark areas did not appear in the histology slices from un-coated MNs. To verify the preliminary results, samples from 48/80-coated MNs were stained again, but this time without using the primary antibody of the kit. The identified darkened areas should not appear on these histology slices without the presence of the primary antibody. Nonetheless, the darkened areas appeared again indicating that it was likely an unspecific binding that caused the local change of color (Figure 5G-H).



**Figure 5: Coating delivery of compound 48/80 using microneedles and immunohistochemistry staining for CD63 in fresh human breast skin samples.** A-B) Plain skin sample without microneedle (MN) insertion. C-D) Skin sample with 60 s insertion of un-coated MNs. E-F) Skin sample with 60 s insertion of 48/80-coated MNs. The black dotted circles indicate darkened stained areas. G-H) Skin sample with 60 s insertion of 48/80-coated MNs, but without using the primary antibody in the IHC staining process. The black dotted circles indicate darkened stained areas.

## 4. Conclusion

In the experimental studies conducted at Cardiff University, it was confirmed that the MNs could penetrate porcine shoulder skin using forces of 5, 10, and 15 N. However, it was determined that 5 N was sufficient for penetrating the upper skin layer and that there was less risk of accidentally breaking the MNs when using this lower force. Based on OCT scans the hole depth, width, and surface damage of the skin were determined, and it was found that the hole depth was dependent on the applied force.

In an additional experiment where one, two, and three rows of MNs were inserted into a porcine neck skin sample it was found that the successful penetration yield (%) decreased with more rows of MNs. If the intention of the improved diagnostic device is to have the MNs aligned in a 2D-array, optimization is needed to ensure 100% successful penetration of all MNs.

As a final test, MNs coated with 48/80 were inserted into fresh human breast skin samples to investigate if activated MCs could be detected via their CD63 surface marker using IHC. This was not possible as the

initially observed response was confirmed to likely be due to unspecific binding. For future studies, it would be ideal if the activation of MCs could be confirmed either by optimizing the IHC process or potentially using flow cytometry, perhaps with a different biomarker. The 48/80 coating should also be optimized, as results presented in manuscript II [2] suggest that only a small amount of coating is delivered.

## 5. Acknowledgements

The authors would like to thank Benedetta Gualeni for instructing how to prepare the skin samples and to Matthew Ivory for helping with the immunohistochemistry.

## 6. Conflict of interest

The authors declare no conflict of interest.

## 7. Data availability statement

All data is available upon request.

## 8. Author contributions

**Stephanie Ingemann Bisgaard:** Methodology, formal analysis, writing – original draft, investigation, visualization. **Long Quang Nguyen:** Resources, investigation. **Mohammad Ramezannezhad:** Resources. **Emma Baczkowski:** Supervision. **James Birchall:** Resources, supervision. **Katrine Lindholm Bøgh:** Supervision, conceptualization, methodology, resources, writing – review & editing, **Stephan Sylvest Keller:** Supervision, funding acquisition, writing – review & editing, project administration.

## 9. Funding

Funding from the Independent Research Fund Denmark (grant no. 8022-00215B), and the LEO Foundation (grant no. LF17046).

## 10. Keywords

Microneedles, porcine skin, human breast skin, compound 48/80, immunohistochemistry.

## 11. References

- [1] S. I. Bisgaard, L. Q. Nguyen, K. L. Bøgh, and S. S. Keller, "Dermal Tissue Penetration of In-plane Silicon Microneedles Evaluated in Skin-simulating Hydrogel, Rat Skin, and Porcine Skin," 2023.
- [2] S. I. Bisgaard *et al.*, "Peanut Allergen Ara h 2 Delivery with In-plane Silicon Microneedles for Test of Allergic Response," 2023.
- [3] W. D. Paton, "Compound 48/80: A potent histamine liberator," *Br. J. Pharmacol. Chemother.*, vol.

6, no. 3, pp. 499–508, 1951.

- [4] S. I. Bisgaard *et al.*, “Birch Pollen Extract and Bet v 1 Allergen Delivery with In-plane Silicon Microneedles for Test of Allergic Response,” 2023.
- [5] J. Elst *et al.*, “Mast cell activation test in chlorhexidine allergy: a proof of concept,” *Br. J. Anaesth.*, vol. 125, no. 6, pp. 970–975, 2020.
- [6] K. Kabashima *et al.*, “Biomarkers for evaluation of mast cell and basophil activation,” *Immunol. Rev.*, vol. 282, no. 1, pp. 114–120, 2018.
- [7] T. Schäfer, P. Starkl, C. Allard, R. M. Wolf, and T. Schweighoffer, “A granular variant of CD63 is a regulator of repeated human mast cell degranulation,” *Allergy Eur. J. Allergy Clin. Immunol.*, vol. 65, no. 10, pp. 1242–1255, 2010.



## Appendix C: Manuscript II

### Manuscript II

Peanut allergen Ara h 2 Delivery with In-plane Silicon Microneedles for Test of Allergic Response.

Stephanie Ingemann Bisgaard, Long Quang Nguyen, Ana Isabel Sancho, Sarah Grundt Simonsen, Gerardo Garcia Zavaleta, Mohammad Ramezannezhad, Emma Baczkowski, James Birchall, Stephan Sylvest Keller, Katrine Lindholm Bøgh, *manuscript in preparation*.

# Peanut Allergen Ara h 2 Delivery with In-plane Silicon Microneedles for Test of Allergic Response

Stephanie Ingemann Bisgaard<sup>a,b</sup>, Long Quang Nguyen<sup>a</sup>, Ana Isabel Sancho<sup>b</sup>, Sarah Grundt Simonsen<sup>b</sup>, Gerardo García Zavaleta<sup>a</sup>, Mohammad Ramezannezhad<sup>a</sup>, Emma Baczkowski<sup>c</sup>, James Birchall<sup>c</sup>, Stephan Sylvest Keller<sup>a</sup>, Katrine Lindholm Bøgh<sup>b,\*</sup>

<sup>a</sup> National Centre for Nano Fabrication and Characterization, Technical University of Denmark, Ørstedss Plads, Building 347 East, 2800 Kgs. Lyngby, Denmark.

<sup>b</sup> National Food Institute, Technical University of Denmark, Kemitovet, Building 202, 2800 Kgs. Lyngby, Denmark.

<sup>c</sup> Welsh School of Pharmacy and Pharmaceutical Sciences, Cardiff University, Redwood Building, King Edward VII Ave, Cardiff CF10 3NB, Great Britain.

\* E-mail of corresponding author: [kalb@food.dtu.dk](mailto:kalb@food.dtu.dk)

## Abstract

Today, allergies are usually first screened using the well-established skin prick test (SPT) method. However, the SPT outcome is qualitative and not quantitative. To improve on the SPT, microneedles (MNs) were tested for allergen delivery by coating the MNs with allergens. First, MNs were coated with fluorescent-labeled molecules by dip-coating to test delivery in Brown Norway (BN) rat abdominal, pig neck, and human breast skin samples. The delivery was visualized by cryostat histology and evaluated by measuring remaining, fluorescent-labeled coating on the MNs after insertion. Second, MNs coated with varying concentrations of peanut protein Ara h 2 allergen were tested *in vivo* using BN rats sensitized with peanut protein extract. Immune responses were confirmed using IgG<sub>1</sub> and IgE enzyme-linked immunosorbent assays (ELISA) and ear swelling tests. MNs coated with compound 48/80 (48/80) and phosphate buffered saline (PBS) were included as respectively positive and negative control for mast cell degranulation. As a further control, intradermal (i.d.) injections were also performed with the same Ara h 2 solution concentrations, as well as 48/80 and PBS. Prior to inserting the MNs or performing the i.d. injections, the rats were intravenously injected with Evans blue for visualization of the blood accumulations, to indicate a local allergic response. The MNs were inserted into the abdominal skin of sedated rats for 60 s whereafter the rats were sacrificed. After sacrificing the rats, the abdominal skin was excised, fixed to its original size, and photographed with the dermis layer facing upwards. Biopsy samples were collected, snap-frozen in liquid nitrogen, and stored at -80 °C until use. The collected biopsy samples were homogenized, and Ara h 2 delivery quantified using both fluorescent-labeled Ara h 2 and Ara h 2 ELISA. Delivery of fluorescent-labeled molecules using MNs was confirmed by histology, but the delivered amount was found to be very small and difficult to accurately quantify. Visualization of the allergic reaction using Evans blue provided clear dose-response curves for some sensitized rats receiving i.d. injections. However, for the coated MNs a reaction different from the negative controls could not be observed using the Evans blue method. Finally, recovery of the delivered Ara h 2 was attempted by performing an Ara h 2 specific ELISA on homogenized biopsy samples and Ara h 2 could be recovered for the highest i.d. injection (18.75 µg Ara h 2). For MN delivery of both fluorescent-labeled Ara h 2 and

pristine Ara h 2 no measurable amount was recovered in the homogenized skin samples. In conclusion, the amount of coating (allergen or positive control) delivered from MNs were insufficient to either elicit a local allergic response or elicit a measurable allergic response using the Evans blue method.

## 1. Introduction

Food allergy is an abnormal reaction caused by the immune system in response to food proteins which are in principle harmless [1]. Even exposure to very small amounts of an allergen can cause an allergic reaction ranging from oral allergy syndrome [2] to anaphylaxis [3]. The term “the big nine” refers to the nine main food allergies caused by cow’s milk, hen’s egg, fish, shellfish, tree nuts, peanut, wheat, soybean, and sesame. Sesame was added to this list officially as of January 1<sup>st</sup>, 2023 [4]. Cow’s milk and hen’s egg allergies are often outgrown by children [5], [6] while others such as peanut, tree nuts, shellfish, and seeds are more persistent food allergies [7]. Peanut allergy is one of the more severe allergies [8] and persist throughout life [9]–[11]. A total of 18 potential allergens in peanut have been registered by the World Health Organization and International Union of Immunological Societies [12] with the major peanut allergens being Ara h 1, 2, 3, and 6 [13], [14].

Diagnosing food allergies is first based on medical history and physical examination [15], and if IgE-mediated food allergy is suspected a blood sample can be collected to test for allergen-specific IgE in the serum [16]. For a definite confirmation of food allergy the current golden standard is the double-blind placebo-controlled food challenge where neither the patient nor the healthcare professional knows if the ingested sample is the suspected food allergen or not [17], [18]. An oral challenge is associated with risk of adverse effects and should always be conducted under medical supervision [19].

Other diagnostic tests include component-resolved diagnosis (CRD) where allergen-specific antibodies are measured and cross-reactive molecules can be identified [20], [21]. Alternatively, the basophil activation test (BAT) may be used where basophils from a blood sample is stimulated with the allergen. As a result of allergen stimulation upregulated surface-bound markers on the basophils such as CD63 or CD203c can be detected using flow cytometry [22].

The skin prick test (SPT) is a well-established method for screening allergies in the clinic and is performed by placing a droplet of allergen extract on the skin of the forearm. The droplet is then pricked through the skin using a SPT needle and this will initiate a local allergic response within the skin, which should become visible within 15-20 min. A healthcare professional will then do a manual readout and evaluate the response based on the diameter ( $\geq 3$  mm) of the wheal [23], [24]. Some food-based allergen extracts are not potent enough to elicit a visible reaction and in these cases the prick-to-prick method may be used. In this case the SPT needle is first pricked into the food and afterwards applied to the skin as in a normal SPT [25], [26].

For determination of allergic responses in controlled animal experiments intravenously injected Evans blue dye has previously been used to stain for the blood accumulation associated with an allergic response [27]–[30]. The method of using dyes to stain for blood accumulations has been used for several years [31], [32].

As an adaptation to the SPT microneedles (MNs) are believed to be able to replace the SPT by making the test less invasive and having a low risk of adverse effects [33], [34]. One study replaced the SPT needle with bare silicon MNs and showed transdermal delivery of allergen extracts and a resulting visual allergic response similar to the SPT [34]. A second study presented allergen delivery to the epidermis of rats using dissolvable MNs and recorded the increase in scratch rate as a measure of successful delivery [33]. MNs have also been used in research for development of cutaneous immunotherapy where peanut extract was coated on solid MNs and delivered into peanut-sensitized mice [35], [36].

The aim of this study was first to investigate the delivery potential of coated MNs using fluorescent-labeled molecules. Secondly, MNs coated with peanut allergen Ara h 2 were pricked into peanut protein extract (PPE)-sensitized Brown Norway (BN) rats to elicit a local allergic response. This allergic response was visualized using Evans blue.

## **2. Materials and methods**

### **2.1 Ara h 2**

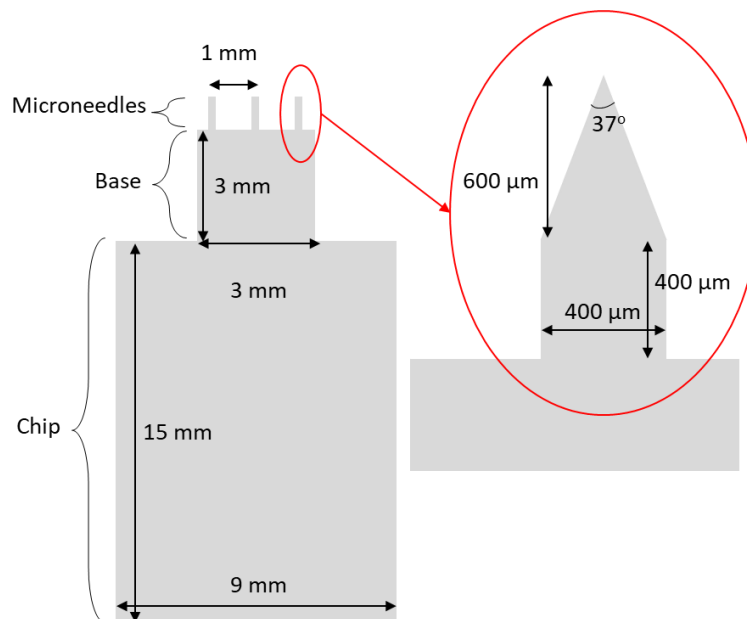
Raw peanuts were obtained from Morrisons market (Leeds, UK), de-skinned and then ground using a Waring blender. The meal was defatted with hexane (1:5, w/v) for 3 h at room temperature (RT) with constant stirring and recovered by filtration on Whatman filter paper number 3 (Merck KGaA, Darmstadt, Germany). The defatting process was repeated, and the meal was allowed to air-dry overnight. Defatted peanut meal proteins were extracted in 20 mM Tris/HCl buffer, pH 8.0 (1:30, w/v) for 2 h at 4 °C. The suspension was centrifuged (12,000 g, 30 min, 4 °C) and the supernatant collected. Ammonium sulphate was added to 40% saturation and the solution stirred for 30 min at 4 °C. After centrifugation at 10,000 g for 20 min at 4 °C, the supernatant was collected, and further addition of ammonium sulphate followed to bring the concentration up to 75% (w/v). The mixture was centrifuged at 10,000 g for 20 min at 4 °C and the pellet was dissolved in 20 mM Tris/HCl buffer, pH 8.0. The solution was dialyzed against 20 mM Tris/HCl buffer, pH 7.2 containing 0.15 M NaCl, overnight at 4 °C using 3.5 kDa MWCO dialysis tubing (Fisher Scientific, Göteborg, Sweden). After filtration with a 0.2 µm syringe filter (Merck), the solution was applied to a HiLoad 16/600 Superdex 75 pg column (Cytiva, Brøndby, Denmark) attached to an ÄKTA Pure 25 M1 (Cytiva), equilibrated with the same buffer using a flow rate of 0.75 mL/min. Absorbance was monitored at 280 nm and 215 nm and fractions were analyzed by SDS-PAGE. Column fractions containing Ara h 2 were collected, pooled, and dialyzed overnight at 4 °C against 20 mM Tris/HCl buffer, pH 7.2 using 3.5 kDa MWCO dialysis tubing (Fisher Scientific). After the ammonium sulfate concentration was adjusted to 1.5 M, the sample was filtered (0.22 µm syringe filter) and loaded onto a HiTrap phenyl HP column (7 x 25 mm, Cytiva) equilibrated with 20 mM Tris/HCl buffer, pH 7.2 containing 1.5 M ammonium sulphate. The column was run at 1 mL/min and eluted with a linear gradient from 1.5 to 0.0 M ammonium sulphate. Column fractions containing Ara h 2 were collected, pooled, dialyzed overnight at 4 °C against PBS (137 mM NaCl, 3 mM KCl, 8 mM Na<sub>2</sub>HPO<sub>4</sub>, 1 mM KH<sub>2</sub>PO<sub>4</sub>, pH 7.2) (3.5 kDa MWCO dialysis tubing) and concentrated by ultrafiltration (3 kDa MWCO Amicon Ultra-15 filter) (Millipore). The purified Ara h 2 was aliquoted and stored at -20 °C for further analysis.

## 2.2 Peanut protein extract

The purification procedure for PPE was almost identical to the procedure for Ara h 2 (section 2.1). The only differences were that the pH of the buffer was 8.5 instead of 8.0, the Tris/HCl buffer ratio was 1:10 instead of 1:30, and the incubation time was 1 h instead of 2 h. The PPE was furthermore dialyzed against PBS instead of 20 mM Tris/HCl buffer, pH 7.2.

## 2.3 Microneedle fabrication

Fabrication of chips with MNs is described in manuscript I [37]. In brief, MNs were fabricated using double-side polished silicon wafers. The MN pattern was designed using CleWin 5 layout editor (WeWin software, Hengelo, The Netherlands). The wafer back and front sides were exposed to spin coating, photo lithography, and dry etch after which the photoresist was removed. The etching step on the back side defined the MN thickness and the photo lithography and etching step on the front side defined the MN shape. The MN shape and dimensions were a pencil shape with a 1000  $\mu\text{m}$  length, 400  $\mu\text{m}$  width, and 180  $\mu\text{m}$  thickness. The chip with MNs is illustrated in Figure 1. It consists of a 15 x 9 mm chip with a 3 x 3 mm extruding part called the base, from which three MNs extrude.



**Figure 1: Schematic illustration of microneedles.** Three pencil-shaped MNs with dimensions of 1000  $\mu\text{m}$  length, 400  $\mu\text{m}$  width, and 180  $\mu\text{m}$  thickness extrude from a base (3 x 3 mm), which itself is extruding from a chip (15 x 9 mm).

## 2.4 Microneedle coating and release

### 2.4.1 Coating solution

Delivery molecules were added to de-ionized water (DI water) in the desired concentration after which carboxymethyl cellulose (CMC) sodium salt (low viscosity) (Sigma-Aldrich, St. Louis, Missouri, USA) was

added to an end concentration of 1% (w/v). PBS was used instead of DI water for all experiments conducted in rats. Coated MNs were stored at 4 °C until use. The maximum storage time was seven days.

Ara h 2 and Rhodamine B-conjugated Ara h 2 were used for coating in addition to the following fluorescent-labeled molecules: Fluorescein isothiocyanate-dextran (FITC-dextran, Sigma-Aldrich), Albumin-fluorescein isothiocyanate conjugate (FITC-BSA, Sigma-Aldrich), and Rhodamine B isothiocyanate-Dextran (Rhodamine B-dextran, Sigma-Aldrich).

#### **2.4.2 Ara h 2 Rhodamine B conjugation**

Rhodamine B was conjugated to Ara h 2 using the Rhodamine B conjugated kit (Fast, Lightning Link, ab188286, abcam, Cambridge, UK) according to manufacturer's instructions.

#### **2.4.3 Dip-coating**

A 3D printed probe for mounting of MNs to a Texture Analyser (TA, Stable Microsystems, Godalming, UK) and wells for coating solutions were prepared using Fusion 360 (Autodesk, CA, USA, V2.0.14793) and sliced using Simplify3D (Simplify3D, OH, USA, version 4.1.2). The probe and wells were printed using fused filament fabrication with Poly(lactic acid) on a Felix Pro Series printer (FELIX Printers, IJsselstein, The Netherlands), as previously described in manuscript I [37].

For optimization experiments the MNs were cleaned by plasma treatment (Diener Electronic Zepto, Diener Electronic GmbH & Co. KG, Ebhausen, Germany) prior to dip-coating. MNs were treated with air-plasma at 40% power (where 10% power = 30 watt) for 75 s using compressed dry air. The MNs were plasma treated on either the front side, back side or both sides.

Using a dip-coating method, the MNs were mounted vertically on the TA using the custom-made probe and moved downwards into the coating solution with a speed of 0.50 mm/s and held in the solution for 10 s. Subsequently, the MNs were removed with a retraction speed of 0.50 mm/s. The MNs were left to dry in an upright position for a few minutes. If the coating contained fluorescence, they were left to dry in darkness.

#### **2.4.4 Coating release**

To determine the proportion of coating released, the remaining, fluorescent-labeled coating on the MNs was measured after insertion. This was done by placing the MNs in the wells of a ProxiPlate-96 Black, Black Opaque 96-shallow well Microplate (PerkinElmer, Waltham, MA, USA) with 90 µL PBS for 5 min to ensure that all remaining coating was released. To confirm that all the remaining coating had been released the MNs were imaged afterwards by fluorescence microscopy (Olympus BX53, Olympus, Shinjuku, TYO, Japan).

The released FITC fluorescence was measured using a Victor X Multilabel Plate Reader (PerkinElmer), after shaking for 1 s, at a measurement height of 13 mm. The Rhodamine B fluorescence was measured using a Multimode Plate Reader EnSpire (PerkinElmer) at an excitation wavelength of 550 nm and an emission wavelength of 570 nm. A standard curve with the relevant fluorescence and PBS as background was included for each plate.

## **2.5 Coating delivery in *ex vivo* pig and human skin samples**

### **2.5.1 *Ex vivo* pig and human skin sample preparation**

Human skin explants were collected from surgical procedures under informed patient consent and local ethical committee approval (South East Wales Research Ethics Committee Ref: 08/WSE03/55).

Excised pig neck and human breast skin samples were frozen at -20 °C until use. Subsequently, the skin samples were thawed at RT for approx. 30 min. Skin samples were prepared under sterile conditions inside a fume hood. Two layers of cork were wrapped in two layers of tin foil and skin samples were placed with the dermis skin layer facing up on the tin foil to remove fat and muscle tissue. After removal, the first tin foil layer was removed to collect the excess fat and muscle tissue, and the skin samples were placed with the epidermis facing up on the tin foiled cork and fixed. The skin surface was gently wiped with ethanol and for pig neck skin samples, the surface was shaved. To prevent the skin from drying they were dapped with PBS every 5-10 min.

### **2.5.2 Cryostat histology with fluorescence delivery in *ex vivo* pig and human skin samples**

MNs were coated as described in section 2.4.3 with 10 mg/mL Rhodamine B-dextran in DI water. The MNs were inserted in pig neck and human breast skin samples for 2, 30 and 60 s at 5 N, measured using a Sauter force gauge (model FH 100, Sauter, Basel, Schweiz). An 8 mm diameter biopsy was taken from the insertion spot of MNs using a biopsy pen (pfm medical ag, Cologne, Germany). The biopsy samples were fixed using formaldehyde and frozen using optimal cutting temperature (OCT) embedding matrix (Carl Roth, Karlsruhe, Germany) at -20 °C and stored at -80 °C until cryosectioning. The frozen biopsy samples were mounted and cryosectioned using a Cryotome FSE cryostat (Thermo Scientific, Waltham, Massachusetts, USA). The cryosectioned slices were 10 µm thick and collected on Thermo Scientific™ SuperFrost™ Microscope Slides, Cut (Fischer Scientific, Waltham, MA, USA). Fluorescence was imaged using an Olympus IX50 microscope with Olympus U-RFL-T burner (Olympus, Shinjuku, TYO, Japan). First, a brightfield microscope picture was taken and subsequently a fluorescence image was taken at the same location and magnification and these pictures were overlaid using ImageJ 1.52a (Wayne Rasband, National Institutes of Health, USA).

## **2.6 Brown Norway rats**

Rat experiments were carried out in the animal facility at the Technical University of Denmark. Ethical approval was given by the Danish Animal Experiments Inspectorate with the authorization number (2020-15-0201-00732-C1). The experiments were overseen by the University's in-house Animal Welfare Committee for animal care and use.

BN rats from the in-house breeding colony at the National Food Institute, Technical University of Denmark with an age of 9-15 weeks were used. Rats were given an in-house produced diet based on potato, fish, and rice proteins, free from legume proteins, for more than 14 generations [38], [39]. Water was provided *ad libitum*. Rats were housed in macrolon cages (n=4/cage) at 22 °C ± 1 °C with a relative humidity of 55 ± 5%. Electric lights were on from 9.00 a.m. to 9.00 p.m. The rats were inspected once a day and body weight noted once a week.

## **2.7 Brown Norway rat experiments**

### **2.7.1 Coating delivery in Brown Norway rat skin (experiment 1)**

To investigate fluorescent-labeled coating delivery, BN rats (n=3, males) were used. Rats were sacrificed by decapitation using hypnorm-midazolam as anesthesia. Subsequently the abdominal skin was shaved, and MNs coated with 10 mg/mL FITC-dextran were tested. MNs were manually inserted into the abdominal skin for 2, 30, 60, and 120 s. The coating delivery was subsequently calculated by subtracting the mean value of remaining, fluorescent-labeled coating on inserted MNs from the mean value of fluorescent-labeled coating on MNs that were not inserted in the skin. The fluorescent-labeled coating on the MNs was measured as described in section 2.4.4.

### **2.7.2 Coating delivery in Brown Norway rat skin (experiment 2)**

To assess FITC-BSA and Rhodamine B-conjugated Ara h 2 coating release, BN rats (n=8, 4/gender) were used. Rats were sedated using hypnorm-midazolam, shaved on the abdomen skin and subsequently 50 µg/mL Rhodamine B-conjugated Ara h 2-coated MNs were inserted in the skin for 2, 30, and 60 s. The rats were then sacrificed by decapitation, and MNs coated with 10 mg/mL FITC-BSA were inserted for 2, 30, and 60 s. The abdominal skin samples were excised and fixed to their original size and samples were taken using an 8 mm biopsy pen, snap-frozen in liquid nitrogen, and stored at -80 °C until use.

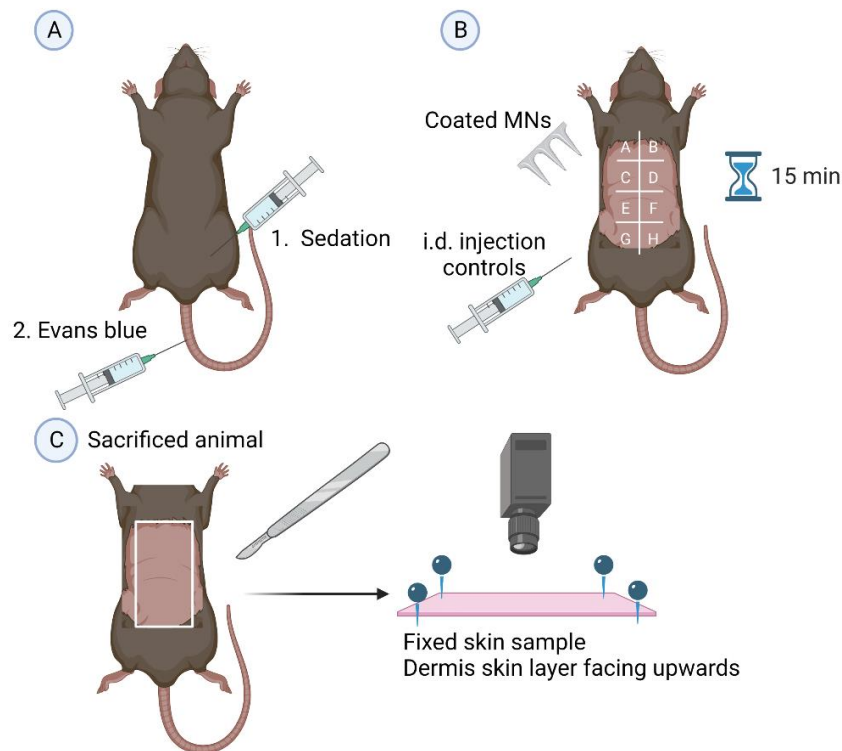
### **2.7.3 Coating delivery of low dosage range of compound 48/80 in Brown Norway rats (experiment 3)**

To evaluate compound 48/80 (Sigma-aldrich) coating delivery and confirm subsequent visualization of the mast cell degranulation response, BN rats (n=8, 4/gender) were used. Rats were sedated using hypnorm-midazolam and 1% Evans blue (Sigma-Aldrich) in PBS was injected into the tail vein at a volume of 2 µL/rat weight (g) (Figure 2A). Evans blue binds to serum albumin in the blood and consequently stains the blood blue, making blood accumulations visible [40]. The rat abdominal skin was shaved and MNs coated as described in section 2.4.3 with either 0 (control), 5, 10, 20, 30 or 40 µg/mL of 48/80 mixed in PBS, were inserted manually into the skin for 60 s. In addition, 30 µL of PBS (negative control) and 30 µL of 20 µg/mL 48/80 (positive control) corresponding to 0.6 µg were i.d. injected for comparison with MN delivery (Figure 2B). After 15 min from the initial Evans blue tail injection, the rats were sacrificed by decapitation. Next, abdominal skin samples were excised and fixed to their original size with the dermis skin layer facing up for visualization of the Evans blue colored blood accumulation. The fixed skin samples were photographed together with a visible ruler for later analysis and comparison (Figure 2C).

### **2.7.4 Coating delivery of high dose range of compound 48/80 in Brown Norway rats (experiment 4)**

A rat experiment similar to experiment 3 (section 2.7.3) was conducted but with a broader range of MN 48/80 coating concentrations (0.1, 1, 10, 100, or 1000 µg/mL 48/80), still using PBS as negative control.

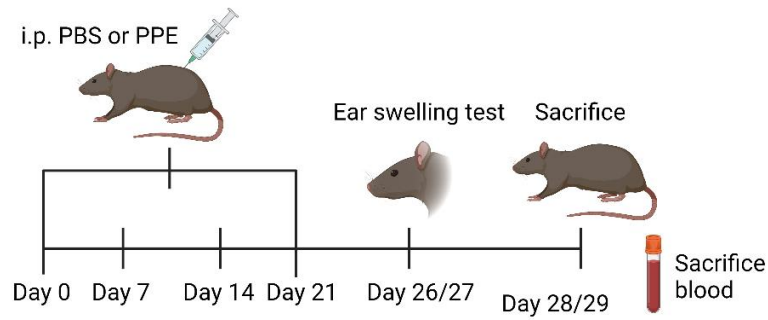




**Figure 2: Illustration of compound 48/80 coating delivery in Brown Norway rats.** A) Rats were sedated using hypnorm-midazolam, 1% Evans blue in PBS was injected into the tail vein and the abdominal skin was shaved. B) Microneedles (MNs) coated with 48/80 were manually inserted for 60 s and 30  $\mu$ L of 20  $\mu$ g/mL 48/80 (0.6  $\mu$ g) and 30  $\mu$ L of PBS were intradermally injected in the rat abdominal skin. C) After 15 min the rats were sacrificed by decapitation, the abdominal skin samples were excised and fixed to their original size with the dermis skin layer facing up and photographed for later analysis. Created with BioRender.com.

### 2.7.5 Delivery of Ara h 2 in naïve or peanut-sensitized Brown Norway rats (experiment 5)

To investigate Ara h 2 coating delivery and mast cell degranulation responses, rats were allocated into six groups (n=8/group, 4/gender) where Group 1, 3, and 5 were intraperitoneally (i.p.) injected with 0.5 mL of PBS as control and Group 2, 4, and 6 were i.p. injected with 0.5 mL of PBS containing 50  $\mu$ g PPE on Day 0, 7, 14, and 21. At Day 26 (Group 3 and 4) and Day 27 (Group 1, 2, 5, and 6) an ear swelling test (EST) was performed as described later in section 2.7.5.1. At Day 28 (Group 1, 2, 4, and 6) and Day 29 (Group 3 and 5) rats were sacrificed by decapitation using hypnorm-midazolam as anesthesia and blood was collected, converted to sera, and stored at -20 °C until analyses (Figure 3).

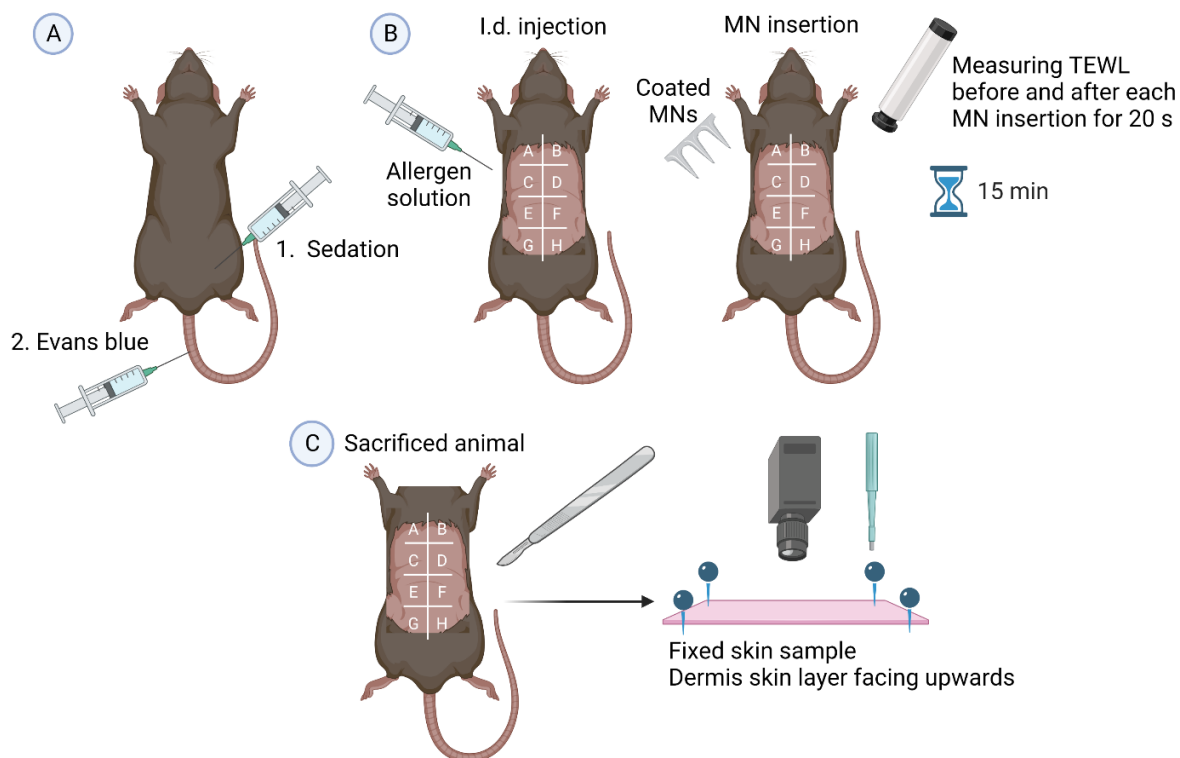


**Figure 3: Rat experimental design.** Rats were immunized with 0.5 mL of phosphate buffered saline (PBS) alone (control groups) or with 0.5 mL PBS containing 50 µg peanut protein extract (PPE) (sensitized groups) on Day 0, 7, 14, and 21. An ear swelling test was performed on Day 26 and 27 and rats were sacrificed on Day 28 and 29 where the blood was collected. Group 1, 3, and 5 were control groups that received PBS while Group 2, 4, and 6 were sensitized groups receiving PPE. Group 1-2 were rats that received an intradermal injection as a control to the microneedle (MN) insertion and Group 3-6 were rats that were pricked with coated MNs. Created with BioRender.com.

Group 1 and 2 were i.d. injected with 30 µL of Ara h 2 in PBS (625, 125, 25, 5, and 1 µg/mL Ara h 2) corresponding to 0.03, 0.15, 0.75, 3.75, and 18.75 µg. As a positive control 30 µL of 20 µg/mL 48/80 corresponding to 0.6 µg was i.d. injected and as a negative control 30 µL of PBS was i.d. injected. Group 1-2 acted as controls for Group 3-6.

Group 3-6 were used for Ara h 2 delivery via MN insertion using the same concentrations of Ara h 2 in the coating solution as for the i.d. injection solutions. Also included were MNs coated with 1000 µg/mL 48/80 as positive MN control and PBS as negative MN control as well as non-coated MNs as a second negative control. The actual amount of allergen or positive control delivered using coated MNs was unknown.

The rats were sedated using hypnorm-midazolam and injected with Evans blue as described in section 2.7.3 and their abdominal skin was shaved (Figure 4A). I.d. injections or manual MN insertions were done for eight randomly assigned locations (A-H) on the abdominal skin 2 min after the Evans blue injection. As a measure for the skin damage posed by the MN insertions, the trans-epidermal water loss (TEWL) was measured for 20 s before and immediately after each MN insertion. When halfway through either the i.d. injections or MN insertions a timer was set for 15 min (Figure 4B) after which the animals were sacrificed. The rats were sacrificed by decapitation. Afterwards, abdominal skin samples were excised, fixed to their original size, and photographed as described in section 2.7.3. Using 8 mm biopsy pens skin samples from the injection/insertion sites were collected, weighed and snap-frozen in liquid nitrogen, and subsequently stored at -80 °C until use (Figure 4C).



**Figure 4: Delivery of Ara h 2 by intradermal injection and microneedle insertion.** A) Rats were sedated using hypnorm-midazolam and 2  $\mu\text{L}/\text{rat weight (g)}$  of 1% Evans blue in phosphate buffered saline was injected into the tail vein. B) Intradermal (i.d.) injections or microneedle (MN) insertions were done after 2 min at eight randomly assigned locations (A-H). Trans-epidermal water loss (TEWL) was measured before and after MN insertion. When halfway through i.d. injections or MN insertions, a timer was set for 15 min whereafter the rats were sacrificed. C) Rats were sacrificed by decapitation. Skin samples were excised, fixed to their original size with the dermis layer facing upwards, and photographed for later Evans blue analysis. Biopsy samples were taken from the eight locations and snap-frozen in liquid nitrogen for  $-80^\circ\text{C}$  storage. Created with BioRender.com.

### 2.7.5.1 Ear swelling test

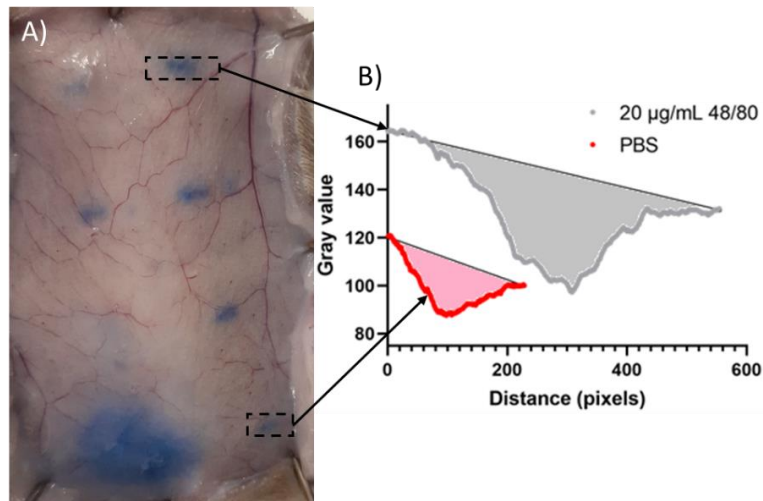
An EST was performed to evaluate the clinical relevance of the PPE sensitization, as previously described [41]. In brief, the rats were anesthetized by injection of hypnorm-midazolam and the initial ear thickness was measured twice using a caliper. The left ear was i.d. injected with 10  $\mu\text{g}$  PPE in 20  $\mu\text{L}$  PBS while 3  $\mu\text{g}$  Ara h 2 in 20  $\mu\text{L}$  PBS was i.d. injected into the right ear. The ear thickness was measured again once after 30 min and the ear swelling, i.e., change in ear thickness ( $\Delta\text{Thickness}$ ) was determined as a measure of the clinical relevance of the PPE sensitization. The PPE sensitization would be considered clinically relevant if  $\Delta\text{Thickness}$  was significantly higher for the sensitized animals compared to the control animals.

## 2.8 ImageJ analysis of Evans blue data

For Evans Blue quantification image analysis was conducted using ImageJ 1.52a (National Institutes of Health, USA). The criterium set for performing an Evans blue quantification analysis was that the positive

control of 48/80 was clearly visible in the skin, thus, if the positive control was not clearly visible the rat was excluded from analysis.

The Evans blue area was measured by setting the length scale according to a ruler in the image. The area was then marked and measured using the freehand selection tool. "Histogram" was used for gray value analysis (color saturation) where the Evans blue area was selected using the rectangle selection tool and a mean value for the gray value was extracted. "Color Profiler" was used for area under the curve (AUC) analysis where the Evans blue area with part of the skin background was selected as illustrated in Figure 5A using the rectangle selection tool and the RGB (red, green, and blue) graph (mean gray value for each column of pixels within the selected area) was extracted (Figure 5B). The red channel was found to give the best color contrast and thus this channel was used henceforth. Upon extraction to Excel (Version 2301, Microsoft 365) a mean value for the background data representing the coloration of the pristine skin was calculated based on the first and last ten data points to establish a baseline. The area of the shaded regions on the gray value by distance graph on Figure 5B were calculated and used as a measure of the Evans blue response AUC.



**Figure 5: Evans blue data extraction for the area under the curve analysis method.** An example of excised skin and illustration of how area under the curve (AUC) data was obtained using ImageJ and analyzed using GraphPad Prism. A) The Evans blue area was selected as illustrated using a rectangle selection tool in ImageJ and the B) "color profiler" tool was used to measure and extract a RGB (red, green, and blue) graph. The red channel was found to be the most sensitive for blue color detection and was therefore used. The areas of the shaded regions were calculated and used as a measure of the Evans blue response.

## 2.9 Enzyme-Linked Immunosorbent Assay

### 2.9.1 Detection of Specific IgG<sub>1</sub> by Indirect ELISA

For detection of the development of a specific immune response, 96-well Maxisorp plates (NUNC, Roskilde, Denmark) were coated with 100 µL/well of 0.1 µg/mL PPE or 0.5 µg/mL Ara h 2 in carbonate buffer (15 mM Na<sub>2</sub>CO<sub>3</sub> x 10 H<sub>2</sub>O, 35 mM NaHCO<sub>3</sub>, pH 9.6) for measurement of PPE-specific IgG<sub>1</sub> and Ara h 2-specific IgG<sub>1</sub>, respectively. Between each step, the plates were washed five times in PBS with 0.01%

(w/v) Tween-20 (Sigma-Aldrich) (PBS-T). After incubation overnight at 4 °C, the plates were incubated for 1 h with 50 µL/well of serial 2-fold diluted blood samples in PBS-T starting at a dilution of 1:8. Next, plates were incubated with 100 µL/well of the secondary antibody, mouse anti-rat IgG<sub>1</sub>, labeled with horseradish peroxidase (HRP, 3060-05, Southern Biotech, Birmingham, AL, USA) diluted 1:20,000 in PBS-T. Afterwards, the plates were washed in tap water and incubated at RT for 12 min with 100 µL/well 3,3',5,5'-tetramethylbenzidine (TMB)-one (4380A, Kementec Diagnostics, Taastrup, Denmark). The reaction was stopped by adding 100 µL/well 0.2 M H<sub>2</sub>SO<sub>4</sub>. The results are expressed as log<sub>2</sub> titer values with a cut-off optical density (OD) of 0.025. Titers are defined as the interpolated dilution of the sample down to the mean absorbance for the negative control +3 x the standard deviation (SD).

### **2.9.2 Detection of Specific IgE by Antibody-Capture ELISA**

For the detection of PPE- or Ara h 2-specific IgE, 96-well Maxisorp plates (NUNC) were coated with 100 µL/well of 0.5 µg/mL mouse anti-rat IgE (HDMAB-123 HydriDomus, Nottingham, UK) in carbonate buffer and incubated overnight at 4 °C. Between each step, the plates were washed five times in PBS-T. Subsequently, plates were blocked for 1 h at 37 °C with 200 µL/well of 3% (w/v) skimmed milk powder (SMP, 70166, Sigma-Aldrich) in PBS-T. Next, serum samples were added in 2-fold serial dilutions starting at 1:8 in PBS-T. Plates were incubated with 50 µL/well of 10:1 digoxigenin (DIG)-coupled PPE diluted to 0.2 µg/mL or Ara h 2 diluted to 0.5 µg/mL in 3% SMP blocking solution. Plates were then incubated with 100 µL/well HRP-labeled sheep-anti-DIG-POD (11633716001, Roche Diagnostics GmbH, Mannheim, Germany) diluted 1:1,000 in PBS-T. Between each step, the plates were washed five times in PBS-T. Afterwards, the plates were washed under tap water and incubated at RT for 12 min with 100 µL/well TMB-one. The reaction was stopped by adding 100 µL/well 0.2 M H<sub>2</sub>SO<sub>4</sub>. The results are expressed as log<sub>2</sub> titer values with a cut-off OD of 0.025. Titers are defined as the interpolated dilution of the sample down to the mean absorbance for the negative control +3 x SD.

### **2.10 Tissue Homogenization**

To investigate molecules in skin samples, tissue homogenization was performed. For homogenization, the frozen skin samples were pulverized using a mortar with a pestle and liquid nitrogen, and 20 µL/mg tissue homogenization lysis buffer (150 mM sodium chloride (Merck, Darmstadt, Germany), 20 mM tris(hydroxymethyl)aminomethane tris(us) (Sigma-Aldrich), 1 mM Ethylene glycol-bis(2-aminoethylether)-N,N,N',N',-tetra acetic acid (EGTA) (Sigma-Aldrich), 1 mM Ethylenediaminetetraacetic acid solution (EDTA (0.5 M)) (Sigma-Aldrich), MilliQ water, 1% w/v IGEPAL (Sigma-Aldrich) with 2% Halt™ Protease Inhibitor Cocktail (100x) (Thermo Fischer Scientific, Waltham, MA, USA)) was added to the mortar and mixed. The samples were collected from the mortar in an Eppendorf tube and one stainless freezer-cold bead (Ø 5 mm) was added. The samples were run in TissueLyser II (QIAGEN, Hilden, Germany) with 30 oscillations/min for 2 min for final homogenization. Afterwards, the samples were incubated on ice for 20 min while being vortexed every 5 min. The samples were centrifuged at 15,000 g for 20 min at 4 °C and the supernatant was harvested and stored at -80 °C until use.

### **2.10.1 Detection of Ara h 2 by Indirect ELISA**

For measurements of Ara h 2 content in the rat skin tissue homogenates (diluted 1:4), an ELISA kit (ARA H 2 ELISA 2.0 KIT – FIVE PLATE (EPC-AH2-5), Indoor Biotechnologies, VA, USA) was performed according to the manufacturer's protocol.

### **2.11 Statistical analysis**

Graphs and statistical analyses were made using Prism V9.5.0 (GraphPad, San Diego, CA, USA). Results regarding coating development and optimization were analyzed using parametric test analyses as this data was deemed to be normally distributed as assessed by D'Agostino-Pearson normality test. For these analyses one-way ANOVA with Tukey's multiple comparisons test and unpaired T-tests with Bonferroni correction were used. A significance level of  $\alpha = 0.05$  was used in all cases.

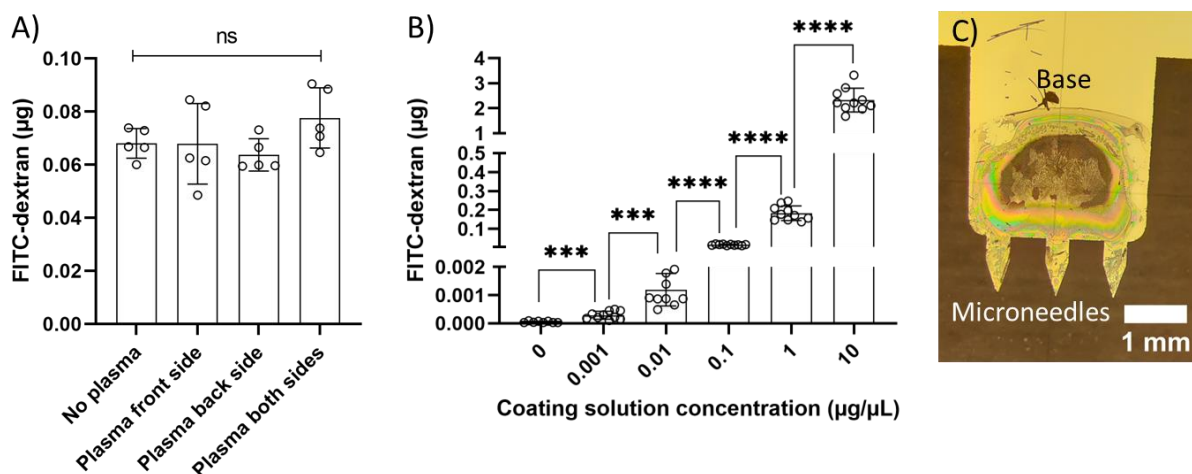
Results obtained from *in vivo* rat experiments were found not to be normally distributed as assessed by D'Agostino-Pearson normality test and was therefore analyzed by non-parametric analyses. For these analyses Kruskal-Wallis test with Dunn's multiple comparisons test and Mann-Whitney test were used. A significance level of  $\alpha = 0.05$  was used in all cases.

## **3. Results**

### **3.1 Microneedle coating and release**

Plasma treatment on the surface of the MNs was investigated as a method for cleaning and increasing hydrophilicity [42] to enhance coating adhesion. No statistically significant differences (one-way ANOVA with Tukey's multiple comparisons test) were revealed when comparing the different plasma treatment strategies of either no, front-side, back-side or both sides plasma treatment of MNs (Figure 6A). Thus, plasma treatment did not aid the coating and was therefore omitted henceforth.

From the initial coating release studies, it was found that by increasing the concentration of FITC-dextran in the coating solution, an increased amount of FITC-dextran was released (Figure 6B). A statistically significant difference (unpaired T-tests with Bonferroni correction,  $\alpha_{\text{Bonferroni}} = 0.01$ ) was found between each tenfold increase in FITC-dextran concentration. It should be noted that to ensure that the MNs were fully coated, the chip was submerged in the FITC-dextran coating solution, and this covered the MNs as well as the base (Figure 6C). Hence, the released amount in this case is a measure of release from both the MNs and the base.



**Figure 6: Optimizing dip-coating of microneedles.** A) Amount of FITC-dextran released (mean  $\pm$  SD,  $n=5$ ) from microneedles (MNs) subjected to plasma surface treatment on either the front, back or both sides. B) Amount of FITC-dextran released (mean  $\pm$  SD,  $n=10$ ) from MNs coated with various FITC-dextran coating solution concentrations. C) Example of an optical microscope image illustrating how the coating is distributed on the MNs and base. For all statistical analyses the statistically significant differences are marked as \*\*\*  $p \leq 0.001$  and \*\*\*\*  $p \leq 0.0001$ .

### 3.2 Coating delivery in Brown Norway rat skin

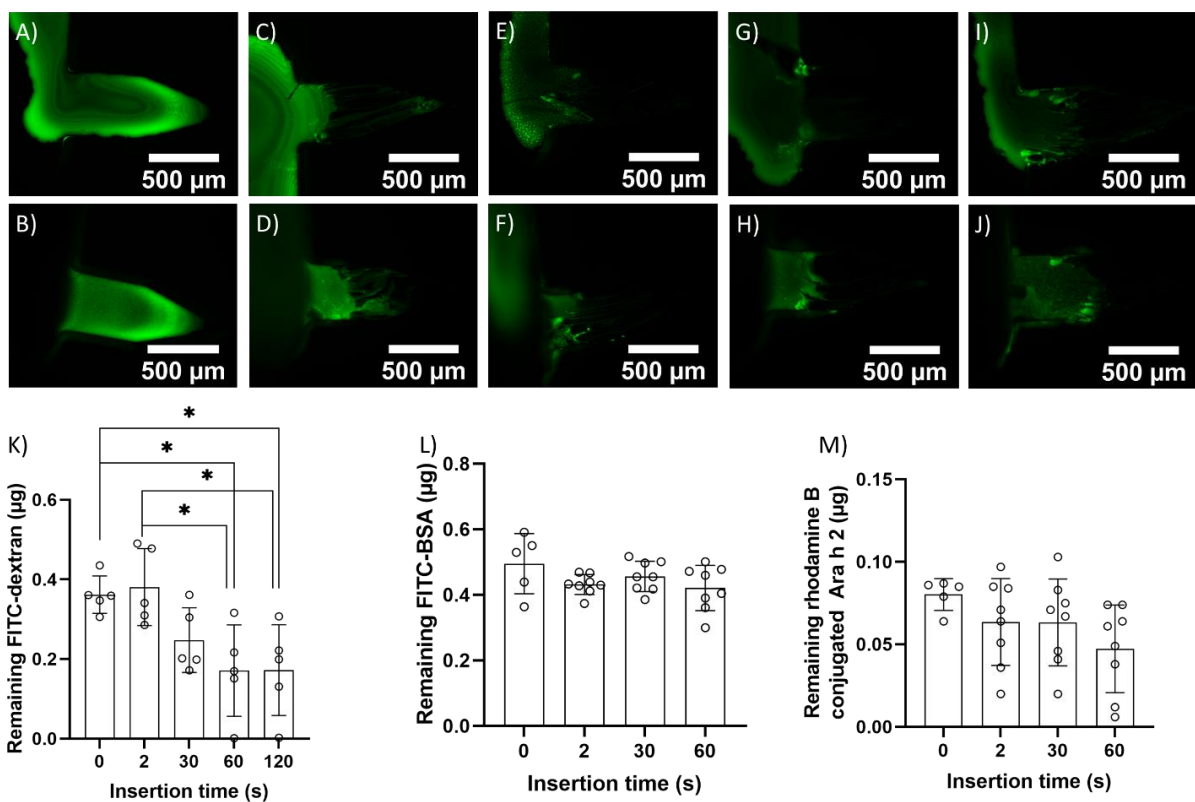
For optimization of insertion time to ensure coating release, sacrificed rats were pricked with FITC-dextran, FITC-BSA, and Rhodamine B-conjugated Ara h 2-coated MNs for different time durations. The fluorescence from the remaining coating on the front as well as back of the MNs was visualized and measured using a fluorescence microscope (Figure 7A-J). Comparing the control MNs (Figure 7A-B), which were not inserted into the rat skin (0 s) with MNs inserted for 2 s (Figure 7C-D), 30 s (Figure 7E-F), 60 s (Figure 7G-H) or 120 s (Figure 7I-J), showed that the coating was released from the MNs when in contact with the skin.

The relative amount of remaining FITC-dextran was compared between the MNs that were not inserted into the rat skin and the MNs inserted for 2, 30, 60, and 120 s respectively. The comparison showed statistically significant differences (one way ANOVA with Tukey's multiple comparisons test) between 0 s (control), and 60 s, and 120 s, respectively, as well as between 2 s and 60 s and 120 s, respectively (Figure 7K). Likewise, the released FITC-dextran was calculated by subtracting the mean fluorescence values of the inserted MNs from the control MNs. From this it was estimated that 2 s insertion caused no (0 ng) release, 30 s insertion caused a release of approx. 27% (90 ng  $\pm$  99 ng release); 60 s insertion caused a release of approx. 49% (166 ng  $\pm$  85 ng release); and 120 s insertion caused a release of approx. 49% (165 ng  $\pm$  116 ng release). It should be noted that these calculations are rough estimates.

To confirm coating release after 60 s of MN insertion, an identical experiment was conducted using FITC-BSA (Figure 7L) and Rhodamine B-conjugated Ara h 2 (Figure 7M). The remaining fluorescence was measured and generally either 30 s and/or 60 s insertion gave a lower mean value of remaining coating (Figure 7L-M) than 0 s (control). For FITC-BSA, 2 s insertion caused approx. 13% (63 ng  $\pm$  97 ng), 30 s insertion caused approx. 8% (39 ng  $\pm$  103 ng), and 60 s insertion caused approx. 15% (74 ng  $\pm$  115 ng)

release while for Rhodamine B-conjugated Ara h 2, 2 s and 30 s insertion both caused approx. 21% ( $17 \text{ ng} \pm 28 \text{ ng}$ ) release while 60 s insertion caused approx. 41% ( $33 \text{ ng} \pm 28 \text{ ng}$ ) release. Based on these results, it appears that the FITC-dextran had the highest release relative to the control after 60 s insertion time with approx. 49% coating release whereas FITC-BSA had a maximum release of approx. 15% and Rhodamine B-conjugated Ara h 2 had approx. 41% release after 60 s. We hypothesize that the difference in release is due to the delivery molecules having a distinct effect on the release of the coating (Figure 7K-M).

To re-find the delivered Rhodamine B-conjugated Ara h 2 in the skin, the Rhodamine B fluorescence intensity was measured in skin homogenates (Figure S1, SI). This revealed that the amount of delivered Ara h 2 was below the limit of detection.



**Figure 7: FITC-dextran, FITC-BSA, and Rhodamine B-conjugated Ara h 2 coating delivery in Brown Norway rat skin.** A-J) Front and back fluorescence microscope images of 450 µg/mL FITC-dextran-coated microneedles (MNs) after insertion. A-B) 0 s control MNs with no insertion. C-D) 2 s insertion. E-F) 30 s insertion. G-H) 60 s insertion. I-J) 120 s insertion. K) Remaining FITC-dextran after 0, 2, 30, 60, and 120 s insertion (mean  $\pm$  SD,  $n=5$ ). L) Remaining FITC-BSA after 0, 2, 30, and 60 s insertion (mean  $\pm$  SD,  $n\geq 5$ ). M) Remaining Rhodamine B-conjugated Ara h 2 after 0, 2, 30, and 60 s insertion (mean  $\pm$  SD,  $n\geq 5$ ). For all statistical analyses the statistically significant differences are marked as \* =  $p \leq 0.05$ .



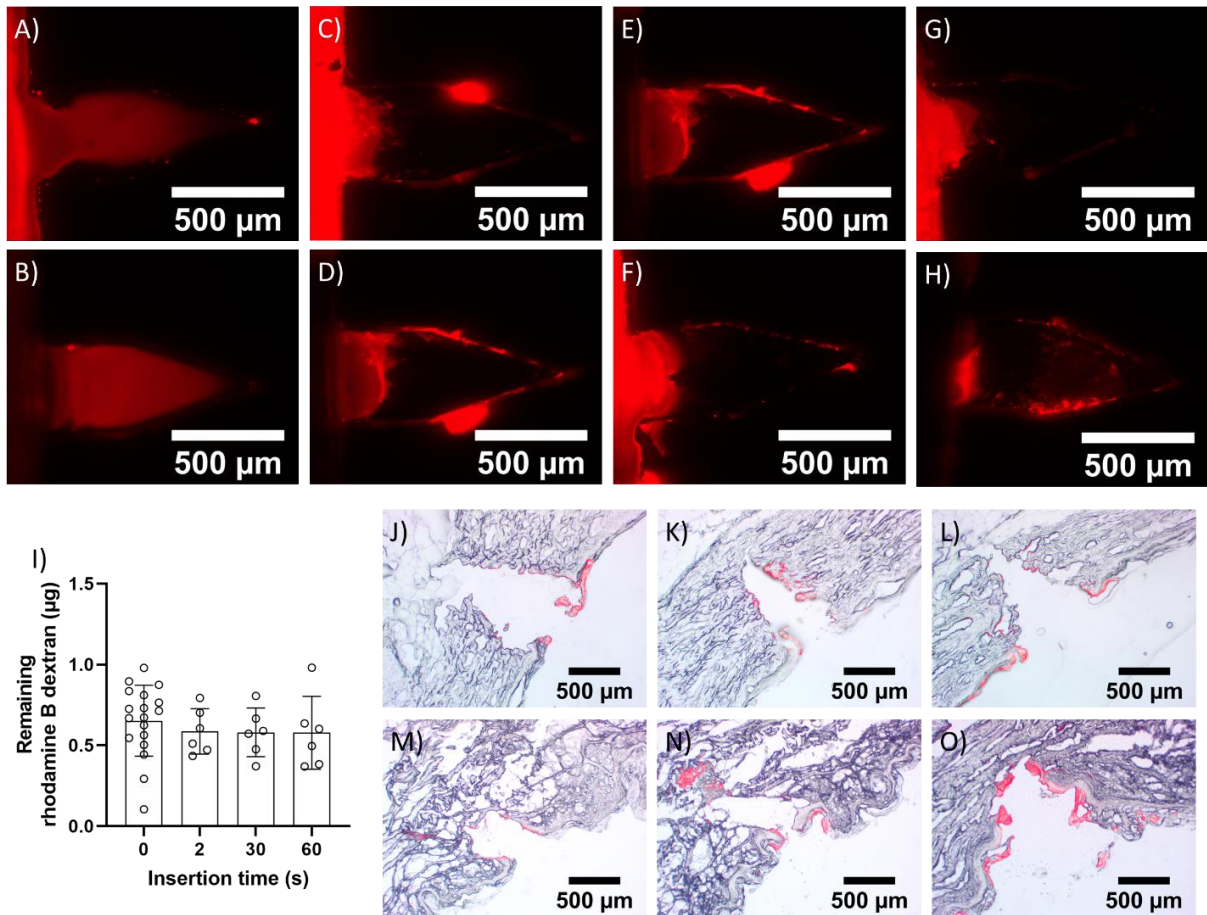
### 3.3 Coating delivery in *ex vivo* pig and human skin samples

Coating delivery was tested in pig neck skin and human breast skin *ex vivo* samples as these have a closer resemblance to the skin of patients than rat skin samples. The released fluorescent-labeled coating was visualized by cryosectioning *ex vivo* skin samples. For this purpose, Rhodamine B-dextran rather than FITC-dextran was used to avoid auto-fluorescence from the skin [43].

The front and back sides of control MNs (Figure 8A-B), and MNs which had been inserted for 2 s (Figure 8C-D), 30 s (Figure 8E-F) or 60 s (Figure 8G-H) were imaged using a fluorescence microscope. It could be observed that inserted MNs had less fluorescent-labeled coating remaining after insertion compared to the control ones.

The remaining Rhodamine B-dextran on the MNs was quantified (Figure 8I), however, the mean fluorescence value after 60 s insertion was not much lower than for the control MNs. The released coating was estimated, and 2 s insertion caused approx. 10% ( $66 \text{ ng} \pm 260 \text{ ng}$ ), 30 s insertion caused approx. 11% ( $72 \text{ ng} \pm 266 \text{ ng}$ ), and 60 s insertion caused approx. 11% ( $75 \text{ ng} \pm 315 \text{ ng}$ ) release. There were no statistically significant differences (one-way ANOVA with Tukey's multiple comparisons test) found for the remaining coating between the different insertion times.

As delivery could not be confirmed statistically by measuring the remaining fluorescence, the pig neck skin (Figure 8J-L) and human breast skin (Figure 8M-O) samples were cryosectioned. Optical as well as fluorescence microscope images were taken of the unstained histology slices, and the images were overlaid. Using this method, delivered Rhodamine B-dextran was visible in the cryosectioned skin samples for all MN insertion times, 2 s (Figure 8J,M), 30 s (Figure 8K,N), and 60 s (Figure 8L,O). Based on this and the previous results, it is likely that small amounts of coating were delivered. It furthermore appears that the insertion time has an impact on the delivery in human breast skin, with increasing delivery times providing more coating to the skin (Figure 8M-O). Collectively, these results demonstrate that a measure of the remaining, fluorescent-labeled coating on the MNs is not the best method for estimating coating delivery. This is likely because the amount of fluorescent-labeled coating delivered from the inserted MNs is so small compared to the coating still present on the MNs and base of the inserted MNs, that the drop in fluorescence signal compared to the not-inserted control MNs becomes insignificant.



**Figure 8: Rhodamine B-dextran fluorescent coating delivery.** A-H) Front and back fluorescence microscope images of 10 mg/mL Rhodamine B-dextran-coated microneedles (MNs) after insertion in pig neck skin samples. A-B) Control MN (no insertion). C-D) MN inserted for 2 s, E-F) 30 s, G-H) 60 s. I) Remaining Rhodamine B-dextran after 0, 2, 30, and 60 s insertion (mean  $\pm$  SD,  $n \geq 6$ ). J-L) Optical and fluorescence microscope images merged to illustrate Rhodamine B-dextran delivery in pig neck skin. J) Coating delivery for 2 s, K) 30 s, or L) 60 s. M-O) Optical and fluorescence microscope images merged to illustrate coating delivery in human breast skin. M) Coating delivery for 2 s, N) 30 s, or O) 60 s.

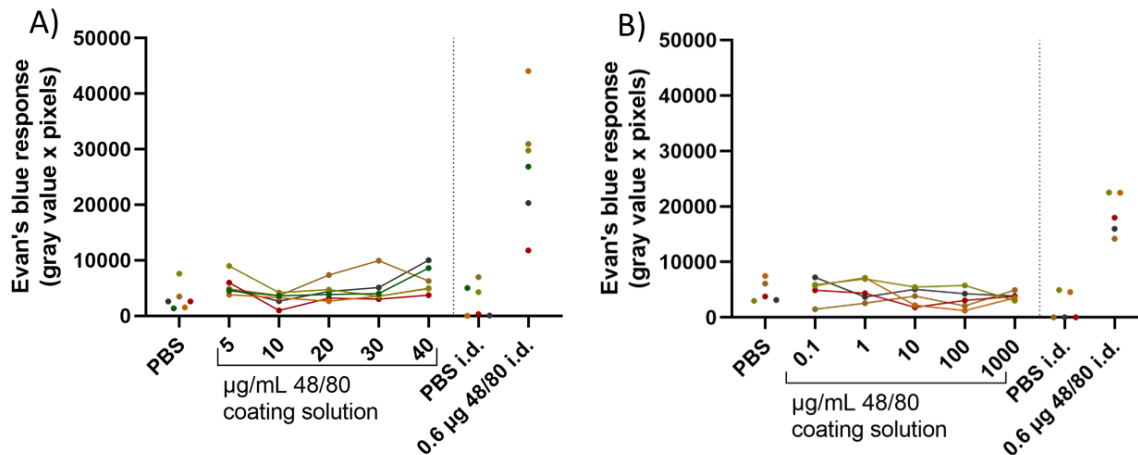
### 3.4 Coating delivery of compound 48/80 in Brown Norway rats

In the present study, the impact of delivered 48/80 on mast cell degranulation was investigated using Evans blue for visualization. MNs coated with various 48/80 coating solution concentrations ranging from 5-40 µg/mL (Figure 9A) or from 0.1 to 100 µg/mL (Figure 9B) were used and compared to 0.6 µg of i.d. delivered 48/80.

Different analysis methods were investigated to quantify the degranulation response using Evans blue staining, as no standard way for analysis of Evans blue data has previously been defined. Parameters such as color saturation (gray value) and Evans blue area (pixels) were investigated (Figure S2A-B, SI) using ImageJ. AUC analysis was conducted to get a combined measure of color saturation and Evans blue area. As evident from Figure S2A-B, SI as well as Figure 9A all three methods could potentially be used for

analysis since the i.d. control injections show the positive control 48/80 eliciting a response compared to the negative control PBS. Nonetheless, as the AUC encompassed both the parameters of color saturation and Evans blue area, this was deemed the most optimal method of analysis (cf. section 2.8).

In Figure 9A-B it can be observed that the MNs coated with varying concentrations of 48/80 did not elicit a response different from PBS.



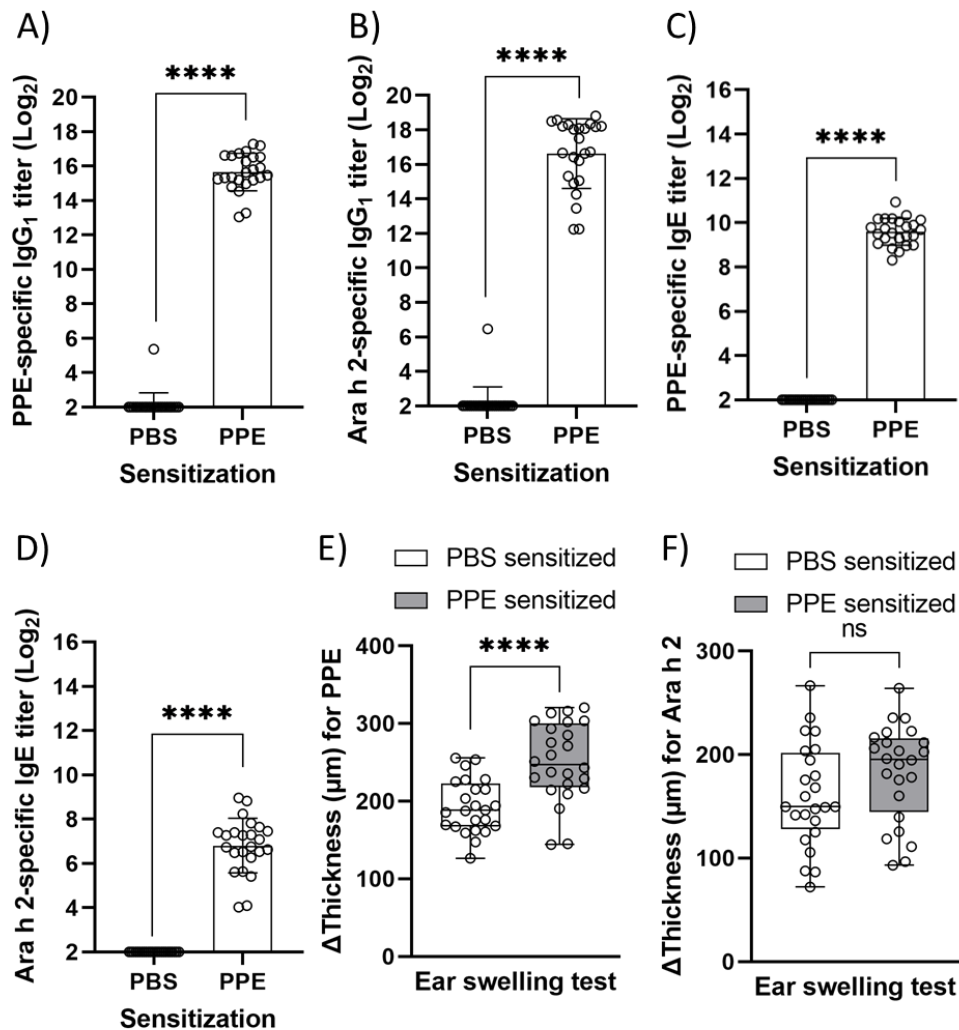
**Figure 9: Dose-response curves for 48/80 delivery in naïve rats using area under the curve analysis.** A-B) Dose-response curves of Evans blue response by area under the curve (AUC) (gray value x pixels) analysis for naïve rats. A) Small range of 48/80 coating solution concentrations: 5, 10, 20, 30, and 40 µg/mL (n=6) and intradermal (i.d.) injection of PBS and 0.6 µg 48/80 (n=6). B) Large range of 48/80 coating solution concentrations: 0.1, 1, 10, 100, and 1000 µg/mL (n=5) and i.d. injection of PBS and 0.6 µg 48/80 (n=5).

### 3.5 Delivery of Ara h 2 coating in Brown Norway rats

#### 3.5.1 Sensitization of Brown Norway rats

Until now the research was conducted on naïve animals only, however, since the idea is to measure an allergic response, the animals were sensitized against PPE. To confirm an initial antibody response PPE- and Ara h 2-specific IgG<sub>1</sub> ELISA assays were performed (Figure 10A-B), and to confirm sensitization PPE- and Ara h 2-specific IgE ELISA assays were performed (Figure 10C-D), along with an EST to confirm a clinically active response against PPE and Ara h 2 (Figure 10E-F).

The IgG<sub>1</sub> and IgE ELISA assays (Figure 10A-D) showed that the PPE-immunized rats developed an immune response and were sensitized towards PPE in contrast to the naïve control rats. Statistically significant differences (Mann-Whitney test) were found for all ELISA assays. The PPE-specific EST (Figure 10E) demonstrated statistically significant difference (Mann-Whitney test) between the control groups (PBS) and sensitized groups (PPE), indicating that the sensitized rats had a clinically active response towards PPE. Even though PPE-sensitized rats all had statistically significant Ara h 2-specific IgE titer values (Figure 10D), this seems to not cause a statistically significant (P=0.1025) clinical response to this single allergen in the EST (Figure 10F).



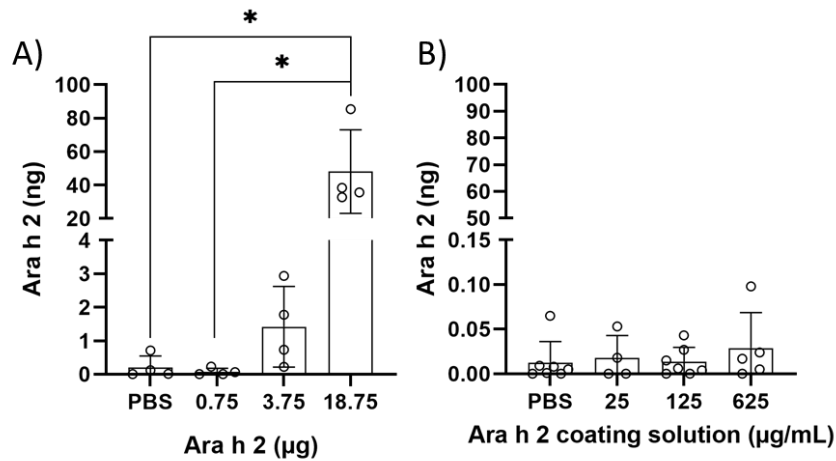
**Figure 10: Immunological response from naïve and sensitized Brown Norway rats.** A) Peanut protein extract (PPE)-specific IgG<sub>1</sub> titer (mean ± SD, n=48). B) Ara h 2-specific IgG<sub>1</sub> titer (mean ± SD, n=48). C) PPE-specific IgE titer (mean ± SD, n=48). D) Ara h 2-specific IgE titer (mean ± SD, n=48). E) Ear swelling test (EST) for PPE (n=48). F) EST for Ara h 2 (n=48). For all statistical analyses the statistically significant differences are marked as \*\*\*\* =  $p \leq 0.0001$ .

During MN insertion in BN rats TEWL was measured to confirm skin penetration. Statistically significant differences in TEWL (Kruskal-Wallis test with Dunn's multiple comparisons test) were observed for the rats before and after MN insertions (Figure S3A, SI) at the individual abdominal skin locations (location A-H, Figure 3B, SI), thus indicating that the MNs penetrated the skin.

### 3.5.2 Retrieval of Ara h 2 after delivery

Delivery of Ara h 2 was also evaluated using an ELISA kit on homogenized skin samples. Ara h 2 could be quantified for one i.d. injection (Figure 11A) and approx. 40 ng corresponding to 0.2% of the initially delivered Ara h 2 could be rediscovered in the skin sample injected with 18.75 μg Ara h 2. This amount was found to be statistically significantly (Kruskal-Wallis test with Dunn's multiple comparisons test)

higher than the amount of Ara h 2 recovered in the PBS and 0.75 µg i.d. injected Ara h 2 skin samples, thus showing that the delivered Ara h 2 could only be recovered if high amounts of Ara h 2 was initially delivered. This indicates that Ara h 2 is either degraded in the skin, taken up by cells or transported away from site of injection. For skin samples with MN insertion, it was not possible to quantify an amount of Ara h 2 in the homogenate (Figure 11B).

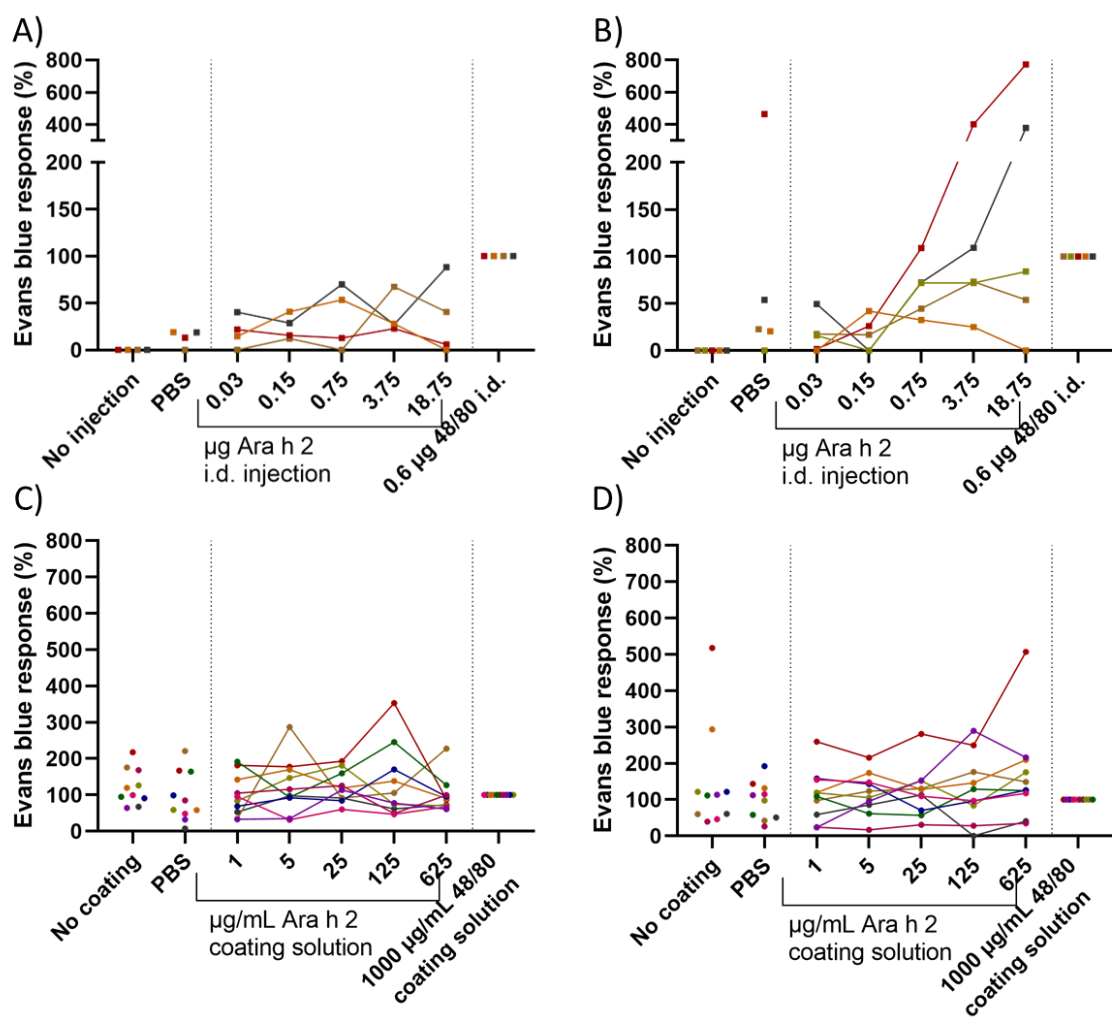


**Figure 11: Retrieval of Ara h 2 in homogenized skin samples after intradermal injection and microneedle insertion.** A) Recovered Ara h 2 in skin samples from rats receiving intradermal injection (mean  $\pm$  SD,  $n=4$ ). B) Recovered Ara h 2 in skin samples from rats receiving microneedle insertion (mean  $\pm$  SD,  $n\geq 4$ ). For all statistical analyses the statistically significant differences are marked as \* =  $p \leq 0.05$ .

### 3.5.3 Evans blue analysis for detection of an allergic response in sensitized Brown Norway rats

To detect an allergic response after i.d. injection or MN delivery of Ara h 2 in the skin, skin coloration by Evans blue was investigated in sensitized and non-sensitized (control) rats. The AUC data (raw data, Figure S4A-D, SI) was analyzed using normalization to the positive control 48/80 (Figure 12A-D) as it was assumed that 48/80 caused max degranulation of mast cells. Only rats for which the positive control was clearly visible were included in the analysis; hence the number of rats vary between the groups in Figure 12.

Rats receiving i.d. injections exhibited in general a low response to PBS and a high response to 48/80 as was expected for both control (Figure 12A) and sensitized rats (Figure 12B), and only sensitized rats reacted to the Ara h 2 with a clear response. For rats receiving MN insertion, no difference in reaction could be observed between the Ara h 2 delivery and PBS in both control (Figure 12C) and sensitized rats (Figure 12D).



**Figure 12: Dose-response curves for intradermal injection and microneedle insertion of Ara h 2 in Brown Norway rats.** A-D) Dose-response curves for Evans blue responses (%) relative to Evans blue response for the positive control (48/80) which in theory represents maximum mast cell degranulation. A) Intradermal (i.d.) injection in naïve control rats (n=4). B) I.d. injection in sensitized rats (n=5). C) Microneedle (MN) insertion in naïve control rats (n=10). D) MN insertion in sensitized rats (n=10).

## 4. Discussion

A correct and precise diagnosis of allergy is important in order for the patient to know the potential severity of the allergy and which precautions should be taken. In this study, coated MNs were investigated with the aim of delivering allergens into the skin to elicit a local allergic response. In the long-term perspective this study is part of developing a new diagnostic method using MNs where an allergen is delivered directly into the skin while measuring *in situ* a local allergic response. Ideally, it will be possible to coat with a different allergen on each MN to test several allergens in a smaller space than the SPT.

First, MNs were coated using dip-coating with a fluorescent-labeled molecule in the coating solution. The delivery of the molecule was evaluated by measuring the remaining, fluorescent-labeled coating on the MNs after insertion and compared to the fluorescent-labeled coating from MNs which were not inserted. It was observed that the coating method, insertion time, and the coating molecule for delivery had an impact on the outcome. The delivery estimations were accompanied by large standard deviations, and it is therefore difficult to say something conclusive regarding the delivered amount.

Studies on delivery using coated MNs generally report varying results. Gill *et al.* developed an optimized method for coating of MNs devoid of coating on the base. They showed a delivery efficiency of 91.4% for Vitamin B after 5 min insertion and their estimation was based on measuring the remaining, fluorescent-labeled coating on the MNs plus the excess amount deposited on top of the skin. Based on these measurements they assumed that the missing amount was delivered in the skin when comparing to MNs which had not been inserted into the skin [44]. We hypothesize that the large standard deviations associated with the delivery estimates in our study could be reduced if the coating was constrained to the MNs only, instead of also covering the base. This would allow for an easier quantification of the amount of released coating solely from the MNs, as the noise from the base coating would be omitted. Shakya *et al.* coated MNs with peanut extract and reported a delivery efficiency of 72.3% by measuring the remaining fluorescence on the MNs and the fluorescence found on top of the skin after insertion [35], just as was done by Gill *et al.* [44]. Landers *et al.* also coated MNs with peanut extract and obtained a delivery efficiency of 65.1% [36] using the same quantification method as Shakya *et al.* [35]. Several studies have investigated MN delivery for different molecules such as Jenkins *et al.* who showed a delivery of just 8% for vaccine delivery for 5 min insertion time [45], while Chen *et al.* estimated a delivery of 90% for sulforhodamine B after 2 min insertion [46], and Kochhar *et al.* reported a delivery of 30% for Rhodamine B after 1 h of insertion [47]. This demonstrates that various parameters such as mode of coating, insertion time, and coating molecules affect the delivery efficacy and hence making a direct comparison between studies difficult. In our study the estimated delivery at 60 s insertion varied greatly depending on whether the molecule was FITC-dextran (49%), FITC-BSA (15%), Rhodamine B-conjugated Ara h 2 (41%) or Rhodamine B-dextran (11%). In short, the coating solution and quantitative measurement methods appeared to have an impact on the estimated delivery.

Rhodamine B-dextran-coated MNs were inserted into pig neck and human breast skin samples which were cut for histology to visualize the delivery in the skin. Here it was clear that Rhodamine B-dextran coating had been delivered into the skin and not only scraped off on the surface.

Having confirmed delivery of Rhodamine B-dextran coating using cryostat histology the allergen of interest, Ara h 2, was conjugated with Rhodamine B and coated onto MNs for delivery. Rhodamine B-conjugated Ara h 2 was not able to be re-found in homogenized skin samples after delivery with the MNs, which is probably due to the delivered amount being below limit of detection of the plate reader. As an alternative to measuring Rhodamine B fluorescence, Ara h 2 in homogenized skin samples was measured using an ELISA kit on i.d. injection and MN delivery samples. It was only possible to re-find Ara h 2 for the highest i.d. injected concentration (625 µg/mL corresponding to 18.75 µg Ara h 2) while none of the MNs gave a measurable Ara h 2 signal indicating that the delivered amount was below the limit of detection for the kit (2.0 ng/mL). Likely, the injected Ara h 2 was either degraded within the skin, taken up by cells

or transported away from the area before the biopsy was taken, as only 0.2% of the initially delivered Ara h 2 could be recovered.

To measure if the amount of delivered Ara h 2 allergen from the MNs was enough to elicit a local allergic response, *in vivo* animal experiments were conducted using PPE-sensitized BN rats. The rats were found to have developed an immunological response by means of specific IgG<sub>1</sub> and IgE towards both PPE as a whole and towards Ara h 2 upon i.p. immunization. Yet, only a statistically significant clinical response was shown for PPE in contrast to Ara h 2 in the EST.

The Evans blue response in i.d. injected rats generally gave a low PBS response and a higher 48/80 response as expected and only PPE-sensitized rats had a visible reaction against Ara h 2. Using i.d. injections as controls for MN coating delivery in rats showed that not enough allergen coating was released from the MNs to either elicit an allergic response or to elicit an allergic response that could be observed using Evans blue. However, using the i.d. injections as controls turned out to be less optimal than anticipated since not all sensitized rats appeared to develop a visual Evans blue response. The general outcome of MNs coated with either 48/80 or Ara h 2 was that no significant measurable reaction could be observed.

In hindsight, PPE-coated MNs should have been included in the experiment since PPE gave a statistically significant clinical response whereas Ara h 2 did not. The PPE consists of several allergens, and it is possible that the main allergen causing an allergic reaction in the rats was not Ara h 2, but one or multiple of the other allergens present in PPE [13], [14] as Ara h 2 only makes up approx. 10% of the PPE [48]. Ideally, different peanut allergens should have been purified, coated on MNs, and tested using i.d. injections and MNs to maximize the chance of a measurable outcome.

The injection of Evans blue into the tail vein proved difficult and required practice. The positive control was therefore not visible for all rats. As a criterium, the positive control on the rat should always be visible to the naked eye, and this was not always the case which is why not all rats could be included in the analysis. This also meant that for some of the analyses only few rats were available which made it even more difficult to reach a conclusion.

For analysis of the Evans blue data several strategies were investigated. As Evans blue is a visualization of coloring of the skin due to blood accumulation, which indirectly points to an allergic response, the analysis tool selected was image analysis. Using ImageJ, the Evans blue area (corresponding to flare (redness) area in the SPT) and the gray value (color saturation) were measured. The AUC measurements were an attempt to combine the Evans blue area and color saturation parameters into a single response parameter. Other previous studies have tried to establish a valid method for Evans blue analysis beyond the visual inspection. Evans blue can be measured and quantified using a spectrophotometer [49], [50], which is done by extracting the Evans blue into formamide and measuring the absorbance at 620 nm using a spectrophotometer. This could be an alternative way for future analysis to try and quantify the allergic response and have it complementary to the AUC measurements as done in our study. Naturally, the fluorescent quantification of the Evans blue dye in this manner would need some optimization to determine the limit of detection and ensure that the skin samples do not auto-fluoresce at this wavelength. Alternatively, other biomarkers could be measured in homogenized samples to confirm an



allergic response such as e.g., tryptase [51],  $\beta$ -hexosaminidase [52] or other molecules that are associated with an allergic reaction and can be measured in a homogenized skin sample.

In regard to the use of MNs to deliver an allergen and elicit an allergic response, only limited prior work exists. Ito *et al.* used dissolvable MNs in rats to deliver the allergen poly-L-arginine. The delivery was confirmed by observing increased scratching from the rats at the site of delivery [33]. Trautmann *et al.* fabricated silicon MNs and tested these in a SPT setting as an alternative to the SPT needle. Using the positive control of histamine normally used for SPT they confirmed delivery when pricking the droplet into the forearm of a volunteer using MNs [34]. In both cases enough allergen was delivered to elicit a response. In the case of Ito *et al.* 300 MNs containing the allergen were used and dissolved within the skin thereby ensuring full delivery [33] while Trautmann *et al.* used a droplet of allergen and thus did not rely on coating delivery [34]. It is possible in our case that an increase in number of MNs or using dissolvable MNs would have increased the delivered allergen dose and resulted in a measurable allergic response.

Assuming that the allergen delivery using coated MNs is sufficient to elicit an allergic response, but insufficient to elicit a measurable response using Evans blue, an alternative measurement method can be used. We envision that the allergic response will be measured quantitatively using MNs with a pyrolytic carbon surface for electrochemical measurements [53], which may prove to be a more sensitive method than Evans blue.

## 5. Conclusions

A dip-coating method was developed for coating MNs with fluorescent-labeled molecules and Ara h 2 allergen for i.d. delivery. Quantifying the delivered coating was attempted by measuring remaining, fluorescent-labeled coating on MNs after insertion into skin, but it was found that the delivered amount was difficult to estimate accurately, probably due to the large background fluorescence from the coating on the base. However, delivery of coating into the skin was confirmed using fluorescence microscopy imaging of cryostat histology, though the delivered amount could not be quantified with this method. It was furthermore observed that the delivery molecule had an impact on the coating solution, and this should therefore be optimized for each individual allergen or molecule to be delivered.

Using Evans blue as a visualization method for quantification of the allergic reaction worked to some degree for the rats receiving i.d. injections, however, no response could be observed for the delivery from MNs. This is likely due to an insufficient delivery of the allergen or positive control. For a future study, PPE-coated MNs should be included alongside Ara h 2 as it appeared that PPE gave a clinically active response in the rats based on the EST results whereas Ara h 2 did not. In general, the quantification method using Evans blue for MN insertion should be further optimized. Nonetheless, this work lays the foundation for the development of a new diagnostic tool for allergies.

## 6. Acknowledgements

The authors would like to thank senior researcher Jeppe Madura Larsen for help with the procedure for performing homogenization of the skin samples using liquid nitrogen. The authors would also like to thank Kresten Hermansen for preparing the peanut protein extract and for purifying Ara h 2. Also, thanks to Ahmad Moukachar for helping with the fluorescence microscopy and ImageJ and Benedetta Gualeni for help with pig and human skin preparations. Thank you to the DTU Animal Facility (BioFacility) for help with the experiments and taking care of the rats. A special thank you to Maja Danielsen for helping with the ear swelling test.

## 7. Conflict of interest

The authors declare no conflict of interest.

## 8. Data availability statement

All data is available upon reasonable request.

## 9. Author contributions

**Stephanie Ingemann Bisgaard:** Methodology, formal analysis, writing – original draft, investigation, visualization. **Long Quang Nguyen:** Resources, investigation. **Ana Isabel Sancho:** Resources. **Sarah Grundt Simonsen:** Investigation. **Gerardo García Zavaleta:** Resources. **Mohammad Ramezannezhad:** Resources. **Emma Baczkowski:** Supervision. **James Birchall:** Resources, supervision. **Stephan Sylvest Keller:** Supervision, funding acquisition, writing – review & editing, project administration. **Katrine Lindholm Bøgh:** Supervision, conceptualization, methodology, resources, writing – review & editing.

## 10. Funding

Funding from the Independent Research Fund Denmark (grant no. 8022-00215B), and the LEO Foundation (grant no. LF17046).

Purification of Ara h 2 was obtained through accessing research infrastructure at National Food Institute, Technical University of Denmark funded by FOODHAY (Food and Health Open Innovation Laboratory, Danish Roadmap for Research Infrastructure).

## 11. Keywords

Brown Norway rats, microneedle, coating, allergy diagnostics, Ara h 2, ear swelling test.

## 12. References

[1] W. Yu, D. M. H. Freeland, and K. C. Nadeau, "Food allergy: Immune mechanisms, diagnosis and

- immunotherapy," *Nat. Rev. Immunol.*, vol. 16, no. 12, pp. 751–765, 2016.
- [2] P. L. Amlot, D. M. Kemeny, C. Zachary, P. Parkes, and M. H. Lessof, "Oral allergy syndrome (OAS): symptoms of IgE-mediated hypersensitivity to foods," *Clin. Exp. Allergy*, vol. 17, no. 1, pp. 33–42, 1987.
- [3] D. Yue, A. Ciccolini, E. Avilla, and S. Wasserman, "Food allergy and anaphylaxis," *J. Asthma Allergy*, vol. 11, pp. 111–120, 2018.
- [4] "U.S. FOOD & DRUG ADMINISTRATION: Food Allergies," *January*, 2023. [Online]. Available: <https://www.fda.gov/food/food-labeling-nutrition/food-allergies>.
- [5] P. Chatchatee, K. M. Järvinen, L. Bardina, K. Beyer, and H. A. Sampson, "Identification of IgE- and IgG-binding epitopes on  $\alpha$ s1-casein: Differences patients with persistent and transient cow's milk allergy," *J. Allergy Clin. Immunol.*, vol. 107, no. 2, pp. 379–383, 2001.
- [6] J. H. Savage, E. C. Matsui, J. M. Skripak, and R. A. Wood, "The Natural History of Egg Allergy," *Pediatrics*, vol. 120, no. 6, pp. 186–187, 2007.
- [7] R. S. Gupta, C. H. Lau, R. G. Hamilton, A. Donnell, and K. K. Newhall, "Predicting Outcomes of Oral Food Challenges by Using the Allergen-Specific IgE-Total IgE Ratio," *J. Allergy Clin. Immunol. Pract.*, vol. 2, no. 3, pp. 300–305, 2014.
- [8] J. A. Lieberman *et al.*, "The global burden of illness of peanut allergy: A comprehensive literature review," *Allergy Eur. J. Allergy Clin. Immunol.*, vol. 76, no. 5, pp. 1367–1384, 2021.
- [9] M. H. K. Ho, W. H. S. Wong, R. G. Heine, C. S. Hosking, D. J. Hill, and K. J. Allen, "Early clinical predictors of remission of peanut allergy in children," *J. Allergy Clin. Immunol.*, vol. 121, no. 3, pp. 731–736, 2008.
- [10] H. S. Skolnick, M. K. Conover-Walker, C. B. Koerner, H. A. Sampson, W. Burks, and R. A. Wood, "The natural history of peanut allergy," *J. Allergy Clin. Immunol.*, vol. 107, no. 2, pp. 367–374, 2001.
- [11] S. A. Bock and F. M. Atkins, "The natural history of peanut allergy," *J. Allergy Clin. Immunol.*, vol. 83, no. 5, pp. 900–904, 1989.
- [12] "WHO/IUIS Allergen Nomenclature Sub-Committee (peanut)." [Online]. Available: <http://allergen.org/search.php?allergen=peanut&search=Search>.
- [13] A. K. Kukkonen, A. S. Pelkonen, S. Mäkinen-Kiljunen, H. Voutilainen, and M. J. Mäkelä, "Ara h 2 and Ara 6 are the best predictors of severe peanut allergy: A double-blind placebo-controlled study," *Allergy Eur. J. Allergy Clin. Immunol.*, vol. 70, no. 10, pp. 1239–1245, 2015.
- [14] S. J. Koppelman, M. Wensing, M. Ertmann, A. C. Knulst, and E. F. Knol, "Relevance of Ara h1, Ara h2 and Ara h3 in peanut-allergic patients, as determined by immunoglobulin E Western blotting, basophil-histamine release and intracutaneous testing: Ara h2 is the most important peanut allergen," *Clin. Exp. Allergy*, vol. 34, no. 4, pp. 583–590, 2004.
- [15] J. A. Boyce *et al.*, *Guidelines for the diagnosis and management of food allergy in the United States: Report of the NIAID-sponsored expert panel*, vol. 126, no. 6 SUPPL. Elsevier Ltd, 2010.
- [16] J. A. Lieberman and S. H. Sicherer, "Diagnosis of food allergy: Epicutaneous skin tests, in vitro tests, and oral food challenge," *Curr. Allergy Asthma Rep.*, vol. 11, no. 1, pp. 58–64, 2011.

- [17] C. D. May, "Objective clinical and laboratory studies of immediate hypersensitivity reactions to foods in asthmatic children," *J. Allergy Clin. Immunol.*, vol. 58, no. 4, pp. 500–515, 1976.
- [18] H. A. Sampson *et al.*, "Standardizing double-blind, placebo-controlled oral food challenges: American Academy of Allergy, Asthma & Immunology-European Academy of Allergy and Clinical Immunology PRACTALL consensus report," *J. Allergy Clin. Immunol.*, vol. 130, no. 6, pp. 1260–1274, 2012.
- [19] T. D. Dang *et al.*, "Increasing the accuracy of peanut allergy diagnosis by using Ara h 2," *J. Allergy Clin. Immunol.*, vol. 129, no. 4, pp. 1056–1063, 2012.
- [20] R. Asero, L. Jimeno, and D. Barber, "Component-resolved diagnosis of plant food allergy by SPT," *Eur. Ann. Allergy Clin. Immunol.*, vol. 40, no. 4, pp. 115–121, 2008.
- [21] N. Suratannon, J. Ngamphaiboon, J. Wongpiyabovorn, P. Puripokai, and P. Chatchatee, "Component-resolved diagnostics for the evaluation of peanut allergy in a low-prevalence area," *Pediatr. Allergy Immunol.*, vol. 24, no. 7, pp. 665–670, 2013.
- [22] A. F. Santos *et al.*, "Basophil activation test discriminates between allergy and tolerance in peanut-sensitized children," *J. Allergy Clin. Immunol.*, vol. 134, no. 3, pp. 645–652, 2014.
- [23] L. Heinzerling *et al.*, "The skin prick test - European standards," *Clin. Transl. Allergy*, vol. 3, no. 1, pp. 1–10, 2013.
- [24] J. Cannon and P. Cullinan, "Skin prick testing," *Occup. Med. (Chic. Ill.)*, vol. 69, no. 4, pp. 298–299, 2019.
- [25] R. Asero *et al.*, "IgE-mediated food allergy diagnosis: Current status and new perspectives," *Mol. Nutr. Food Res.*, vol. 51, no. 1, pp. 135–147, 2007.
- [26] F. Rancé, A. Juchet, F. Brémont, and G. Dutau, "Correlations between skin prick tests using commercial extracts and fresh foods, specific IgE, and food challenges," *Allergy Eur. J. Allergy Clin. Immunol.*, vol. 52, no. 10, pp. 1031–1035, 1997.
- [27] E. Jensen-Jarolim *et al.*, "Allergen mimotopes in food enhance type I allergic reactions in mice," *FASEB J.*, vol. 13, no. 12, pp. 1586–1592, 1999.
- [28] I. Schöll *et al.*, "Allergen-loaded biodegradable poly(D,L-lactic-co-glycolic) acid nanoparticles down-regulate an ongoing Th2 response in the BALB/c mouse model," *Clin. Exp. Allergy*, vol. 34, no. 2, pp. 315–321, 2004.
- [29] U. Baranyi *et al.*, "Tolerization of a Type I Allergic Immune Response through Transplantation of Genetically Modified Hematopoietic Stem Cells," *J. Immunol.*, vol. 180, no. 12, pp. 8168–8175, 2008.
- [30] K. L. Bøgh, V. Barkholt, and C. B. Madsen, "Characterization of the Immunogenicity and Allergenicity of Two Cow's Milk Hydrolysates - A Study in Brown Norway Rats," *Scand. J. Immunol.*, vol. 81, no. 5, pp. 274–283, 2015.
- [31] Z. Ovary, "Immediate Reactions in the Skin of Experimental Animal Provoked by Antibody-Antigen Interaction," *Progr. Allergy*, vol. 5, pp. 459–508, 1958.
- [32] M. W. Chase, "Studies on the Sensitization of Animals With Simple Chemical Compounds: X. Antibodies inducing immediate-type skin reactions," *J. Exp. Med.*, vol. 86, no. 6, pp. 489–514,

1947.

- [33] Y. Ito *et al.*, "Dissolving microneedles as skin allergy test device," *Biol. Pharm. Bull.*, vol. 40, no. 4, pp. 531–534, 2017.
- [34] A. Trautmann, F. Heuck, R. Denfeld, P. Ruther, and O. Paul, "Detachable Silicon Microneedle Stamps For Allergy Skin Prick Testing," *19th IEEE Int. Conf. Micro Electro Mech. Syst.*, pp. 434–4237, 2006.
- [35] A. K. Shakya *et al.*, "Microneedles coated with peanut allergen enable desensitization of peanut sensitized mice," *J. Control. Release*, vol. 314, no. October, pp. 38–47, 2019.
- [36] J. J. Landers *et al.*, "Targeted allergen-specific immunotherapy within the skin improves allergen delivery to induce desensitization to peanut," *Immunotherapy*, 2022.
- [37] S. I. Bisgaard, L. Q. Nguyen, K. L. Bøgh, and S. S. Keller, "Dermal Tissue Penetration of In-plane Silicon Microneedles Evaluated in Skin-simulating Hydrogel, Rat Skin, and Porcine Skin," 2023.
- [38] S. Kroghsbo, K. L. Bøgh, N. M. Rigby, E. N. C. Mills, A. Rogers, and C. B. Madsen, "Sensitization with 7S globulins from peanut, hazelnut, soy or pea induces ige with different biological activities which are modified by soy tolerance," *Int. Arch. Allergy Immunol.*, vol. 155, no. 3, pp. 212–224, 2011.
- [39] K. L. Bøgh *et al.*, "Digested Ara h 1 has sensitizing capacity in Brown Norway rats Clinical & Experimental Allergy," pp. 1611–1621, 2009.
- [40] M. A., "Comparison of Evans Blue Injection Routes," *J. Neurosci. Methods*, vol. 195, no. 2, pp. 206–210, 2011.
- [41] A. V. Locke, J. M. Larsen, K. B. Graversen, T. R. Licht, M. I. Bahl, and K. L. Bøgh, "Amoxicillin does not affect the development of cow's milk allergy in a Brown Norway rat model," *Scand. J. Immunol.*, vol. 95, no. 5, pp. 1–13, 2022.
- [42] A. U. Alam, M. M. R. Howlader, and M. J. Deen, "Oxygen Plasma and Humidity Dependent Surface Analysis of Silicon, Silicon Dioxide and Glass for Direct Wafer Bonding," *ECS J. Solid State Sci. Technol.*, vol. 2, no. 12, pp. P515–P523, 2013.
- [43] R. Na, I. M. Stender, L. Ma, and H. C. Wulf, "Autofluorescence spectrum of skin: Component bands and body site variations," *Ski. Res. Technol.*, vol. 6, no. 3, pp. 112–117, 2000.
- [44] H. S. Gill and M. R. Prausnitz, "Coated microneedles for transdermal delivery," *J. Control. Release*, vol. 117, no. 2, pp. 227–237, 2007.
- [45] D. Jenkins, S. Corrie, C. Flaim, and M. Kendall, "High density and high aspect ratio solid micro-nanoprojection arrays for targeted skin vaccine delivery and specific antibody extraction," *RSC Adv.*, vol. 2, no. 8, pp. 3490–3495, 2012.
- [46] Y. Chen, B. Z. Chen, Q. L. Wang, X. Jin, and X. D. Guo, "Fabrication of coated polymer microneedles for transdermal drug delivery," *J. Control. Release*, vol. 265, no. March, pp. 14–21, 2017.
- [47] J. S. Kochhar, W. J. Goh, S. Y. Chan, and L. Kang, "A simple method of microneedle array fabrication for transdermal drug delivery," *Drug Dev. Ind. Pharm.*, vol. 39, no. 2, pp. 299–309, 2013.

- [48] T. K. S. Sztuk *et al.*, "Dose and route of administration determine the efficacy of prophylactic immunotherapy for peanut allergy in a Brown Norway rat model," *Front. Immunol.*, vol. 14, no. February, pp. 1–13, 2023.
- [49] H. Evans, K. E. Killoran, and E. Mitre, "Measuring local anaphylaxis in mice," *J. Vis. Exp.*, no. 92, pp. 1–6, 2014.
- [50] H. L. Wang and T. W. Lai, "Optimization of Evans blue quantitation in limited rat tissue samples," *Sci. Rep.*, vol. 4, pp. 1–7, 2014.
- [51] D. D. Metcalfe *et al.*, "Biomarkers of the involvement of mast cells, basophils and eosinophils in asthma and allergic diseases," *World Allergy Organ. J.*, vol. 9, no. 1, pp. 1–15, 2016.
- [52] S. Wernersson and G. Pejler, "Mast cell secretory granules : armed for battle," vol. 14, no. JULY, 2014.
- [53] S. E. Tehrani, "3D Pyrolytic Carbon for Monitoring Type I Allergic Reactions," Technical University of Denmark (DTU), 2022.

## 12. List of abbreviations

| Abbreviation        | Meaning  |
|---------------------|--|
| AUC                 | Area under the curve   |
| BAT                 | Basophil activation test   |
| BN                  | Brown Norway   |
| CMC                 | Carboxymethyl cellulose  |
| CRD                 | Component-resolved diagnosis   |
| DI water            | De-ionized water   |
| DIG                 | Digoxigenin  |
| EDTA                | Ethylenediaminetetraacetic acid solution                             |
| EGTA                | Ethylene glycol-bis(2-amino-ethylether)-N,N,N',N',-tetra acetic acid |
| ELISA               | enzyme-linked immunosorbent assay                                    |
| EST                 | Ear swelling test  |
| FITC-BSA            | Albumin-fluorescein isothiocyanate conjugate                         |
| FITC-dextran        | Fluorescein isothiocyanate-dextran                                   |
| HRP                 | Horseradish peroxidase   |
| i.d.                | Intradermal  |
| i.p.                | Intraperitoneal  |
| MN                  | Microneedle  |
| MWCO                | MW cut off   |
| OCT                 | Optimal cutting temperature  |
| OD                  | Optical density  |
| PBS                 | Phosphate buffered saline  |
| PBS-T               | Phosphate buffered saline with 0.01% Tween-20                        |
| PPE                 | Peanut protein extract   |
| RGB                 | Red, green, and blue   |
| Rhodamine B-dextran | Rhodamine B isothiocyanate-Dextran                                   |
| RT                  | Room temperature   |
| SD                  | Standard deviation   |
| SMP                 | Skimmed milk powder  |
| SPT                 | Skin prick test  |
| TA                  | Texture analyser   |
| TEWL                | Trans-epidermal water loss   |
| TMB-one             | 3,3',5,5'-tetramethylbenzidine                                       |
| w/v                 | Weight per volume  |
| 48/80               | Compound 48/80   |

## Peanut allergen Ara h 2 delivery for test of allergic response with in-plane Si microneedles – Supporting information

Stephanie Ingemann Bisgaard<sup>a,b</sup>, Long Quang Nguyen<sup>a</sup>, Ana Isabel Sancho<sup>b</sup>, Sarah Grundt Simonsen<sup>b</sup>, Gerardo García Zavaleta<sup>a</sup>, Mohammad Ramezannezhad<sup>a</sup>, Emma Baczkowski<sup>c</sup>, James Birchall<sup>c</sup>, Stephan Sylvest Keller<sup>a</sup>, Katrine Lindholm Bøgh<sup>b,\*</sup>

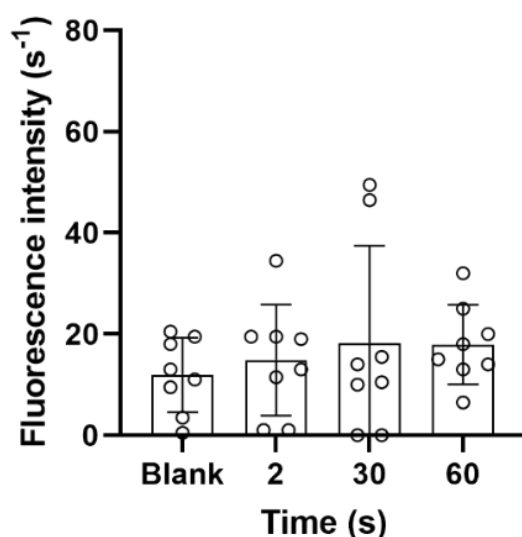
<sup>a</sup> National Centre for Nano Fabrication and Characterization, Technical University of Denmark, Ørsteds Plads, Building 347 East, 2800 Kgs. Lyngby, Denmark.

<sup>b</sup> National Food Institute, Technical University of Denmark, Kemitovet, Building 202, 2800 Kgs. Lyngby, Denmark.

<sup>c</sup> Welsh School of Pharmacy and Pharmaceutical Sciences, Cardiff University, Redwood Building, King Edward VII Ave, Cardiff CF10 3NB, Great Britain.

\* E-mail of corresponding author: [kalb@food.dtu.dk](mailto:kalb@food.dtu.dk)

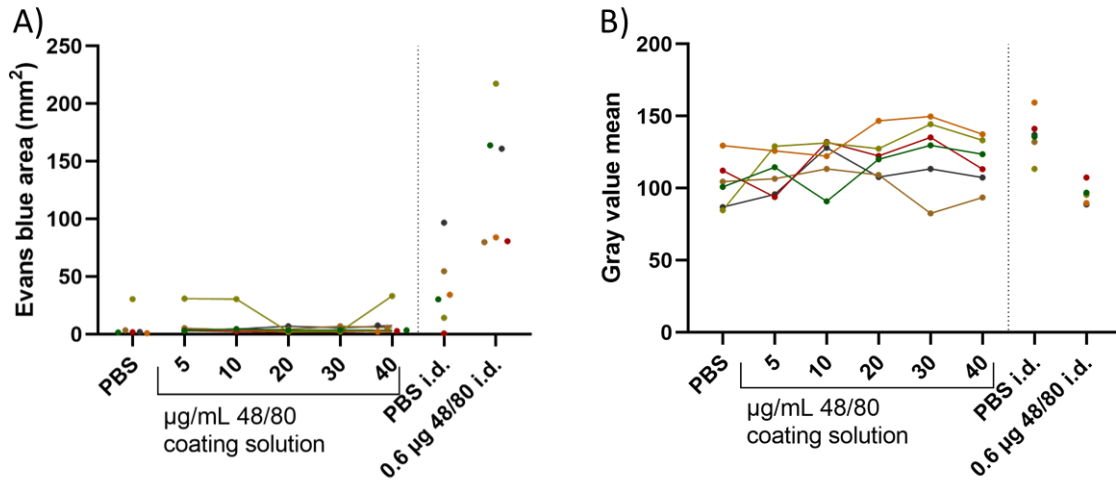
### S1 Coating delivery



**Figure S1: Rhodamine B-conjugated Ara h 2 delivered in Brown Norway rat abdominal skin samples.** Fluorescence of homogenized skin samples after Rhodamine B-conjugated Ara h 2 release from microneedles (mean  $\pm$  SD, n=8).

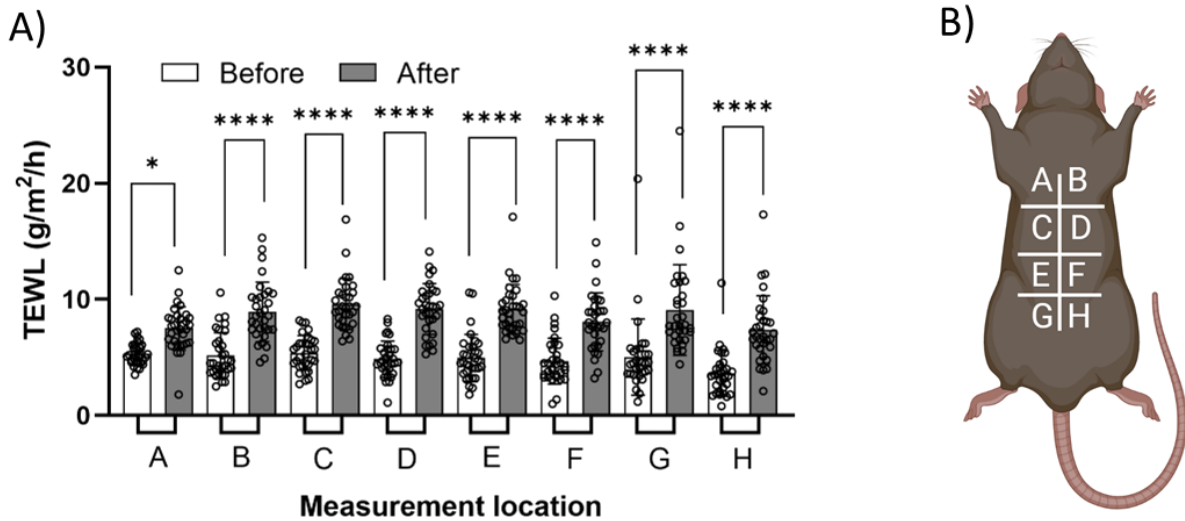


## S2 Positive control coating delivery in Brown Norway rats



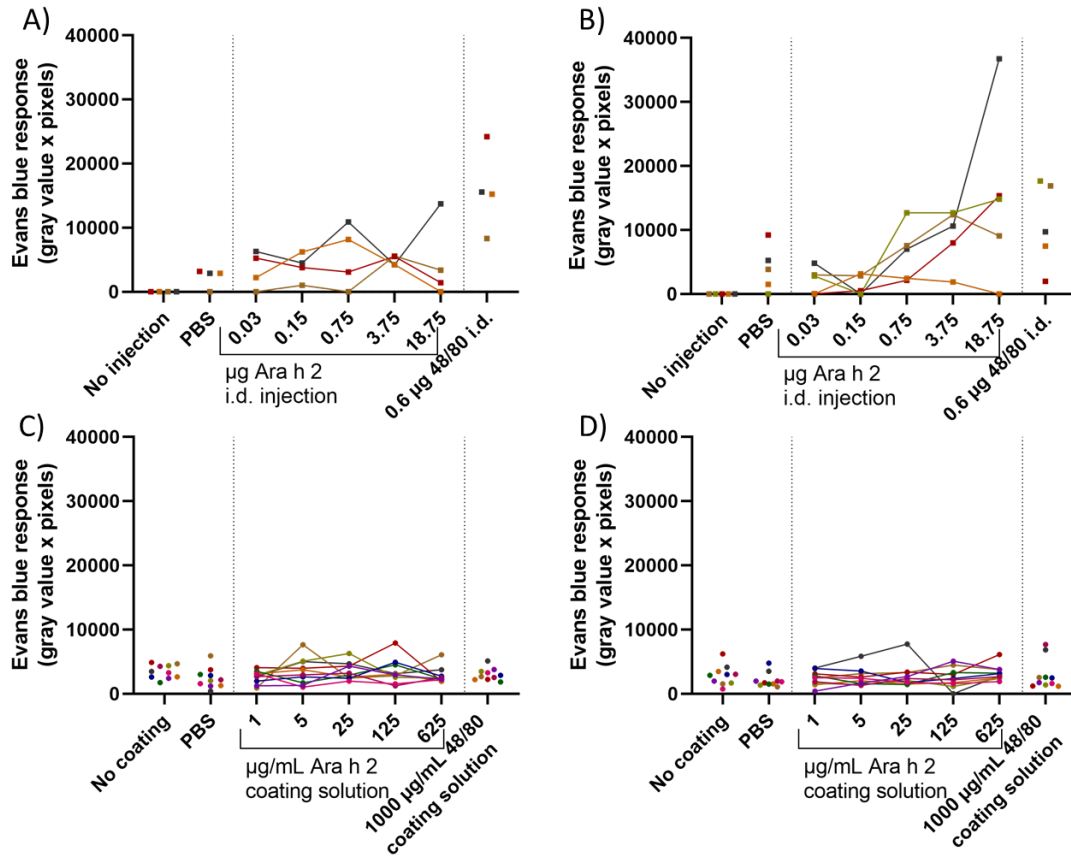
**Figure S2: Dose-response curves for analysis methods of Evans blue.** A) Dose-response curves for Evans blue area in naive rats (n=6). B) Dose-response curves for gray value mean (color saturation) in naive rats (n=6). The lower the value the darker the coloring and the higher the value the lighter the coloring, i.e., more intense Evans blue coloration will be represented by a lower gray value.

## S3 Trans-epidermal water loss



**Figure S3: Confirming microneedle penetration of skin.** A) Trans-epidermal water loss (TEWL) was measured for 20 s before and after microneedle insertion (60 s) at locations A-H (mean  $\pm$  SD, n=48). B) Schematic illustrating the TEWL measurement locations A-H. For all statistical analyses the statistically significant differences are marked as \* =  $p \leq 0.05$ , \*\*\*\* =  $p \leq 0.0001$ . Created with BioRender.com.

## S4 Ara h 2 delivery in Brown Norway rats



**Figure S4: Dose-response curves of Evans blue response.** A-D) Evans blue response calculated using area under the curve (gray value x pixels) analysis. A) Intradermal (i.d.) injection in naïve rats (n=4), B) i.d. injection in sensitized rats (n=5), C) microneedle (MN) insertion in naïve rats (n=10) and D) MN insertion in sensitized rats (n=10). Based on raw AUC data the MNs did not appear to cause more damage than the i.d. injection as the Evans blue response was within the same range.

## **Appendix D: Study report II**

### **Study report II**

Birch Pollen Extract and Bet v 1 Allergen Delivery with In-plane Silicon Microneedles for Test of Allergic Response. Stephanie Ingemann Bisgaard, Long Quang Nguyen, Sarah Grundt Simonsen, Gerardo García Zavaleta, Mohammad Ramezannezhad, Stephan Sylvest Keller, Katrine Lindholm Bøgh.

# Birch Pollen Extract and Bet v 1 Allergen Delivery with In-plane Silicon Microneedles for Test of Allergic Response

Stephanie Ingemann Bisgaard<sup>a,b</sup>, Long Quang Nguyen<sup>a</sup>, Sarah Grundt Simonsen<sup>b</sup>, Gerardo García Zavaleta<sup>a</sup>, Mohammad Ramezannezhad<sup>a</sup>, Stephan Sylvest Keller<sup>a</sup>, Katrine Lindholm Bøgh<sup>b,\*</sup>

<sup>a</sup> National Centre for Nano Fabrication and Characterization, Technical University of Denmark, Ørsted Plads, Building 347 East, 2800 Kgs. Lyngby, Denmark.

<sup>b</sup> National Food Institute, Technical University of Denmark, Kemitorget, Building 202, 2800 Kgs. Lyngby, Denmark.

\* E-mail of corresponding author: [kalb@food.dtu.dk](mailto:kalb@food.dtu.dk)

## Abstract

The skin prick test (SPT) is used in the clinic to screen for allergies but has the disadvantage of being a qualitative rather than quantitative estimation. The objective of this study was to deliver birch pollen extract (BPE) and the birch pollen allergen Bet v 1 into the skin using coated microneedles (MNs) to elicit a local allergic response as a first step to improving the SPT method. MNs were dip-coated in coating solution containing various concentrations of either BPE or Bet v 1 as well as compound 48/80 as a positive control and phosphate buffered saline (PBS) as a negative control. Evans blue was injected intravenously into the tail vein for visualization of blood accumulation indicating a local allergic response. Coated MNs were tested *in vivo* in either naïve or BPE-sensitized Brown Norway rats. Sensitization to BPE and Bet v 1 was confirmed by IgE ELISAs and the clinical response confirmed by an ear swelling test. For one group of rats, the coated MNs were inserted in the abdominal skin for 60 s after sedation, whereas another group of rats were given intradermal (i.d.) injections of the same allergens, as well as the positive control 48/80 and negative control PBS. The rats were sacrificed, and the abdominal skin was excised and fixed to its original size with the dermis layer facing upwards. The skin samples were photographed for subsequent Evans blue analysis. Based on the Evans blue analysis, clear dose-response curves were observed for sensitized rats receiving i.d. injections. However, sensitized rats receiving MN insertion did not provide a reaction against BPE or Bet v 1 that was significantly different from the reaction of the naïve control rats. As no difference in response could be detected using Evans blue for delivery of BPE or Bet v 1 using coated MNs it was concluded that the delivered amount of allergen was either too low to elicit an allergic response or the allergic response was too small to be measured with Evans blue.

## 1. Introduction

Birch trees are predominantly found in Northern and Central Europe [1] and due to climate changes the level of birch pollen has increased and the birch pollen season has been extended [2]. Birch pollen can cause allergic rhinitis and sometimes asthma symptoms [3] and with cross-reactivity to food allergens the severity of birch pollen allergy increases [4]. Eight allergens from birch pollen are recognized by the International Allergen Nomenclature Sub-committee [5] with Bet v 1 as the main allergen [6], [7].

Diagnostic tools include examination of the clinical history and radioallergosorbent test (RAST) [8] where allergen specific IgE antibodies are detected using a secondary radiolabeled antibody [9]. Additional tests such as histamine release test and inhalation provocation test [10] also exist. For screening of birch pollen allergy, the skin prick test (SPT) is an established method. It is performed by placing a droplet of allergen on the skin of the forearm and the allergen is then pricked into the skin using a SPT needle. After 15-20 min a visual response in the form of a wheal and flare will appear and this is then evaluated by a health care professional [11]. A blood test for birch pollen specific IgE is also an option and it is often more reliable than the SPT [12], [13].

For visualization of allergic reactions in animal experiments intravenous injection of Evans blue has been utilized [14]–[17]. This method is well-established and has been used for a long time for visualization of blood accumulations [18], [19].

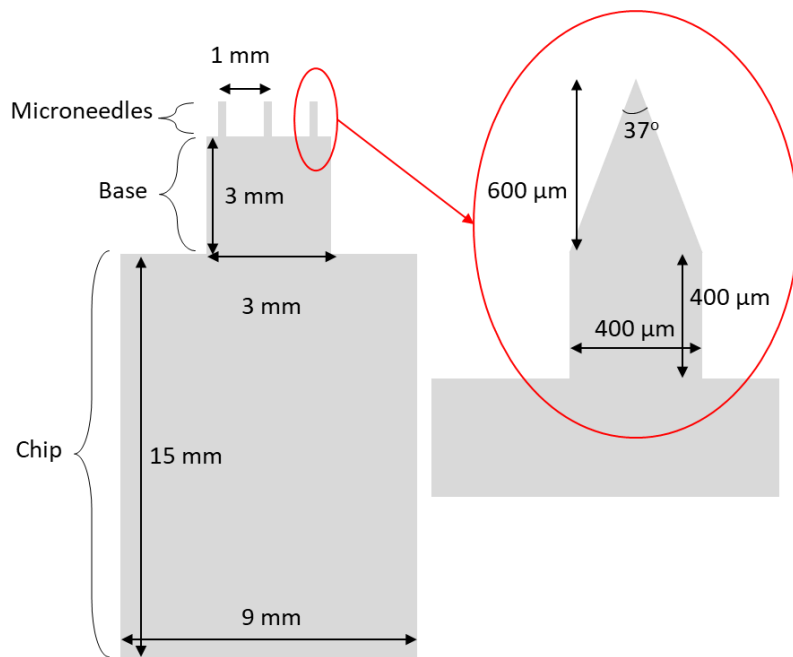
Microneedles (MNs) are being investigated as an alternative diagnostic tool to the SPT [20], [21]. They are also being researched for their potential in vaccination [22] and immunotherapy of airway allergies where allergen extract is coated on MNs for cutaneous delivery [23].

The aim of this study was to coat MNs with birch pollen extract (BPE) or Bet v 1 allergen and deliver this intradermally (i.d.) upon manual insertion into naïve or BPE-sensitized Brown Norway (BN) rats to elicit a local allergic reaction. The allergic reaction was visualized using Evans blue.

## **2. Materials and methods**

### **2.1 Microneedle fabrication**

The fabrication, dimensions and shape of MNs are described in manuscript I [24]. Briefly explained silicon wafers were exposed to spin coating, photo lithography, and dry etching to determine the thickness and shape of the MNs, whereafter excess photoresist was removed. As illustrated in Figure 1 the MNs were pencil shaped with a total length of 1000  $\mu\text{m}$ , thickness of 180  $\mu\text{m}$ , and width of 400  $\mu\text{m}$  and each chip always contained three such MNs extruding from a 3 x 3 mm base which sat on a 9 x 15 mm chip for handling.



**Figure 1: Illustration of microneedle shape and dimensions.** Schematic of the 1000  $\mu\text{m}$  long, 400  $\mu\text{m}$  wide, and 180  $\mu\text{m}$  thick, pencil-shaped microneedles. Three MNs extrude from the base which is attached to the chip. Adopted from manuscript II [25].

## 2.2 Coating solution

The coating solution was described in manuscript II [25], but in brief it consisted of 1% (w/v) carboxymethylcellulose (CMC) sodium salt (low viscosity) (Sigma-Aldrich, St. Louis, Missouri, USA) in phosphate buffered saline (PBS, 137 mM NaCl, 3 mM KCl, 8 mM  $\text{Na}_2\text{HPO}_4$ , 1 mM  $\text{KH}_2\text{PO}_4$ , pH 7.2) with different concentrations (6, 60, and 600  $\mu\text{g}/\text{mL}$ ) of either birch pollen extract (BPE, DST, Schwerin, Germany) or Bet v 1 allergen extract (DST).

## 2.3 Dip-coating

The dip-coating method was outlined in manuscript II [25], but in short a Texture Analyser was used to lower a mounted chip with MNs at the speed of 0.5 mm/s into a coating solution, holding the MNs in the solution for 10 s, and retracting the MNs again at a speed of 0.5 mm/s. The MNs were left to dry for a few min afterwards.

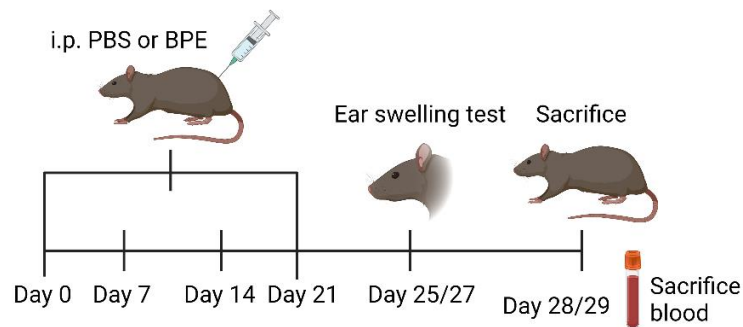
## 2.4 Brown Norway rats

Rat experiments were conducted in the Technical University of Denmark's animal facility. Ethical approval was given by The Danish Animal Experiments Inspectorate with the authorization number (2020-15-0201-00732-C1). The University's in-house Animal Welfare Committee for animal care and use were in charge of overseeing the rat experiments.

BN rats 9-12 weeks old were used for the experiments. The rats originated from the in-house breeding colony at the National Food Institute, Technical University of Denmark. An in-house produced diet based on potato, fish, and rice proteins was fed to the BN rats for more than 14 generations [26], [27] and water was available *ad libitum*. Macrolon cages were used to house the BN rats (n=4/cage) at a temperature of 22 °C ± 1 °C with a humidity of 55 ± 5%. Light was on from 9.00 a.m. to 9.00 p.m. The rats were inspected once daily, and body weight recorded once weekly.

### 2.4.1 Rat experiment: Delivery of birch pollen extract and Bet v 1 in Brown Norway rats

To assess BPE and Bet v 1 allergen delivery using coated MNs, rats were allocated into four groups (n=8/group, 4/gender) where Group 1 and 3 were intraperitoneally (i.p.) injected with 0.5 mL PBS as control and Group 2 and 4 were i.p. injected with 0.5 mL PBS containing 50 µg BPE on Day 0, 7, 14, and 21. On Day 25 (Group 1-2) and Day 27 (Group 3-4) an ear swelling test (EST) was performed as described later in section 2.4.2. On Day 28 (Groups 1, 2, and 4) and Day 29 (Group 3) the rats were sacrificed by decapitation using hypnorm-midazolam as anesthesia and blood was collected (Figure 2).



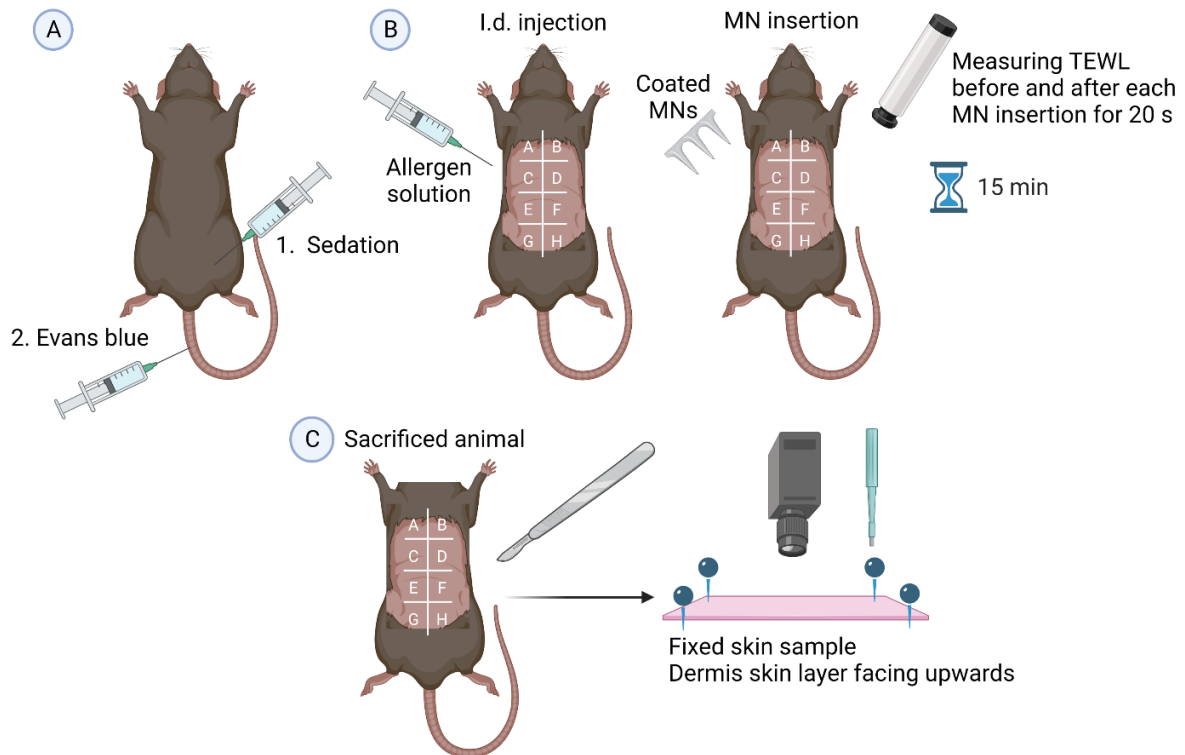
**Figure 2: Rat experiment design.** Rats were intraperitoneally injected with 0.5 mL phosphate buffered saline (PBS) (control groups) or 50 µg birch pollen extract in 0.5 mL PBS (sensitized groups) on Day 0, 7, 14, and 21 to induce sensitization. An ear swelling test was performed on Day 25 and 27 and rats were sacrificed on Day 28 and 29 where blood was collected. Group 1-2 were rats receiving intradermal injections and Group 3-4 were rats receiving microneedle insertions. Created with BioRender.com. Adapted from manuscript II [25].

Group 1-2 were i.d. injected with 30 µL of BPE or Bet v 1 (6, 60 or 600 µg/mL) in PBS giving a total amount of 0.18, 1.80, or 18 µg. In addition, 30 µL of 20 µg/mL 48/80 (48/80, Sigma-Aldrich) was i.d. injected corresponding to 0.6 µg as a positive control and an i.d. injection of 30 µL of PBS was used as a negative control.

Group 3-4 had MNs inserted that were coated with the same concentrations of allergen solution as was used for the i.d. injections. Yet, the amount coated on the MNs, and the amount of allergen delivered in the skin is unknown but anticipated to be much below the amount delivered with i.d. injections. As positive control 1000 µg/mL 48/80-coated MNs were used, and as a negative control PBS-coated MNs were used.

The rat experiment was conducted as described in manuscript II [25]. In brief, the rats were sedated using hypnorm-midazolam, 2 µL/rat weight (g) of 1% Evans blue in PBS was injected into the tail vein and the abdominal skin was shaved (Figure 3A). After 2 min the rats were subjected to either i.d. injection or

manual MN insertion at eight locations (A-H) randomly assigned on the abdominal skin. Trans-epidermal water loss (TEWL) measurements were performed prior to and after each MN insertion for assessing tissue damage. When halfway through i.d. injections or MN insertions, a timer was set for 15 min (Figure 3B) whereafter the rats were sacrificed by decapitation. Afterwards, the abdominal skin was excised and fixed to its original size with the dermis skin layer facing upwards and the Evans blue coloration was photographed for subsequent analysis. A skin biopsy was collected for each of the locations (A-H) and weighed. The biopsy samples were snap-frozen in liquid nitrogen and stored at -80 °C (Figure 3C).



**Figure 3: Delivery of birch pollen extract and Bet v 1 by intradermal injection or microneedle insertion.** A) The rats were sedated using hypnorm-midazolam and 2  $\mu$ L/rat weight (g) of 1% Evans blue in phosphate buffered saline was injected into the tail vein. B) After 2 min, either intradermal (i.d.) injection or microneedle (MN) insertion was done at eight randomly assigned locations (A-H) and trans-epidermal water loss was measured prior to and after MN insertions to assess tissue damage. When halfway through the i.d. injections or MN insertions, a timer was set for 15 min and the rats were sacrificed when the timer ran out. C) The skin with i.d. injections or MN insertions were excised, fixed to its original size, and photographed for subsequent Evans blue analysis. Biopsy samples were taken from the eight locations (A-H) and snap-frozen in liquid nitrogen for storage at -80 °C. Created with BioRender.com. Adopted from manuscript II [25].

### 2.4.2 Ear swelling test

An EST was done to evaluate the clinical relevance of the BPE sensitization, as previously described [25], [28]. Briefly, the rats were anesthetized using hypnorm-midazolam and the initial ear thickness was



measured twice. The left ear was i.d. injected with 10 µg BPE in 20 µL PBS and the right ear was i.d. injected with 3 µg Bet v 1 in 20 µL PBS. The thickness was measured again, once, after 30 min.

## **2.5 ImageJ analysis of Evans blue data**

ImageJ 1.52a (National Institutes of Health, USA) was used for all image analysis as described in manuscript II [25]. In brief, “Color Profiler” was used for area under the curve (AUC) analysis where the Evans blue area was selected using the rectangle selection tool and the RGB (red, green, and blue) graph for the Evans blue area and background surrounding it was extracted. Based on the extracted RGB graphs for the data in the red channel, AUC was calculated for the background and Evans blue area which were then subtracted from each other. This gave a quantitative value for the parameters of surface area as well as color saturation with the unit of the AUC being “gray value x pixels”.

## **2.6 Enzyme-Linked Immunosorbent Assay**

### **2.6.1 Detection of specific IgG<sub>1</sub> by indirect ELISA**

The procedure for specific IgG<sub>1</sub> was generally as described in manuscript II [25], with the exception that the 96-well Maxisorp plates (NUNC, Roskilde, Denmark) were coated overnight at 4 °C with 100 µL/well of 10 µg/mL BPE in carbonate buffer (15 mM Na<sub>2</sub>CO<sub>3</sub> x 10 H<sub>2</sub>O, 35 mM NaHCO<sub>3</sub>, pH 9.6). The results are expressed as log<sub>2</sub> titer values with a cut-off optical density (OD) of 0.1. The titer values are defined as the interpolated dilution of the sample down to the mean absorbance for the negative control +3 x the standard deviation (SD).

### **2.6.2 Detection of specific IgE by indirect ELISA**

The procedure for specific IgE was generally as described in manuscript II [25], with the exception that the detection of BPE-specific IgE was performed with 50 µL/well of 10:1 digoxigenin (DIG)-coupled BPE diluted to 1 µg/mL in 3% skimmed milk powder (SMP, 70166, Sigma-Aldrich) blocking solution. The results are expressed as log<sub>2</sub> titer values with a cut-off OD of 0.1. The titer values are defined as the interpolated dilution of the sample down to the mean absorbance for the negative control +3 x SD.

## **2.7 Statistical analysis**

Graphs and statistical analyses were generated using Prism V9.5.0 (GraphPad, San Diego, CA, USA). The results were analyzed using non-parametric analyses as the data was found to not be normally distributed as assessed by D’Agostino-Pearson normality tests. The performed tests were therefore Mann-Whitney tests and Kruskal-Wallis tests with Dunn’s multiple comparisons test using a significance level of  $\alpha=0.05$  in all cases.

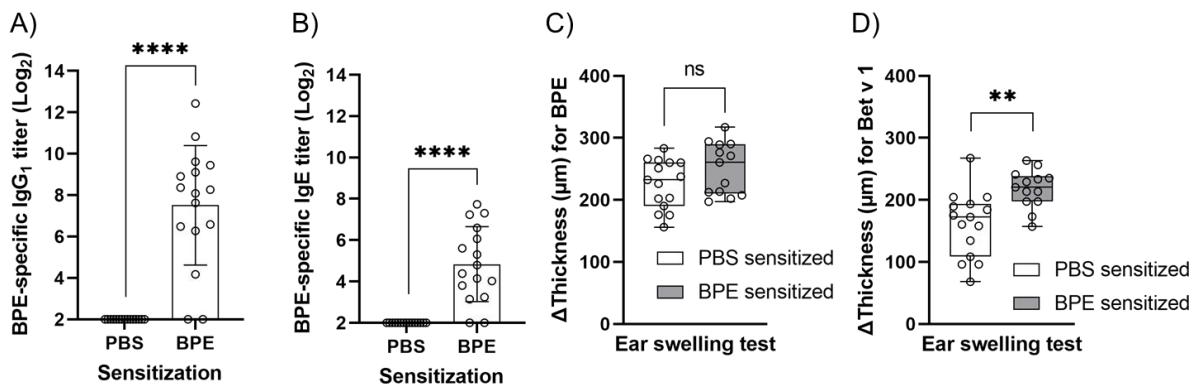
### 3. Results

#### 3.1 Delivery of birch pollen extract and Bet v 1 allergen in Brown Norway rats

##### 3.1.1 Sensitization of Brown Norway rats

BPE-specific IgG<sub>1</sub> enzyme-linked immunosorbent assay (ELISA) was performed to confirm an initial antibody response (Figure 4A) and BPE-specific IgE ELISA assay was done to confirm sensitization towards BPE (Figure 4B). The IgG<sub>1</sub> and IgE ELISAs showed that most of the BPE immunized rats, except from three, had developed an immune response and were found to be sensitized towards BPE in contrast to the PBS control rats. The three non-sensitized rats were omitted from the remaining analysis of this study.

An EST was done for BPE (Figure 4C) and Bet v 1 (Figure 4D) where a statistically significant difference (Mann-Whitney test) between the control group (PBS) and sensitized group (BPE) was found for the Bet v 1 EST indicating that the sensitized rats had a clinically active response towards Bet v 1. No statistically significant difference was found for BPE ( $P=0.1001$ ), thus a clinically active response towards BPE was not shown.



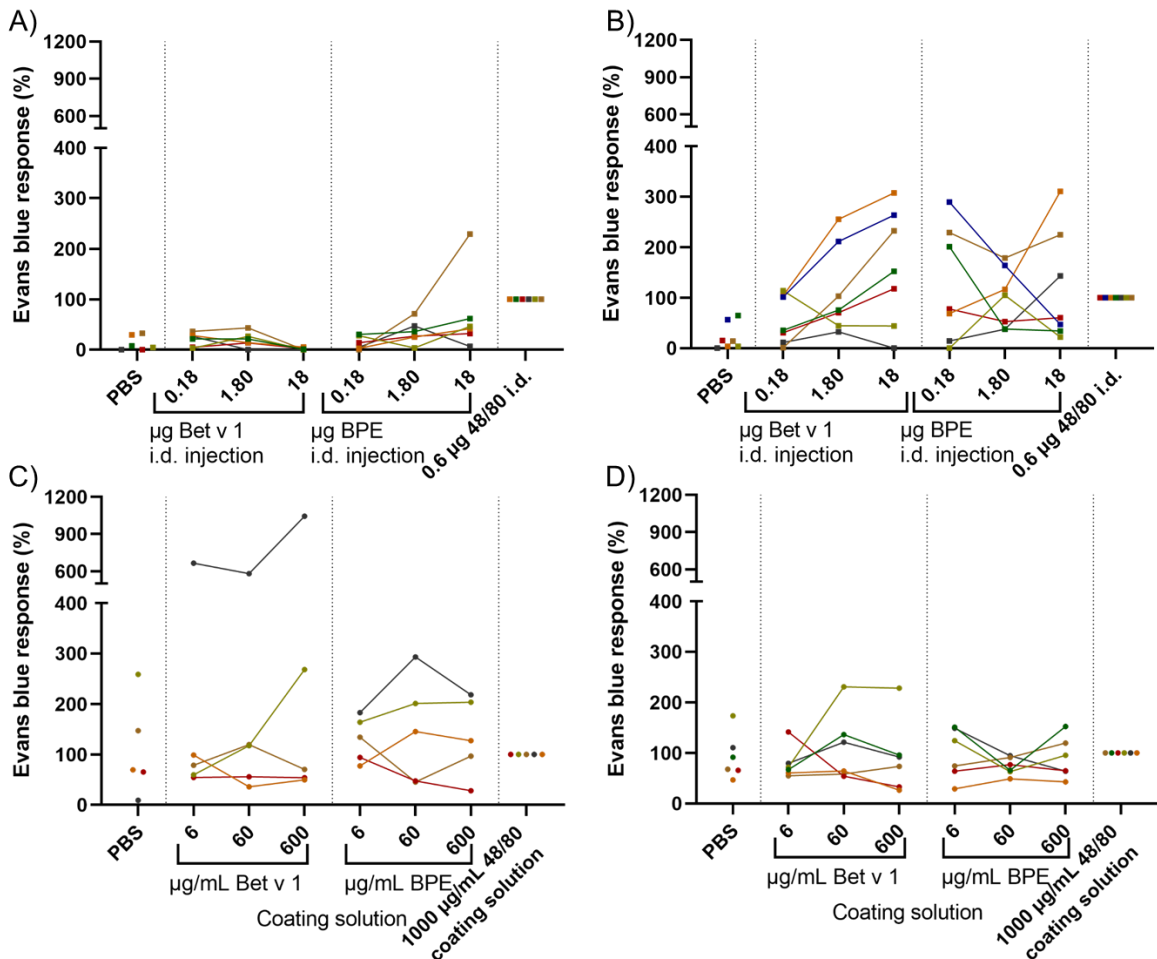
**Figure 4: Immune response in Brown Norway rats.** A) Birch pollen extract (BPE)-specific IgG<sub>1</sub> titer (n=31). B) BPE-specific IgE titer (n=31). C) Ear swelling test (EST) for BPE (n=28). D) EST for Bet v 1 (n=28). For all statistical analyses the significant differences are marked as \*\* =  $p \leq 0.01$ , \*\*\*\* =  $p \leq 0.0001$ .

TEWL (Figure S1A, SI) was measured for 20 s prior to and after MN insertion at the specific locations A-H (Figure S1B, SI) to confirm MN penetration of the skin. Although it seemed that MN insertion caused an increase in TEWL in all cases, only three locations (D, E, and G) showed a statistically significant difference (Kruskal-Wallis test with Dunn's multiple comparisons test) between the TEWL before and after measurements.

##### 3.1.2 Area under the curve analysis

The Evans blue response was measured relative to the positive control of 48/80 assuming this provided max degranulation of mast cells (for raw AUC data see Figure S2A-D in SI). Only rats where the positive control 48/80 was clearly visible were included in the analysis hence the number of rats varied between the groups.

The rats receiving i.d. injections exhibited a low response to PBS and a high response to 48/80 (Figure 5A-B). Sensitized rats appeared to respond to both Bet v 1 and BPE (Figure 5B) compared to naïve rats (Figure 5A). There was no difference in the measurable reaction towards Bet v 1, BPE, or 48/80 for rats receiving MN insertions compared to the negative control (PBS-coated MNs), and there was no difference between the reactions in naïve (Figure 5C) and sensitized rats (Figure 5D).



**Figure 5: Dose-response curves for Evans blue response (%) relative to Evans blue response for the positive control (compound 48/80).** A) Intradermal (i.d.) injection in naïve rats (n=6). B) i.d. injection in sensitized rats (n=7). C) Microneedle (MN) insertion naïve male rats (n=5). D) MN insertion in sensitized rats (n=6).

## 4. Discussion

MNs were investigated for their potential role in allergy diagnostics by testing their ability to deliver allergens via coating and initiate a local allergic response. This study included MNs coated with the primary allergen Bet v 1 and MNs coated with BPE.

Using an EST, a statistically significant difference was found for Bet v 1 between the sensitized and naïve rats, however, this was not found for BPE. Ideally, the concentration of Bet v 1 in BPE should be

established. Focke *et al.* performed an analysis where they found a tenfold variation in the concentration of Bet v 1 in commercially available BPEs and they found that 1.62 µg/mL – 19.61 µg/mL Bet v 1 was present in the tested extracts [29]. Assuming that this translates to the BPE used in our study and based on the outcome of the EST, the estimated concentration of Bet v 1 in BPE appears to not be high enough to elicit a clinical response towards BPE with Bet v 1 being the main allergen and contributor to an allergic reaction. It is therefore hypothesized that the rats were sensitized towards the Bet v 1 in the BPE and that the concentration of Bet v 1 was too small in the BPE to elicit a clinical response whereas the pure Bet v 1 extract had a high enough concentration for a clinical response to occur.

The difference in TEWL before and after MN insertion was found to not be statistically significant in all locations, which could indicate that the MNs did not pierce the skin. It could also be that the MNs did not completely reach the interstitial fluid or a blood vein, thereby not eliciting as high a water loss. However, the trend was that the TEWL mean values were higher after the penetration in all cases, so the skin was likely pierced.

For rats receiving i.d. injections the Evans blue AUC method gave some promising dose response curves for BPE and Bet v 1. For the rats receiving MN insertions, the Evans blue response for the BPE, Bet v 1 or 48/80-coated MNs was no different from the Evans blue response from PBS-coated MNs. This could be due to the MNs not piercing the skin sufficiently as indicated by the lack of statistically significant differences for the TEWL measurements. Yet, it is more likely that the amount of delivered allergen or 48/80 using coated MNs was too small to either elicit a response in the first place or at least to elicit a measurable reaction using the Evans blue method.

In other studies Evans blue has been quantified by extracting the Evans blue from the biological sample and measuring the absorbance at 620 nm using a spectrophotometer [30], [31]. Other ways of quantifying the Evans blue response would be beneficial to complement the image analysis. As a final note, it would be beneficial if other biomarkers for mast cell activation such as tryptase or histamine [32] could be measured in skin sample biopsies taken from the site of i.d. injection and MN insertion to confirm a local allergic response. As an alternative method to using Evans blue we envision using the MNs with a pyrolytic carbon layer to perform electrochemical measurements of the allergic response [33].

## 5. Conclusions

In this study BPE and Bet v 1-coated MNs were tested for their ability to deliver allergen within the skin to elicit a local allergic response. Evans blue quantification using the AUC analysis method was found to be viable for rats receiving i.d. injections of BPE and Bet v 1. However, for the rats receiving MN insertions no significant reaction could be obtained. It is likely that the MNs did not deliver enough BPE or Bet v 1 to either elicit an allergic response in the first place or elicit a response measurable by the Evans blue method.

For a future study, the dip-coating method for the MNs should be further optimized and the coating solution should be optimized for the individual allergen. Other ways of Evans blue quantification or other

analyses methods entirely should also be explored to complement image analysis, and finally the amount of Bet v 1 present in the BPE should be established.

## 6. Acknowledgements

The authors would like to thank the DTU Animal Facility (BioFacility) for help with the animal experiment and taking care of the animals. A special thank you to Maja Danielsen for help with the ear swelling test.

## 7. Conflict of interest

The authors declare not conflict of interest.

## 8. Data availability statement

All data is available upon reasonable request.

## 9. Author contributions

**Stephanie Ingemann Bisgaard:** Methodology, formal analysis, writing – original draft, investigation, visualization. **Long Quang Nguyen:** Resources, investigation. **Sarah Grundt Simonsen:** Investigation. **Gerardo García Zavaleta:** Resources. **Mohammad Ramezannezhad:** Resources. **Stephan Sylvest Keller:** Supervision, funding acquisition, writing – review & editing, project administration. **Katrine Lindholm Bøgh:** Supervision, conceptualization, methodology, resources, writing – review & editing.

## 10. Funding

Funding from the Independent Research Fund Denmark (grant no. 8022-00215B), and the LEO Foundation (grant no. LF17046).

## 11. Keywords

Brown Norway rats, microneedles, birch pollen extract, Bet v 1, coating, Texture Analyser, ImageJ, allergy

## 12. References

- [1] M. Smith *et al.*, “Geographic and temporal variations in pollen exposure across Europe,” *Allergy Eur. J. Allergy Clin. Immunol.*, vol. 69, no. 7, pp. 913–923, 2014.
- [2] C. Canova *et al.*, “The influence of sensitisation to pollens and moulds on seasonal variations in asthma attacks,” *Eur. Respir. J.*, vol. 42, no. 4, pp. 935–945, 2013.
- [3] T. Biedermann, L. Winther, S. J. Till, P. Panzner, A. Knulst, and E. Valovirta, “Birch pollen allergy in Europe,” *Allergy Eur. J. Allergy Clin. Immunol.*, vol. 74, no. 7, pp. 1237–1248, 2019.
- [4] F. Wölbing, J. Kunz, W. E. Kempf, C. Grimm, J. Fischer, and T. Biedermann, “The clinical

- relevance of birch pollen profilin cross-reactivity in sensitized patients," *Allergy Eur. J. Allergy Clin. Immunol.*, vol. 72, no. 4, pp. 562–569, 2017.
- [5] "WHO/IUIS Allergen Nomenclature Sub-Committee (Birch)." [Online]. Available: <http://allergen.org/search.php?allergenname=&allergensource=birch&TaxSource=&TaxOrder=&foodallerg=all&bioname=>.
- [6] L. Li, C. Chang, and K. Guan, "Birch Pollen Allergens," *Curr. Protein Pept. Sci.*, vol. 23, no. 11, pp. 731–743, 2022.
- [7] H. Ipsen and H. Løwenstein, "Isolation and immunochemical characterization of the major allergen of birch pollen (*Betula verrucosa*)," *J. Allergy Clin. Immunol.*, vol. 72, no. 2, pp. 150–159, 1983.
- [8] G. Petersson, S. Djueborg, and R. Ingestad, "Clinical History, Skin Prick Test and RAST in the Diagnosis of Birch and Timothy Pollinosis," *Allergy*, vol. 41, no. 6, pp. 398–407, 1986.
- [9] B. Chinoy, E. Yee, and S. L. Bahna, "Skin testing versus radioallergosorbent testing for indoor allergens," *Clin. Mol. Allergy*, vol. 3, no. 1d, pp. 1–7, 2005.
- [10] M. Osterballe, R. Scheller, P. Stahl Skov, K. E. Andersen, and C. Bindsvlev-Jensen, "Diagnostic value of scratch-chamber test, skin prick test, histamine release and specific IgE in birch-allergic patients with oral allergy syndrome to apple," *Allergy Eur. J. Allergy Clin. Immunol.*, vol. 58, no. 9, pp. 950–953, 2003.
- [11] L. Heinzerling *et al.*, "The skin prick test - European standards," *Clin. Transl. Allergy*, vol. 3, no. 1, pp. 1–10, 2013.
- [12] G. Menz *et al.*, "Serological and skin-test diagnosis of birch pollen allergy with recombinant Bet v I, the major birch pollen allergen," *Clin. Exp. Allergy*, vol. 26, no. 1, pp. 50–60, 1996.
- [13] M. Miguères *et al.*, "Types of sensitization to aeroallergens: Definitions, prevalences and impact on the diagnosis and treatment of allergic respiratory disease," *Clin. Transl. Allergy*, vol. 4, no. 1, pp. 1–8, 2014.
- [14] E. Jensen-Jarolim *et al.*, "Allergen mimotopes in food enhance type I allergic reactions in mice," *FASEB J.*, vol. 13, no. 12, pp. 1586–1592, 1999.
- [15] I. Schöll *et al.*, "Allergen-loaded biodegradable poly(D,L-lactic-co-glycolic) acid nanoparticles down-regulate an ongoing Th2 response in the BALB/c mouse model," *Clin. Exp. Allergy*, vol. 34, no. 2, pp. 315–321, 2004.
- [16] U. Baranyi *et al.*, "Tolerization of a Type I Allergic Immune Response through Transplantation of Genetically Modified Hematopoietic Stem Cells," *J. Immunol.*, vol. 180, no. 12, pp. 8168–8175, 2008.
- [17] K. L. Bøgh, V. Barkholt, and C. B. Madsen, "Characterization of the Immunogenicity and Allergenicity of Two Cow's Milk Hydrolysates - A Study in Brown Norway Rats," *Scand. J. Immunol.*, vol. 81, no. 5, pp. 274–283, 2015.
- [18] Z. Ovary, "Immediate Reactions in the Skin of Experimental Animal Provoked by Antibody-Antigen Interaction," *Progr. Allergy*, vol. 5, pp. 459–508, 1958.
- [19] M. W. Chase, "Studies on the Sensitization of Animals With Simple Chemical Compounds: X.

- Antibodies inducing immediate-type skin reactions," *J. Exp. Med.*, vol. 86, no. 6, pp. 489–514, 1947.
- [20] A. Trautmann, F. Heuck, R. Denfeld, P. Ruther, and O. Paul, "Detachable Silicon Microneedle Stamps For Allergy Skin Prick Testing," *19th IEEE Int. Conf. Micro Electro Mech. Syst.*, pp. 434–4237, 2006.
- [21] Y. Ito *et al.*, "Dissolving microneedles as skin allergy test device," *Biol. Pharm. Bull.*, vol. 40, no. 4, pp. 531–534, 2017.
- [22] A. K. Shakya, C. H. Lee, and H. S. Gill, "Cutaneous vaccination with coated microneedles prevents development of airway allergy," *J. Control. Release*, vol. 265, no. August, pp. 75–82, 2017.
- [23] A. K. Shakya, C. H. Lee, and H. S. Gill, "Microneedle-Mediated Allergen-Specific Immunotherapy for the Treatment of Airway Allergy in Mice," *Mol. Pharm.*, vol. 17, no. 8, pp. 3033–3042, 2020.
- [24] S. I. Bisgaard, L. Q. Nguyen, K. L. Bøgh, and S. S. Keller, "Dermal Tissue Penetration of In-plane Silicon Microneedles Evaluated in Skin-simulating Hydrogel, Rat Skin, and Porcine Skin," 2023.
- [25] S. I. Bisgaard *et al.*, "Peanut Allergen Ara h 2 Delivery with In-plane Silicon Microneedles for Test of Allergic Response," 2023.
- [26] S. Kroghsbo, K. L. Bøgh, N. M. Rigby, E. N. C. Mills, A. Rogers, and C. B. Madsen, "Sensitization with 7S globulins from peanut, hazelnut, soy or pea induces ige with different biological activities which are modified by soy tolerance," *Int. Arch. Allergy Immunol.*, vol. 155, no. 3, pp. 212–224, 2011.
- [27] K. L. Bøgh *et al.*, "Digested Ara h 1 has sensitizing capacity in Brown Norway rats Clinical & Experimental Allergy," pp. 1611–1621, 2009.
- [28] A. V. Locke, J. M. Larsen, K. B. Graversen, T. R. Licht, M. I. Bahl, and K. L. Bøgh, "Amoxicillin does not affect the development of cow's milk allergy in a Brown Norway rat model," *Scand. J. Immunol.*, vol. 95, no. 5, pp. 1–13, 2022.
- [29] M. Focke, K. Marth, and R. Valenta, "Molecular composition and biological activity of commercial birch pollen allergen extracts," *Eur. J. Clin. Invest.*, vol. 39, no. 5, pp. 429–436, 2009.
- [30] H. Evans, K. E. Killoran, and E. Mitre, "Measuring local anaphylaxis in mice," *J. Vis. Exp.*, no. 92, pp. 1–6, 2014.
- [31] H. L. Wang and T. W. Lai, "Optimization of Evans blue quantitation in limited rat tissue samples," *Sci. Rep.*, vol. 4, pp. 1–7, 2014.
- [32] D. D. Metcalfe *et al.*, "Biomarkers of the involvement of mast cells, basophils and eosinophils in asthma and allergic diseases," *World Allergy Organ. J.*, vol. 9, no. 1, pp. 1–15, 2016.
- [33] S. E. Tehrani, "3D Pyrolytic Carbon for Monitoring Type I Allergic Reactions," Technical University of Denmark (DTU), 2022.

### 13. List of abbreviations

| Abbreviation | Meaning                    |
|--------------|----------------------------|
| AUC          | Area under the curve       |
| BN           | Brown Norway               |
| BPE          | Birch pollen extract       |
| ELISA        | enzyme-linked immunoassay  |
| EST          | Ear swelling test          |
| i.d.         | Intradermal                |
| i.p.         | Intraperitoneal            |
| MN           | Microneedle                |
| OD           | Optical density            |
| PBS          | Phosphate buffered saline  |
| RGB          | Red, green and blue        |
| SD           | Standard deviation         |
| TEWL         | Trans-epidermal water loss |
| w/v          | Weight per volume          |
| 48/80        | Compound 48/80             |



# Birch pollen extract and allergen Bet v 1 delivery for test of allergic response with in-plane Si microneedles – Supporting information

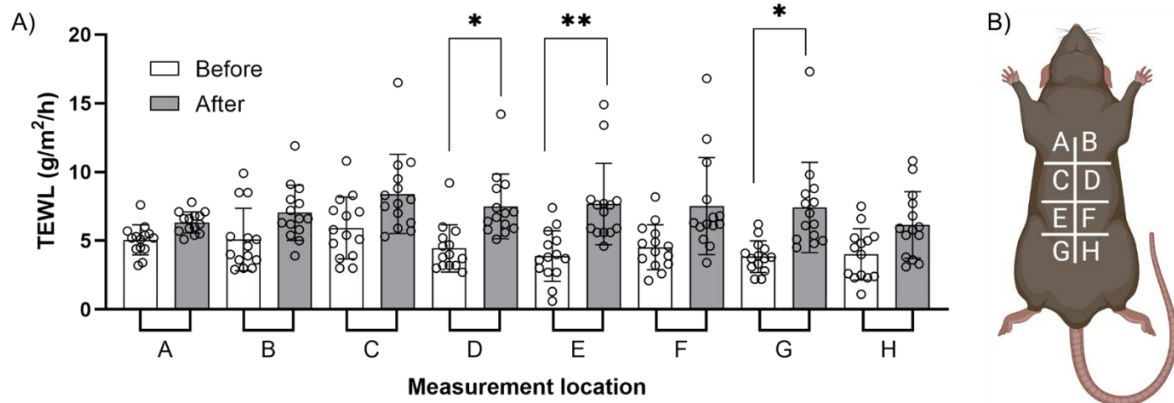
Stephanie Ingemann Bisgaard<sup>a,b</sup>, Quang Long Nguyen<sup>a</sup>, Sarah Grundt Simonsen<sup>b</sup>, Gerardo García Zavaleta<sup>a</sup>, Mohammad Ramezannezhad<sup>a</sup>, Stephan Sylvest Keller<sup>a</sup>, Katrine Lindholm Bøgh<sup>b,\*</sup>,

<sup>a</sup> National Centre for Nano Fabrication and Characterization, Technical University of Denmark, Ørsteds Plads, Building 347 East, 2800 Kgs. Lyngby, Denmark.

<sup>b</sup> National Food Institute, Technical University of Denmark, Kemitovet, Building 202, 2800 Kgs. Lyngby, Denmark.

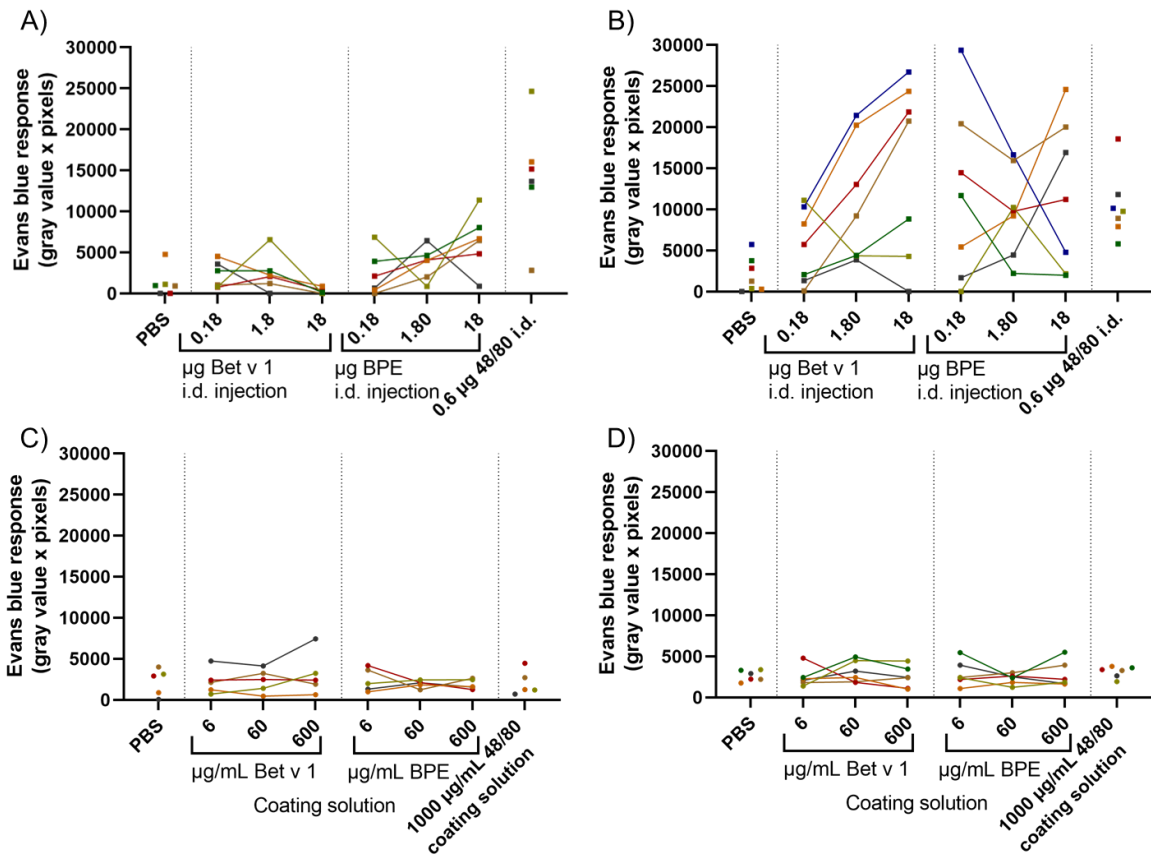
\* E-mail of corresponding author: [kalb@food.dtu.dk](mailto:kalb@food.dtu.dk)

## S1 Trans-epidermal water loss



**Figure S1: Trans-epidermal water loss measurements and the measurement locations.** A) Trans-epidermal water loss (TEWL) was measured for 20 s before and after microneedle insertion (60 s) at locations A-H (mean  $\pm$  SD, n=48). B) Schematic illustrating the TEWL measurement locations A-H. Created with BioRender.com.

## S2 Area under the curve analysis



**Figure S2: Dose-response curves for Evans blue response by AUC (gray value x pixels) analysis.** A) Intradermal (i.d.) injection in naïve rats (n=6). B) i.d. injection in sensitized rats (n=7). C) Microneedle (MN) insertion in naïve rats (n=5). D) MN insertion in sensitized rats (n=6).